



HAL
open science

Multi-modality quality assessment for unconstrained biometric samples

Xinwei Liu

► **To cite this version:**

Xinwei Liu. Multi-modality quality assessment for unconstrained biometric samples. Image Processing [eess.IV]. Normandie Université; Gjøvik University College (Norvège), 2018. English. NNT : 2018NORMC284 . tel-02299278

HAL Id: tel-02299278

<https://theses.hal.science/tel-02299278>

Submitted on 27 Sep 2019

HAL is a multi-disciplinary open access archive for the deposit and dissemination of scientific research documents, whether they are published or not. The documents may come from teaching and research institutions in France or abroad, or from public or private research centers.

L'archive ouverte pluridisciplinaire **HAL**, est destinée au dépôt et à la diffusion de documents scientifiques de niveau recherche, publiés ou non, émanant des établissements d'enseignement et de recherche français ou étrangers, des laboratoires publics ou privés.



Normandie Université

THÈSE

Pour obtenir le diplôme de doctorat

Spécialité INFORMATIQUE

Préparée au sein de l'Université de Caen Normandie

En cotutelle internationale avec Gjøvik University College (HIG) , NORVEGE

Multi-modality quality assessment for unconstrained biometric samples

Présentée et soutenue par
Xinwei LIU

Thèse soutenue publiquement le 22/06/2018
devant le jury composé de

M. AMINE NAÏT-ALI	Professeur des universités, université Paris-est créteil (UPEC)	Rapporteur du jury
Mme SOPHIE TRIANTAPHILLIDOU	Professeur, University of Westminster	Rapporteur du jury
M. PATRICK BOURS	Professeur, Department of Information Security	Membre du jury
Mme CHRISTINE FERNANDEZ-MALOIGNE	Professeur des universités, Université de Poitiers	Président du jury
M. FREDERIC JURIE	Professeur des universités, Université Caen Normandie	Membre du jury
M. LUDOVIC MACAIRE	Professeur des universités, Université Lille 1 Sciences Et Technolog	Membre du jury
M. MARIUS PEDERSEN	Professeur, Department of Computer Science	Membre du jury
M. CHRISTOPHE CHARRIER	Maître de conférences HDR, Université Caen Normandie	Directeur de thèse

Thèse dirigée par **CHRISTOPHE CHARRIER**, Groupe de recherche en informatique, image, automatique et instrumentation



UNIVERSITÉ
CAEN
NORMANDIE



Abstract

The aim of this research is to investigate multi-modality biometric image quality assessment methods for unconstrained samples. Studies of biometrics noted the significance of sample quality for a recognition system or a comparison algorithm because the performance of the biometric system depends mainly on the quality of the sample images. The need to assess the quality of multi-modality biometric samples is increased with the requirement of a high accuracy multi-modality biometric systems.

In this thesis we describe the work carried out to use no-reference image quality metrics for the assessment of multi-modality biometric sample images. The intended behavior of such metrics is to evaluate or predict the quality of natural image as human observers would perceive it.

Following an introduction and background in biometrics and biometric sample quality, we introduce the concept of biometric sample quality assessment for multiple modalities. Recently established ISO/IEC quality standards for fingerprint, iris, and face are presented. In addition, sample quality assessment approaches which are designed specific for contact-based and contactless fingerprint, near-infrared-based iris and visible wavelength iris, as well as face are surveyed. Following the survey, approaches for the performance evaluation of biometric sample quality assessment methods are also investigated.

Based on the knowledge gathered from the biometric sample quality assessment challenges, we propose a common framework for the assessment of multi-modality biometric image quality. We review the previous classification of image-based quality attributes for a single biometric modality and investigate what are the common image-based attributes for multi-modality. Then we select and re-define the most important image-based quality attributes for the common framework. In or-

der to link these quality attributes to the real biometric samples, we develop a new multi-modality biometric image quality database which has both high quality sample images and degraded images for contactless fingerprint, visible wavelength iris, and face modalities. The degradation types are based on the selected common image-based quality attributes. Another important aspect in the proposed common framework is the image quality metrics and their applications in biometrics. We first introduce and classify the existing image quality metrics and then conducted a brief survey of no-reference image quality metrics, which can be applied to biometric sample quality assessment. Plus, we investigate how no-reference image quality metrics have been used for the quality assessment for fingerprint, iris, and face biometric modalities.

From the fingerprint quality ISO/IEC standard we already know what kind of degradations that can affect the performance of a fingerprint recognition system, however, it is not clear if the system performance will be influenced, or to what extent. Therefore, an experiment is conducted to investigate how a number of selected image degradations influence the performance of a fingerprint recognition system, and, influence the performance of a fingerprint quality assessment approach.

According to the availability of open source biometric recognition applications, the existing contact-based fingerprint recognition algorithms have difficulties to extract the minutiae from the high quality contactless fingerprint images from our database. Therefore, we review 10 existing methods for the enhancement of contact-based fingerprint and select two suitable methods to verify whether they can be applied to contactless fingerprint. Finally, we propose an improved 3-step contactless fingerprint image enhancement approach for the minutia extraction. However, after the image enhancement process, the number of detected minutiae is still under an acceptable level. We decide to leave contactless fingerprint for our further study.

The experiments for the performance evaluation of no-reference image quality metrics for visible wavelength face and iris modalities are conducted. The experimental results indicate that there are several no-reference image quality metrics that can assess the quality of both iris and face biometric samples. Lastly, we optimize the best metric by re-training it. The re-trained image quality metric can provide better recognition performance than the original. Through the work carried out in this thesis we have shown the applicability of no-reference image quality metrics for the assessment of unconstrained multi-modality biometric samples.

Sammendrag

Målet med denne forskningen er å undersøke biometrisk bildekvalitet med flere modaliteter i ukontrollerte omgivelser. Tidligere forsknings innen biometri har påpekt betydningen av bildekvalitet for et gjenkjennelsessystem eller sammenligningsalgoritmer fordi ytelsen til det biometriske systemet avhenger hovedsakelig av kvaliteten av bildene. Behovet for å vurdere kvaliteten på multimodale biometriske bilder øker med kravet om høy nøyaktighet i multimodale biometriske systemer. I denne avhandlingen beskriver vi arbeidet som utføres for å gjøre beregninger av bildekvalitet uten referansebilder for vurdering av biometriske bilder med flere modaliteter. Den tiltenkte oppgaven til slike beregninger er å evaluere eller forutsi kvaliteten på det naturlige bildet som menneskelige observatører ville oppleve det. Etter en introduksjon og bakgrunn i biometri og biometrisk kvalitet, presenterer vi begrepet biometrisk bildekvalitet vurdering for flere modaliteter. Nylig etablerte ISO / IEC kvalitetsstandarder for fingeravtrykk, iris og ansikt blir presentert. I tillegg tilnærmes bildekvalitetsvurdering som er konstruert spesifikt for kontaktbaserte og kontaktløse fingeravtrykk, nærinfrarødbasert iris og synlig bølgelengde iris, samt ansikt blir undersøkt. Etter dette, undersøker vi ytelseevaluering av biometriske bildekvalitetsmetoder. Basert på kunnskap samlet fra dagens utfordringer innen biometriske bildekvalitetsevaluering, foreslår vi et felles rammeverk for vurdering av multimodal biometrisk bildekvalitet. Vi går igjennom tidligere klassifisering av bildebaserte kvalitetsattributter for hver biometrisk modalitet og undersøker hva som er vanlig bildebaserte attributter for multimodale biometriske systemer. Basert på dette velger vi og definerer de viktigste bildebaserte kvalitetsattributter for det felles rammeverket. For å knytte disse kvalitetsattributene til de virkelige biometriske bildene utvikler vi en ny biometrisk bildekvalitetsdatabase med flere modaliteter, som har både høy kvalitets bilder og forringede bilder for kontaktløse fingeravtrykk, synlig bølgelengde iris og ansikt. Forringede

bilder er basert på vanlige bildebaserte kvalitetsattributter. Et annet viktig aspekt i det foreslåtte rammeverket er bildekvalitetsmålinger og deres applikasjoner i biometri. Først introduserer og klassifiserer vi eksisterende bildekvalitetsmetriker og deretter viser vi en oversikt over ikke-referanse bildekvalitetsmetriker uten referansebilde som kan brukes til biometrisk bildekvalitetsvurdering. I tillegg undersøker vi hvordan bildekvalitetsmetriker har blitt brukt til kvalitetsvurdering for fingeravtrykk, iris og ansikt.

Fra ISO / IEC-standarden for fingeravtrykkskvalitet vet vi allerede hva slags forringelse av bildene som kan påvirke ytelsen til et fingeravtrykks-gjenkjenningssystem. Det er imidlertid ikke klart om systemytelsen vil bli påvirket, eller i hvilken utstrekning. Derfor utføres et eksperiment for å undersøke hvordan et antall valgte bildeforringelser påvirker ytelsen til et fingeravtrykks-gjenkjenningssystem, og sammenhengen mellom kvalitetsvurdering av bildene og ytelsen av systemet. I henhold til tilgjengeligheten av åpen kildekode biometrisk anerkjennelsesprogrammer, har de eksisterende kontaktbaserte fingeravtrykks-gjenkjenningssystemene problemer med å trekke ut referansepunkter fingeravtrykksbildene med høy kvalitet fra vår database. På grunn av dette tester vi 10 eksisterende metoder for forbedring av kontaktbasert fingeravtrykk, og velger to egnede metoder for å kontrollere om de kan brukes til kontaktløse fingeravtrykk. Til slutt foreslår vi et forbedret 3-trinns bildeforbedringsmetode for kontaktløse fingeravtrykk. Imidlertid, etter bildeforbedringsprosessen, er antall referansepunkter fortsatt under et akseptabelt nivå. Vi bestemmer oss for å ikke fortsette forskningen på kontaktløse fingeravtrykk i våre videre studier. Resten av avhandlingen omfatter eksperimenter for ytelseevaluering av kvalitetsmetriker uten referansebilde for synlig bølgelengde ansiktsbilder og iris. De eksperimentelle resultatene indikerer at det er flere bildekvalitetsmetriker som kan vurdere kvaliteten på både iris- og ansiktsbilder. Til slutt optimaliserer vi den beste metrikken, og den optimaliserte metrikken gir bedre ytelse enn originalen. Gjennom arbeidet i denne avhandlingen har vi vist anvendeligheten av bildekvalitetsmetriker for vurdering av biometriske bilder med flere modaliteter.

Résumé

L'objectif de ces travaux de recherche est d'étudier les méthodes d'évaluation de la qualité des images biométriques multimodales sur des échantillons acquis de manière non contrainte. De nombreuses études ont noté l'importance de la qualité de l'échantillon pour un système de reconnaissance ou un algorithme de comparaison, puisque la performance du système biométrique est intrinsèquement dépendant de la qualité des images de l'échantillon. Dès lors, la nécessité d'évaluer la qualité des échantillons biométriques pour plusieurs modalités (empreintes digitales, iris, visage, etc.) est devenue primordiale notamment avec l'apparition de systèmes biométriques multimodaux de haute précision.

Dans cette thèse, nous décrivons le travail effectué pour étudier l'adaptabilité des métriques de qualité d'image sans référence pour l'évaluation d'images biométriques de plusieurs modalités. Le comportement attendu de ces métriques est d'évaluer ou de prédire la qualité de l'image naturelle telle que le font les observateurs humains.

Après une introduction présentant un historique de la biométrie et des préceptes liés à la qualité des échantillons biométriques, nous présentons le concept d'évaluation de la qualité des échantillons pour plusieurs modalités. Les normes de qualité ISO / CEI récemment établies pour les empreintes digitales, l'iris et le visage sont présentées. De plus, des approches d'évaluation de la qualité des échantillons conçues spécifiquement pour les empreintes digitales avec et sans contact, pour l'iris (dont une image est capturée en proche infrarouge et dans le domaine visible), ainsi que le visage sont étudiées. Finalement, des techniques d'évaluation des performances des mesures de qualité des échantillons biométriques sont également étudiées.

Sur la base des conclusions formulées suite à l'étude des solutions algorithmiques

portant sur l'évaluation de la qualité des échantillons biométriques, nous proposons un cadre commun pour l'évaluation de la qualité d'image biométrique pour plusieurs modalités. Après avoir étudié les attributs de qualité basés sur l'image par modalité biométrique, nous examinons quelle intersection existe pour l'ensemble des modalités. Ensuite, nous sélectionnons et redéfinissons les attributs de qualité basés sur l'image qui sont les plus importants afin de définir un cadre commun. Afin de relier ces attributs de qualité aux vrais échantillons biométriques, nous développons une nouvelle base de données de qualité d'image biométrique multi-modalité qui contient des images échantillons de haute qualité et des images dégradées pour l'empreinte digitale acquise sans contact, l'iris (dont l'acquisition est réalisée dans le spectre visible) et le visage. Les types de dégradation appliqués sont liés aux attributs de qualité qui sont communs aux diverses modalités et qui sont basés sur l'image. Un autre aspect important du cadre commun proposé est la qualité de l'image et ses applications en biométrie. Nous avons d'abord introduit et classifié les métriques de qualité d'image existantes, puis effectué un bref aperçu des métriques de qualité d'image sans référence, qui peuvent être appliquées pour l'évaluation de la qualité des échantillons biométriques. De plus, nous étudions comment les mesures de qualité d'image sans référence ont été utilisées pour l'évaluation de la qualité des empreintes digitales, de l'iris et des modalités biométriques du visage.

D'après la norme ISO / CEI portant sur la qualité des empreintes digitales, nous connaissons les types de dégradations qui peuvent affecter les performances d'un système de reconnaissance d'empreintes digitales. Cependant, il n'est pas clair dans quelle mesure les performances du système sont influencées. Par conséquent, une expérience est menée pour étudier de quelle manière les dégradations appliquées sur les images influencent les performances d'un système de reconnaissance d'empreintes digitales, et dans quelle mesure elles influencent les performances des mesures de qualité des empreintes digitales.

Les algorithmes existants de reconnaissance d'empreintes digitales acquises par contact ne sont pas nécessairement performants lors de la phase d'extraction des minuties sur les images d'empreintes digitales acquises sans contact et de haute qualité présentes dans notre base de données. Par conséquent, dix méthodes d'amélioration des images d'empreinte digitale acquises avec contact extraites de l'état de l'art sont étudiées. Seules les deux meilleures méthodes sont sélectionnées afin de vérifier dans quelle mesure elles sont applicables pour des images d'empreinte digitale acquises sans contact. Finalement, nous proposons une approche d'amélioration des images d'empreinte digitale acquises sans contact pour l'extraction de minuties. Cependant, après application du processus d'amélioration d'image, le nombre de minuties détectées est toujours inférieur à un niveau acceptable. Ceci

fera l'objet de travaux ultérieurs afin d'aboutir à un processus d'extraction de minuties cohérent.

Des expériences pour l'évaluation de la performance des métriques de qualité d'image sans référence sur les images de visage et de l'iris sont effectuées. Les résultats expérimentaux indiquent qu'il existe plusieurs métriques qui peuvent évaluer la qualité des échantillons biométriques de l'iris et du visage avec un fort coefficient de corrélation. La méthode obtenant les meilleurs résultats en terme de performance est ré-entraînée sur des images d'empreintes digitales, ce qui permet d'augmenter significativement les performances du système de reconnaissance biométrique.

À travers le travail réalisé dans cette thèse, nous avons démontré l'applicabilité des métriques de qualité d'image sans référence pour l'évaluation d'échantillons biométriques multi-modalité non contraints.

Acknowledgement

There are many people who deserve to be acknowledged, without their support and help it would not have been possible to complete this work. First of all, I would like to thank my two main supervisors, Professor Marius Pedersen from Norwegian University of Science and Technology, who introduced me to the field of image quality, and Associate Professor Christophe Charrier from University of Caen Lower Normandy, who brought me the knowledge of biometrics. Many thanks goes to my third supervisor Professor Patrick Bours from Norwegian University of Science and Technology. His assistance, feedback, and support has been invaluable. My deepest gratitude to all of you for your guidance and support during this work.

I would also like to thank the members of the Norwegian Color and Visual Computing Laboratory at Norwegian University of Science and Technology: Faouzi Alaya Cheikh, Aditya Sole, Hilda Deborah, Haris Ahmad Khan, and Congcong Wang. Many thanks go to the members of the E-payment & Biometrics Research Unit at GREYC Laboratory from National School of Engineers of Caen: Christophe Rosenberger, Morgan Barbier, Estelle Cherrier, Ndiaga Faye, Alexandre Ninassi, Baptiste Hemery, Benoit Vibert, Germain Jolly, Thomas Gougeon, Antoine Cabana, and others.

Thanks also goes out to those who participated in my time consuming experiments. Thanks for your time and contribution.

My deepest appreciation is due to my family and friends, their support has been invaluable. Finally, I would like to express my gratitude to my wife Nian, who has borne my increasing absence with good will.

Thank you all.

Caen, France
April 2018
Xinwei Liu

Contents

List of Tables	xxii
List of Figures	xxviii
Abbreviations	xxix
1 Introduction	1
1.1 Motivation	2
1.2 Aims and research questions	2
1.3 Publications	3
1.4 Thesis outline	5
2 Background	7
2.1 What is biometrics?	7
2.1.1 Biometrics	7
2.1.2 Fingerprint recognition	9
2.1.3 Face recognition	11
2.1.4 Iris recognition	12
2.1.5 Performance of a biometric system	14

2.1.6	Biometric databases	16
2.2	What is quality?	18
2.2.1	Image quality	18
2.2.2	Biometric sample quality	19
3	Biometric sample quality assessment	21
3.1	Fingerprint quality assessment	22
3.1.1	Fingerprint ISO quality standard: ISO/IEC 29794-4 – In- information technology – Biometric sample quality – Part 4: Finger image data	22
3.1.2	Contact-based fingerprint quality assessment	23
3.1.3	Contactless fingerprint quality assessment	24
3.2	Face quality assessment	24
3.2.1	Face ISO quality standard: ISO/IEC 29794-5 – Informa- tion technology – Biometric sample quality – Part 5: Face image data	24
3.2.2	Face quality assessment methods	27
3.3	Iris quality assessment	27
3.3.1	Iris ISO quality standard: ISO/IEC 29794-6 – Information technology – Biometric sample quality – Part 6: Iris image data	27
3.3.2	NIR-based iris quality assessment	28
3.3.3	VW iris quality assessment	28
3.4	Performance evaluation of biometric sample quality assessment methods	29
3.5	Summary	29
4	A common framework for the assessment of multi-modality biometric image quality	31
4.1	Multi-modality biometric system	31

4.2	The proposed framework	32
4.3	Common image-based image attributes of multi-modality sample quality assessment for unconstrained biometric system	33
4.3.1	Previous classification of image-based attributes	33
4.3.2	Investigation of common image-based quality attributes	34
4.3.3	Classification of most important image-based attributes and their definitions	34
4.4	GC ² : A new multi-modality biometric image quality database	39
4.5	IQMs and their applications in biometrics	44
4.5.1	Introduction and classification of IQMs	44
4.5.2	A brief survey of no-reference IQMs	45
4.5.3	Fingerprint sample quality assessment using no-reference IQMs	46
4.5.4	Face sample quality assessment using no-reference IQMs	46
4.5.5	Iris sample quality assessment using no-reference IQMs	47
4.6	Summary	47
5	How image degradations influence the performance of fingerprint biometrics	49
5.1	Introduction	49
5.2	Experimental setup	50
5.2.1	Selection and implementation of fingerprint degradations	50
5.2.2	Fingerprint recognition system	51
5.2.3	Fingerprint database	53
5.2.4	Computation environment	53
5.3	Experimental results	53
5.3.1	Histogram of comparison scores	53
5.3.2	Distributive tendency of comparison score	53

5.3.3	DET curve	55
5.3.4	Equal Error Rate	57
5.3.5	Fingerprint image quality assessment and its evaluation	58
5.4	Summary	59
6	Contactless fingerprint image quality enhancement	63
6.1	Introduction	64
6.2	A review of existing contact-based fingerprint quality enhancement approaches	65
6.2.1	Method 1: fingerprint enhancement by directional Fourier filtering	65
6.2.2	Method 2: fingerprint enhancement by estimating local ridge orientation and frequency	67
6.2.3	Method 3: fingerprint enhancement by using filtering techniques	68
6.2.4	Method 4: knowledge based fingerprint enhancement	72
6.2.5	Method 5: fingerprint enhancement by using dyadic scale-space	74
6.2.6	Method 6: wavelet based fingerprint enhancement	75
6.2.7	Method 7: fingerprint enhancement by separable Gabor filter realization	76
6.2.8	Method 8: fingerprint enhancement by using short time Fourier transform analysis	77
6.2.9	Method 9: fingerprint enhancement by robust orientation field estimation	78
6.2.10	Method 10: fingerprint enhancement by orientation field estimation	80
6.3	Experiment of applying contact-based fingerprint enhancement methods on contactless fingerprint images	82
6.3.1	Comparing enhancement performance between three methods	82

6.3.2	Comparing computation speed between three methods . . .	83
6.4	An improved 3-step contactless fingerprint image enhancement method	85
6.4.1	Step 1: Color-grayscale fingerprint image enhancement . . .	86
6.4.2	Step 2: Fingerprint local ridge orientation and frequency estimation in high reliability area	86
6.4.3	Step 3: Prior knowledge based latent fingerprint orientation field estimation in low reliability area	89
6.4.4	Performance evaluation of proposed method	92
6.5	Summary	96
7	How color space affect the performance of biometric systems	97
7.1	Influence of color space for the performance of degraded face image recognition	97
7.1.1	Related works of color space for the face recognition . . .	98
7.1.2	Experimental setup	99
7.1.3	Experimental results	101
7.1.4	Discussion	105
7.1.5	Summary	106
7.2	Influence of color space for the performance of degraded visible wavelength iris image recognition	106
7.2.1	Related works of color space for the visible wavelength iris recognition	106
7.2.2	Experimental setup	107
7.2.3	Experimental results	109
7.2.4	Histogram of the comparison scores and the difference of their mean values	109
7.2.5	Summary	112
7.3	Conclusion	112

8	Performance evaluation of no-reference image quality metrics for face and iris biometric images	113
8.1	Introduction	114
8.2	Experimental setup	116
8.2.1	Database and biometric systems	116
8.2.2	No-reference IQMs and their classification	116
8.3	Experimental results for face modality	117
8.3.1	Histogram of the comparison scores and their mean values	117
8.3.2	DET curve and EER	120
8.3.3	Performance comparison between selected IQMs and ISO proposed IQMs	126
8.3.4	Re-training ILNIQE2 on face database	127
8.3.5	Discussion	132
8.3.6	Summary	135
8.4	Experimental results for iris modality	135
8.4.1	Histogram of the comparison scores and their mean values	135
8.4.2	DET curve and EER	137
8.4.3	Re-training ILNIQE2 on VW iris database	143
8.4.4	Summary	146
8.5	Conclusion	146
9	Conclusion	149
	Bibliography	172
	Appendix	172
A	Figures of histogram of the comparison scores and their mean values	173

- B Figures of DET curves with EER for comparison score with and without omitting low quality samples 181**
- C Figures of EER values with omitting low quality face samples one by one until the best quality sample left 189**

List of Tables

2.1	Biometric databases	16
3.1	Characterization of facial quality	25
5.1	EER of NBIS fingerprint system D2O	58
5.2	EER of NBIS fingerprint system D2D	58
5.3	Spearman’s rank correlation.	59
6.1	Average computation time per image for three enhancement methods	84
6.2	Average number of detected minutiae.	95
6.3	Fingerprint enhancement experiment protocol	95
6.4	Biometric system performance results over the private contactless fingerprint database	95
6.5	Computational costs of three methods	96
7.1	Color space experiment protocol for face modality	99
7.2	EER obtained from face recognition by using different color com- ponents. Values in red represents the lowest EER for the acquisi- tion devices.	105
7.3	Color space experiment protocol for iris modality	107

7.4	EER obtained from iris recognition by using different color components	111
8.1	Classification of the selected IQMs	116
8.2	Overview of the performance of selected IQMs for face modality .	126
8.3	Overview of the performance of selected IQMs for iris modality .	143

List of Figures

1.1	Overview of thesis structure and relation to the publications.	6
2.1	Identification schemes.	8
2.2	Examples of human characteristics that can be used as biometric traits for identification.	9
2.3	Flow chart of a fingerprint recognition system.	10
2.4	Example of fingerprint images from FVC2002 database.	10
2.5	Flow chart of a face recognition system.	12
2.6	A front-on view of the eye.	13
2.7	Flow chart of an iris recognition system.	14
2.8	An example of a DET curve and a ROC curve.	15
2.9	The reference model for distinguishing between character, fidelity, and utility.	20
4.1	Common framework for the assessment of multi-modality biometric image quality.	33
4.2	The image-based quality attributes tree generated from the commonly measured ones.	35
4.3	Simple Venn diagram with four folds.	36

4.4	An example of sample images from different modalities and cameras.	40
4.5	Degraded iris samples in all five levels.	41
4.6	Degraded face samples in all five levels.	42
5.1	Fingerprint image degradations in different levels.	52
5.2	The histogram of genuine comparison score for original and degraded fingerprints.	54
5.3	The histogram of genuine comparison score for original and degraded fingerprints.	54
5.4	The D2O distributive tendency plots for four degradations in five levels.	56
5.5	The D2D distributive tendency plots for four degradations in five levels.	56
5.6	DET curve for blur and JPEG degradations in five levels of the NBIS system (D2O).	57
5.7	The scatter plots of the NFIQ quality measurement values.	59
5.8	The histogram of the NFIQ quality assessment results for original fingerprints.	60
5.9	The histogram of the NFIQ quality assessment results for four degradations in five levels.	60
6.1	An example of fingerprint ridge ending and bifurcation.	64
6.2	An example of high quality fingerprint sample and low quality fingerprint sample.	64
6.3	Flow chart of the fingerprint enhancement method 1.	66
6.4	Experimental results from method 1.	67
6.5	The flowchart of core stages of fingerprint enhancement method 2.	68
6.6	Some experimental results from method 2.	69
6.7	Flowchart of the binarization-based method 3.1.	70
6.8	Experimental results of the binarization-based method 3.1.	70

6.9	Fingerprint enhancement results method 3.2.	71
6.10	Demonstration of rules for method 4.	73
6.11	Flowchart of fingerprint enhancement method 4.	74
6.12	An experimental result of fingerprint enhancement method 4.	74
6.13	Experimental results of fingerprint enhancement method 5.	75
6.14	An example of experimental result from fingerprint enhancement method 6.	76
6.15	The flowchart of the proposed method 8.	78
6.16	Experimental results from method 8.	79
6.17	An example of experimental result from method 9.	79
6.18	The flowchart of the proposed method 10.	81
6.19	Some experimental results from the method 10.	81
6.20	Examples of binary fingerprint obtained directly from segmented original fingerprints.	83
6.21	Enhancement results from reflex camera.	83
6.22	Enhancement results from smartphone.	84
6.23	Enhancement results from LFC	84
6.24	The framework of the proposed 3-step contactless fingerprint enhancement approach.	85
6.25	An example of the enhancement result after the first step.	87
6.26	An example of the enhancement result after the second step.	90
6.27	An example of the experimental result from the third step.	92
6.28	The comparison between three fingerprint enhancement methods.	93
6.29	Examples of the minutiae extraction results.	94
7.1	Comparison scores and the difference of their mean values from three cameras by using different color space components.	102
7.2	DET curves from three cameras by using different color space components.	104

7.3	Comparison score and the difference of their mean values from left and right eye for LFC.	109
7.4	Comparison score and the difference of their mean values from left and right eye for smartphone.	110
7.5	Comparison score and the difference of their mean values from left and right eye for reflex camera.	110
8.1	Comparison scores and their mean values for GF+KFA recognition algorithm for the three cameras.	118
8.2	Examples of comparison scores and their mean values with omitting low quality samples.	119
8.3	Tendency of mean comparison scores with omitting low quality samples.	121
8.4	Examples of DET curves with EER for score with and without omitting low quality samples.	122
8.5	Tendency of EER values with and without omitting low quality samples.	124
8.6	Examples of EER values with omitting low quality face samples one by one.	125
8.7	DET curves with EER for LFC by using ISO proposed IQMs.	127
8.8	EER values for reflex camera by using ISO proposed IQMs.	128
8.9	Comparison of EER between original and re-trained method.	129
8.10	Comparison of EER for each distortion.	130
8.11	Comparison of ERC between original and re-trained method.	131
8.12	Examples of comparison scores and their mean values with omitting low quality samples.	136
8.13	Tendency of mean comparison scores with omitting low quality samples.	138
8.14	Examples of DET curves with EER for score with and without omitting low quality samples.	139

8.15	Tendency of EER values with and without omitting low quality samples.	140
8.16	Examples of EER values with omitting low quality iris samples one by one.	141
8.17	Examples of EER values with omitting low quality iris samples one by one.	142
8.18	Examples of EER values with omitting low quality iris samples one by one.	142
8.19	Comparison of EER between original and re-trained method. . . .	144
8.20	Comparison of ERC between original and re-trained method. . . .	145
A.1	Comparison scores and their mean values with omitting low quality face samples for LFC.	174
A.2	Comparison scores and their mean values with omitting low quality face samples for smartphone.	175
A.3	Comparison scores and their mean values with omitting low quality face samples for reflex camera.	176
A.4	Comparison scores and their mean values with omitting low quality iris samples for LFC.	177
A.5	Comparison scores and their mean values with omitting low quality iris samples for smartphone.	178
A.6	Comparison scores and their mean values with omitting low quality iris samples for reflex camera.	179
B.1	DET curves with EER for comparison score with and without omitting low quality face samples for LFC.	182
B.2	DET curves with EER for comparison score with and without omitting low quality face samples for smartphone.	183
B.3	DET curves with EER for comparison score with and without omitting low quality face samples for reflex.	184
B.4	DET curves with EER for comparison score with and without omitting low quality iris samples for LFC.	185

B.5	DET curves with EER for comparison score with and without omitting low quality iris samples for smartphone.	186
B.6	DET curves with EER for comparison score with and without omitting low quality iris samples for reflex.	187
C.1	EER with omitting low quality samples one by one until the best quality face sample left for LFC.	190
C.2	EER with omitting low quality samples one by one until the best quality face sample left for smartphone.	191
C.3	EER with omitting low quality samples one by one until the best quality face sample left for reflex camera.	192
C.4	EER with omitting low quality samples one by one until the best quality iris sample left for LFC.	193
C.5	EER with omitting low quality samples one by one until the best quality iris sample left for smartphone.	194
C.6	EER with omitting low quality samples one by one until the best quality iris sample left for reflex camera.	195

Abbreviations

DET Detection Error Tradeoff

DPI Dots Per Inch

EER Equal Error Rate

ERC Error versus Reject Curves

FMR False Match Rate

FNMR False Non-Match Rate

GF Gabor Filtering

GMR Genuine Match Rate

IQMs Image Quality Metrics

KFA Kernel Fisher Analysis

LFC Light Field Camera

MVG MultiVariate Gaussian

NBIS National Institute of Standards and Technology Biometric Image Software

NFIQ National Institute of Standards and Technology Fingerprint Image Quality

NIR Near InfraRed

NIST National Institute of Standards and Technology

NSS Natural Scene Statistics

PC Phase Congruency

ROC Receiver Operating Characteristic

VW Visible Wavelength

Chapter 1

Introduction

In an increasingly digital world, verifying users' identities when accessing a remote service (payment, social networks, border control) becomes a key issue. In this context, biometric recognition appears as the only security technique of user identity verification. Password based techniques or use of a smart card will always carry a risk on the verification [1]. The quality of a biometric sample is one of the main criteria having a direct influence on the overall performance of a biometric recognition system [2]. Poor quality samples will have a direct negative affect to the enrollment, which will lead to a decrease in system performance. Therefore, without quality assessment, it is illusory to develop a reliable and robust recognition system. There are many existing researches focusing on biometric sample quality assessment, but different evaluation approaches measure different quality attributes and most of them focus on measuring modality-based attributes. Meanwhile, different biometric modalities seem to be isolated from each other in the image quality evaluation process. In this Ph.D research, we investigate image-based multi-modality quality assessment for unconstrained biometric samples. The novelty of this research is that, the selected appropriate image-based quality attributes will be applied to the quality assessment in three biometric modalities: contactless fingerprint, visible wavelength iris, and face. In addition, we evaluate the performance of selected no-reference [Image Quality Metrics \(IQMs\)](#) on unconstrained biometric samples. Based on the evaluation results, we optimize the [IQMs](#) that have better performance for multi-modality samples. As a result, an optimized biometric sample quality assessment method is presented, which can be used for multi-modality biometric samples.

1.1 Motivation

Biometric recognition is a mature technology used in many government and civilian applications such as e-passports, ID cards, and border control [1]. However, during the past several years, biometric sample quality assessment became a significant issue because of biometric systems' poor performance on degraded samples [2]. Studies and benchmarks have shown that biometric sample quality have a direct influence on the overall performance of a biometric recognition system [2, 3]. Indeed, the recognition of the person cannot be ensured with a high level of accuracy when using a poor quality biometric sample (fingerprint, face, iris, etc.). For example, a too dark or too fuzzy or too noisy sample image may require an extra processing step (e.g. image enhancement) to be able to identify the sample in the system. The biometric sample quality assessment issue has nevertheless received little research attention compared to the primary feature-extraction and pattern-recognition tasks.

Generally, the biometric data is obtained from a sensor that can generate an image. However, because of changes in physical characteristics of human beings (glasses, scars, etc.), the acquisition environment (indoor, outdoor, etc.) and existing hardware solutions, image degradations that have been introduced during the acquisition process can affect the system performance. So, ensuring strict quality control of the acquired data is an essential process in the development of an efficient biometric recognition system.

Many techniques have been proposed in literature to assess the quality of a biometric sample that is affected by different degradations. Samples from different modalities usually have their own modality-specific degradation (e.g. scars in fingerprint image or eyes closed in face image) so that the most commonly way to measure sample quality is to use modality-based image quality metrics. However, metrics that can evaluate multi-modality biometric sample quality are rarely considered [4]. The link of sample quality evaluation between different modalities can be established by using image-based quality metrics, which are able to assess image-based quality attributes (e.g. illuminant, sharpness). This could be the solution of developing multi-modality biometric sample quality assessment approaches especially when the data are captured under unconstrained environment by using low-cost devices.

1.2 Aims and research questions

In order to overcome the challenges mentioned in the motivation section, the main objective of this Ph.D research is to investigate the common image-based multi-modality biometric sample quality assessment framework. Based on this frame-

work, we select the most important image-based quality attributes for the assessment of multi-modality biometric samples. Based on the selected attributes we evaluate the performance of existing no-reference IQMs on unconstrained multi-modality biometric samples. The evaluation results can assist us to further optimize appropriate no-reference IQMs. Finally, the optimized metric can be used for the quality assessment for unconstrained multi-modality biometric samples.

Regarding to the objectives mentioned above, we can formulate the following research questions:

1. How to design a common framework to assess the quality of multi-modality biometric image samples?
2. What are the most important image-based quality attributes in the common framework?
3. How to use no-reference IQMs to assess the quality of multi-modality biometric image samples, and what is their performance?
4. How to optimize the no-reference IQMs in order to improve their performance on multi-modality biometric image samples?

1.3 Publications

The current study has led to the publication of several papers in international and national peer-reviewed conferences. One article has also published in an international journal. The relations between the publications and the thesis can be seen in Figure 1.1. Listed below are the main publications.

Journal publication

- Article G** Xinwei Liu, Marius Pedersen, Christophe Charrier, Patrick Bours,
[5] "Performance evaluation of no-reference image quality metrics for face biometric images," Journal of Electronic Imaging 27(2), 023001 (2018), DOI: 10.1117/1.JEI.27.2.023001.

International conference publications

- Article A** Xinwei, Liu, Pedersen Marius, and Charrier Christophe. "Image-based attributes of multi-modality image quality for contactless biometric samples." In *3rd International Conference on Signal Processing and Integrated Networks (SPIN)*. pp. 106-111, Noida, India, Feb. 2016.
[6]
- Article B** Liu, Xinwei, Marius Pedersen, Christophe Charrier, Patrick Bours, and Christoph Busch. "The influence of fingerprint image degradations on the performance of biometric system and quality assessment." In *Biometrics Special Interest Group (BIOSIG), 2016 International Conference of the*, pp. 1-6. IEEE, Darmstadt, Germany, Sep. 2016.
[7]
- Article C** Liu, Xinwei, Marius Pedersen, Christophe Charrier, Faouzi Alaya Cheikh, and Patrick Bours. "An improved 3-step contactless fingerprint image enhancement approach for minutiae detection." In *Visual Information Processing (EUVIP), 6th European Workshop on*, pp. 1-6. IEEE, Marseille, France, Oct. 2016.
[8]
- Article E** Liu, Xinwei, Christophe Charrier, Marius Pedersen, and Patrick Bours. "Study on color space for the performance of degraded face image recognition." *Electronic Imaging 2018*. pp. 1-5, Burlingame, United States, Jan. 2018.
[9]
- Article F** Liu, Xinwei, Marius Pedersen, Christophe Charrier, and Patrick Bours. "Can no-reference image quality metrics assess visible wavelength iris sample quality?." In *IEEE International Conference on Image Processing*. pp. 1-6, Beijing, China, Sep. 2017.
[10]

National conference publications

- Article D** Liu, Xinwei, Christophe Charrier, Marius Pedersen, and Patrick Bours. "Study on color space for the performance of degraded visible wavelength iris recognition." In *Compression and Representation of Audiovisual Signals*. pp. 1-5, Caen, France. Oct. 2017.
[11]

Supporting publications

- Article H** [12] Liu, Xinwei, Christophe Charrier, Marius Pedersen, and Patrick Bours. "Performance Evaluation of No-Reference Image Quality Metrics for Visible Wavelength Iris Biometric Images." In *26th European Signal Processing Conference (EUSIPCO 2018)*. Rome, Italy. Sep. 2018.
- Article I** [13] Liu, Xinwei, Marius Pedersen, Christophe Charrier, and Patrick Bours. "Can image quality enhancement methods improve the performance of biometric systems for degraded face images?." In *The 9th Colour and Visual Computing Symposium 2018 (CVCS 2018)*. Gjøvik, Norway. Sep. 2018.

1.4 Thesis outline

An overview of the thesis outline is shown in Figure 1.1 on the next page, linking chapters and the publications listed in Section 1.3. This thesis is intended to provide the reader with the understanding required to use no-reference IQMs to assess the quality of unconstrained multi-modality biometric sample images. The thesis is structured into 9 chapters to guide the reader through the different topics of the thesis. Chapters 1 and 2 introduce important background knowledge to the reader. Chapter 3 illustrates the state-of-the-art issues in the biometric sample quality assessment field. A common framework for the assessment of multi-modality biometric sample quality is proposed in Chapter 4, to give an in-depth introduction to the core of this thesis. Chapter 5 investigates how different image degradations affect the performance of a fingerprint recognition system and fingerprint image quality assessment method. In Chapter 6, we develop a contactless fingerprint enhancement method in order to adapt contactless fingerprint to the traditional contact-based recognition systems. Based on the experimental results from Chapter 6, we decided to only investigate face and visible wavelength iris modalities in the following chapters. In Chapter 7, we conduct experiments to know how color spaces affect the performance of biometric systems. Then, we evaluate the performance of no-reference IQMs on unconstrained biometric samples for face and visible wavelength iris modalities in Chapters 8. Finally, the conclusions are given in Chapter 9.

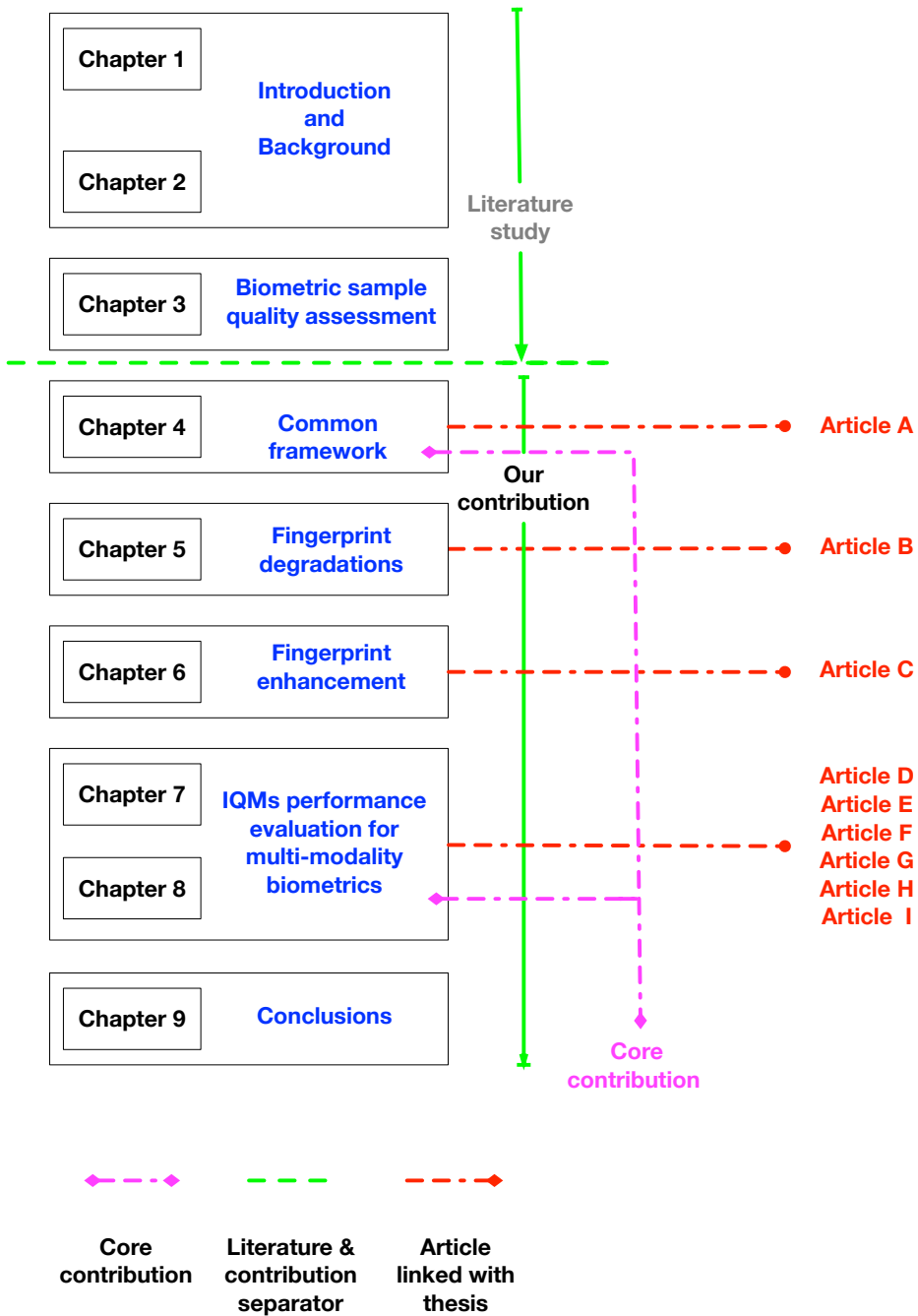


Figure 1.1: Overview of thesis structure and relation to the publications.

Chapter 2

Background

2.1 What is biometrics?

In this section, we introduce what is biometrics and fingerprint, face, and iris recognition. We also have an overview of biometric databases.

2.1.1 Biometrics

The early biometric application can be traced back to 1891 when Juan Vucetich, who was an Argentine police official, started a collection of fingerprints of criminals [14]. The first literature that discussed biometrics was "Finger Print", published by Francis Galton in 1892 [15]. Then, the question is: what is biometrics? There are several definitions for biometrics: Ross *et al.* [1] introduced biometrics as the science of establishing the identity of an individual based on the physical, chemical or behavioral attributes of the person; Jain *et al.* [16] indicated any human physiological or behavioral characteristic could be a biometrics provided it has four desirable properties: 1) universality, 2) uniqueness, 3) permanence, and 4) collectability; ISO/IEC standard 2382-37, Information Technology – Vocabulary – Part 37 : Biometrics [17] defined the term 'biometrics' is automated recognition of individuals based on their biological and behavioral characteristics. In recent modern society, the need for large-scale identity applications strengthen the link between biometrics and our daily life. Such biometric systems require a high level of accuracy for the identification of an individual in the context of other systems.

The aim of a biometric identity application is to verify if an individual's identity is who he or she claims to be. It can prevent impostors from accessing protected resources. We are still using many traditional approaches that set up an individual's identity that include knowledge-based (e.g. passwords) and token-based

(e.g. ID cards) mechanisms. However, these established identities can be lost, shared, manipulated or stolen thereby compromising the intended security. Under this premise, biometrics provides a natural and reliable way to perform individual recognition based on their biological characteristics [18]. The use of biometrics in identification tasks can change the inquire to 'Who you are?' instead of 'What do you possess?' (such as an ID card) or 'What do you remember?' (such as a password). Figure 2.1 shows examples of traditional and biometric-based methods in identification schemes.

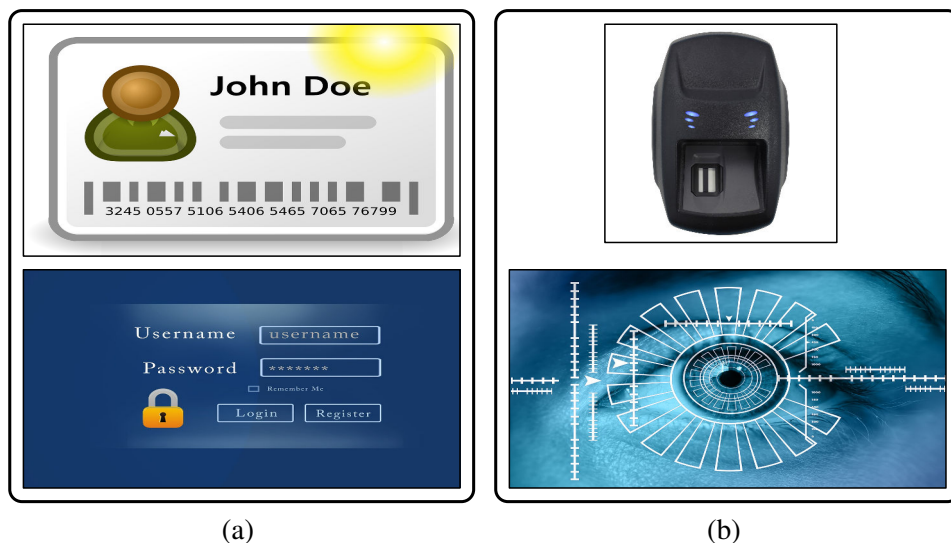


Figure 2.1: Identification schemes. (a) represents the traditional schemes use ID cards or passwords to recognize an individual. (b) represents the biometric-based schemes uses fingerprint or iris to verify an individual. Figures reproduced from <https://pixabay.com>, visited 05/03/2018.

Compared to the biometric-based identification, the traditional applications have many drawbacks that make the system to be easily attacked. O’Gorman [19] illustrated six possible attacks if the traditional identification methods are used: 1) client attack (e.g. guessing passwords); 2) host attack (e.g. accessing plain text file containing passwords); 3) eavesdropping (e.g. ‘shoulder surfing’ for passwords); 4) repudiation (e.g. claiming lost of token); 5) Trojan horse attack (e.g. deleting data from computer); 6) denial of service (e.g. disabling the system by deliberately supplying an incorrect password several times). However, for example, password has a higher key-space than most other authenticators, and token provides compromise detection since its absence is observable [19]. On the other hand, biometrics provide some strengths that can’t be given by traditional methods, for example, negative recognition and non-repudiation [20]. But biometrics may have

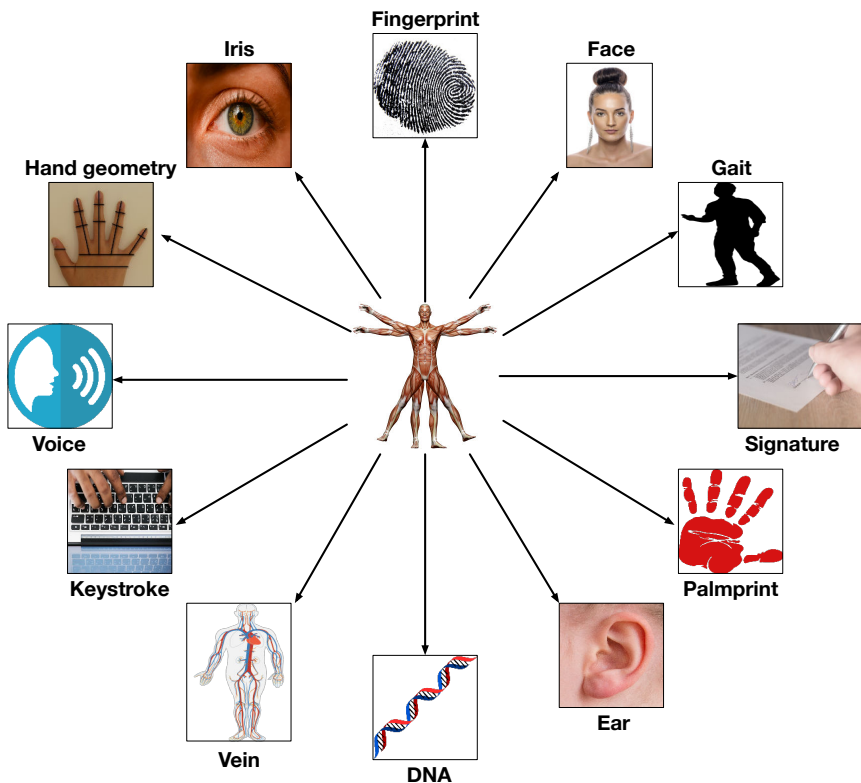


Figure 2.2: Examples of human characteristics that can be used as biometric traits for identification. Figures reproduced from <https://pixabay.com>, visited 05/03/2018.

user privacy issues.

Biometric systems use a number of physical or behavioral characteristics, such as fingerprint, face, iris, hand geometry, retina, signature, gait, palmprint, or voice (see Figure 2.2) [21]. These characteristics are also referred to as traits or most commonly called biometric modalities. Biometric systems have their own problems (e.g. privacy issues) [22], but biometric systems do increase user convenience by alleviating the need to design and remember passwords [18].

2.1.2 Fingerprint recognition

A fingerprint in its narrow sense is an impression left by the friction ridges of a human finger. In biometrics, a fingerprint consists of a pattern of interleaved ridges and valleys from the epidermis of a finger [23]. One of the important approaches of forensic science is the rehabilitation of fingerprint from a crime scene. Fingerprints are easily deposited on suitable surfaces (such as glass or metal or

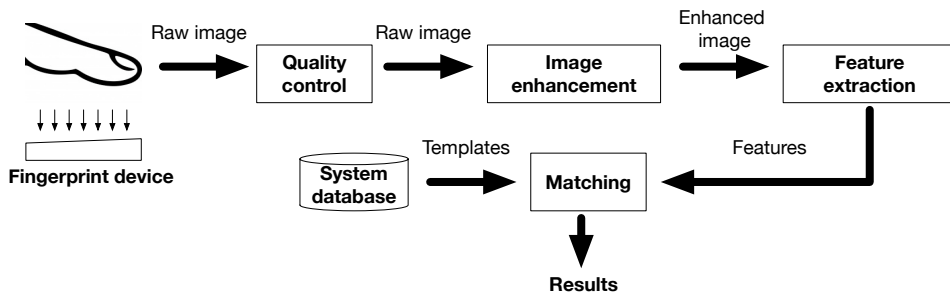


Figure 2.3: Flow chart of a fingerprint recognition system. Reproduction inspired by Maltoni *et al.* [23].

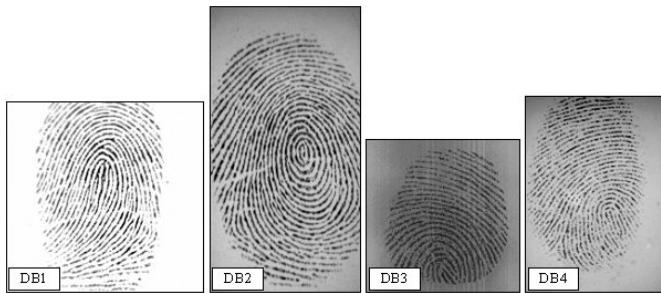


Figure 2.4: Example of fingerprint images from FVC2002 database [25].

polished stone) by the natural secretions of sweat from the eccrine glands that are present in epidermal ridges. Human fingerprints are detailed, nearly unique, difficult to change, and durable over the life of an individual, making them suitable as long-term markers of human identity [23]. Thus, police or other authorities can use fingerprints to identify individuals for different purposes. Since the early 20th century, the police started to analyze fingerprints and it has led to many crimes being solved [24]. Automatic fingerprint recognition technology has now rapidly grown beyond forensic applications and into civilian applications. Together with face, fingerprint is one of the main biometric modalities for electronic documents (e-passport, visas, ID cards, etc) used to enforce border control and security. In addition, due to the development of fingerprint recognition technologies, the fingerprint-based biometric systems are becoming popular by using low-cost acquisition devices, such as smartphone and webcam.

The flow chart of a fingerprint recognition system is illustrated in Figure 2.3. In general, a fingerprint recognition system has four modules: quality control, image enhancement, feature extraction, and matching. Firstly, a fingerprint is captured by a sensor, which acquires a digital fingerprint sample image. The common fin-

gerprint devices have a 500 **Dots Per Inch (DPI)** and produce an 8-bit grayscale raw fingerprint image (see Figure 2.4). A quality control procedure is then applied to the captured raw fingerprint image in order to ensure whether the quality of the fingerprint image meets the requirement of feature extraction. In case the quality is not good enough, either the acquisition process has to be re-conducted, or the system enhance the quality of the image. The image enhancement procedure aims to improve the clarity of the ridge pattern, especially in noisy regions, to simplify the subsequent feature extraction. During this procedure, a commonly used special filtering technique called contextual filtering [23] is used. The re-captured or enhanced fingerprint image is then passed to the feature extraction module. The extracted feature set usually contains minutiae. Nevertheless, depending on the used matching algorithm, other features (e.g. local orientation, local frequency, singularities, ridge shapes, ridge counts, parts of the enhanced image, etc.) can be extracted along with (or replace with) minutiae. Finally, the feature set extracted from the current fingerprint sample is compared with one or more templates retrieved from a system database at the matching module. Most of the matching algorithms compare two fingerprints by searching the spatial correspondence of a minimum number of minutiae which is following the well-established manual method. The comparison is a challenging issue due to large variations (e.g. displacement, rotation, skin condition, distortion, noise, etc.) that can characterize two fingerprint images acquired from the same finger at different times. There are two modes of matching: verification and identification. In the verification mode, the system only retrieves one fingerprint template from the database and compares with the current sample since the user has been required to claim his identity. However, the current sample is compared with all the templates from the database to identify who the user is. For more introduction, we refer the reader to Maltoni *et al.* [23].

2.1.3 Face recognition

Face recognition is a task that humans perform routinely and effortlessly in our daily lives [26]. Besides being natural and nonintrusive, face recognition has a very important advantage that it can be acquired from a distance to the individual and in a covert manner, compared to contact-based traditional fingerprint recognition. Face recognition has become increasingly important owing to rapid advances in imaging devices (surveillance cameras, camera in smartphones), availability of huge amounts of face images on the internet, and increased demands for higher security. The history of automatic face recognition dates back to 1970, when Michael David Kelly developed the first face recognition system in his thesis [27]. There was a dormant period in automatic face recognition until the work by Sirovich and Kirby [28] on a low dimensional face representation.

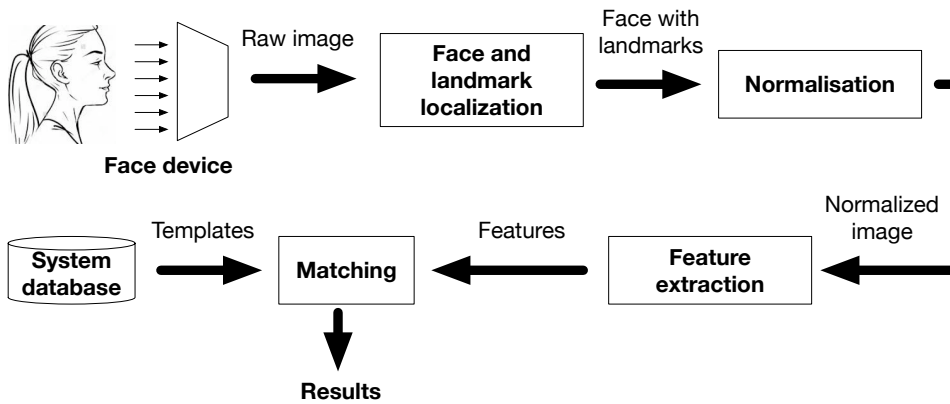


Figure 2.5: Flow chart of a face recognition system. Reproduction inspired by Jain *et al.* [26].

The commonly used face recognition application is based on two-dimensional face sample images. However, three-dimensional (depth or range) face images or multi-spectrum face images can improve the level of security of the application. An automatic face recognition system generally has four modules: face localization, normalization, feature extraction, and matching, as shown in Figure 2.5. Face localization separates the face region from the background. It also gives a coarse estimate of the face location and scale. Facial landmarks, such as eyes, nose, mouth, and facial outline, are also localized in this stage. Then, face normalization is conducted to normalize the face geometrically and photometrically. The face has to be cropped, warped, or morphed in order to be transformed into a standard frame for geometrical normalization. The photometric normalization process normalizes the face based on properties (e.g. illumination and gray scale). Face feature extraction is performed on the normalized face to extract salient information that is useful for distinguishing faces of different persons and is robust with respect to the geometric and photometric variations. The extracted face features are used for face matching. Finally, the matching module conducts the comparison between current face features and the template from the system database. For more introduction, we refer the reader to Jain *et al.* [26].

2.1.4 Iris recognition

The iris is a thin, circular structure in the eye, responsible for controlling the diameter and size of the pupil and thus the amount of light reaching the retina. Eye color is defined by the color of the iris. In optical terms, the pupil is the eye's aperture, while the iris is the diaphragm [29]. A front-on view of the eye region in-

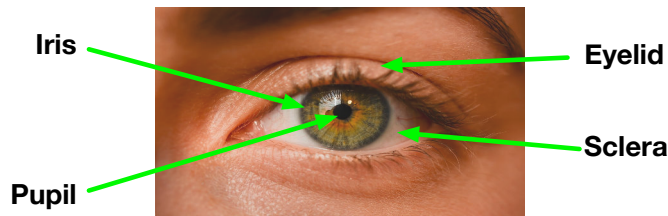


Figure 2.6: A front-on view of the eye. Figure reproduced from <https://pixabay.com>, visited 05/03/2018.

cludes the iris as illustrated in Figure 2.6. The iris has an unique epigenetic pattern that remains stable throughout adult life and it is an externally protected organ [30]. Using iris to identify individuals in biometrics benefits from the iris characteristics. Features can be extracted from the captured iris sample image by using image processing methods. The features are used to generate a template, which is an objective mathematical representation of the unique information stored in the iris, is then saved in a database. Similar to fingerprint recognition, if an individual uses an iris recognition system for identification, the extracted features from the current iris image are compared to other templates in the system database. The first, most successful, and best known automatic iris recognition system, was implemented by John Daugman, who was a scientific researcher at Cambridge in the early 19th century [31].

The flow chart of an iris recognition system is illustrated in Figure 2.7. In general, an iris recognition system has four modules: segmentation, normalization, feature extraction and encoding, and matching. The first module of iris recognition is to segment the iris region from the eye image. There are approximately two circles in the iris region: the first circle is the boundary between pupil and iris, and the second circle is the boundary between iris and sclera (see Figure 2.6). The eyelids and eyelashes are also necessary to segment because they can occlude the upper and lower area of the iris region. In addition, the specular reflections caused by the illumination can sometimes corrupt the iris pattern within the iris region. Therefore, they also need to be isolated. The segmentation stage is used for the exclusion of above mentioned occlusions in the iris region, meanwhile, locating the circular iris region. In the next module, the transformation is applied to the segmented iris region in order to have fixed dimensions for further use. In general, iris can be stretched in eye images because of pupil dilation from different levels of illumination and it causes the dimensional inconsistencies. Moreover, the distance between the device and the individual, device position, and head tilt can also be sources of inconsistency. In order to overcome these issues, the normalization module is used to keep iris regions, which may under different acquisition condi-

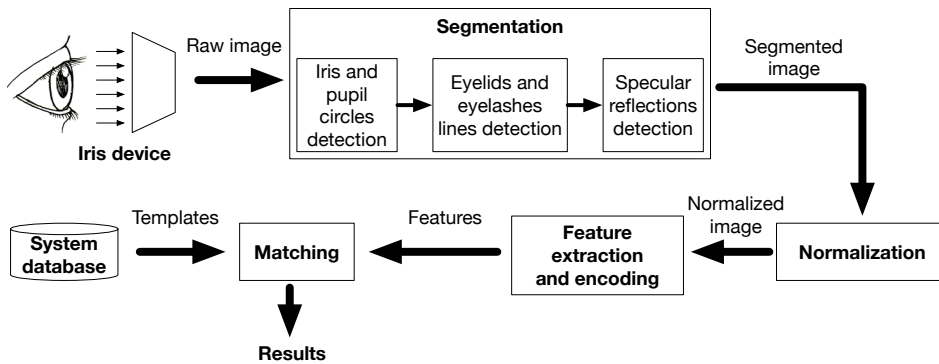


Figure 2.7: Flow chart of an iris recognition system. Reproduction inspired by Daugman [31].

tions, to have constant dimensions and characteristic features at the same spatial location. In the iris feature extraction module, the discriminating features in an iris pattern are extracted. The extracted significant features are then encoded for the matching process. The commonly used approach for template creation is band pass decomposition [31]. Finally, the matching stage conducts the comparison between current encoded iris features and the template from the system database. For more introduction, we refer the reader to Daugman [31].

2.1.5 Performance of a biometric system

An individual's identity can be easily validated if the current input password matches the password stored in the database. However, it is impossible to have two biometric sample images exactly the same, which are captured under different conditions and at different time. This can be explained by having variations in the biometric samples. There are two kinds of variability that can be found in the biometric feature set: intra-class variation and inter-class variation [32]. The variability in feature sets from the same individual is intra-class variation, and the variability in feature sets from different individuals is inter-class variation. The intra-class variation can be explained by having sensing condition issues (e.g. noise of the biometric acquisition device); the issues of changed individual's biometric characteristic (e.g. scars on fingerprint); the issues of changed environment (e.g. different lighting angles in face recognition); and individual-device interaction issues (e.g. closed eyes or partial fingerprints). Thus, two feature sets originating from the same biometric trait of a user are never exactly the same. A useful feature set should present small intra-class variation and large inter-class variation [32].

A similarity score represents the similarity between two biometric feature sets. If

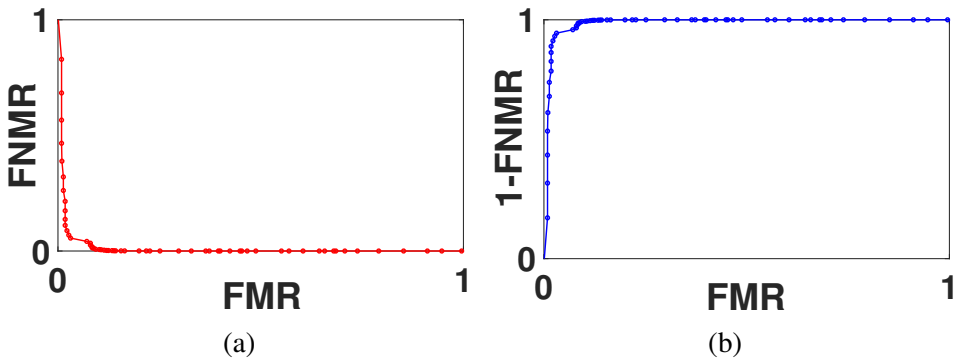


Figure 2.8: An example of a DET curve and a ROC curve. (a) represents the DET curve. (b) represents the ROC curve.

the comparison is conducted between two biometric samples from the same biometric trait, the similarity score is called genuine score. On the other hand, if the comparison is conducted between two biometric samples from two different biometric traits, the similarity score is then called imposter score. In general, genuine score should be higher than the imposter score. A biometric system makes a decision by comparing the comparison score to a threshold. Such threshold is the point at which it becomes reasonably certain that a biometric sample matches a particular reference template. When a genuine score is lower than a threshold τ , a false non-match decision is made. When an imposter score is higher than the threshold τ , a false match decision is made. The False Non-Match Rate (FNMR) of a biometric system can be given as the probability that the system fails to detect a match between the input sample and a template from the same individual in the database. It measures the percentage of valid inputs that are incorrectly rejected [32]. Similarly, the False Match Rate (FMR) of a system may be given as the probability that the system incorrectly matches the input sample to a template from different individuals in the database [32]. It measures the percentage of invalid inputs that are incorrectly accepted. Although the FNMR and the FMR values are affected by the threshold τ , it is impossible to decrease both FNMR and FMR at the same time for a certain biometric system. A Detection Error Tradeoff (DET) curve [33] that plots the FNMR against the FMR at different threshold τ on a normal deviate scale and interpolates between these points is usually (see Figure 2.8 (a)) used to reflect the system performance. A Receiver Operating Characteristic (ROC) curve shows FMR against Genuine Match Rate (GMR). $GMR=1-FNMR$ (see Figure 2.8 (b)). The main difference between the DET curve and the ROC curve is that they are vertically mirrored. Another commonly used indicator to represent the performance of a biometric system is Equal Error Rate (EER), which

is a single-valued representation. **EER** can be found when the **FNMR** and **FMR** are the same [32]. The lower the **EER** value the better the biometric system performance.

An important aspect that needs to be considered is that the **FNMR** and **FMR** are not evenly distributed between different individuals in a biometric system. There are inherent differences in the 'recognizability' of different users [32]. Dodding-ton *et al.* [34] proposed to categorize individuals into four groups (sheep, goats, lambs, and wolves) based on their inherent differences. This categorization also called 'Dodding-ton's zoo' was used for speaker recognition, nevertheless, it is still valuable for other biometric modalities.

2.1.6 Biometric databases

Many biometric recognition systems claim that they have an excellent performance according to the test results. However, many of the test data they used to make such demonstration are usually not publicly available [35]. This issue motivate the development of biometric databases that can be publicly available for research purposes. Biometric databases are used for the evaluation of the performance of biometric systems. They can be either single modality databases which contain only one biometric modality, or multi-modality databases which collect several modalities. There are many existing single modality databases, however, the number of multi-modality biometric image databases is limited. We briefly introduce some commonly used single modality and multi-modality biometric databases in this section. Table 2.1 gives an overview of relevant databases based on the available detailed information from their origin.

Table 2.1: Biometric databases

Single modality databases	
Fingerprint databases	
Name	Description
FVC databases [23]	There are four versions of FVC databases: FVC2000, FVC2002, FVC2004, and FVC2006. FVC2006 contains four distinct databases, and each database is 150 fingers wide and 12 samples per finger in depth (e.g. it consists of 1800 fingerprint images). More details can be found at http://bias.csr.unibo.it/fvc2000(or 2002, 2004, 2006)/databases.asp .

NIST 8-Bit grayscale database [36]	It contains 2000 8-bit gray scale fingerprint image pairs. Each image is 512-by-512 pixels with 32 rows of white space at the bottom. 400 fingerprint pairs from each of the five classifications (Arch, Left and Right Loops, Tented Arch, and Whirl). Each of the fingerprint pairs are two completely different rollings of the same fingerprint and 19.7 pixels per millimeter resolution.
MCYT database [37]	The fingerprint portion of the MCYT database contains 79200 fingerprint images collected from 330 subjects with two sensors (one optical and one capacitive, 12 impressions per finger, all 10 fingers per subject). A subset of 24000 images (all images from 100 subjects) is freely available. The full dataset is available by license.
Face databases	
Yale database B [38]	The database contains 5760 single light source images of 10 subjects each seen under 576 viewing conditions (9 poses x 64 illumination conditions). For every subject in a particular pose, an image with ambient (background) illumination was also captured. Hence, the total number of images is in fact $5760+90=5850$.
AT & T database [39]	There are ten different images of each of 40 subjects. For some subjects, the images were taken at different times, varying the lighting, facial expressions and facial details (glasses / no glasses). All the images were taken against a dark homogeneous background with the subjects in an upright, frontal position.
FERET database [40]	The FERET database was collected in 15 sessions. It contains 1564 sets of images for a total of 14,126 images that includes 1199 individuals and 365 duplicate sets of images.
AR database [41]	It contains over 4,000 color images corresponding to 126 people's faces (70 men and 56 women). Images feature frontal view faces with different facial expressions, illumination conditions, and occlusions. The pictures were taken under strictly controlled conditions. No restrictions on wear, make-up, hair style, etc. were imposed to participants.

Iris databases	
CASIA databases [42]	There are four versions of CASIA iris database (1.0, 2.0, 3.0, and 4.0). The latest version 4.0 contains a total of 54601 iris images from more than 1800 genuine subjects and 1000 virtual subjects. All iris images are 8 bit gray-level JPEG files, collected under near infrared illumination or synthesized.
UBIRIS databases [43, 44]	The first version of the UBIRIS database is composed of 1877 images collected from 241 persons. The second version has over 11 000 images and more realistic noise factors.
UTIRIS database [45]	It has two datasets: Visible Wavelength (VW) iris data and Near InfraRed (NIR) iris data. The database is constructed with 1540 images from 79 individuals from both right and left eyes demonstrated in 158 classes in total.
Multi-modality databases	
Name	Modalities
MyIdea database [46]	Fingerprint, Video Face, Voice, Signature, Palm print
MCYT database [47]	Fingerprint, Signature
BIOMET database [48]	Face, Audio, Face infrared, Hand, Fingerprint, 3D Face
WVU database [49]	Iris, Fingerprint, Palm, Hand, Voice, Face

2.2 What is quality?

In this section, we introduce what is image quality and what is biometric sample quality.

2.2.1 Image quality

Research on image quality has a long history. The concept of image quality originated in the optical field. Optics, as a science and technology, dates back to about 1200 B.C. with the invention of curved mirrors. In the 20th century, the pace of development of television and digital imaging technologies had a significant speed-up. Image quality has never been the top level design criteria during the early stage of research in the imaging technology history. The image quality became popular when the television and digital imaging started to be investigated. The topic which discussed the rendering of tones that comprise the image was the first research topic about image quality followed by the spatial structure or the image details. Finally, the research focuses have moved to the color image quality. Image quality

has several definitions given in the research field that have been widely accepted: Engeldrum [50] defined image quality as the integrated set of perceptions of the overall degree of excellence of the image. Janssen [51] suggested the quality of an image is the adequacy of this image as input to visual perception, and the adequacy of an image as input to visual perception is given by the discriminability and identifiability of the items depicted in the image.

2.2.2 Biometric sample quality

Generally, a biometric sample is of good quality if it is suitable for personal recognition [2]. The term 'quality' is used to describe several different aspects of a biometric sample that contribute to the overall performance of a biometric system. For the purposes of standardization, the recent standardization efforts (ISO/IEC 29794-1 Information technology – Biometric sample quality – Part 1: Framework [52]) have defined terms, and a reference model for distinguishing between these different aspects of quality, illustrated in Figure 2.9. Depending on context, three prevalent uses are to subjectively reflect [52]:

- the **character** of a sample. It is an expression of quality based on the inherent features of the source from which the biometric sample is acquired. For instance, a fragmentary fingerprint has poor character;
- the **fidelity** of a sample to the source from which it is acquired. It is an expression of quality, which is based on the fidelity that reflects the degree of its similarity to its source. Biometric sample fidelity is comprised of fidelity components contributed by different processes;
- the **utility** of a sample within a biometric system. It is an expression of quality based on utility reflects the predicted positive or negative contribution of an individual biometric sample to the overall performance of a biometric system. Both character and fidelity can influence utility-based biometric sample quality.

The term 'quality' should not only represents the captured attributes of the biometric sample, for instance, image brightness, sharpness, resolution, or contrast. These quality attributes may influence biometric sample utility and could affect the quality evaluation results and biometric system performance. The 'quality' should be an indicator of the biometric system performance. Furthermore, 'quality' is related to one biometric sample but system performance is related to the full biometric system, which is an issue that makes the evaluation not straightforward and difficult.

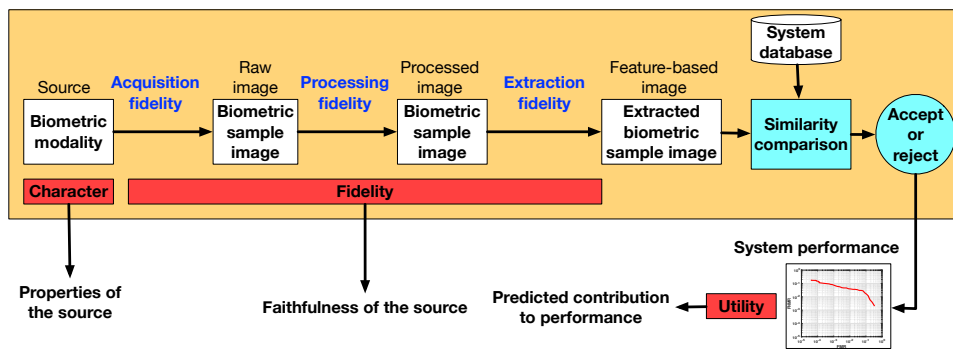


Figure 2.9: The reference model for distinguishing between character, fidelity, and utility. Reproduction inspired by Alonso *et al.* [2].

Chapter 3

Biometric sample quality assessment

The continuous studies of biometrics noted the significance of sample quality for a recognition system or a comparison algorithm because the performance of the biometric system is mainly dependent on the quality of the sample image. Over the last decade, researchers developed plenty of biometric sample quality assessment algorithms mainly for fingerprints [53, 54, 55, 56, 57, 58, 59], irises [60, 61, 62, 63, 64, 65], faces [66, 67, 68, 69, 70, 71]. The most important functionality we expect is that a quality measurement method can achieve is to predict the sample's utility. In response to this, samples that have higher image quality are able to result in better recognition or verification performance. Unfortunately, the standardizations and methodologies [72, 73, 74] for biometric sample quality evaluation have only recently formalized means that most of the sample quality assessment approaches have been developed and tested under limited, heterogeneous frameworks [2]. In the same words, not every recognition method uses the same quality attributes for processing, and different attributes may influence their performance. For instance, an iris recognition method named *Ic1* is sensitive to the iris distance to the camera, whereas recognition method *Ic2* is insensitive to such changes. In this case, a sample quality assessment method that measures the iris distance to the camera can predict *Ic1*'s performance very well but not *Ic2*'s. Therefore, the performance of the sample quality assessment method is always dependent on specific quality attributes or a single modality that link to the recognition or verification algorithm.

3.1 Fingerprint quality assessment

In this section, we introduce fingerprint ISO standard, contact-based and contact-less fingerprint quality assessment methods.

3.1.1 Fingerprint ISO quality standard: ISO/IEC 29794-4 – Information technology – Biometric sample quality – Part 4: Finger image data

A fingerprint image captured from a device can not always have good quality. Many defects can be introduced to the image. This standard [72] categorized these defects to four groups:

1. Defect caused by user character: a) Extreme skin conditions such as very wet, very dry, etc.; b) Scars; c) Wrinkles; d) Blisters; e) Eczema; f) Impurities such as dirt, latent print, etc.
2. Defect caused by imaging: a) Sampling error; b) Low contrast or signal-to-noise ratio; c) Distortion; d) Erroneous or streak lines; e) Uneven background; f) Insufficient dynamic range; g) Non-linear or non-uniform gray-scale output; h) Pixels not available due to hardware failure; i) Aliasing problems.
3. Defect caused by user behavior: a) Elastic deformation; b) Improper finger placement such as too low, rotated, etc.; c) Insufficient area of finger image.
4. Defect caused by environment: a) Humidity; b) Light; c) Impurities on the scanner surface.

The above mentioned defects can affect the performance of a fingerprint recognition system. So it is necessary to compute the quality score of the captured fingerprint image. This standard [72] proposed some aspects that can be used for the computing of the fingerprint quality score. Such quality score should be system independent and device independent, moreover, it should reflect the performance of a fingerprint recognition system. These aspects are divided to local analysis and global analysis, the aspects for local and global analysis are listed below:

- Local analysis
 - Orientation certainty level analysis
 - Ridge-valley structure analysis
 - Frequency domain analysis
 - Uniformity analysis

- Global analysis
 - Orientation flow analysis
 - Ridge-valley uniformity analysis
 - Radial power spectrum analysis

In order to obtain a single or unified output from several or all the quality analyses, it is necessary to combine the results (scores) of the analysis described above and produce a single scalar quality score as wanted in the quality research field. Each of the quality score is normalized to a single scalar range, for instance, between 0 and 1, before combining them. The combination of quality analysis methods is also important so that the final quality score can reflect the performance of the biometric system.

3.1.2 Contact-based fingerprint quality assessment

For contact-based fingerprint, Lim *et al.* [53] proposed to use a local-feature-based quality metric that computes orientation certainty level, ridge frequency, ridge thickness, and ridge-to-valley thickness ratio. Shen *et al.* [54] presented Gabor filters for fingerprint quality measurement. Vatsa *et al.* [55] used redundant discrete wavelet transform to compute dominant ridge activity to assess fingerprint quality. Olsen *et al.* [56] proposed a quality evaluation method based on assessing Gabor filter responses of a fingerprint image. Chen *et al.* [57] measure the quality of ridge samples by energy spectral density concentration in particular frequency bands obtained by discrete Fourier transform. The most commonly used fingerprint quality assessment method is proposed by [National Institute of Standards and Technology \(NIST\)](#) and named [National Institute of Standards and Technology Fingerprint Image Quality \(NFIQ\)](#) [58]. This approach proposed fingerprint image quality as a classification method. It computes a feature vector using the quality image 'map' and minutiae quality statistics produced by a minutiae detection algorithm. The feature vector is then used as inputs to a multi-layer perceptron neural network classifier, and the output activation level of the neural network is used to determine the fingerprint's image quality level. There are five quality levels with 1 being the highest quality and 5 being the lowest quality. Recently, [NFIQ 2.0](#) [59] was introduced with a similar learning-based quality measurement framework in which many new image-based attributes are included. Alonso-Fernandez *et al.* [75] presented a comparative study of several fingerprint quality metrics, in which these metrics are divided into global and local algorithms. Most of above mentioned methods have high correlation with the system performance. However, different correlation values are obtained depending on the biometric systems,

sensors, databases, and so on. It suggests that fingerprint quality assessment approaches can work differently in different test conditions, which will be a source of further investigation. Due to their different properties, some assessment methods could not be suitable for a certain kind of conditions. On the other hand, different quality measures could provide complementary information, and its combination may improve the process of assessing the quality of a fingerprint. It is interesting to study the effects of low quality fingerprints in systems that use alternative methods for minutiae extraction, or alternative features for fingerprint comparison.

3.1.3 Contactless fingerprint quality assessment

For contactless-based fingerprint, Derawi *et al.* [76] stated that image contrast should be enhanced in order to improve sample quality. Song *et al.* [77] presented that image defocusing, low ridge-valley contrast are quality issues in contactless fingerprint samples. Labati *et al.* [78] proposed that non-uniform resolution, out of focus and noise are commonly distortions in contactless fingerprint images. Similar research [79, 80, 81, 82] also indicated that illumination, distance to the camera, contrast, motion blur, and complex background play important roles in contactless fingerprint sample quality evaluation. To overcome above quality issues, Yang *et al.* [83] proposed a one-stop-shop quality assessment approach for smartphone-camera (contactless) fingerprint samples by using a 12-dimensional quality feature vector. Lee *et al.* [84] and Hiew *et al.* [85] presented image pre-processing methods of contactless fingerprint samples to evaluate their quality. Some of these methods applied only image-based quality attributes to the assessment process, some of them used both image-based and modality-based quality attributes. Moreover, different contactless fingerprint systems can be sensitive to different quality attributes. Therefore, a review and evaluation of existing contactless fingerprint quality assessment methods is needed in order to understand which are the most important quality attributes to be assessed.

3.2 Face quality assessment

In this section, we introduce face ISO standard and quality assessment methods.

3.2.1 Face ISO quality standard: ISO/IEC 29794-5 – Information technology – Biometric sample quality – Part 5: Face image data

There are different factors that can affect the performance of face recognition system. An ideal system has to take into account the biometric characteristics of the subject and a number of factors that influence these characteristics. The environmental conditions in the acquisition process, such as the influence of subjects characteristics and the influence of the acquisition process are also need to be considered. In addition, it is necessary to distinguish between static and dynamic char-

acteristics and properties: a) static subjects characteristics are related to anatomical characteristics of the subject; b) dynamic subject characteristics are related to subjects behavior during the acquisition process; c) static properties of the acquisition process are related to physical properties of the capturing device and effects caused by the sample processing chain; d) dynamic properties of the acquisition process are related to environmental conditions during the capturing process. The standard in [73] classified the dynamic versus static properties as well as the subject versus the acquisition process characteristics affecting facial quality, which are given in Table 3.1.

Table 3.1: Characterization of facial quality

	Subject characteristics	Acquisition process
Static	Biological characteristics: <ul style="list-style-type: none"> • anatomical characteristics (e.g. head dimensions, eye positions) • injuries and scars • ethnic group • impairment Other static characteristics: <ul style="list-style-type: none"> • heavy facial wears, such as thick or dark glasses • makeup • permanent jewellery 	Acquisition process and capture device properties, like: <ul style="list-style-type: none"> • image enhancement and data reduction process • physical properties (e.g. image resolution and contrast) • optical distortions • static properties of the background, e.g. wallpaper • sensor resolution • geometric distortion

Dynamic	Subject characteristics and behavior: <ul style="list-style-type: none">● closed eyes● (exaggerated) expression● hair across the eye● head pose● subject posing (frontal / non frontal to camera)	Scenery: <ul style="list-style-type: none">● dynamic characteristics of the background like moving objects● variation in lightning and related potential defects● subject posing● acquisition process and capture device properties
----------------	---	--

Based on the factors given in Table 3.1, face image quality assessment should analyze different aspects, which were proposed in the standard [73]:

1. Dynamic subject characteristics

- subject's behaviour
- analysis based on statistical differences of the left and right half of the face: lighting symmetry and pose symmetry

2. Static characteristics of the acquisition process

- image resolution and size
- noise: image acquisition noise and compression noise

3. Characteristics of image acquisition

- image properties
- image appearance
- illumination intensity
- image brightness
- image contrast
- exposure
- focus, blur and sharpness
- color
- subject-camera distance

3.2.2 Face quality assessment methods

There are two different face image quality measurement techniques: still-face image-based methods and video-based methods. As the focus of this Ph.D is on still images, we will only present this. Sang *et al.* [66] proposed a face image evaluation for face standards. In this study, several algorithms for face image quality assessment were presented. Illumination conditions and facial pose were evaluated in terms of facial symmetry, and implemented based on Gabor wavelet features. Similarly, Hsu *et al.* [67] presented a quality evaluation framework that complies with the requirement of ISO face quality standard [73] for facial biometrics. Subasic *et al.* [68] proposed an assessment scheme of a set of 17 automatic tests in conjunction with the international civil aviation organization face image presentation standards for automatic quality assessment. Klare and Jain [69] presented a perceived uniqueness measure of a given face sample and comparison scores from any face matcher. The measure computes the distance of a comparison score to a set of imposter scores, thus indicating face uniqueness. Gao *et al.* [70] proposed the use of asymmetry in local binary pattern features [71] as a measure of the face sample quality. All of above mentioned methods measure the quality attributes recommended by the face ISO standard [73].

3.3 Iris quality assessment

In this section, we introduce iris ISO standard, NIR-based and VW iris quality assessment methods.

3.3.1 Iris ISO quality standard: ISO/IEC 29794-6 – Information technology – Biometric sample quality – Part 6: Iris image data

Iris quality involves the conditions required to obtain sufficient image sharpness at satisfactory resolution. In order to be able to extract the iris from the eye region, the contrast in the iris also need to be sufficient. In addition, another important aspect is the positioning of the subject's iris in the camera's field of view with good focus while minimizing or eliminating impairments, such as specular reflections. A list of requirements for the assessment of iris image quality is proposed in this standard [74]:

- Usable iris area
- Iris-sclera contrast
- Iris-pupil contrast
- Pupil boundary circularity

- Grey scale utilization
- Iris radius
- Pupil dilation
- Iris pupil concentricity
- Margin adequacy
- Sharpness

3.3.2 NIR-based iris quality assessment

Li *et al.* [60] presented three novel approaches that measure defocus, motion blur, and off-angle in an iris sample to estimate iris image quality. Belcher and Du [61] proposed an approach that automatically selects the portions of the iris with the most distinguishable changing patterns to measure the feature information. The combination of occlusion and dilation determines the amount of iris region available and is considered in the metric. Kalka *et al.* [62] extended their previous work by analyzing the effect of seven quality factors: defocus blur, motion blur, off-angle, occlusion, specular reflection, lighting, and pixel-counts on the performance of traditional iris recognition system. Wei *et al.* [63] presented a novel method to select clear images in the image sequence. He *et al.* [64] proposed a fast iris image quality evaluation approach based on weighted information entropy combining iris image segmentation through localization. Chen *et al.* [65] presented a quality metric for iris based on the spectral energy in local regions. It seems that blur is the common distortion considered by most of these assessment methods for NIR-based iris images. In addition, the iris image quality can affect the segmentation process. An incorrect segmented iris can also result low iris recognition performance. Therefore, NIR-based iris quality assessment approaches should be taking into account the performance of iris segmentation and the performance of recognition.

3.3.3 VW iris quality assessment

Recent interest in non-ideal iris imagery has sparked research on iris recognition in the Visible Wavelength. Proença [86] presented a quality evaluation algorithm for operation on VW iris imagery. In his study, six iris quality attributes were assessed: focus assessment, motion assessment, off-angle assessment, occlusions assessment, levels of iris pigmentation, pixel count, and pupillary dilation and amount of information. This is the only available sample image quality assessment method for VW iris. This method took into account both system performance and

human perceptual for the term 'quality'. However, the implementation of this method is not publicly available for performance evaluation.

3.4 Performance evaluation of biometric sample quality assessment methods

Tabassi *et al.* [58], Alonso-Fernandez *et al.* [2], and Breitenbach *et al.* [87] employed correlation analysis to evaluate image quality assessment methods. In short, they believed that a quality measure is highly correlated (statistically) with comparison scores obtained from a classifier is the most desirable. They observed that high quality biometric samples could generate relatively high genuine scores, which are well separated from impostor scores. Some researchers [57, 88, 89, 90] proposed to use quality-bin based approaches to evaluate the image quality assessment methods. They believed that excluding a certain percentage of low quality samples from the dataset would decrease the **EER** would decrease. Therefore, dividing the entire dataset into several quality bins and conducting comparison experiments individually can evaluate the performance of quality metrics. In addition, Chen *et al.* [57] suggested to use a distance metric that incorporate their method in the formulation of Hamming Distance matcher to show improved results when compared to simple Hamming Distance. An alternative approach for the evaluation of sample quality assessment methods could be by computing the cross-correlation between the given metric and various existing metrics [89]. Grother *et al.* [3] proposed five aspects to evaluate the performance of sample quality metrics: combining two samples' quality values; rank-ordered **DET** characteristics; **Error versus Reject Curves (ERC)**; generalization to multiple matchers; and number of level of quality. Finally, Jain *et al.* [18] stated that **ROC** curve, **FNMR**, and **FMR** could also be an indicator of biometric sample image quality metric performance.

3.5 Summary

In this chapter, we introduced biometric sample quality assessment for contact-based and contactless fingerprint, face, and **NIR** and **VW** iris. We surveyed several approaches for the performance evaluation of biometric sample quality assessment methods.

Chapter 4

A common framework for the assessment of multi-modality biometric image quality

The contributions of this Ph.D thesis start from this chapter. In this chapter, the Section 4.3 is based on the Article A [6], which is introduced in Section 1.3.

4.1 Multi-modality biometric system

The most commonly used biometric systems are usually using a single modality to conduct recognition. With the proliferation of biometric-based solutions in civilian and law enforcement applications, it is important that the vulnerabilities and limitations of these systems are clearly understood. There are four main challenges that can significantly affect the performance of single modality biometric systems [91]:

1. Degraded raw images: the captured biometric images may introduce degradations due to unconstrained acquisition conditions or device errors. Degraded raw images can result in an individual being incorrectly recognized as another individual thereby increasing the errors of the system [91].
2. Non-universality: the biometric system may fail to capture high quality images from a subset of individuals. It can highly reduce the system performance. Therefore, a re-acquisition process is needed in order to capture useful sample images for all individuals.
3. Upper bound on recognition accuracy: due to the limitation of feature extraction and matching algorithms, it is impossible to continuously improve

the performance a single modality biometric system. So there is an implicit upper bound on the system performance.

4. Spoof attacks: behavioral modalities such as voice and signature are subject spoofed by an impostor attempting to mimic the modality corresponding to legitimately enrolled subjects [92, 93]. Physical modalities such as face and iris can also be spoofed by inscribing similar structures on synthetic material [91]. Targeted spoof attacks can undermine the security afforded by the biometric system and, consequently, mitigate its benefits [94].

In order to overcome the above mentioned limitations of single modality biometric system, systems that use multiple modalities for the identification/recognition purpose can be developed. Such systems, known as multi-modality biometric systems [95, 96], can improve the system performance and avoid spoof attacks.

4.2 The proposed framework

We have discussed the quality assessment issues in Chapter 3 for single modality biometric systems, such as fingerprint, iris, and face. However, the image quality assessment approaches that can be used for multi-modality biometric systems are rarely considered. The solution of developing multi-modality biometric sample quality assessment approaches is to measure image-based quality attributes for multiple modalities. In this section, we propose a common framework which can be used for the development of quality assessment methods for multi-modality biometric system. We illustrate this framework in Figure 4.1.

In this framework, we first need to select appropriate image-based quality attributes from each single biometric modality. As introduced in Chapter 3, many existing quality assessment approaches are used for measuring biometric sample quality which are based on the factors that affect system performance. It is important to select appropriate common image-based quality attributes related to those factors for multiple modalities. These attributes include, for example, sharpness, illumination, contrast, noise and so on. In the proposed framework, we consider three biometric modalities: contactless fingerprint, face, and **Visible Wavelength** iris. Then a multi-modality biometric image quality database is created. Even though there are many single modality biometric sample databases for fingerprint, iris, or face, a multi-modality database that contains degraded biometric image samples caused by the selected quality attributes with different degradation levels does not exist. This database is used for the evaluation of biometric quality assessment approaches in the next stages of this framework. The next stage in this framework is to select suitable **Image Quality Metrics (IQMs)** that are designed for natural images for the assessment of biometric images. The performance of selected **IQMs**

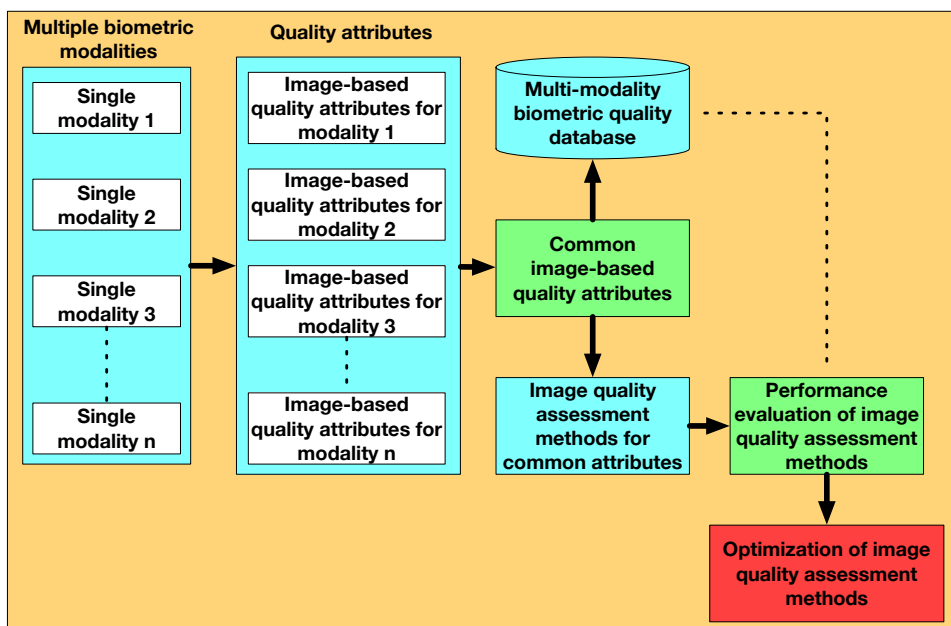


Figure 4.1: Common framework for the assessment of multi-modality biometric image quality.

is evaluated by using our database. Finally, IQMs that result in better system performance will be optimized.

4.3 Common image-based image attributes of multi-modality sample quality assessment for unconstrained biometric system

4.3.1 Previous classification of image-based attributes

In order to better understand image quality evaluation in biometrics, it is necessary to inspect the different image-based quality attributes that are commonly measured in biometric samples. Bharadwaj *et al.* [4] have classified image-based attributes into four groups:

1. Blurring: Image blurring is a common attribute that occurs due to defocus, motion, or certain environmental factors.
2. Illumination: Non-uniform lighting is essential for the acquisition of a bad quality biometric sample. Adversely directed lighting drastically affects the performance of fingerprint, face, and iris recognition.

3. Noise/Compression: An image may contain noise due to environmental factors, incorrect use of sensors, and transmission errors. Depending on the compression levels, various image encoding techniques can produce artifacts.
4. Optical distortions: Non-conformity to rectilinear projection causes distortion in the captured images.

Degradations of aforementioned image-based attributes usually occur due to the limitation of sensor technology or the condition of image acquisition. As the constraints on human beings during acquisition are not well controlled, the impact of these attributes on the performance of biometric systems increased drastically [4]. Consequently, the assessment of these attributes is critical for developing effective and robust biometric systems.

4.3.2 Investigation of common image-based quality attributes

The first step in the common framework is to identify the relevant and important image-based attributes. We took the approach of doing a survey of the existing literature. Many attributes have been considered as important and evaluated by researchers to quantify biometric sample quality for fingerprint, face, and iris. These image-based attributes include, motion blur [77, 82, 85, 80, 62, 63, 60, 74, 97], CCD background noise [77, 80], lighting [77, 78, 67, 62], contrast [77, 84, 82, 85, 81, 79, 78, 76, 67, 70, 73, 61, 74], image noise [84, 78, 81], image background noise [82], defocus [85, 80, 62, 63, 61, 60, 78], image focus [78, 98], illumination [78, 79, 99, 70, 66], blurring effects [78, 97], illuminance [76], clarity [76], compression artifacts [67], exposure [67, 73], sharpness [67, 70, 100, 97, 66, 73, 74], color [67, 73], brightness [100, 73], salt and pepper noise [97], luminance [73], artifacts [73, 74], gray scale utilization [74].

4.3.3 Classification of most important image-based attributes and their definitions

When reducing these attributes we surveyed, we need to consider several important issues. A long term goal of this research is to find the solution of multi-modality biometric sample quality assessment. With this intention, the quality attributes have to be general enough to be assessed in all three modalities, while they should play an important role in each modality. In addition, the quality attributes have to be suitable for IQMs to address the intended assessment methods. An overview of common image-based attributes is illustrated in Figure 4.2. The existing sets of quality attributes do not fulfill all of these requirements, and therefore a new set of quality attributes is needed.

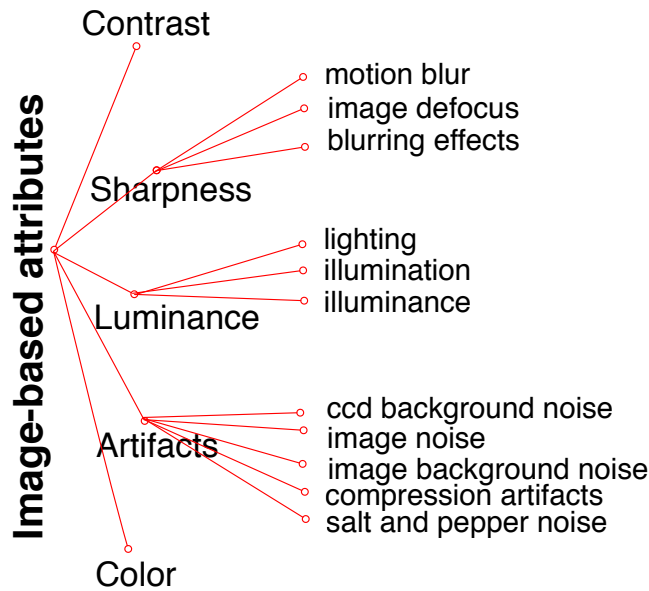


Figure 4.2: The image-based quality attributes tree generated from the commonly measured ones.

Many of the aforementioned quality attributes are similar and have common denominators, which allow them to be grouped within more general attributes to reduce the dimensionality and create a more manageable evaluation of sample quality. Usually a compromise is necessary between generality and accuracy when it comes to dimensionality. A smaller set of general attributes results in lower accuracy but also lower complexity, and vice versa [101]. According to the consideration stated above and the aspect of the assessment of IQMs, we classify the reviewed quality attributes to the following five different dimensions:

1. The **contrast** attribute has two aspects: local contrast and global contrast. The local contrast can be defined as the average difference between neighboring pixels. The global contrast is defined as the weighted sums of the overall local contrast for different resolutions.
2. The **sharpness** attribute is defined as the clarity of biometric sample structure and details.
3. The **luminance** attribute can be defined as the intensity of the biometric sample illumination.
4. The **artifacts** attribute is given as any undesired alteration in biometric sample

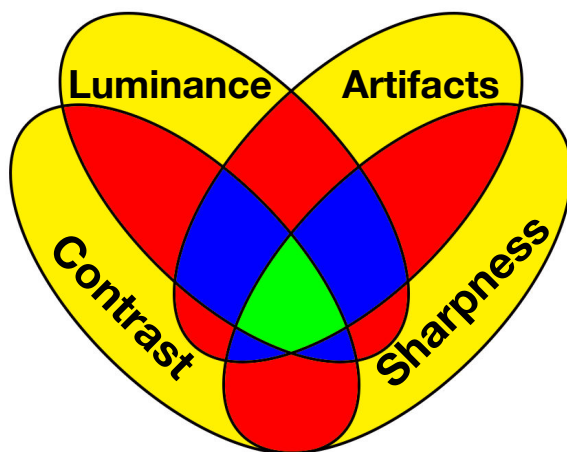


Figure 4.3: Simple Venn diagram with four folds used for an abstract illustration of four image-based quality attributes and the interactions between them. Overall biometric sample quality can be affected by one (yellow), two (red), three (blue), or four (green) of the attributes.

introduced during its digital processing, such as noise, compression and so on.

5. The **color** attribute is defined as the color information that can be additionally used for biometric recognition in order to improve sample quality and system performance.

We used a Venn diagram to create simple and intuitive illustration of the image-based attributes and their influence on overall biometric sample quality. Venn diagram can be used to show possible logical relations between these four attributes. Color information is known not to affect current biometric recognition performance of major biometric system [73], but more and more researchers start paying attention to the color attribute to improve biometric sample quality and system performance [102, 103, 104]. Therefore, we illustrated the image-based attributes using only four folds, leaving the color attribute out for future research interests.

The Venn diagram in Figure 4.3 shows how the overall biometric sample quality can be affected by one, two, three, or four of the image-based attributes. Some attributes are interdependent [105], addressing image quality to a multidimensional problem [106], in this case four dimensions. The folds in Figure 4.3 may have different sizes or positions because the attributes can affect the overall biometric sample quality in different ways. In addition, there is always a trade off between preserving independence and reducing all of the existing image-based attributes to

five dimensions. By taking into account the aspects of biometric sample quality as much as possible, it is not easy to keep the balance.

These five image-based attributes are a good starting point for the multi-modality biometric sample quality assessment. Each attribute may have specific meanings in different biometric modalities. Furthermore, these attributes may also have sub-attributes. Such issues will be discussed when we take a closer look at the different image-based attributes in the following sections.

Contrast

While contrast for simple images is well defined, contrast for complex images is not [107]. Real world images, and therefore biometric images, can be considered as complex images while simple images rather contain test patterns like sinusoidal gratings [73]. Contrast as an image attribute is usually defined as the ratio between the brightest and the darkest spots in the image. The human perception of the image contrast does not completely correspond to this definition. Therefore, it is necessary to investigate different contrast definitions.

There are several commonly used definitions for contrast in the literature, such as Michelson contrast [108], Weber contrast [109], and band-limited contrast [110]. A recent proposed method for computing contrast, a global contrast factor [111] was recommended by the ISO face quality standard [73]. This method is based on local contrast at a given position in its neighborhood. Based on this local contrast, the global contrast is given as the weighted sums of the overall local contrast for different resolutions.

Contrast is clearly difficult to define, and its definition changes according to the application. Considering the property of fingerprint, face, and iris biometric sample images, the definition of our contrast attribute can refer to the definition of local and global contrast as proposed in [111].

In order to evaluate fingerprint image contrast, we need a method for measuring the contrast of the ridge-valley structure. According to the definition stated above, the given position $f(x, y)$ could be a pixel on the ridge and the neighboring pixels could be the corresponding valley pixels. For iris images, we should not only calculate the contrast for iris structure, but also compute the iris-sclera contrast and iris-pupil contrast. For face images, we can apply the proposed method to calculate the contrast on the face structure. In conclusion, the aforementioned contrast definition is suitable for defining contrast in multiple modalities.

Sharpness

We consider sharpness as another important image-based attribute because it has been commonly used in biometric sample quality assessment. Caviedes and Oberti [112] defined sharpness as the clarity of detail and edge in an image. Bouzit and MacDonald [113] also suggested that sharpness is related to details and edges. Fedorovskaya [114] proposed to define sharpness as the overall impression of clarity of edges observed within the entire image. ISO fingerprint quality standard [72] used ridge-valley clarity to represent fingerprint sample sharpness. ISO iris quality standard [74] presented a method for iris sharpness by measuring the degree of focus present in a iris sample image. ISO face quality standard [73] stated that the sharpness of a face image refers to the degree of clarity in both coarse and fine details in the face region. By taking into account all the aspects stated above, we can define our sharpness attribute as the clarity of biometric sample structure and details.

Image-based attributes that are suitable to group within the sharpness attribute are diverse and many, including sharpness [67, 70, 100, 97, 66, 73, 74], motion blur [77, 82, 85, 80, 62, 63, 60, 74, 97], defocus [85, 80, 62, 63, 61, 60, 78], image focus [78, 98], and blurring [78, 97].

Luminance

A common definition of luminance is the intensity of light emitted from a surface per unit area in a given direction. Here we define luminance as the intensity of the biometric sample illumination. It is important to evaluate whether the biometric sample illumination is too strong or too weak. In addition, whether the intensity of the illumination is uniform or not also plays an important role in biometric sample quality assessment. Many image-based attributes used by other researchers can be included within our luminance attribute, such as lighting [77, 78, 67, 62], illumination [78, 79, 99, 70, 66], and illuminance [76].

Artifacts

Many artifacts were discovered by other researchers in biometric samples, for example, noise, compression degradations, etc. Three most common sub-attributes that can be classified in our artifacts attribute: noise, compression distortions, and optical distortions. The noise in biometric images depends on the different processes that are required to generate a digital image. The introduced noise in particular related to the sensor or processing involved. Relevant noise sources include: 1) digital image acquisition sensors (e.g. digital camera); 2) analogue image acquisition devices; 3) image scanning devices; and 4) digital transmission errors. Compression artifacts are noticeable distortions of images caused by the applic-

ation of lossy data compression. It contains several different distortions so it is complex. The majority component in compression artifacts is block artifact. The last sub-attribute is optical distortions. Any effect of optical distortion including spherical aberration, chromatic aberration, astigmatism, and coma that an biometric sample image may exhibit should be assessed to ensure that they cause no significant worsening of error performance for the designed configuration. There are a variety of assessment approaches for each artifact. Therefore we will not discuss any particular method here.

We can link the artifacts attribute with several of the attributes used in the literature. For instance, CCD background noise [77, 80], image noise [84, 78, 81], image background noise [82], compression artifacts [67], salt and pepper noise [97], and artifacts [73, 74].

Color

Even though color information is known not to affect current biometric recognition performance of major biometric systems, if the color of the background is known, it can be used to calibrate the image (e.g. 18% gray). Furthermore, more and more research start considering the color information in order to improve biometric sample quality [102, 103, 104]. We believe that color attributes will be an important image-based biometric attribute in the near future.

4.4 GC²: A new multi-modality biometric image quality database

Since we only focus on image-based quality attributes, we need to choose a specific multi-modality biometric database that only contains image-based distortions, but without modality-based degradations. In order to evaluate the performance of no-reference IQMs, as well as the biometric recognition system, the common way is to use images in different levels of degradations. All existing databases contain both image-based and modality-based degradations, and the degradations are not presented in different levels. Therefore, we create a new database 'GC² Multi-Modality Biometric Image Quality Database' for the specific requirements in this research. The name of the database 'GC²' came from both institutions which funded my Ph.D: Greyc laboratory from University of Caen in Caen, France, and Colorlab from NTNU in Gjøvik, Norway.

This database has three biometric modalities: contactless fingerprint, VW iris, and face. Three cameras are used for the acquisition: 1) a Lytro [115] first generation Light Field Camera (LFC) (11 Megapixels), 2) a Google Nexus 5 embedded camera (8 Megapixels), and 3) a Canon D700 with Canon EF 100mm f/2.8L Macro

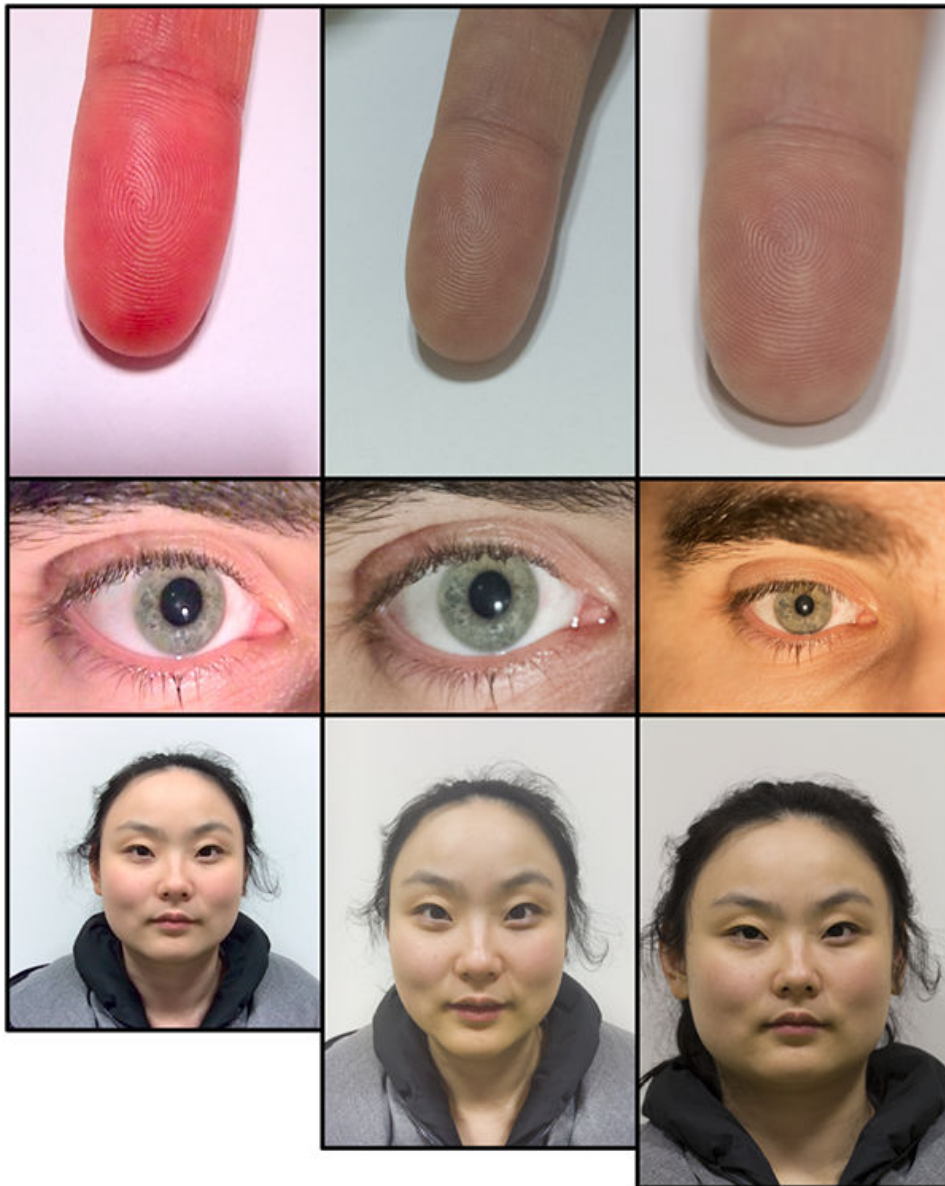


Figure 4.4: An example of sample images from different modalities and cameras. The first row represent the fingerprint modality, the second row represent the iris modality, and the last row represents the face modality. The first column represents images captured by LFC, the second column represents images captured by smartphone, and the last column represents images captured by reflex camera.

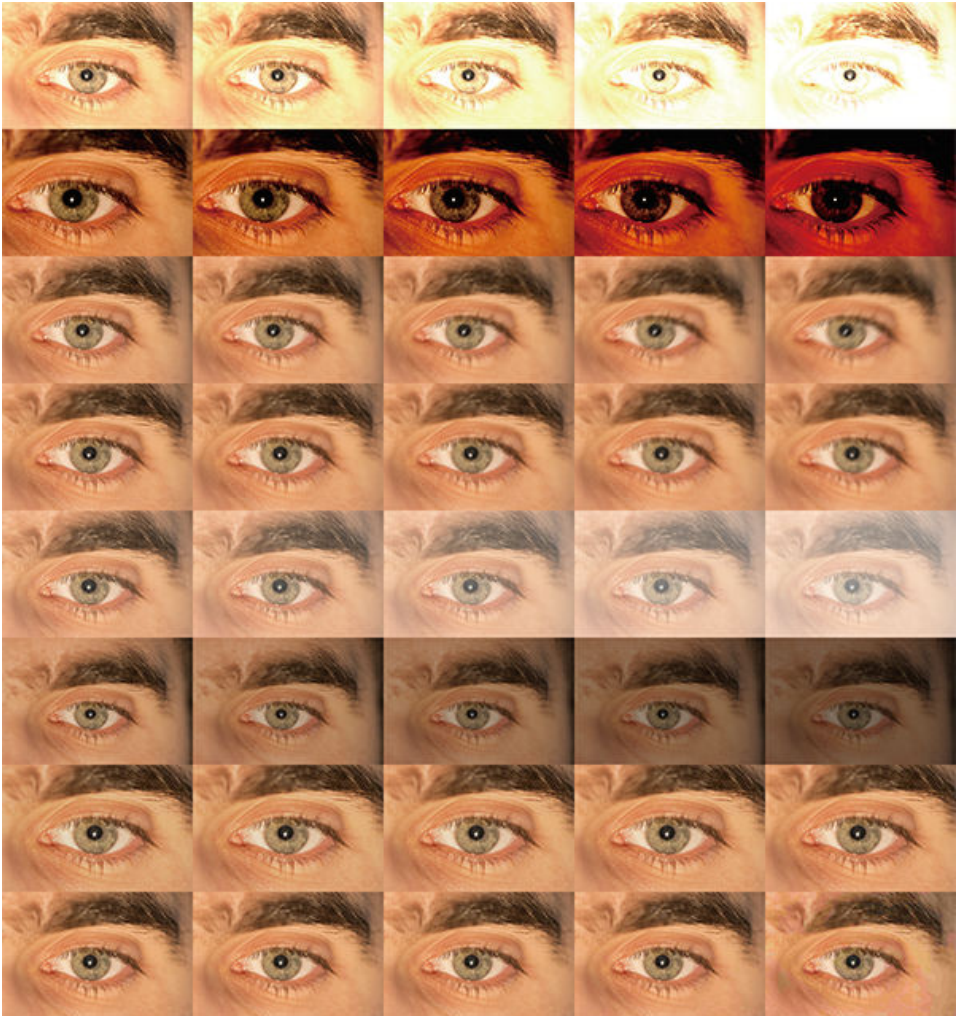


Figure 4.5: Degraded iris samples in five levels, the first column represents the degradation level 1 (little degraded) and the last column represents the degradation level 5 (highly degraded). The first row represents too high contrast iris images; the second row represents too low contrast iris images; the third row represents motion blurred iris images; the fourth row represents the Gaussian blurred iris images; the fifth row represents high luminance iris images; the sixth row represents low luminance iris images; the seventh row represents iris images containing poisson noise; the last row represents JPEG compressed iris images.

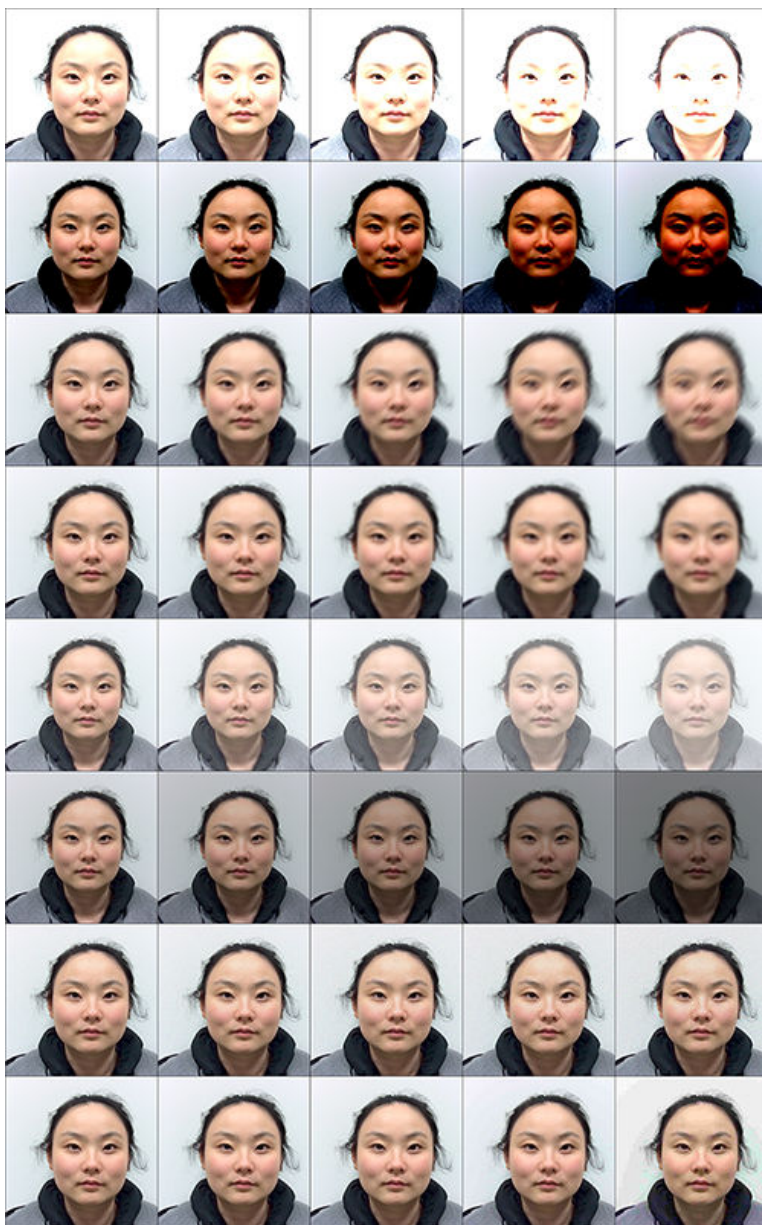


Figure 4.6: Degraded face samples in five levels, the first column represents the degradation level 1 (little degraded) and the last column represents the degradation level 5 (highly degraded). The first row represents too high contrast face images; the second row represents too low contrast face images; the third row represents motion blurred face images; the fourth row represents the Gaussian blurred face images; the fifth row represents high luminance face images; the sixth row represents low luminance face images; the seventh row represents face images containing poisson noise; the last row represents JPEG compressed face images.

Lens (18 Megapixels). An example of sample images from different modalities and cameras is illustrated in Figure 4.4. 50 subjects participated in the acquisition, seven of them are female and 43 of them are male. For the fingerprint modality, three fingers (index finger, middle finger, and ring finger) per hand and 15 sample images per finger per camera have been acquired. Each subject was asked to put their fingers on a white paper during the acquisition. Normal office light was used for lighting condition. There are 15 samples per finger per hand \times 3 fingers \times 2 hands \times 50 subjects \times 3 cameras = 13500 raw fingerprint images in the database. For the iris modality, 15 iris samples per eye per camera have been acquired. Each subject was asked to sit in a dark room with only an incandescent lamp in front of the face to avoid reflection in the iris. There are 15 samples per eye \times 2 eyes \times 50 subjects \times 3 cameras = 4500 raw iris images in the database. For the face modality, 15 samples per subject \times 50 subjects \times 3 cameras = 2250 raw face images are obtained in the database. Each subject was asked to sit in front a white wall with normal office light. In order to obtain image-based distortions correlated to the attributes redefined in Section 4.3.3, we need to artificially degrade sample images in the database. Inspired by the techniques used in CID:IQ image quality database [116], we degrade sample images for iris modality and face modality into five degradation levels (one to five, from little degraded to highly degraded) for each distortion as follows (all image processing is conducted by using Matlab R2016 a):

- **Contrast distortions.** There are two kinds of contrast distortions: too low and too high contrast. We use Matlab function `'J = imadjust(I, [lowin; highin], [lowout; highout])'`, which maps the values in I (original image) to new values in J (degraded sample image) such that values between low_{in} and $high_{in}$ map to values between low_{out} and $high_{out}$. For low contrast, the low_{in} and $high_{in}$ values are set to 0.2 and 1 for the degradation level 1 (little degraded), low_{out} and $high_{out}$ values are set to 0 and 1. The low_{in} increases 0.1 for each degradation level and the other variables remains the same values. For high contrast, the low_{in} and $high_{in}$ values are set to 0 and 0.8 for the level 1, low_{out} and $high_{out}$ values are set to 0 and 1. The $high_{in}$ decreases 0.1 for each degradation level and the other variables remain the same values.
- **Sharpness distortions.** We generate two sharpness distortions: motion blur and Gaussian blur. For motion blur we use Matlab function `'h = fspecial('motion', len, theta)'`, which returns a filter to the linear motion of a camera by `len` pixels, with an angle of `theta` degrees in a counterclockwise direction. The `len` value is set to 10 for degradation level 1 and `theta` is set to 45. The `len` increases 15 for each degradation

level and the other variables remain the same values. For Gaussian blur we use the function `h = fspecial('gaussian', hsize, sigma)`, which returns a rotationally symmetric Gaussian lowpass filter of size `hsize` with standard deviation `sigma` (positive). The `hsize` value is set to [25 25] and the `sigma` is set to 2 for the degradation level 1. The `sigma` increases 2 for each degradation level and the `hsize` changes according to the value of `sigma`.

- **Luminance distortion.** There are two kinds of luminance distortions: too low and too high luminance. We use Matlab function `J = imadjust(I, [lowin; highin], [lowout; highout])`, again to simulate luminance distortions. For low luminance, the `lowin` and `highin` values are set to 0 and 1, `lowout` and `highout` values are set to 0 and 0.9 for degradation level 1. The `highout` decreases 0.1 for each degradation level and the other variables remain the same values. For high luminance, the `lowin` and `highin` values are set to 0 and 1, `lowout` and `highout` values are set to 0.1 and 1 for degradation level 1. The `lowout` increases 0.1 for each degradation level and the other variables remain the same values.
- **Artifacts.** We introduce two artifacts to the raw sample images: poisson noise and JPEG compression artifacts. We use Matlab function `J = imnoise(I, 'poisson')` to add poisson noise for degradation level 1. We add another layer of poisson noise for each degradation level. The JPEG compression ratio is set to 0.9 for degradation level 1. The ratio decreases 0.2 for each degradation level.

Including the degraded sample images, there are 317250 sample images in the database. An example of degraded sample images in five levels for iris modality is given in Figure 4.5, and for face modality is given in Figure 4.6. We plan to make the database publicly available.

4.5 IQMs and their applications in biometrics

4.5.1 Introduction and classification of IQMs

There are many existing **IQMs** that have been developed for the assessment of natural images' quality [117]. Based on the availability of a reference image, **IQMs** can be classified into full-reference, reduced-reference, and no-reference methods [118]. Full reference **IQMs** can assess the quality of images, which have original undistorted visual stimulus along with the distorted stimulus are available. Reduced-reference **IQMs** can assess the quality of images, which have the distorted stimulus and some additional information about the original stimulus available.

No-reference IQMs can assess the quality of images, which have only the distorted stimulus available. According to the properties of biometric sample images, only no-reference IQMs might be suitable for the assessment of biometric sample image quality. It is interesting to evaluate the performance of such kind of IQMs on biometric images in order to assess the possibility of developing image-based multi-modality sample quality assessment methods.

4.5.2 A brief survey of no-reference IQMs

Here we give a brief survey of no-reference IQMs that can be used to assess the five image-based quality attributes presented in Section 4.3.3.

There are many distortion-specific no-reference IQMs in the research field. Fang *et al.* [119] proposed a method for no-reference quality assessment of contrast distorted images based on the principle of natural scene statistics. Panetta *et al.* [120] presented a no-reference metric for measuring image contrast. Gu *et al.* [121] propose no-reference metric that generates an overall quality estimation of a contrast-distorted image by properly combining local and global considerations. Ferzli *et al.* [122] present a perceptually-based no-reference image sharpness metric by integrating the concept of just noticeable blur into a probability summation model. Han *et al.* [123] propose an algorithm for no-reference blurred image quality assessment based on block-based discrete cosine transform statistics and linear prediction method. Leclaire and Moisan [124] present a no-reference image blur metric based on Fourier phase information. Blanchet and Moisan [125] propose a sharpness index that is closely related to the notion of global phase coherence. Zhu and Karam [126] introduce a no-reference metric based on perceptually weighted local noise. Wang *et al.* [127] develop a no-reference quality measurement algorithm for JPEG compressed images.

There are also many holistic IQMs, which are for generalized purposes. Gabarda and Cristobal [128] propose a no-reference metric based on measuring the variance of the expected entropy of a given image upon a set of predefined directions. Moorthy and Bovik [129] propose a two-step framework for no-reference image quality assessment based on natural scene statistics. Saad *et al.* [130] propose a general-purpose, distortion-agnostic, no-reference image quality assessment algorithm based on a natural scene statistics model of discrete cosine transform coefficients. Mittal *et al.* [131] propose a natural scene statistic-based distortion-generic no-reference metric that operates in the spatial domain. Zhang *et al.* [132] present a feature-enriched no-reference metric based on a multivariate Gaussian model. Liu *et al.* [133] develop a general-purpose no-reference metric that utilizes local spatial and spectral entropy features on distorted images. A recent no-reference IQM is proposed by Liu *et al.* [134] which applies relative gradient

statistics and adaboosting neural network techniques.

Different IQMs have their pros and cons. Distortion-specific IQMs may have better performance only measuring given distortion. On the other hand, generalized IQMs can assess different types of distortions, however, they may not perform as good as distortion-specific IQMs for certain distortion. In addition, some IQMs are Natural Scene Statistics (NSS) based metrics and some of them have been trained on image quality databases. NSS based IQMs can better assess the quality of natural images, and trained IQMs have better performance on images that similar to trained databases. But for the other types of images these IQMs cannot guarantee their performance.

4.5.3 Fingerprint sample quality assessment using no-reference IQMs

There are quite a few studies investigating fingerprint quality assessment by using no-reference IQMs. El Abed *et al.* [135] presented a quality assessment metric of fingerprints. Its main originality lies in the use of a no-reference quality metric. The proposed quality metric combines two types of parameters through a weighted sum optimized by a genetic algorithm: a) image quality criterion, and b) pattern-based quality criteria (salient and patch-based features). Yao *et al.* [136] proposed a utility based quality assessment method of fingerprints by considering several complementary aspects: a) image quality assessment without any reference which is consistent with human conception of inspecting quality, b) textural features related to the fingerprint image, and c) minutiae features which correspond to the most used information for matching. The proposed quality metric is obtained by a linear combination of these features and is validated with a reference metric using different approaches. There are also some metrics proposed by the fingerprint quality standard [72]. All of these studies are for contact-based fingerprint quality assessment. Contactless fingerprint technology has not been widely used, so the quality assessment for contactless fingerprint is rarely considered.

4.5.4 Face sample quality assessment using no-reference IQMs

There are several existing studies using no-reference IQMs to assess face sample quality. Abaza *et al.* [137] evaluated no-reference IQMs that can measure image quality factors in the context of face recognition. Then they proposed a face image quality index that combines multiple quality measures. Dutta *et al.* [138] proposed a data driven model to predict the performance of a face recognition system based on image quality features. They modeled the relationship between image-based quality features and recognition performance measures using a probability density function. Hua *et al.* [139] investigated the impact of out-of-focus blur on face recognition performance. Fiche *et al.* [140] introduced a blurred face recogni-

tion algorithm guided by a no-reference blur metric. There are also some metrics proposed by the face quality standard [73]. From these studies we can see that, no-reference IQMs can be used for the assessment of face sample quality. The performance is comparable to some metrics proposed in face quality standard [73] which are designed for specific face modality. However, the above mentioned studies have two common shortages: a) the image-based quality attributes in these studies do not cover all the five important attributes indicated in Section 4.3.3; and b) the databases used in these studies contain both image-based distortions and modality-based distortions. Due to these two shortcomings, the performance of no-reference IQMs could be affected.

4.5.5 Iris sample quality assessment using no-reference IQMs

For NIR iris quality assessment, most of the quality assessment approaches are designed specific for iris modality. Therefore, no-reference IQMs that can only assess image-based distortions are not commonly used. However, for VW iris quality assessment, only Proença *et al.* [86] proposed an approach for quality assessment. In this study, both image-based metrics and modality-based metrics are combined to assess VW iris quality. Generally speaking, no-reference IQMs have not been tested on iris images.

4.6 Summary

In this chapter, we proposed a common framework for the assessment of multi-modality biometric image quality, which addressed the first research question formulated in Section 1.2. In this framework, we selected the most important common image-based quality attributes of multi-modality sample quality assessment for unconstrained biometric systems, which addressed the second research question in Section 1.2. We created a multi-modality biometric image quality database for the performance evaluation purpose. Existing IQMs are introduced and classified in order to discover their applications for fingerprint, face, and iris biometrics.

Chapter 5

How image degradations influence the performance of fingerprint biometrics

This chapter is based on Article B [7], which is introduced in Section 1.3.

5.1 Introduction

During the past several years, biometric sample quality assessment became a significant issue because of biometric systems poor performance on degraded image samples. Studies and benchmarks have shown that biometric sample quality have a direct influence on the overall performance of a biometric recognition system [2, 3]. Indeed, using a poor quality biometric sample in the enrollment phase of the subject, the recognition of the person cannot be ensured with a high level of accuracy. For example, a blurry sample image at enrollment may require an extra processing step to be able to identify the sample in the system. This operationally important topic has nevertheless received little research compared to the primary feature-extraction and pattern-recognition tasks. Generally, the biometric data is obtained from a sensor that can generate an image. However, because of changes in physical characteristics of human beings (glasses, scars, etc.), the acquisition environment (indoor, outdoor, etc.) and existing hardware solutions, defects of the overall system performance are dominant on the acquisition process. So, ensuring strict quality control of the acquired data is an essential process in the development of an efficient biometric recognition system. From the fingerprint quality standard [72] we already know what kinds of degradations that can affect the performance of a fingerprint recognition system, however, it is not clear to what extent

the system performance will be influenced. Therefore, an experiment is conducted to investigate how image degradations influence the performance of fingerprint recognition system, and the performance of fingerprint quality assessment approach. First, we select normal degradations and apply them to fingerprint samples. Then, the system performance comparison between original and degraded fingerprints will be conducted in order to illustrate the impact of each degradation on biometric system performance. Finally, we use NFIQ fingerprint image quality metric to measure its performance on selected degradations.

5.2 Experimental setup

In this section, we present the selected degradations, used fingerprint recognition system and the fingerprint database.

5.2.1 Selection and implementation of fingerprint degradations

According to biometric sample quality standards [52, 72] and existing research we surveyed [53, 54, 55, 56, 57, 58, 59, 75], we select four degradations for the experiment: low contrast, motion blur, JPEG lossy compression artifact, and JPEG 2000 lossy compression artifacts. It has been clearly and widely proved that low contrast between fingerprint ridge and valley area and clarity of fingerprint are two of most common degradations that decrease fingerprint recognition system performance. Many of fingerprint image quality metrics analyze the contrast and clarity of fingerprint as an indicator for fingerprint image quality [141, 142, 143, 144, 145, 58]. Additionally, due to the dry skin condition of the subjects and too low pressure during acquisition process, low contrast of the fingerprint is anticipated in normal fingerprint processing. However, we should keep in mind that the low contrast caused by dry skin is different from the low contrast caused by wet skin. In this experiment we only take into account the low contrast degradation due to dry skin. In fingerprint quality standard [72], JPEG and JPEG 2000 lossy compression algorithms are used for fingerprint image data coding. So it is also necessary to investigate the impact of JPEG and JPEG 2000 compression artifacts. Based on the reasons above, four types of degradation are selected. Each fingerprint sample will be degraded into five levels (from little degraded to significantly degraded fingerprint image). The implementation of each level is described as follow:

- Motion blur: $h = f_{special}('motion', len)$ is used to generate motion blur to original fingerprint images. It returns a filter to approximate, once convolved with an image, the linear motion of a camera by len pixels. The filter becomes a vector for horizontal and vertical motions. The len is defined as 3, 6, 9, 12, 15 for level 1 to level 5, which corresponds to a motion of 3, 6, 9, 12, 15 pixels;

- JPEG compression artifacts: the compression ratio for JPEG lossy compression are 0.95, 0.75, 0.55, 0.35, and 0.15 for level 1 to level 5, respectively;
- Contrast distortion: $J = imadjust(I, [low_{in}; high_{in}], [low_{out}; high_{out}])$ is used to generate low contrast fingerprint. It maps the values in I to new values in J such that values between low_{in} and $high_{in}$ map to values between low_{out} and $high_{out}$. The low_{out} value is defined as 15, 30, 45, 60, 75 for level 1 to level 5;
- JPEG 2000 compression artifacts: the compression ratio for JPEG 2000 lossy compression are $\frac{1}{2}$, $\frac{1}{3}$, $\frac{1}{5}$, $\frac{1}{7}$, and $\frac{1}{9}$ for level 1 to level 5, respectively.

All image processing is completed using Matlab R2015b 64bit. Some examples of original fingerprints compared to degraded images are shown in Figure 5.1.

From Figure 5.1 we can see that, for degradation type blur and low contrast, the differences between each level are visually distinguishable. In contrast, the differences between each level in both JPEG lossy compression and JPEG 2000 lossy compression artifacts are not obvious. However, this does not mean that these degradations influence fingerprint recognition system in the same way as what we see from here.

5.2.2 Fingerprint recognition system

In order to investigate how these degradations influence fingerprint recognition performance, we use [National Institute of Standards and Technology Biometric Image Software \(NBIS\)](#) [146]. The NBIS distribution is developed by the NIST for the Federal Bureau of Investigation and Department of Homeland Security. In NBIS, three core applications will be used in this experiment:

1. **MINDTCT**, a minutiae detector. It locates and records ridge ending and bifurcations in a fingerprint image. The location, type, orientation, and quality of minutiae are stored and used for further processing (e.g. fingerprint comparison);
2. **BOZORTH3**, a comparison algorithm. It is a minutiae based fingerprint comparison algorithm. It will do both one-to-one and one-to-many comparison operations. It accepts minutiae generated by the MINDTCT algorithm. The output is a comparison score between two fingerprints;
3. **NFIQ**, a fingerprint image quality metric. It analyses a fingerprint image and assigns a quality level of 1 (highest quality) 5 (lowest quality) to the image.



Figure 5.1: Fingerprint image degradations in different levels. Column (A) represents the original fingerprint; (B) represents the degradation level 1 (little degraded); (C) represents the degradation level 2; (D) represents the degradation level 3; (E) represents the degradation level 4; and (F) represents the degradation level 5 (significant degraded). The first row is blur degradation; the second row is JPEG lossy compression artifacts; the third row is low contrast degradation; and the last row is JPEG 2000 lossy compression artifacts. All fingerprint samples in this figure are from FVC 2002 DB1 dataset [25].

Higher quality images should produce significantly better performance with comparison algorithms.

5.2.3 Fingerprint database

The fingerprint database used for fingerprint image degradation generation and fingerprint recognition is FVC 2002 DB1 [25]. The acquisition sensor is optical sensor "TouchView II" by Identix. This database contains 100 fingers and 8 samples per finger. Totally, 800 fingerprints are obtained from the database.

5.2.4 Computation environment

The computer used for conducting image processing and fingerprint minutiae extraction and comparison is DELL LATITUDE E6540 laptop. It has an Intel(R) Core(TM) i7-4800MQ CPU @2.7GHz processor and 16GB memory. The operating system is Windows 7 Professional 64 bit. All executable NBIS applications are called in Matlab R2015b.

5.3 Experimental results

Due to the expensive computation for MINDTCT and BOZORTH3 by using Matlab, we reduce the full size of FVC 2002 DB1 to 50 fingers and 4 samples per finger. Therefore, 200 fingerprints are used in the experiment.

5.3.1 Histogram of comparison scores

The histograms of genuine comparison score for original fingerprints and degraded fingerprint are shown in Figure 5.2 and Figure 5.3. The difference between two Figures is that the scores in Figure 5.2 are the comparison between degraded fingerprints (probe) and original fingerprints (as reference images) (we call it D2O). Whereas, the scores in Figure 5.3 are the comparison between degraded fingerprints (probe) and degraded fingerprints (as reference images) (we call it D2D). From both Figures 5.2 and 5.3 we can observe that, only blur degradation has a significant negative affect on NBIS fingerprint recognition system. This is because that from degradation level one to level five, more and more genuine comparison score move from high value to low value. In addition, there is no significant difference between D2O histogram and D2D histogram. Histograms of probe comparison score have the similar properties to the genuine comparison scores.

5.3.2 Distributive tendency of comparison score

Similar to histogram, we also plot the distribution of the genuine/probe comparison scores. It is the genuine/probe comparison scores for degraded fingerprints versus the genuine/probe comparison scores for original fingerprints. The distributive

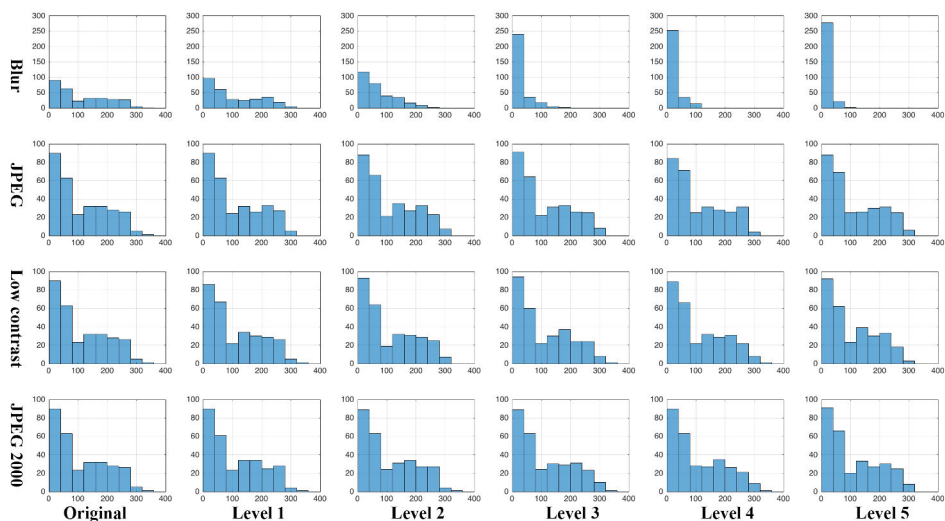


Figure 5.2: The histogram of genuine comparison score for original and degraded fingerprints. The scores of degraded fingerprints are the comparison between degraded fingerprints (probe) and original fingerprints (reference). The x axis represents the comparison score and y axis represents the number of score.

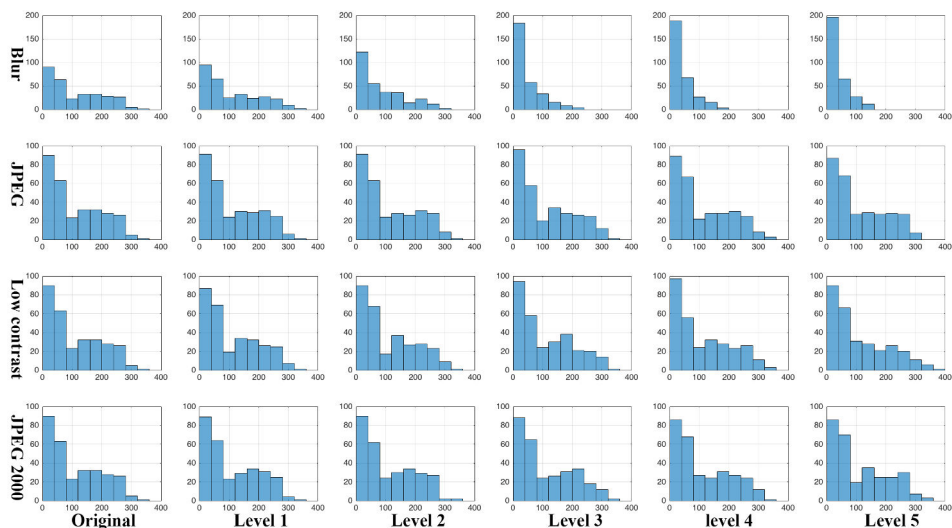


Figure 5.3: The histogram of genuine comparison score for original and degraded fingerprints. The scores of degraded fingerprints are the comparison between degraded fingerprints (probe) and degraded fingerprints (reference). The x axis represents the comparison score and y axis represents the number of score.

tendency plots make it easier for us to see the tendency of the scores change due to the effect of the introduced degradation in different levels. Both D2O and D2D distribution plots are illustrated in Figure 5.4 and Figure 5.5, respectively. The x axis represents the degraded genuine score and the y axis represents the original genuine score. The reference line is $y = x$. The lower area which is the triangle area under the reference line indicates that the original genuine score from a given fingerprint sample is lower than the degraded genuine score from the same fingerprint sample. The upper area which is the triangle area above the reference line indicates that the original genuine score from a given fingerprint sample is higher than the degraded genuine score from the same fingerprint sample. In our case, if more and more score points in the plot move to the upper area after introducing a higher level of degradation, it means that NBIS fingerprint recognition performance is negatively affected by the given degradation. On the other hand, if more and more score points in the plot move to the lower area after introducing higher level of degradation, it means that NBIS fingerprint recognition performance is positively affected by the given degradation. The more score points are centralized around the reference line, the less influence there is of such degradation to the NBIS fingerprint recognition performance.

From Figure 5.4 we can see that, after fingerprints become more blurred, more and more score points move to the upper area and very close to the y axis. As we introduced before, this shows that blur degradation on fingerprint samples has a high negative correlation to the NBIS fingerprint recognition system performance. For JPEG lossy compression artifacts, no significant scores change tendency that can be observed. However, when the compression ratio is increasing, more score points move away from the reference line, but to both lower and upper direction. Similar tendencies can be found for both low contrast and JPEG 2000 lossy compression artifacts. This means that, in our case, these three degradations slightly affect NBIS fingerprint recognition performance but no strong trend. By comparing the D2O distributive tendency plots to D2D plots for blur degradation, we can see that score points in D2D plot move not as much as the points in D2O plot for each level. This is also because blur has the significant impact on the NBIS fingerprint recognition performance in our conditions. Distributive tendency plots of probe comparison score have the similar properties to the genuine comparison scores.

5.3.3 DET curve

Here, we use DET curves (see Figure 5.6) to illustrate the influence of different degradations on NBIS fingerprint recognition system performance. From the DET curves we can see that the influence of blur degradation is higher than the JPEG degradation (the DET curves for the other two degradations are very similar to

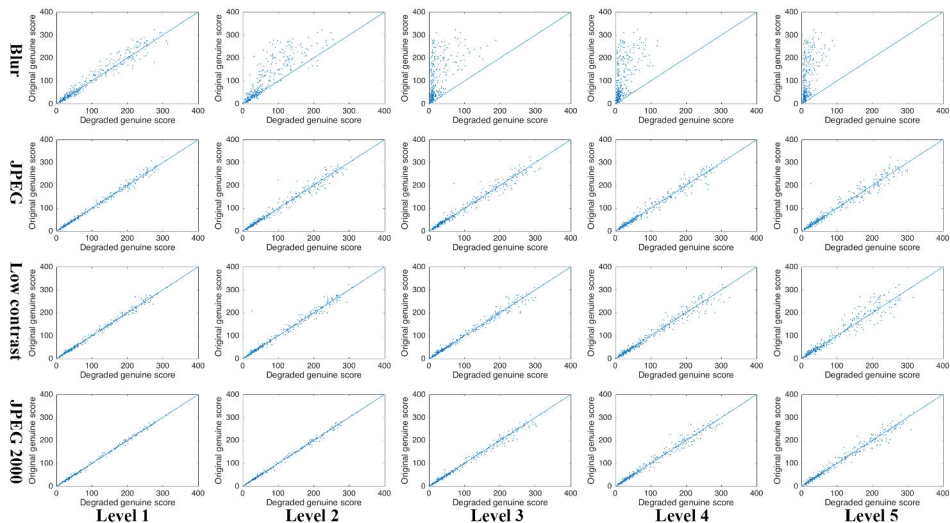


Figure 5.4: The D2O distributive tendency plots for four degradations in five levels. The x axis represents the degraded genuine score while the y axis represents the original genuine score.

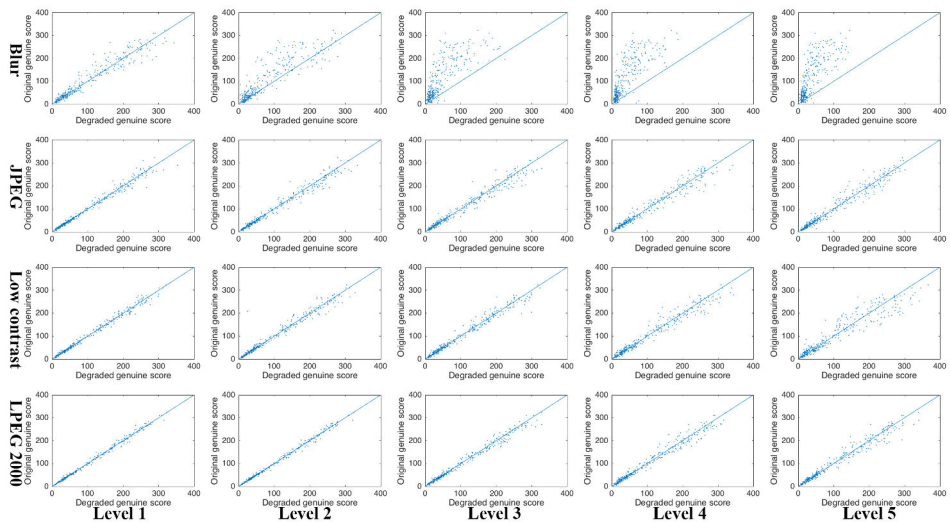


Figure 5.5: The D2D distributive tendency plots for four degradations in five levels. The x axis represents the degraded genuine score while the y axis represents the original genuine score.

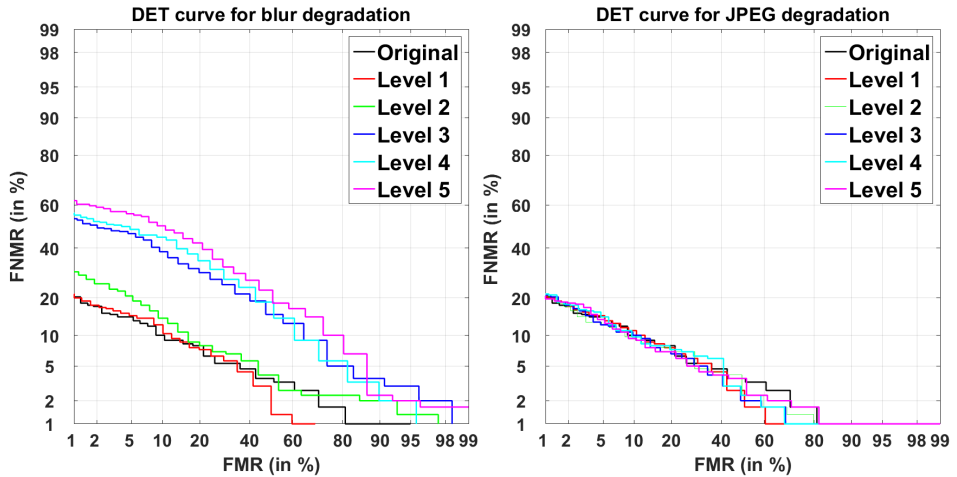


Figure 5.6: DET curve for blur and JPEG degradations in five levels of the NBIS system (D2O).

JPEG), which is very similar to what we observed before. Moreover, system performance has a dramatic decrease between level 2 and level 3 (between the green curve and the blue curve) in blur degradation. This phenomenon can be observed only from DET curves, but not so much from the histogram nor distributive tendency plots.

5.3.4 Equal Error Rate

Finally, we use EER to investigate the influence of the degradations on the NBIS fingerprint system. EER is the value where FNMR and FMR are equal. Lower EER values indicate a better performance of the system. We can compare EER in different degradations and in different levels in order to know the impact of each degradations. Table 5.1 and Table 5.2 are EER values from D2O and D2D comparison scores, respectively. The red color value in the top-left cell is the EER from original comparison scores.

From Tables 5.1 and 5.2 we can learn again that blur degradation has a significant negatively effect on the NBIS fingerprint recognition system. There is a bigger difference of EER between blur level 2 and blur level 3 than between other levels. These two findings are the same as we saw from DET curves. EER for JPEG are fluctuating in both tables. Except the JPEG level 3 EER in Table 5.1, all values for JPEG are greater than the original comparison EER value. It is interesting that the low contrast EER value first decreases from level 1 to level 3 in Table 5.1 (value decrease can be found from level 1 to level 2 in Table 5.2). This phenomenon

Table 5.1: EER of NBIS fingerprint system D2O

0.0885	Level 1	Level 2	Level 3	Level 4	Level 5
Blur	0.0991	0.1229	0.2824	0.2890	0.3100
JPEG	0.0909	0.0932	0.0880	0.0934	0.0896
Low contrast	0.0899	0.0870	0.0866	0.0921	0.1004
JPEG 2000	0.1002	0.1021	0.0953	0.0870	0.0910

Table 5.2: EER of NBIS fingerprint system D2D

0.0885	Level 1	Level 2	Level 3	Level 4	Level 5
Blur	0.0971	0.1089	0.2411	0.2509	0.2871
JPEG	0.0945	0.0927	0.0953	0.0894	0.0893
Low contrast	0.0981	0.0905	0.0965	0.0976	0.0993
JPEG 2000	0.0893	0.0914	0.0987	0.0972	0.0887

could be explained as, when the contrast of the fingerprint decrease, it may reduce some of the noise and also reduce the degradation of low contrast between ridge and valley that caused by wet skin (this is opposite to the dry skin low contrast degradation). But the EER values increase and are greater than the very first levels at the end. EER values are also fluctuated for JPEG 2000 degradation in both tables and no obvious trend of value changes can be found. EER values from low contrast in level 2 and JPEG 2000 in level 4 in Table 5.1 are lower than the original comparison EER value. However, we can observe that EER values have an overall decrease when applying degradations on fingerprint samples.

5.3.5 Fingerprint image quality assessment and its evaluation

Furthermore, we will use one fingerprint image quality assessment method, NFIQ 1.0 [58], to measure the quality of original and degraded fingerprints. Then compare the quality assessment results with the comparison scores to evaluate the performance of NFIQ on selected degradations in five levels.

If we look at Figures 5.7, 5.8, and 5.9 together, we can see that when blur level increases, the comparison scores decrease while more and more fingerprints get higher NFIQ fingerprint quality values (higher NFIQ values indicate lower fingerprint quality). For the rest of degradations, neither comparison scores nor the NFIQ assessment results have significant variation. These are the same as what we observed from previous results. It means that there is a correlation between NFIQ measurement results and the system performance.

In addition, we compute the Spearman's rank correlation coefficient [147] ρ as a

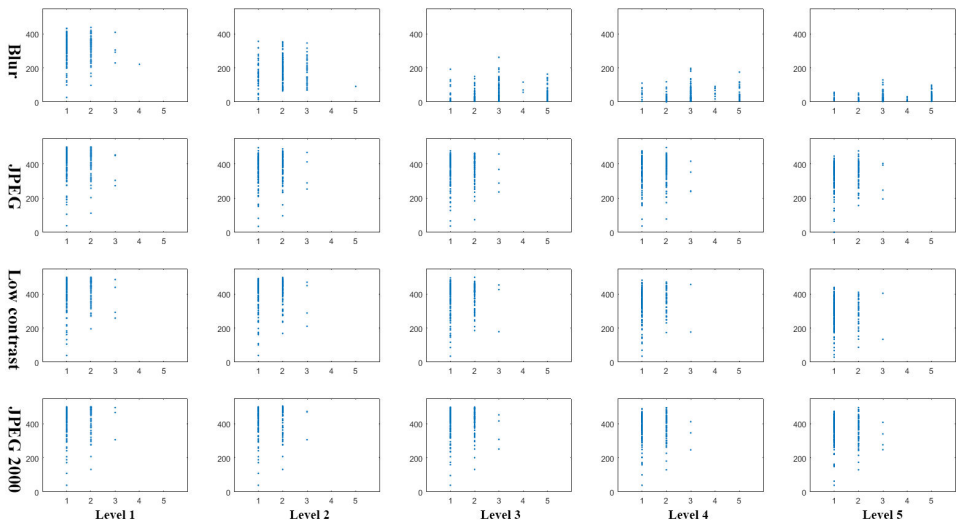


Figure 5.7: The scatter plots of the NFIQ quality measurement values (x axis) versus the comparison scores (y axis) for four degradations in five levels.

Table 5.3: Spearman’s rank correlation coefficients p under four degradations in five levels using the normalized comparison scores as ground truth for NFIQ quality values.

p	Level	Level 2	Level 3	Level 4	Level 5
Blur	0.5192	0.5187	0.4868	0.5110	0.5326
JPEG	0.5246	0.5281	0.5286	0.5059	0.5486
Low contrast	0.5386	0.5286	0.5431	0.5530	0.4937
JPEG 2000	0.5264	0.5406	0.5055	0.5222	0.5090

quantitative method to analyze how well the **NFIQ** quality assessment results and **NBIS** system performance correlate. The results are given in Table 5.3 with four degradations in five levels for generating the normalized comparison scores. The results show that the **NFIQ** fingerprint quality assessment is accurate to assess the samples’ quality in all degradations and levels assuming the normalized comparison score for each sample as the ground truth of sample quality.

5.4 Summary

In order to investigate how fingerprint image degradations influence recognition system performance, we selected four types of degradation, blur, JPEG lossy compression artifacts, low contrast, and JPEG 2000 lossy compression artifacts. Each degradation has been applied to fingerprint samples from part of the FVC 2002 DB1 database in five different levels. The fingerprint recognition system we used

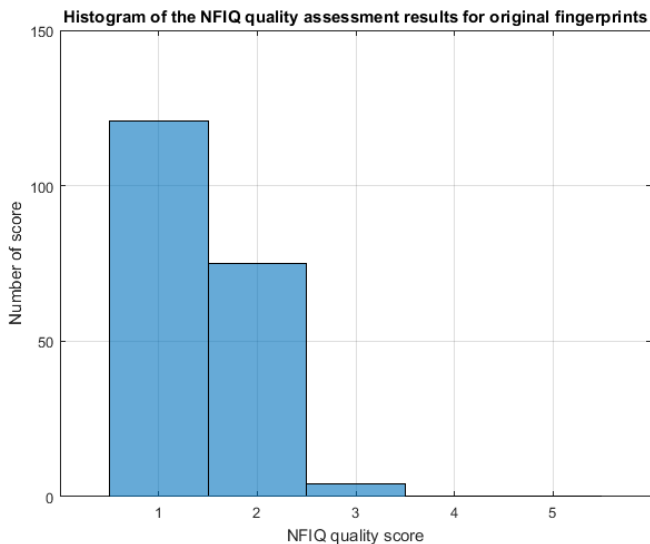


Figure 5.8: The histogram of the NFIQ quality assessment results for original fingerprints.

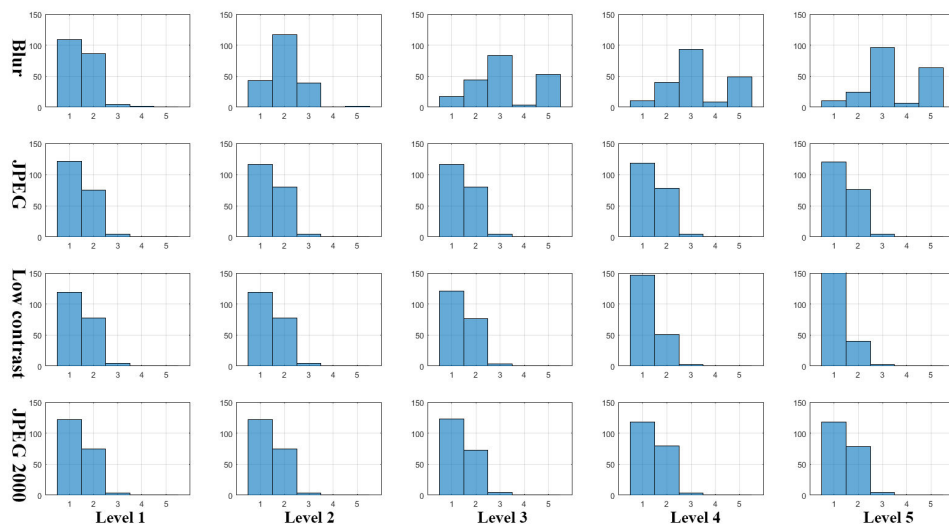


Figure 5.9: The histogram of the NFIQ quality assessment results for four degradations in five levels.

is two applications from **NBIS**: a minutiae detector called MINDTCT and a fingerprint comparison algorithm called BOZORTH3. According to the histograms of comparison scores, distributive tendency plots, **DET** curves generated from experimental results, we learnt that blur degradation significant negatively affect **NBIS** fingerprint recognition system performance based on certain steps between degradation levels. The performance of **NBIS** fingerprint recognition system is not apparently affected by the rest of degradations. However, we did observe **EER** values have an overall decrease when applying degradations on fingerprint samples. There is no big difference between D2O and D2D results. Finally, we employed NFIQ to evaluate the quality of original and degraded fingerprint samples. We generated the scatter plots of the NFIQ quality measurement values versus the comparison scores, the histogram of the NFIQ quality assessment results, and Spearman's rank correlation coefficients using the normalized comparison scores as ground truth for NFIQ quality values. By investigating these results we can analyze how well the NFIQ quality assessment results and **NBIS** system performance correlate. The results show that the NFIQ fingerprint quality assessment is accurate to assess the samples quality in all degradations and levels assuming the normalized comparison score for each sample as the ground truth of sample quality.

Chapter 6

Contactless fingerprint image quality enhancement

As introduced in the proposed framework in Section 4.2, we selected three modalities for the multi-modality quality assessment task: contactless fingerprint, **Visible Wavelength** iris, and face. Contactless fingerprint and **VW** iris have not been widely used in the market, so the number of available biometric systems is limited, especially for those publicly available system. Fortunately, the differences between **Near InfraRed** iris and **Visible Wavelength** iris are not very big, so it is possible to adapt **VW** iris sample images to the biometric systems designed for **NIR** iris [148, 149, 150]. However, the differences between contact-based fingerprint and contactless fingerprint is quite big and the existing contact-based fingerprint biometric systems cannot handle contactless fingerprint images very well. This is due to the low quality of captured contactless fingerprint images. Therefore, in order to be able to use contactless fingerprint images, either new systems have to be developed or introduce contactless fingerprint quality enhancement approaches. Unfortunately, there is few contactless fingerprint quality enhancement approach is publicly available. Those available methods do not perform good enough to improve the quality of contactless fingerprint that result in sufficient system performance. Therefore, we need to investigate whether existing contact-based fingerprint quality enhancement approaches can be used for contactless fingerprint images. In this chapter, we first review existing approaches for contact-based fingerprint enhancement. Then we apply suitable methods to contactless fingerprint to investigate whether the enhanced sample images can achieve sufficient system performance. This chapter is based on Article C [8], which is introduced in Section 1.3.



Figure 6.1: An example of fingerprint ridge ending (left) and bifurcation (right). Figures reproduced from [8].

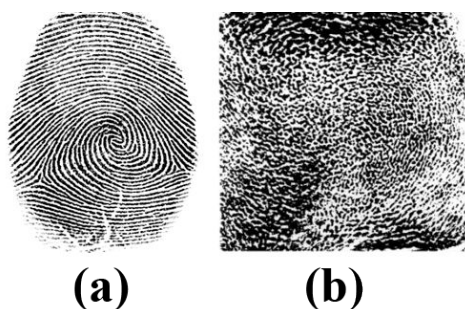


Figure 6.2: An example of (a) high quality fingerprint sample, and (b) low quality fingerprint sample.

6.1 Introduction

Fingerprints are basically oriented texture fields of quasi-periodic and smooth pattern of ridges and valleys having dominant frequency that reside in mid frequency range. Ridge orientation, ridge spatial frequency and more significantly structure of minutiae and their distribution in the fingerprint image, are the main intrinsic features of a given fingerprint. Most commonly used fingerprint recognition systems are based on minutiae matching [151]. Minutiae characteristics are local discontinuities in the fingerprint pattern which represent terminations and bifurcations. A ridge termination is defined as the point where a ridge ends abruptly. A ridge bifurcation is defined as the point where a ridge forks or diverges into branch ridges [152]. Figure 6.1 illustrates an example of ridge ending and bifurcation. A critical step in fingerprint recognition is to automatically and reliably extract minutiae from the given fingerprint samples, which is a challenging mission. The performance of a minutiae extraction method relies heavily on the quality of the given fingerprint samples. Figure 6.2 (a) shows an example of high quality fingerprint sample and an example of fingerprint sample of very low quality, in which minutiae characteristics are totally corrupted, is shown in Figure 6.2 (b).

In order to ensure that the performance of the minutiae extraction method will be robust with respect to the quality of given fingerprint samples, a fingerprint image enhancement approach that can be used for the improvement of the minutiae characteristics clarity is desired.

There are numerous existing fingerprint enhancement and pre-processing methods and different methods have their own strengths. In recent years, the contactless fingerprint recognition is gaining more popularity, due to the enormous development in imaging technology that can be used to overcome the limitations of existing contact based fingerprint sensors. By using contactless fingerprint recognition, a wide range of advantages [82, 84] can be observed, such as: distortion (caused due to the contact pressure) free fingerprint acquisition, free from hygienic problems, no presence of latent fingerprint and so on. However, the use of contactless fingerprint recognition is also very challenging because of (1) uncontrolled illumination and background; (2) scaling is essential since fingerprint samples from same subject are captured at different distance; (3) the depth of field in contactless sensor is small and will result in a non-uniform focus while acquiring the image; (4) low contrast between ridges and valleys increases the challenge to extract minutiae features for accurate fingerprint recognition [153].

6.2 A review of existing contact-based fingerprint quality enhancement approaches

In this Section, we will review ten commonly used contact-based fingerprint enhancement approaches in the research field.

6.2.1 Method 1: fingerprint enhancement by directional Fourier filtering

Sherlock *et al.* [154] proposed a fingerprint enhancement method using directional Fourier filtering technology. Spatial domain technology involves spatial convolution of the image with filter masks. They used Fourier domain filtering and pre-filtered fingerprint in order to convolve the fingerprint samples with filters of full image size, since the 2D fast Fourier transform algorithm can be applied to calculate convolutions efficiently. As a result, such directional filtering is performed using information from the whole fingerprint image rather than from a small neighborhood of the filtered point, and this leads to more effective noise reduction in the filtered image.

In method 1, the fingerprint enhancement has two steps: the first step is filtering and the second step is thresholding. The first step generates a directionally smoothed version of the fingerprint from which most of the non-fingerprint area has been removed. This image has the useful information, such as ridge structure

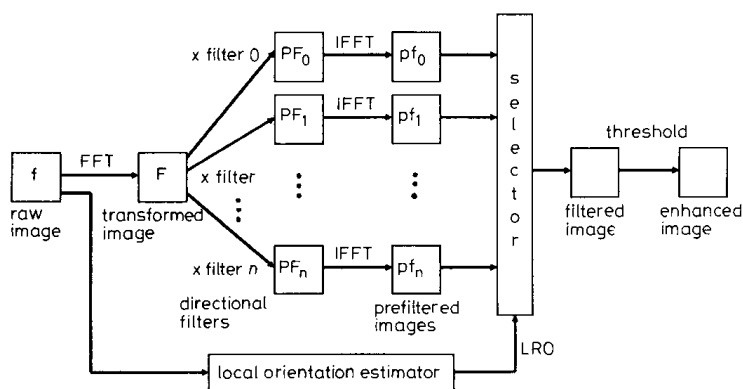


Figure 6.3: Flow chart of the fingerprint enhancement method proposed by Sherlock *et al.* [154].

and minutiae etc. The second step will generate the binarized (enhanced) fingerprint image.

The fingerprint image contains local ridge orientation and ridge spacing. This enhancement method considers this property by filtering the fingerprint image with a position-dependent directional Fourier domain filter whose passband is everywhere matched to the local ridge orientation and spacing [154].

The flow chart of this fingerprint enhancement method is shown in Figure 6.3. Several position-independent Fourier filters have been developed even though the directional filter is position-dependent. Some newly designed directional filters were employed to the original fingerprint image, yielding some directionally filtered images. These steps can be found as 'pre-filtered images' in Figure 6.3.

For each pixel value, the pre-filtered image is then built up by selecting the value which has the shortest distance to the actual ridge orientation. There, the actual ridge orientation was investigated so that the enhancement method can conduct the above mentioned selection procedure. In the end, the binarization will be performed on the directionally filtered fingerprint image by using a local average as the threshold surface in the thresholding step.

Some experimental results from Sherlock's method is illustrated in Figure 6.4. Compared to the original low quality fingerprint sample images, the enhanced images have certain quality improvement and this demonstrates the usefulness of position-dependent Fourier domain filtering in the fingerprint image enhancement technologies.

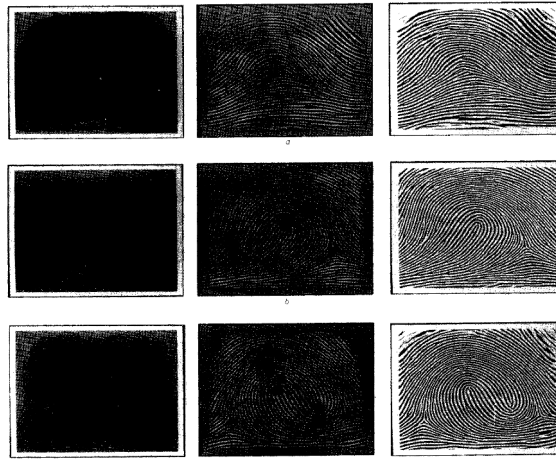


Figure 6.4: Experimental results from method proposed by Sherlock *et al.* [154]. The first column represents the original fingerprint images, the second column represents the directionally filtered images, and the last column represents the thresholded enhanced fingerprint images.

6.2.2 Method 2: fingerprint enhancement by estimating local ridge orientation and frequency

Hong *et al.* [155] presented a fast fingerprint enhancement method that can enhance the clarity of ridge and valley structure of given fingerprint samples by estimating local ridge orientation and frequency. In this method, five core stages have been applied to a fingerprint image:

- **Fingerprint normalization:** an original fingerprint sample image need to be normalized so that it has a pre-specified mean and variance;
- **Fingerprint local orientation estimation:** estimating the local orientation from the normalized original fingerprint sample;
- **Fingerprint local frequency estimation:** calculating fingerprint ridge frequency from the estimated orientation fingerprint sample;
- **Fingerprint region mask estimation:** computing the region mask by classifying each block in the normalized original fingerprint sample into a recoverable or an unrecoverable block (a pixel in the fingerprint image can be either a *non-ridge-and-valley* (unrecoverable) pixel or a *ridge-and-valley* (recoverable) pixel);

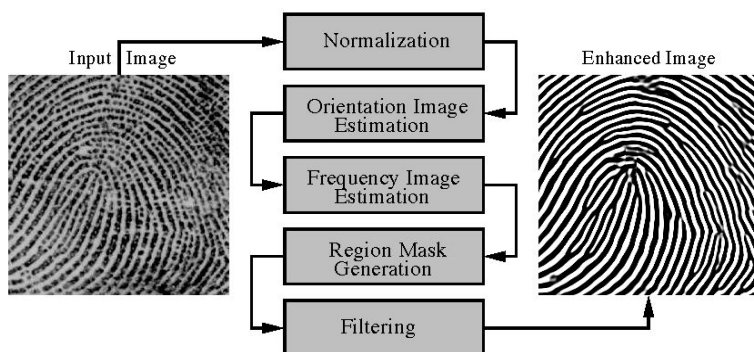


Figure 6.5: The flowchart of core stages of fingerprint enhancement method proposed by Hong *et al.* [155].

- **Fingerprint filtering:** a bank of Gabor filters which is tuned to local ridge orientation and ridge frequency is employed to the recoverable pixels in the normalized original fingerprint sample to generate a final enhanced fingerprint image.

A flowchart of above mentioned five core stages is given in Figure 6.5.

By using this enhancement approach, fingerprint quality enhancement can be observed subjectively by a visual assessment of some enhancement results. These experimental results are shown in Figure 6.6. From the results we can see that after using this approach, the clarity of fingerprint ridge and valley structures have been improved.

6.2.3 Method 3: fingerprint enhancement by using filtering techniques

Greenberg *et al.* [152] proposed two approaches to enhance fingerprint image quality. The first one is applying local histogram equalization, Wiener filtering, and image binarization to a fingerprint image. The second approach will employ a unique anisotropic filter for direct grayscale enhancement for a fingerprint sample.

A binarization-based method

In this first method, the combination of filters and noise removal techniques were applied in both preprocessing and post processing stages. The flowchart of this method is presented in Figure 6.7. As shown in the flowchart, four main steps are applied to the original fingerprint images:

- **Fingerprint contrast enhancement:** a local histogram equalization is employed to the original fingerprint by using a local block process;

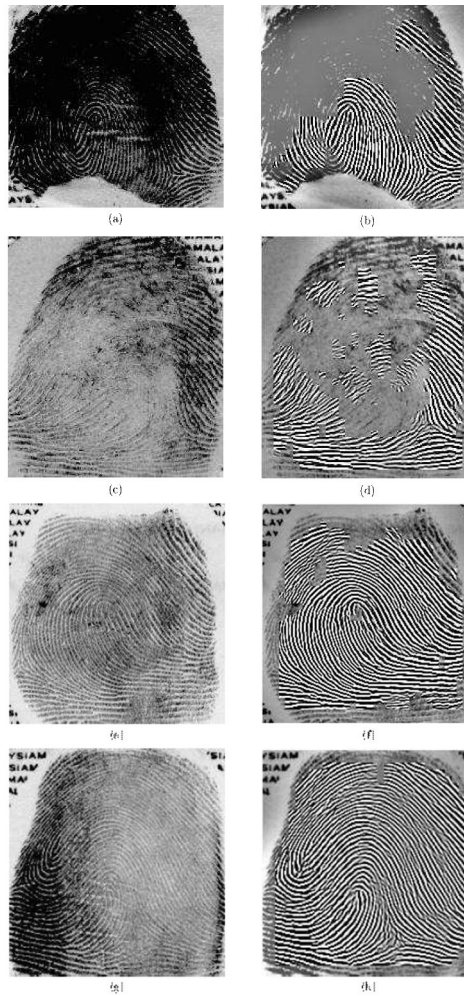


Figure 6.6: Some experimental results from method 2. (a), (c), (e), and (g) represent the original fingerprint samples; (b), (d), (f), and (h) represent the enhanced fingerprint images with recoverable regions superimposed on the corresponding original fingerprint images.

- **Fingerprint Wiener filtering noise removal:** a pixel-wise adaptive Wiener filter is applied to remove noise in the contrast enhanced fingerprint image;
- **Fingerprint binarization and thinning:** the binarization process is conducted by applying an adaptive thresholding. Thinned ridge-lines are obtained using morphological thinning operations;
- **Fingerprint post processing and binary filtering:** a newly designed algorithm is used to remove false ridge lines and gaps between true ridge line.

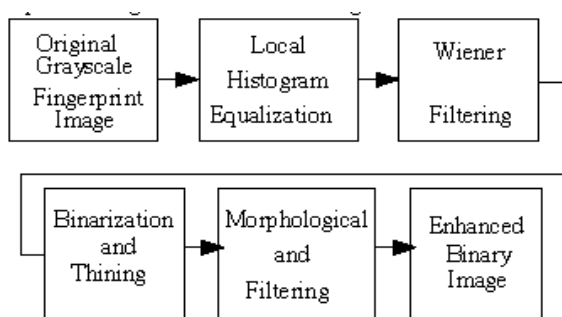


Figure 6.7: Flowchart of the binarization-based method. Figure reproduced from [152].

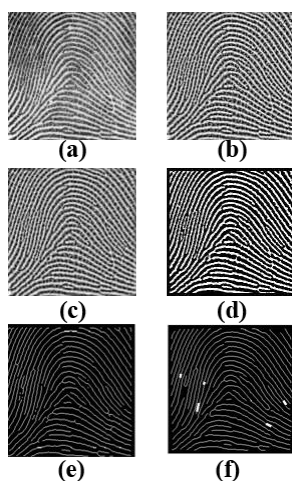


Figure 6.8: Experimental results of the binarization-based method. (a) is the original fingerprint, (b) is the contrast enhanced image, (c) is the Wiener filtered image, (d) is the binarized image, (e) is the thinned image, and (f) is the final enhanced fingerprint sample.

Some experimental results from this first method is given in Figure 6.8.

A direct gray scale enhancement method

Based on fingerprint enhancement algorithms proposed by Maio *et al.*[156] and Hong *et al.*[155], the second method modified the original algorithm from [155] and then improve fingerprint image quality by using an anisotropic filter.

In the first stage, a modification of the Gabor-based algorithm is conducted. In the algorithm proposed by Hong *et al.* [155], a bank of Gabor filters, which is tuned to local ridge orientation and ridge frequency, is applied to the ridge and valley pixels in the normalized input fingerprint image to obtain an enhanced fingerprint



Figure 6.9: Fingerprint enhancement results (clock-wise from up-left): original fingerprint, Gabor filtered image, modified Gabor filtered image, and final anisotropic filter fingerprint.

image. The filters are used as bandpass filters to remove the noise and preserve true ridge and valley structures. Greenberg *et al.* [152] proposed to replace the original scheme by a local gradient operations from [156] which is used for more precise orientation estimation. Then fine tuning of some parameters in the original method results in an efficient and more robust algorithm. In order to decrease the standard deviation in all directions perpendicular to the ridge direction, some values have been modified. The new parameter settings create fewer spurious ridges and make the filter more robust to noise. Next, by cutting down the valid frequency range, wrong estimation of the frequency in blocks which do not form a well-defined frequency is avoided. Finally, for better definition of the block's center, in the ridge frequency algorithm [155], normalizing the image into a block of odd size 15x15 is changed to 16x16.

In the second stage, a new direct gray scale approach based on a unique anisotropic filter [157] is applied. A structure adaptive anisotropic filtering technique is proposed by Yang *et al.* [158] for image filtering. Instead of using local gradients as a means of controlling the anisotropism of filters. It uses both a local intensity orientation and an anisotropic measure to control the shape of the filter. Then they modified this anisotropic filter by shaping the filter kernel and applied it to fingerprint images [157]. The basic idea is that the kernel is allowed to be shaped or scaled according to local features within a given neighborhood. By applying this modified filter, only orientation information is required, thus, it makes this method faster than [155].

Experimental results from this approach illustrate in Figure 6.10.

6.2.4 Method 4: knowledge based fingerprint enhancement

Luo *et al.* [159] presented a rule-based method to enhance fingerprint samples. They employed human knowledge about fingerprints into the enhancement process in the form of rules and simulate what an expert will do to enhance a fingerprint image. In their approach, the skeleton image is used to provide ridge structure for the enhancement of the binary fingerprint. The flowchart of this method is given in Figure 6.11. There are six key rules in this method and the demonstration of each rule is illustrated in Figure 6.9:

- **Bridge processing:** If two bifurcation points A and B are connected by an edge shorter than a predefined threshold, and both points satisfy the loose bridge condition. Then, connect related end points C and D of the other type in the binary image. Delete A and B from the set of bifurcation points. Delete C and D from the set of end points;
- **Breaks processing:** If two end points A and B of the same type faces each other, and their distance is within a predefined threshold, and the line connecting A and B will not cross any edge of the same type as A. Then, connect A and B in the binary image. Delete A and B from the set of end points. Delete the related bifurcation C and D of the other type from the set of bifurcation points. C and D may not satisfy the loose bridge condition and can not be taken as bridge;
- **Complex connection processing:** If A is a cross point, and one of the edges connect with A also connects with a bifurcation point B which satisfies strict bridge condition, and the edge connecting A and B is shorter than a predefined threshold as in rule bridge processing. Then, take A and B as a bridge, do the same as in rule bridge processing. Then set A as a bifurcation point;
- **Blur processing:** If two bifurcation points A and B are connected by an edge shorter than a predefined threshold. Then, connect the related end points C and D of the other type in the binary image. Delete A and B from the set of bifurcation points. Delete C and D from the set of end points;
- **Scar processing:** If a bifurcation point A satisfies strict bridge condition, and two of the edges having the largest between-edge angle among the three edges connect with point A also connects with point B and C respectively. Then, connect A and D, B and E, C and F in the binary image. Break the connection of A and B, A and C. Delete A, B, C, D, E and F from the corresponding point sets;

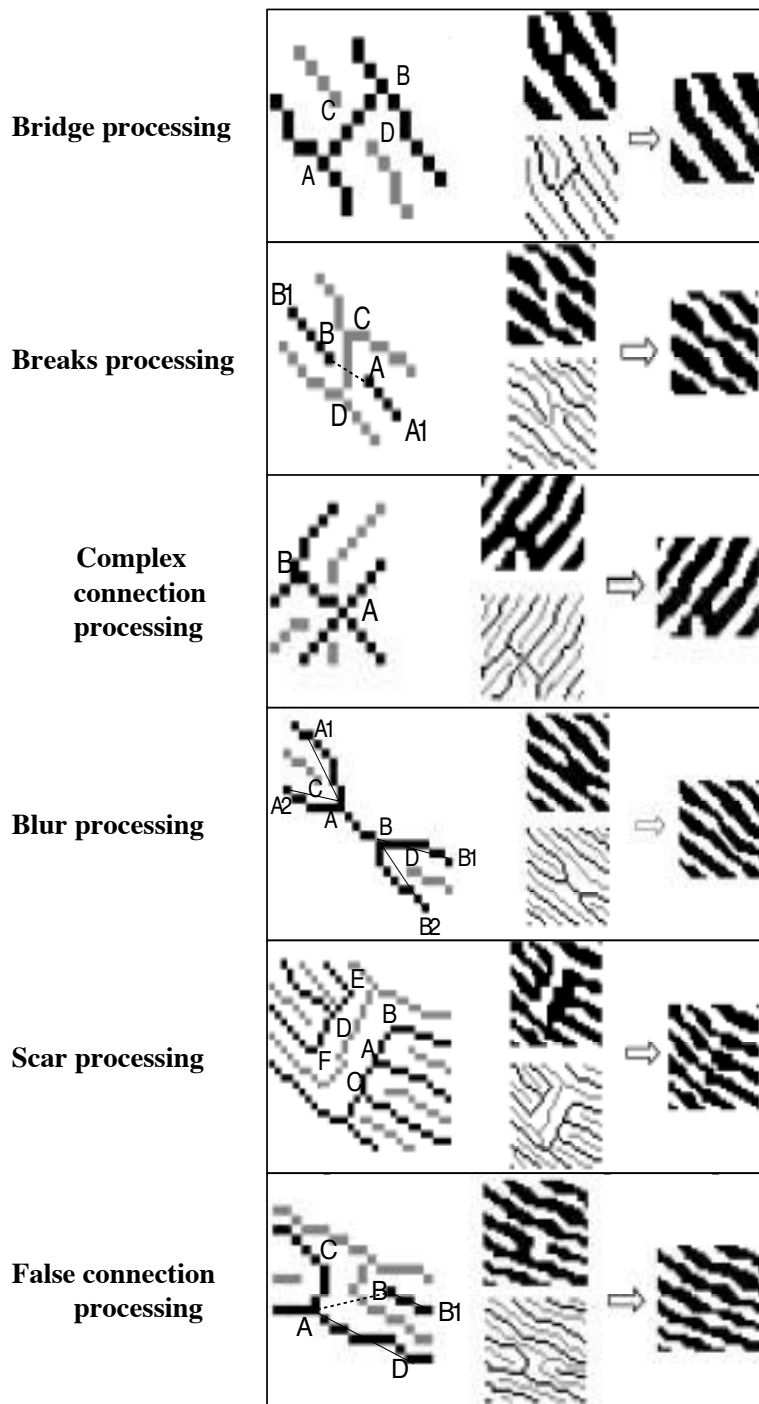


Figure 6.10: Demonstration of rules for method 4. Figures reproduced from Luo *et al.* [159].

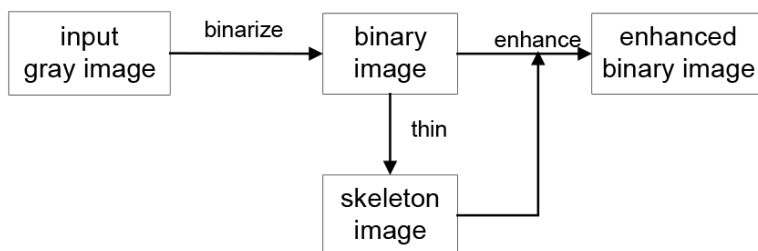


Figure 6.11: Flowchart of fingerprint enhancement method proposed by Luo *et al.*[159].

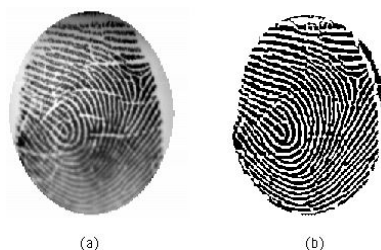


Figure 6.12: An experimental result of fingerprint enhancement method proposed by Luo *et al.*[159]. (a) represents the original fingerprint, and (b) represents the enhanced image.

- False connection processing:** If a bifurcation point A and an end point B of the same type face each other, and their distance is within a predefined threshold, and the line connecting A and B will not cross any edge of the same type as A. Then, connect B and C in the binary image. Break the connection between A and C. Where C is a point in the edge connect with point A, B and C are on the same side of line AD. Delete A and B from the set of Bifurcation points and the set of end points respectively.

An experimental result is shown in Figure 6.12.

6.2.5 Method 5: fingerprint enhancement by using dyadic scale-space

Cheng and Tian [160] presented the scale space theory in the computer vision to enhance the fingerprint. In the enhancement process, decomposing a fingerprint into a set of images and organize the images by a courser to finer scheme. Then a global and integrate interpretation is generated and it makes it possible to avoid the influence of noise to the largest extent. There are four important stages in this method:

- Fingerprint preprocessing with dyadic scale-space:** the algorithm first decomposes the fingerprint image into a series of images to avoid the noise

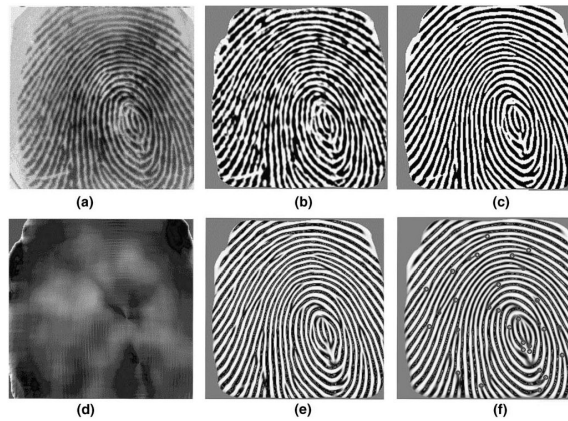


Figure 6.13: Experimental results of fingerprint enhancement method proposed by Cheng and Tian [160]. (a) represents the original fingerprint image, (b) and (c) represents the decomposed images, (d) represents the ridge width image, (e) represents the final enhanced fingerprint, and (f) represents the detected minutiae in the fingerprint after enhancement.

in different scales. Then it combines the images to get a more credible image. Each time reduce the noise to some extent. After several iterations, a preprocessed fingerprint is available;

- **Fingerprint orientation estimation:** after generating a decomposed image, it will be segmented to foreground and background. All the processing after segmentation is applied to the foreground region only, which could reduce computation time. The fingerprint orientation estimation method proposed by Jain *et al.* [161] is then employed;
- **Fingerprint ridge width calculation:** in order to control the iterative times, the mean ridge width is calculated based on the binary fingerprint image;
- **Fingerprint minutiae extraction:** after through several iterations, the binarized fingerprint is produced. Then, fingerprint thinning approach proposed by Naccache and Shinghal [162] is used.

Experimental results in the process dyadic scale-space is presented in Figure 6.13.

6.2.6 Method 6: wavelet based fingerprint enhancement

Because of the spatial localization property and capability to use oriented wavelets such as Gabor wavelet filtering, Hatami *et al.* [163] proposed a two-step fingerprint enhancement algorithm:

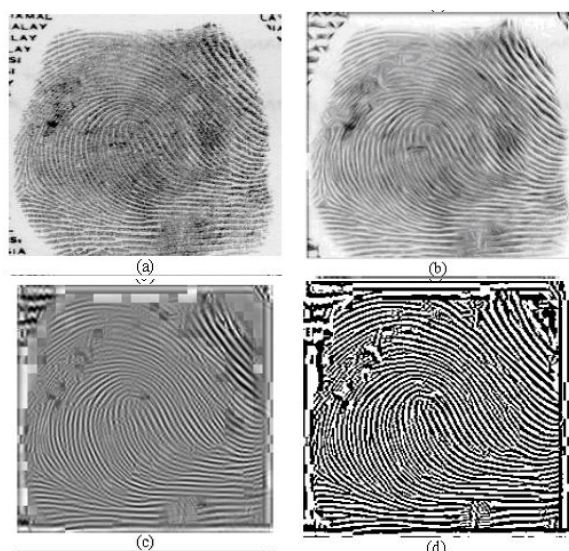


Figure 6.14: An example of experimental result from fingerprint enhancement approach proposed by Hatami *et al.*[163]. (a) is the original fingerprint, (b) is smoothed image, (c) is the Gabor filtered image, and (d) is the final enhanced binary fingerprint image.

Step 1: smoothing

In the first step, first apply a Gaussian filter to the original fingerprint image in equally spaced directions with K directions that is specified by the user. Then divide the filtered image into $K \times K$ blocks, where K is chosen such that frequency of the ridges are retained. Finally, choose the filtered block that is in the orientation of the ridge and reconstruct the final enhanced fingerprint by adjoining these blocks.

Step 2: Gabor wavelet filtering

In the second step, first divide the image to the $K \times K$ blocks. Then apply Gabor wavelet decomposition in the direction orthogonal to direction chosen in the first step and at different scales. Finally, reconstruct the final enhanced fingerprint based on adjoining chosen filtered blocks.

An example of experimental results is given in Figure 6.14.

6.2.7 Method 7: fingerprint enhancement by separable Gabor filter realization

Areekul and Tantaratana [164] proposed to use a separable Gabor filter realization for fast fingerprint enhancement due to 2D Gabor filter can be divided into a 1D

Gaussian band-pass filter and a 1D low-pass filter. In addition, the separation will reduce computation complexity. This method can be divided into three steps. The first step is to define and interpolate consecutive sequences of pixels to form a new image along selected convolutional orientation and its perpendicular with the cheapest complexity as possible. Second, two continuous 1D Gabor filters are generated with suitable parameters, and resampled with uniform space between pixels, which related to resampling image from the first step. Finally, separable convolution can be performed along any selected orientation using tessellated and interleaved patterns.

6.2.8 Method 8: fingerprint enhancement by using short time Fourier transform analysis

Chikkerur *et al.* [165] introduced a new method for fingerprint enhancement based on short time Fourier transform analysis. This approach simultaneously estimates all the intrinsic properties of the fingerprints such as the foreground region mask, local ridge orientation, and local ridge frequency. Four core stages are included in this method (see flowchart of this method in Figure 6.15):

- **Fingerprint short time Fourier transform analysis:** in order to resolve the properties of the image both in space and also in frequency. It is necessary to extend the traditional one dimensional time-frequency analysis to two dimensional image signals to perform short (time/space)-frequency analysis;
- **Fingerprint orientation estimation:** assuming that the orientation θ is a random variable that has the probability density function $p(\theta)$. The expected value of the orientation may then be obtained by using a vector averaging according to

$$E(\theta) = \frac{1}{2} \tan^{-1} \frac{\int_{\theta} \sin(2\theta) d\theta}{\int_{\theta} \cos(2\theta) d\theta}. \quad (6.1)$$

The terms $\sin(2\theta)$ and $\cos(2\theta)$ are used to resolve the orientation ambiguity between orientations $\pm 180^\circ$;

- **Fingerprint ridge frequency estimation:** the average ridge frequency is estimated in a manner similar to the ridge orientation. We can assume the ridge frequency to be a random variable with the probability density function;
- **Fingerprint region mask:** an energy image $E(x, y)$ is defined, where each value indicates the energy content of the corresponding block. The fingerprint region may be differentiated from the background by thresholding the

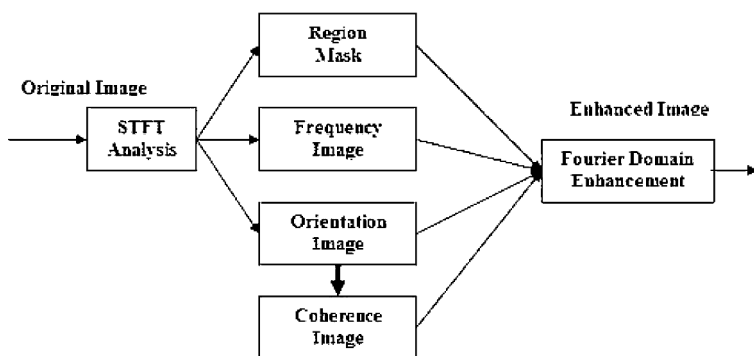


Figure 6.15: The flowchart of the proposed method by Chikkerur *et al.*[165].

energy image. The region mask is obtained by thresholding. Otsu's optimal thresholding [166] technique is used to automatically determine the threshold. The resulting binary image is processed further to retain the largest connected component and binary morphological processing.

Some experimental results are demonstrated in Figure 6.16.

6.2.9 Method 9: fingerprint enhancement by robust orientation field estimation

Yoon *et al.* [167] introduced a fingerprint enhancement method that expects manually marked region of interest and singular points. The core of this method is a robust orientation field estimation algorithm for fingerprint. Short time Fourier transform is used to generate multiple orientation components in each image block. This is followed by a hypothesize-and-test paradigm based on randomized RANSAC, which obtains a group of hypothesized orientation fields. There are four key steps in this approach:

- **Manual markup of region of interest and singular points:** singularities observed in almost all the fingerprints fall into one of the following categories: (i) no singularity (e.g. arch type of fingerprints), (ii) one core and one delta (e.g. loop and tented arch type), and (iii) two cores and two deltas (e.g. whorl and twin loop type);
- **Fingerprint orientation element estimation:** a popular approach to compute the orientations in a block is based on the short time Fourier transform [165], which detects the peaks in the magnitude spectrum of the local image;

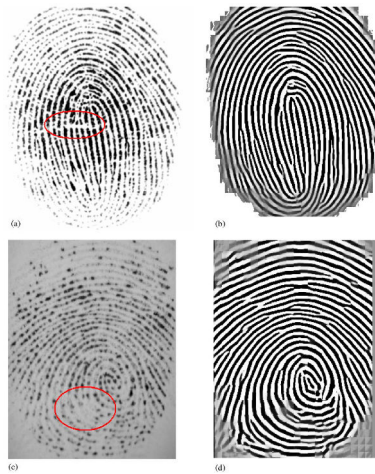


Figure 6.16: Experimental results from method proposed by Chikkerur *et al.*[165]. The left column is original fingerprint images and the right column is images after enhancement.

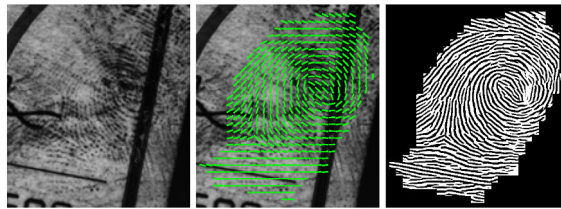


Figure 6.17: An example of experimental result from method proposed by Yoon *et al.* [167]. The left first image is original fingerprint images and the middle image is orientation estimated fingerprint, and the last image is the final enhanced binary fingerprint.

- **Fingerprint orientation field estimation:** in this step, a two-level approach is used to estimate the orientation field of a fingerprint: (i) the orientation elements in a neighborhood are merged into an orientation group whose elements are compatible with each other, and (ii) a global orientation field is robustly estimated by a set of orientation groups;
- **Fingerprint filtering:** the last step in this method is using Gabor filtering technique to enhance the orientation estimated fingerprint image.

An example of the experimental result is shown in Figure 6.17.

6.2.10 Method 10: fingerprint enhancement by orientation field estimation

A similar fingerprint enhancement approach comparable to Yoon *et al.* [167] is proposed by Feng *et al.* [168]. The main motivation behind this method is that a major limitation of conventional algorithms is that they do not utilize prior knowledge of the ridge structure in fingerprints. Inspired by spelling correction techniques in natural language processing, a novel fingerprint orientation field estimation algorithm based on prior knowledge of fingerprint structure is presented. The prior knowledge of fingerprints using a dictionary of reference orientation patches, which is constructed using a set of true orientation fields, and the compatibility constraint between neighboring orientation patches is introduced here. Orientation field estimation for fingerprints is posed as an energy minimization problem, which is solved by loopy belief propagation.

From Figure 6.18 we can observe that this method has an off-line dictionary construction stage and an on-line orientation field estimation stage. In the off-line stage, a set of good quality fingerprints of various pattern types (arch, loop, and whorl) are manually selected and their orientation fields are used to construct a dictionary of orientation patches. In the on-line stage, given a fingerprint image, its orientation field is automatically estimated using the following steps:

- **Fingerprint pre-estimation:** the initial orientation field is obtained using a local orientation estimation method, such as local Fourier analysis;
- **Fingerprint dictionary lookup:** the initial orientation field is divided into overlapping patches. For each initial orientation patch, its six nearest neighbors in the dictionary are viewed as candidates for replacing the noisy initial orientation patch;
- **Fingerprint context-based correction:** the optimal combination of candidate orientation patches is found by considering the compatibility between neighboring orientation patches.

Some experimental results are illustrated in Figure 6.19.

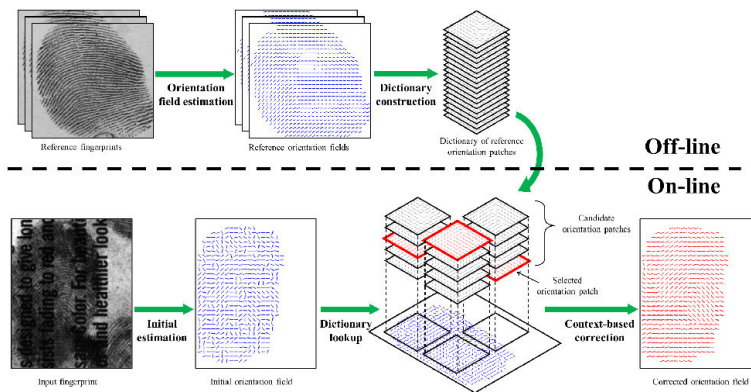


Figure 6.18: The flowchart of the proposed method by Feng *et al.*[168]. This approach contains an off-line dictionary construction stage and an on-line orientation field estimation stage.

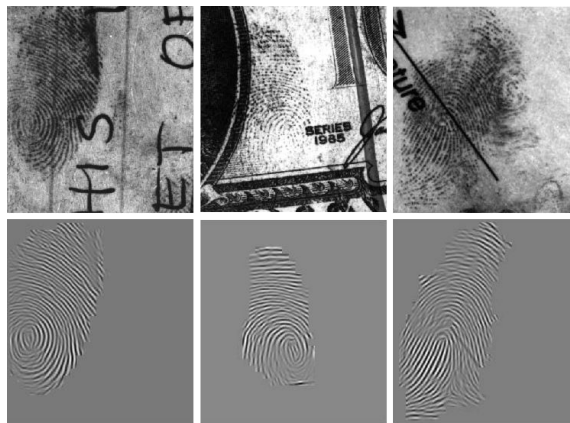


Figure 6.19: Some experimental results from the method proposed by Feng *et al.*[168]. The top row represents the original fingerprint images and the bottom row represents the enhanced fingerprints corresponding to the original ones.

6.3 Experiment of applying contact-based fingerprint enhancement methods on contactless fingerprint images

In the previous section we introduced 10 image enhancement techniques for contact-based fingerprint. Due to the lack of fingerprint enhancement approaches for contactless samples, it would be interesting to investigate the performance of these contact-based methods on contactless fingerprint images. In this section, we select three above listed methods which are suitable for contactless fingerprint and conduct a test experiment by applying them to contactless fingerprint images. The database used for this experiment is the fingerprint subset from GC² database. The selected approaches are: method 2 proposed by Hong *et al.* [155], method 3 proposed by Greenberg *et al.* [152], and method 10 proposed by Feng *et al.* [168]. We will compare these three methods in two aspects, the first aspect is the performance of enhancement under human visual opinion, and the second aspect is computation speed.

6.3.1 Comparing enhancement performance between three methods

In order to compare the performance of the three methods, except the segmented original RGB fingerprint we generate a binary fingerprint image by using a commonly used image normalization and binarization protocol. Some examples of binary fingerprints are presented in Figure 6.20. From the binary images we can see that without any fingerprint enhancement, almost no ridge and valley structure can be observed. These fingerprint samples can hardly be used for biometric recognition. So it is necessary to enhance the fingerprint samples especially for contactless images.

After applying three enhancement approaches to the segmented fingerprint in our database, some experimental results can be found in Figures 6.21, 6.22, and 6.23 representing the enhancement results from reflex camera, smartphone, and [Light Field Camera](#), respectively.

The performance of three enhancement approaches can be assessed subjectively by our visual inspection of these experimental results. It is obvious to see that after employing three enhancement approaches, the quality of contactless fingerprint image has been significantly improved. The ridge and valley structure can be easily used to conduct the minutiae extraction and biometric recognition. However, due to the low contrast between ridge and valley in the contactless fingerprint images, all three methods cannot enhance and estimate the entire fingerprint ridge orientation (the black holes represent the ridge and valley structure in certain area is too weak to be enhanced). On the other hand, the number of black holes in method 10 is less than method 2 and method 3, but method 2 has more black holes

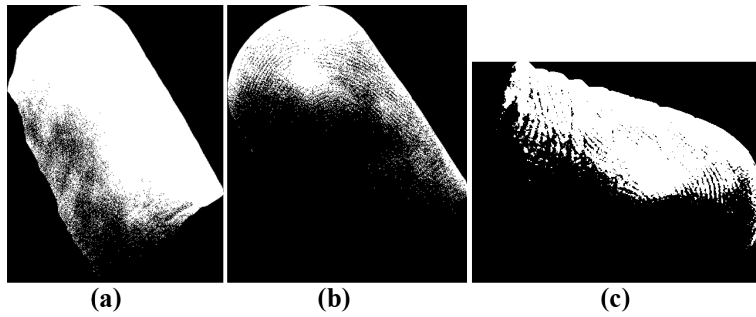


Figure 6.20: Examples of binary fingerprint obtained directly from segmented original fingerprints.(a) represents the binary fingerprint from reflex camera, (b) represents the binary fingerprint from smartphone, and (c) represents the binary fingerprint from Light field camera.

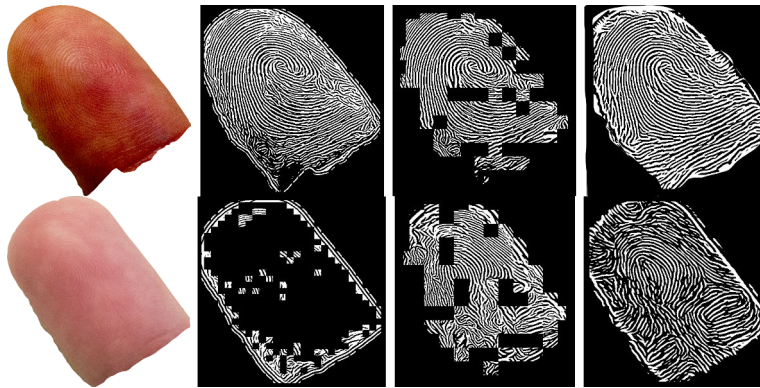


Figure 6.21: Enhancement results from reflex camera. The first column is the segmented original RGB fingerprint, the second column is the results of method 2, the third column is the results of method 3, and the last column is the results of method 10.

than the other two approaches. Even though the quality of contactless fingerprint images have been improved, but the accuracy of estimated ridge orientation is still not very high.

6.3.2 Comparing computation speed between three methods

Additionally, we calculate the average computation time for all contactless fingerprint samples in our database as an indicator to represents the speed between three methods. The results are demonstrated in Table 6.1. From the table we can see that method 3 is the fastest method and method 10 is slower than the other two approaches.

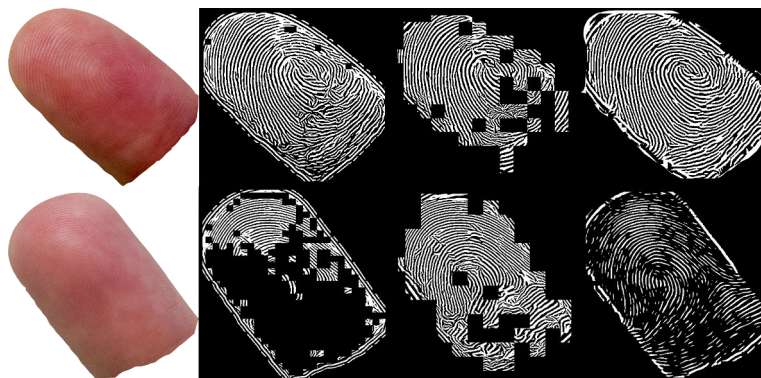


Figure 6.22: Enhancement results from smartphone. The first column is the segmented original RGB fingerprint, the second column is the results of method 2, the third column is the results of method 3, and the last column is the results of method 10.

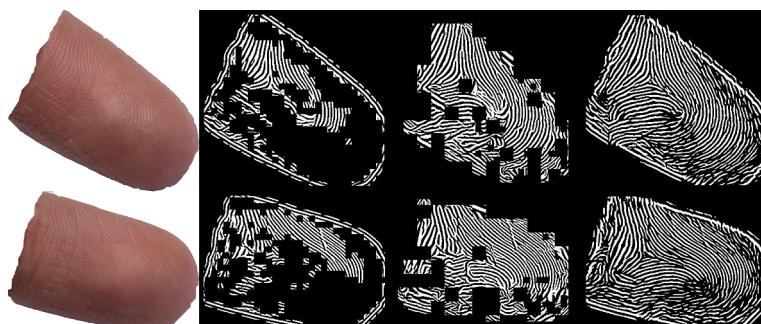


Figure 6.23: Enhancement results from LFC. The first column is the segmented original RGB fingerprint, the second column is the results of method 2, the third column is the results of method 3, and the last column is the results of method 10.

Table 6.1: Average computation time per image for three enhancement methods

Method	Time (seconds)
Method 2 by Hong <i>et al.</i> [155]	2.55
Method 3 by Greenberg <i>et al.</i> [152]	1.26
Method 10 by Feng <i>et al.</i> [168]	7.53

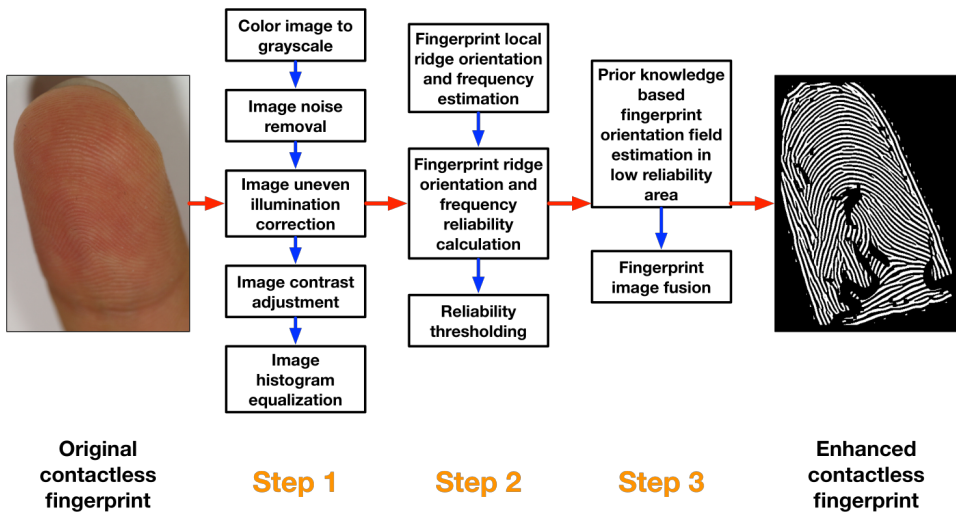


Figure 6.24: The framework of the proposed 3-step contactless fingerprint enhancement approach.

6.4 An improved 3-step contactless fingerprint image enhancement method

From the experiment results presented in the last section, three selected methods for contact-based fingerprint enhancement will have an unsatisfactory performance on contactless fingerprint samples. Therefore, we propose a 3-step contactless fingerprint enhancement approach, which is a combination of ordinary and optimized contact-based fingerprint enhancement methods.

The first step converts the RGB original contactless fingerprint image to grayscale and then applies ordinary image enhancement methods (e.g. noise removal, illumination correction, etc.) to the grayscale sample. After the first step, the fingerprint image will be enhanced by using an optimized local ridge orientation and frequency estimation method proposed by Hong *et al.* [155]. The last step is using a prior knowledge based fingerprint orientation field estimation approach [168] to process low reliability areas that cannot be estimated in step two. Finally, we fuse the enhancement results from step two and three as the final result. The framework of the proposed method is given in Figure 6.24, more details about each step will be presented in the following sub-sections.

6.4.1 Step 1: Color-grayscale fingerprint image enhancement

In this step, we first convert the RGB contactless fingerprint to the grayscale image by forming a weighted sum of the R, G, and B components [169]:

$$F_g = 0.2989 \times F_r + 0.5870 \times F_g + 0.1140 \times F_b \quad (6.2)$$

where F_g represents the grayscale fingerprint and F_r, F_g, F_b represent the R, G, B components of the original RGB fingerprint. Then a 2D adaptive noise-removal filtering [170] which lowpass-filters a grayscale image that has been degraded by constant power additive noise. This filter estimates the local mean μ and variance σ around each pixel:

$$\mu = \frac{1}{NM} \sum_{n_1, n_2 \in \eta} a(n_1, n_2) \quad (6.3)$$

and

$$\sigma^2 = \frac{1}{NM} \sum_{n_1, n_2 \in \eta} a^2(n_1, n_2) - \mu^2, \quad (6.4)$$

where η is the N -by- M local neighborhood of each pixel in the fingerprint. The filter then creates a pixelwise Wiener filter using these estimates:

$$b(n_1, n_2) = \mu + \frac{\sigma^2 - v^2}{\sigma^2} (a(n_1, n_2) - \mu), \quad (6.5)$$

where v^2 is the noise variance. If the noise variance is not given, the filter uses the average of all the local estimated variances. After the noise removal, a Top-Hat filtering [171] is applied to correct uneven illumination. Next, we adjust the fingerprint contrast by finding limits to stretch contrast. Finally, the contrast-limited adaptive histogram equalization [172] is used to enhance the fingerprint. An example of using the first step fingerprint enhancement approach is illustrated in Figure 6.25.

6.4.2 Step 2: Fingerprint local ridge orientation and frequency estimation in high reliability area

In this step, an optimized fingerprint local ridge orientation and frequency estimation method [155] will be applied to the enhanced contactless fingerprint from step 1. There are five stages in this step:

Normalization

Let $F(i, j)$ represents the gray level value at pixel (i, j) in the fingerprint, M and V represent the image mean and variance of F , respectively, and N is the normalized fingerprint. Therefore, the normalization can be given as:

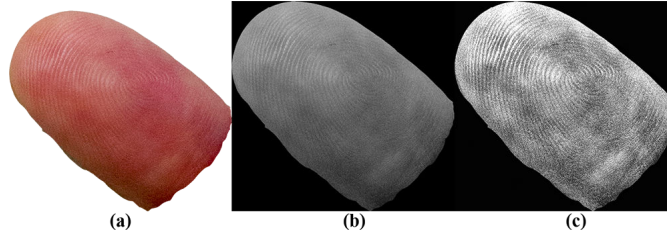


Figure 6.25: An example of the enhancement result after the first step. (a) represent the original RGB contactless fingerprint, (b) represents the grayscale fingerprint, and (c) represent the enhanced fingerprint after the step 1.

$$N(i, j) = \begin{cases} M_d + \sqrt{\frac{V_d(F(i, j) - M)^2}{V}}, & \text{if } F(i, j) > M \\ M_d - \sqrt{\frac{V_d(F(i, j) - M)^2}{V}}, & \text{otherwise} \end{cases} \quad (6.6)$$

where M_d and V_d represent the desired mean and variance values respectively.

Orientation estimation

The fingerprint orientation image is an intrinsic property of the fingerprint images and defines invariant coordinates for ridges and valleys in a local neighborhood. Several methods have been developed to estimate image local orientation [173, 174, 175, 176]. Here, we optimize the original mean square orientation estimation method:

- Divide N into 4×4 size blocks;
- Calculate the gradients $\partial_x(i, j)$ and $\partial_y(i, j)$ at each pixel (i, j) . The Sigma of the Gaussian weighting used to sum the gradient moments is optimized as 10;
- Estimate the local orientation of each block centered at pixel (i, j) using:

$$\nu_x(i, j) = \sum_{u=i-w/2}^{i+w/2} \sum_{v=j-w/2}^{j+w/2} 2\partial_x(u, v)\partial_y(u, v), \quad (6.7)$$

$$\nu_y(i, j) = \sum_{u=i-w/2}^{i+w/2} \sum_{v=j-w/2}^{j+w/2} (\partial_x^2(u, v)\partial_y^2(u, v)), \quad (6.8)$$

$$\theta(i, j) = \frac{1}{2} \tan^{-1} \left(\frac{\nu_y(i, j)}{\nu_x(i, j)} \right), \quad (6.9)$$

where $\theta(i, j)$ is the least square estimate of the local ridge orientation;

- Because of the presence of noise, corrupted ridge and valley structures, minutiae, and so on, the orientation image needs to be converted into a continuous vector field, which is given as:

$$\phi_x(i, j) = \cos(2\theta(i, j)), \quad (6.10)$$

$$\phi_y(i, j) = \sin(2\theta(i, j)), \quad (6.11)$$

where ϕ_x and ϕ_y are the x and y components of the vector field respectively;

- Finally, we can compute the local ridge orientation at (i, j) by employing:

$$O(i, j) = \frac{1}{2} \tan \left(\frac{\phi_x(i, j)}{\phi_y(i, j)} \right). \quad (6.12)$$

With such equation, a smooth orientation field estimate can be generated and the Sigma of the Gaussian used to smooth the final orientation vector field is optimized as 5.

Orientation reliability calculation

If the ridge and valley structure in the given contactless fingerprint has a high level of degradation (e.g. blurred, very low contrast), the error rate of the orientation estimation will increase significantly. Therefore, we calculate the reliability of the estimated orientation and then apply another method (in step 3) on those areas with low reliability values.

Here we calculate the area moment about the orientation axis (this will be the minimum moment) and an axis perpendicular (which will be the maximum moment). The reliability measure is given by:

$$Re = 1 - \frac{\zeta_{min}}{\zeta_{max}}, \quad (6.13)$$

where Re is the reliability and ζ_{min} and ζ_{max} represent the minimum and the maximum moment, respectively. The reasoning being that if the ratio of the minimum to maximum moments is close to one we have little orientation information.

Ridge frequency estimation

Let N represents the normalized fingerprint and O represents the estimated orientation fingerprint, then the x-signature can be calculated by:

$$Q[k] = \frac{1}{w} \sum_{d=0}^{w-1} N(u, v), \quad k = 0, 1, \dots, l-1, \quad (6.14)$$

$$u = i + \left(d - \frac{w}{2}\right) \cos O(i, j) + \left(k - \frac{l}{2}\right) \sin O(i, j), \quad (6.15)$$

$$v = j + \left(d - \frac{w}{2}\right) \sin O(i, j) + \left(\frac{l}{2} - k\right) \cos O(i, j), \quad (6.16)$$

Let $T(i, j)$ be the average number of pixels between two consecutive peaks in the x-signature, then the ridge frequency $\Omega(i, j)$ is $\frac{1}{T(i, j)}$. The window length used to identify peaks is optimized as 9, the minimum and maximum ridge wavelengths, in pixels, is optimized as 1 and 50 respectively.

Gabor filtering

Since Gabor filters have both frequency-selective and orientation-selective properties and have optimal joint resolution in both spatial and frequency domain [177, 178]. So it is necessary to employ Gabor filters as bandpass filters to remove undesired noises and preserve the true ridge and valley structure.

Finally, we use the orientation reliability values masking the Gabor filtered fingerprint and an binarized fingerprint within reliability over 50% is obtained after the step 2 enhancement. An example of the enhancement results introduced in step 2 is given in Figure 6.26.

6.4.3 Step 3: Prior knowledge based latent fingerprint orientation field estimation in low reliability area

After step 2, we will apply a prior knowledge based fingerprint orientation field estimation method on the low reliability area (reliability lower than 50%) which is obtained from the previous step. Thanks to the latent fingerprint enhancement method, we could consider the low reliability area as latent fingerprint due to its low quality of ridge and valley structure and biometric information.

Dictionary creation

A number of orientation patches with the same size are included in the dictionary. An orientation patch has $e \times e$ orientation elements and an orientation element refers to the dominant orientation in a block of size 16×16 pixels. These orientation patches are generated from a group of high quality reference fingerprint

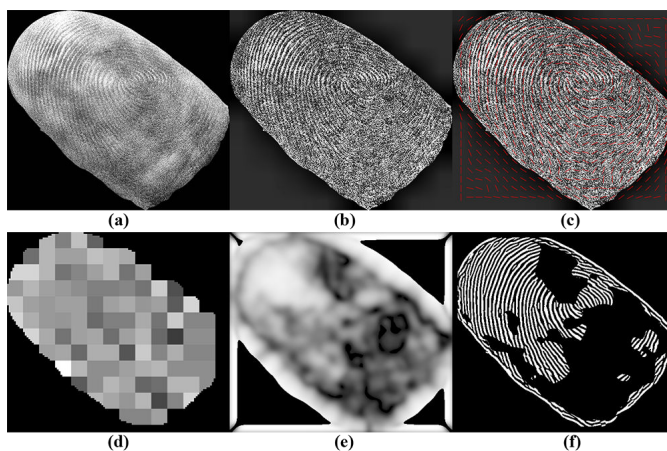


Figure 6.26: An example of the enhancement result after the second step. (a) represents the enhanced fingerprint after the step 1, (b) represents the normalized fingerprint, (c) represents the estimated orientation fingerprint, (d) represents the estimated ridge frequency fingerprint, (e) represents the orientation reliability, and (f) represents the final masked Gabor filtering fingerprint.

samples and the orientation elements are estimated by VeriFinger 6.2 SDK [179]. Since the orientation elements of the latent fingerprint are unknown, so each orientation patch is rotated by 21 different angles $\{i \cdot 5^\circ, -10 \leq i \leq 10\}$ to generate additional orientation patches.

Fingerprint orientation pre-estimation

The fingerprint orientation field pre-estimation is obtained using a simple method proposed by Jain *et al.* [180]. The dominant orientation in a 16×16 block is computed by detecting the peak in the magnitude spectrum of the local image. Due to the poor quality of latents, the initial orientation field is usually very noisy. However, orientation field smoothing should be avoided in this stage because correct orientation elements may even be degraded by strong noise in the neighboring regions. The problem of correcting noisy orientation field is left to the later stages, which utilize prior knowledge of fingerprints.

Fingerprint dictionary lookup

Given an initial orientation patch that contains at least one foreground block, a list of candidate reference orientation patches from the dictionary need to be retrieved, which are sorted according to their similarity with the initial patch. In order to retrieve the correct orientation patches at high rank, proper similarity measure and retrieval strategy need to be designed.

The similarity $S(\alpha, \beta)$ between an initial orientation patch α and a reference orientation patch β is computed by comparing corresponding orientation elements. Let n_i is the number of orientation elements in the initial orientation patch. Let n_r is the number of orientation elements whose differences are less than a predefined threshold (empirically set as $\pi/12$). The similarity between two patches then is given as:

$$S(\alpha, \beta) = \frac{n_r}{n_i} \quad (6.17)$$

Orientation field correction is posed as a combinational optimization problem. The total number of possible solutions is $n_l^{n_p}$, where n_l is the length of candidate list, and n_p is the number of patches in the input fingerprint.

Fingerprint context-based correction

After a dictionary lookup, a list of $c_i (1 \leq c_i \leq n_l)$ candidate orientation patches are obtained. $\beta_i = \{\beta_{i,1}, \beta_{i,2}, \dots, \beta_{i,c_i}\}$, for an initial orientation patch α_i . Contextual information needs to be utilized in order to resolve the ambiguity. Then this issue will be figured out by searching for a set of candidates r^* , which minimizes an energy function $E(r)$:

$$E(r) = E_s(r) + \omega_c E_c(r) \quad (6.18)$$

where $E_s(r)$ represents the similarity term, $E_c(r)$ represents the compatibility term, and ω_c represents the weight of compatibility term. The similarity term is given as:

$$E_s(r) = \sum_{i \in V} (1 - S(\alpha_i, \beta_{i,r_i})) \quad (6.19)$$

where V is the set of foreground patches and $S(\cdot)$ is defined in Equation 6.17. The compatibility term is given as:

$$E_c(r) = \sum_{(i,j) \in N} (1 - C(\beta_{i,r_i}, \beta_{j,r_j})) \quad (6.20)$$

where N represents the set of adjacent foreground patches which are four-connected neighbors. The compatibility between two neighboring orientation patches β_{i,r_i} and β_{j,r_j} is measured by the similarity of orientation in the overlapping blocks. Let $\{\theta_n\}_{n=1}^{N_o}$ and $\{\lambda_n\}_{n=1}^{N_o}$ are the set of orientation is the N_o overlapping blocks of two orientation patches. Finally, the compatibility is defined as:

$$C(\beta_{i,r_i}, \beta_{j,r_j}) = \frac{1}{N_o} \sum_{n=1}^{N_o} |\cos(\theta_n - \lambda_n)| \quad (6.21)$$

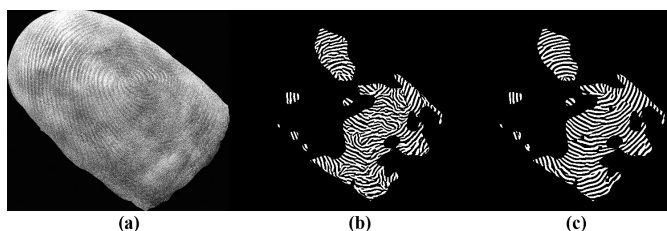


Figure 6.27: An example of the experimental result from step 3. (a) represents the enhanced fingerprint after the step 1, (b) represents the low reliability area enhancement result by step 2, (c) represents the low reliability area enhancement result by the third step.

An example of the experimental result from step 3 and the comparison of low reliability area enhancement results between step 2 and step 3 are given in Figure 6.27. It is very obvious that the approach introduced in step 3 has a better performance in the low reliability area. The reason of why to not use step 3 to enhance the entire contactless fingerprint is that the method presented in step 3 has good performance only on low reliability area. Our experimental results shown that if we apply Feng *et al.* [168]’s method on high reliability area, the enhancement results is not as good as Hong *et al.* [155]’s method.

Finally, we fuse the high reliability area orientation estimation results from step 2 and low reliability area orientation estimation results from step step 3 and then apply Hong *et al.* [155]’s method on the fused enhancement result.

6.4.4 Performance evaluation of proposed method

Both subjective and objective assessments are conducted to evaluate the performance of the proposed contactless fingerprint enhancement approach. We consider human visual assessment as the subjective evaluation method, meanwhile, minutiae extraction and biometric system performance are two indicators for objective evaluation. In order to conduct the evaluation process, we use contactless fingerprint modality from GC² database. However, due to the insufficient quality, fingerprint images taken by LFC cannot be recognized by the enhancement methods. Thus, we only use fingerprint images taken by smartphone and reflex camera.

Figure 6.28 illustrates the enhancement results for smartphone and reflex camera as an example from three methods: Hong *et al.* [155]’s method, Feng *et al.* [168]’s method, and the proposed approach. By comparing the results we can see that, the proposed method has an obvious improvement over the other two. The enhanced fingerprint samples have very clear ridge and valley structure, especially the orientation and directional field presented in the proposed enhancement approach is better than the other methods.

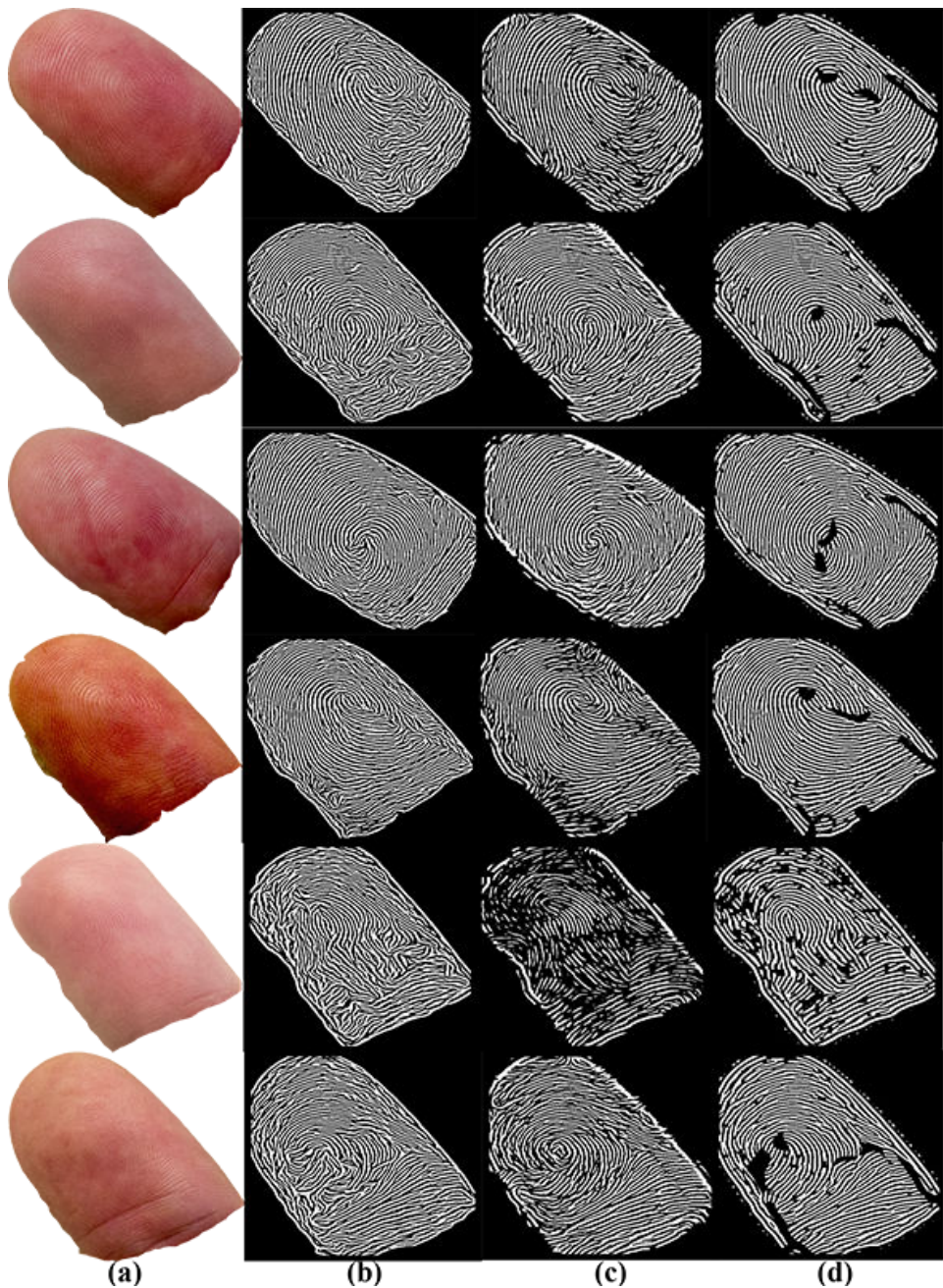


Figure 6.28: The comparison between three fingerprint enhancement methods. The first three rows are fingerprint samples taken by smartphone, the last three rows are fingerprint samples acquired by reflex camera. Column (a) represents the original RGB contactless fingerprint, column (b) represents the enhancement results from Hong *et al.* [155]'s method, column (c) represents the enhancement results from Feng *et al.* [168]'s method, and column (d) is the enhancement results from proposed method.

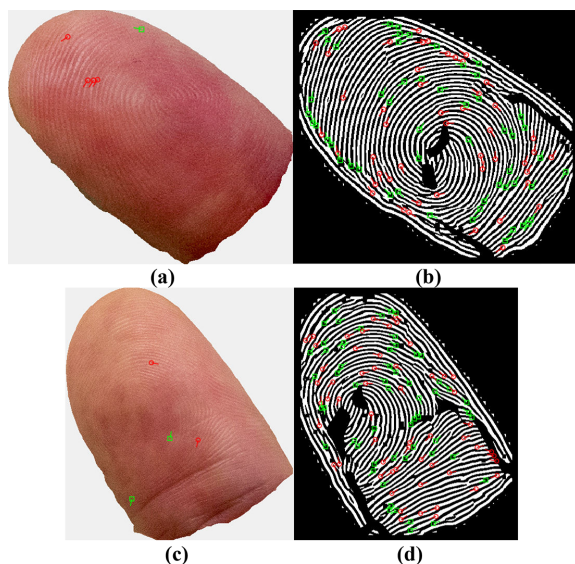


Figure 6.29: Examples of the minutiae extraction results from (a) original contactless fingerprint of sample S1 (5 minutiae detected); (b) enhanced contactless fingerprint of sample S1 (105 minutiae detected); (c) original contactless fingerprint of sample S2 (4 minutiae detected); (d) enhanced contactless fingerprint of sample S2 (112 minutiae detected).

We use [National Institute of Standards and Technology Biometric Image Software](#) to detect and extract minutiae from the original contactless fingerprint and the enhanced fingerprint obtained from the proposed approach. This system also includes minutiae quality assessment based on local image conditions. The minutiae extraction results are shown in Figure 6.29. The minutiae quality threshold is set to 0.3 for original contactless fingerprint and 0.7 for enhanced fingerprint sample. From the Figure 6.29 we can see that, very few minutiae (4 or 5) can be detected by the detector from the original contactless fingerprint due to the low contrast between ridge and valley and out of focus. After the enhancement, the number of detected minutiae (high quality level) has a significant increasing (105 and 112). The average number of detected minutiae is given in Table 6.2. The average number of detected minutiae increased with about 30 and 40 compared to Hong *et al.* [155]'s method and Feng *et al.* [168]'s method, respectively. We also conducted a Sign test statistic to investigate the improvement of detected minutiae number. The p-values are always less than $2.2e^{-16}$ when comparing the proposed method to the original fingerprints without enhancement and existing enhancement methods. It means that the proposed fingerprint enhancement approach can improve the quality of the contactless fingerprint for minutiae detection effectively.

While the effect of the enhancement algorithm may be gauged visually, the final

Table 6.2: Average number of detected minutiae.

	Original	Hong [155]	Feng [168]	Proposed
Number of minutiae	4	38	29	67

Table 6.3: Experiment protocol

	Enroll samples	Probe samples	Total samples
Smartphone	5 samples per finger * 3 fingers * 2 hands * 50 subjects = 1500 samples	10 samples per finger * 3 fingers * 2 hands * 50 subjects = 3000 samples	1500 + 3000 = 4500 samples
Reflex	5 samples per finger * 3 fingers * 2 hands * 50 subjects = 1500 samples	10 samples per finger * 3 fingers * 2 hands * 50 subjects = 3000 samples	1500 + 3000 = 4500 samples

objective of the enhancement process is to increase the accuracy of the recognition system. We also evaluate the effect of our enhancement on our database. The experiment protocol is give in Table 6.3. We use the fingerprint matching algorithm, BOZORTH3 from NBIS. The biometric system performance results are provided in Table 6.4. The parameters of BOZORTH3 are default. Considering the computational costs of each of these approaches, we also illustrate the average computation time for each method on all contactless fingerprint samples in the private database (see Table 6.5). From the results we can see that, EER for proposed method is 7% and 15% lower than existing methods, respectively. The FMR @ FNMR=0.01 for proposed method is lower than the others. The speed of the proposed method is, however, slower than the other two approaches.

Table 6.4: Biometric system performance results over the private contactless fingerprint database

	Original	Hong [155]	Feng [168]	Proposed
EER	37.9%	25.4%	33.7%	18.2%
FMR @ FNMR = 0.01	45%	39.1%	42.9%	30.3%

Table 6.5: Computational costs of three methods

Enhancement method	Computation time (seconds)
Hong et al. [155]	3.57
Feng et al. [168]	9.74
Proposed method	16.92

6.5 Summary

In this Chapter, we first review 10 existing contact-based fingerprint quality enhancement approaches. Then apply three of them to contactless fingerprint images. The adaption results show that these approaches cannot very well enhance contactless fingerprint images. Finally, we developed an improved 3-step contactless fingerprint image enhancement approach. The proposed approach is based on: 1) color-grayscale fingerprint image enhancement, 2) fingerprint local ridge orientation and frequency estimation in high reliability area, and 3) prior knowledge based latent fingerprint orientation field estimation in low reliability area. Both subjective and objective assessment methods are used to evaluate the performance of the proposed method. From the human visual aspect we can see that, after the enhancement the ridge and valley structure in the contactless fingerprints are much more visible and clear. From the minutiae extraction and biometric system performance aspects we can see that, the proposed approach can significantly improve the performance of minutiae recognition and the EER and FMR are lower than some of the existing methods. The computational costs of the proposed method is higher than the other two original methods. However, by using the proposed method, EERs are still higher than an accepted level for fingerprint recognition. So we can neither use the raw contactless fingerprint images nor the enhanced images for the evaluation of IQMs for multi-modality biometric sample quality assessment.

Chapter 7

How color space affect the performance of biometric systems

Color provides important information and features for face and visible wavelength iris recognition. Different color spaces possess different characteristics and are suitable for different applications. In this chapter, we propose to investigate how different color space components influence the performance of degraded face and visible wavelength iris recognition. Towards this goal, several color space components are selected for the evaluation. In addition, four different types and totally eight image-based degradations are applied to face and visible wavelength iris image samples in order to discover the impact on the performance of the biometric system. In this chapter, Section 7.1 is based on Article E [9], and Section 7.2 is based on Article D [11], which are introduced in Section 1.3.

7.1 Influence of color space for the performance of degraded face image recognition

Biometrics are more and more popular in recent years. Among all the existing biometric modalities, face recognition is one of the well known technologies. Thanks to the development of color imaging technology and biometric recognition application, face images captured under unconstrained conditions by classical devices such as smartphone, webcams or low-cost cameras can be used for face recognition [26]. However, many of the existing face recognition approaches are only using grayscale images converted from RGB images by taking the average of the three color components. The drawback of this method is that we do not consider the impact of each color component in an RGB image, and, moreover, we ignore

the influence of other color spaces than the RGB space. Back to 1999, color information has been noticed due to its importance in face recognition [181]. Unlike grayscale images, color face images are represented in the most commonly used RGB color space. By including color information in face recognition, the unique characteristics that are exclusive to color face images have become relevant to recognition performance [26]. The impact of color components on recognition performance lead us to further analyze the representation of color information. We can investigate through various color spaces to explore additional information from the color image that can be used to increase recognition performance. Another factor that influences the performance of face recognition is the quality of face sample images. The color face images can be captured under unconstrained environment conditions. Therefore, some image-based degradations could be introduced during the acquisition process. Using such face images for recognition is a more challenging issue [26].

7.1.1 Related works of color space for the face recognition

There are many researches using color face image for recognition. Choi *et al.* [182] proposed to use color local Gabor wavelets and color local binary pattern for the purpose of face recognition. Jones and Abbott [183] explored the extraction of features from color face images by using an extended hypercomplex Gabor filtering method. Wang *et al.* [184] represented a color face recognition approach based on two-dimensional principal component analysis. Yang and Liu [185] presented a general discriminant model for color face recognition. Choi *et al.* [186] proposed a metric called 'variation ratio gain', which aimed to prove theoretically the significance of color effect on low-resolution faces within well-known subspace face recognition frameworks. It quantitatively characterizes how color features affect the recognition performance with respect to changes in face resolution. They also conducted performance evaluation studies to show the effectiveness of color on low-resolution faces. However, the number of studies that investigate the influence of color information on face recognition is limited. Yip and Sinha [187] suggested that color cues play a role in face recognition and their contribution becomes evident when shape cues are degraded. Under such conditions, recognition performance with color images is significantly better than with grayscale images. Their experimental results indicated that the contribution of color may lie not so much in providing diagnostic cues to identity as in aiding low-level image-analysis processes such as segmentation. Torres *et al.* [181] stated that a common feature found in practically all technical approaches proposed for face recognition is the use of only the luminance information associated to the face image. It is necessary to know if this is due to the low importance of the color information in face recognition or due to other less technical reasons. They performed a variety of

Table 7.1: Experiment protocol for face

	Enroll samples	Probe samples	Total samples
LFC	5 samples per subject * 8 distortions * 5 levels * 50 subjects = 10000 samples	10 samples per subject * 8 distortions * 5 levels * 50 subjects = 20000 samples	10000 + 20000 = 30000 samples
Smart-phone	5 samples per subject * 8 distortions * 5 levels * 50 subjects = 10000 samples	10 samples per subject * 8 distortions * 5 levels * 50 subjects = 20000 samples	10000 + 20000 = 30000 samples
Reflex	5 samples per subject * 8 distortions * 5 levels * 50 subjects = 10000 samples	10 samples per subject * 8 distortions * 5 levels * 50 subjects = 20000 samples	10000 + 20000 = 30000 samples

tests using a global eigen approach, which was modified to cope with the color information. Their results show that the use of the color information embedded in an eigen approach can improve the recognition rate when compared to the same scheme which uses only the luminance information. Yoo *et al.* [188] presented color processing for face recognition systems and the results showed that color information helps the performance of face recognition and found that specifically YCbCr and YCg'Cr' color spaces are the most appropriate for face recognition. Bours and Helkala [189] investigated whether using one of the three color layers of the RGB image could give better recognition performance compared to the grey-scale converted image. Finally, Hemery *et al.* [190] studied different color spaces for representing an image for the face authentication application. They used a generic algorithm based on a matching of key points using SIFT descriptors computed on one color component. Ten color spaces have been studied on four large and significant benchmark databases. The results showed that all color spaces do not provide the same efficiency and the use of the color information allows an interesting improvement of verification results.

7.1.2 Experimental setup

The degraded face images are from GC² Multi-modality Biometric Database. The experiment protocol is illustrated in Table 7.1.

Color space

According to the analysis results from [187, 188, 190], seven different color spaces are selected for our experiment: grayscale space, RGB space, CIELab space,

YCbCr space, HSV space, LSLM space, and CIEXYZ space. Therefore, we evaluate the performance of face recognition system by representing face image in nine color components:

- Grayscale: computed from the three components of RGB color space by using the equation: $grayscale = 0.299R + 0.587G + 0.114B$;
- Red, Green, and Blue components from RGB color space;
- L (LAB_L) component from CIELab color space: The CIELab color space describes mathematically all perceivable colors in three dimensions; L for lightness and a and b for the color opponents green-red and blue-yellow;
- Y component from YCbCr color space: The YCbCr color space is widely used for digital video. In this format, luminance information is stored as a single component (Y), and chrominance information is stored as two color-difference components (Cb and Cr).
- V component from HSV color space: HSV (Hue, Saturation, Value) is one of the alternative representations of the RGB color space. The HSV representation models the way paints of different colors mix together, with the saturation dimension resembling various shades of brightly colored paint, and the value dimension resembling the mixture of those paints with varying amounts of black or white paint;
- L (LSLM_L) component from LSLM color space: LSLM is a color space represented by the response of the three types of cones of the human eye, named for their responsively (sensitivity) peaks at long, medium, and short wavelengths;
- Z component from CIEXYZ color space: X, Y and Z are extrapolations of RGB created mathematically to avoid negative numbers and are called Tristimulus values. Y means luminance, Z is somewhat equal to blue, and X is a mix of cone response curves chosen to be orthogonal to luminance and non-negative.

The color space transformations have been done in Matlab R2016a by using default scripts.

Face recognition system

The open source face recognition system is 'The PhD (Pretty helpful Development functions for) face recognition toolbox' [191], which is a collection of Matlab functions and scripts for face recognition. The toolbox was produced as a

byproduct of Štruc and Pavešić's [192] research work and is freely available for download. Three face feature extraction algorithms are used:

Kernel Fisher Analysis (KFA)

This feature extraction algorithm uses only **KFA** [193] on the original image without Gabor filtering technique. The **KFA** method first performs nonlinear mapping from the input space to a high-dimensional feature space, and then implements the multi-class Fisher discriminant analysis in the feature space. The significance of the nonlinear mapping is that it increases the discriminating power of the **KFA** method, which is linear in the feature space but nonlinear in the input space. The analyzed feature vector will be finally used for face recognition.

Gabor Filtering (GF) + KFA

In this feature extraction algorithm, a bank of complex Gabor filters defined in the spatial and frequency domains will be constructed first. Then, the algorithm computes the magnitude responses of a face image filtered with a filter bank of complex Gabor filters. The magnitude responses of the filtering operations are normalized after downscaling using zero-mean and unit variance normalization [192]. After that they are converted as the feature vector. Before we use the feature vector to perform face recognition, a **KFA** [193] is applied to it.

Phase Congruency (PC) + KFA

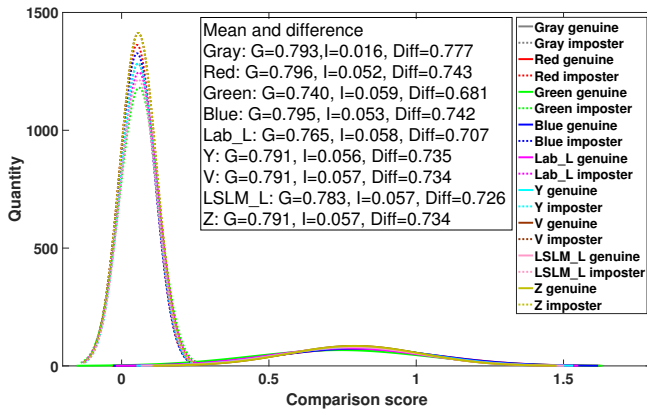
The first step in this feature extraction algorithm is the same as **GF + KFA**, a bank of complex Gabor filters defined in the spatial and frequency domains will be constructed first. But then the algorithm computes phase congruency features from a face image using a precomputed filter bank of complex Gabor filters [194]. After that they are converted as the feature vector. The feature vector is employed **KFA** before used for face recognition.

As described above, three face feature extraction algorithms are used in the experiment: **KFA**, **GF + KFA**, and **PC + KFA**. The classification method is based on the nearest neighbor classifier [192]. This classification method is capable of performing comparison similarity scores between two feature vectors.

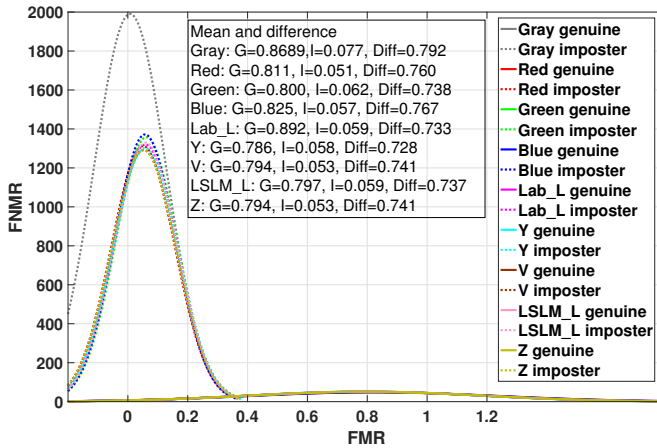
7.1.3 Experimental results

Histogram of the comparison scores and the difference of their mean values

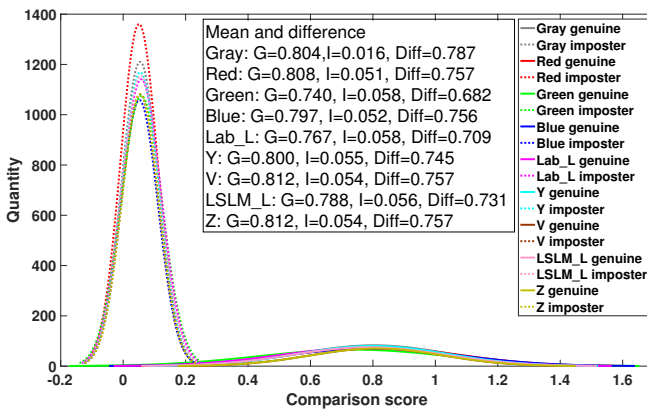
In order to evaluate the performance of a face recognition system on degraded face images when taking into account color space components, we first plot the fitted histogram of the comparison scores and the difference of their mean values in Fig-



(a) LFC



(b) Smartphone



(a) Reflex

Figure 7.1: Comparison scores and the difference of their mean values from three cameras by using different color space components.

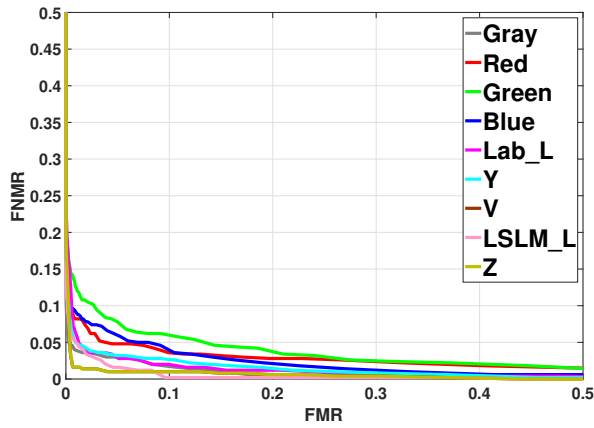
Figure 7.1. The x-axis represents the score and the y-axis represents the quantity of the comparison. The comparisons are between all face images (original and degraded) for each capture device. The reference images are created from each captured sample face image per subject per device. The line plots (continuous lines for genuine comparison and dotted lines for imposter comparison) is the fitted line for the histogram of the comparison score. The mean values and their differences when using different color components to represent the face images are also given in the figures. The G means the genuine comparison and the I means the imposter comparison. The gray color represents the comparison score from grayscale face images, the red lines represent the red channel from RGB color space, the green lines represent the green channel from RGB color space, the blue lines represent the blue channel from RGB color space, the magenta lines represent the L channel from CIELab color space, the light blue lines represent the Y channel from the YCbCr color space, the brown lines represent the V channel from HSV color space, the pink lines represent the L channel from the LSLM color space, and the chartreuse lines represent the Z channel from CIEXYZ color space.

From Figure 7.1 we can see that, when the color space changed there is no big difference between the fitted histogram and the mean of the comparison score. It means that using different components from selected color spaces cannot significantly affect the performance of the face recognition system on degraded face images. However, the biggest differences between the genuine score and the imposter score for three cameras are always from the grayscale face images. It means that grayscale face images have an overall better performance for all three cameras when considering only the μ values and ignoring the σ values.

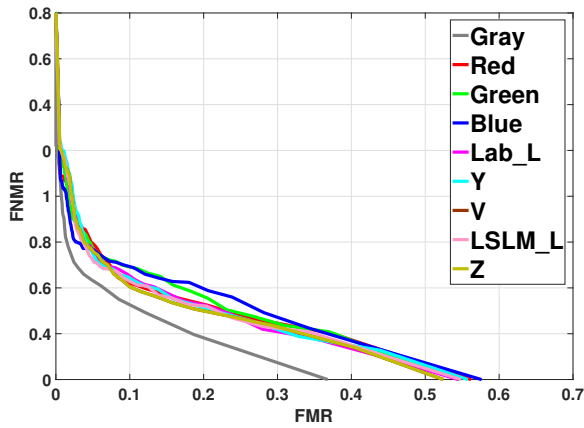
DET curve

As mentioned before, we also obtain the DET curve as an indicator to examine the performance of face recognition system by using different color components to represent degraded face images. The DET curves for three cameras are given in Figure 7.2. The x-axis represents the FMR and the y-axis represents the FNMR. If a DET curve is closer to the bottom-left point, it means that this set of data lead to a higher face recognition performance.

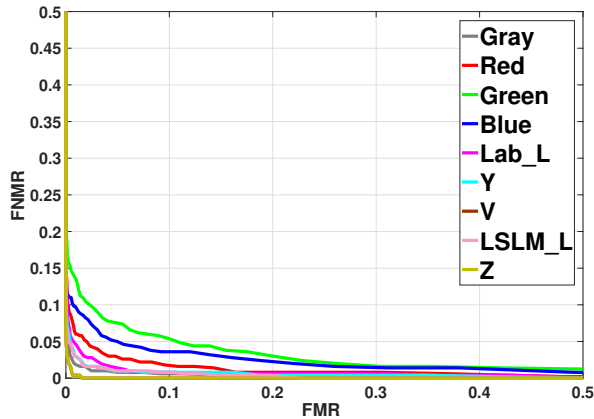
From Figure 7.2 we can see that, DET curves are overlapping with each other for smartphone, except for grayscale component. The grayscale component has better performance than the other components for smartphone. For LFC and reflex camera, the better performing color component is the Z channel from CIEXYZ color space because the chartreuse lines are closer to the bottom-left point. On the other hand, the green channel from RGB color space always gives lower performance because the green lines are furthest from the bottom-left point compared to the



(a) LFC



(b) Smartphone



(a) Reflex

Figure 7.2: DET curves from three cameras by using different color space components.

Table 7.2: EER obtained from face recognition by using different color components. Values in red represents the lowest EER for the acquisition devices.

Color component	LFC	Smartphone	Reflex
Gray	0.036	0.0302	0.020
Red	0.048	0.0317	0.034
Green	0.064	0.0316	0.066
Blue	0.056	0.0318	0.050
Lab_L	0.036	0.0304	0.028
Y	0.036	0.0302	0.018
V	0.014	0.0310	0.006
LSLM_L	0.028	0.0310	0.018
Z	0.014	0.0310	0.006

other lines.

EER

Finally, we use **EER** as another indicator to illustrate the performance of the face recognition system when using different color component representing degraded face images. The lower the **EER**, the better the system performance. In Table 7.2 we can discover similar findings to the **DET** curves: by using different color components to represent degraded face images, the face recognition performance is slightly affected. For face images taken by smartphone, **EERs** obtained from gray components and the Y channel from the YCbCr color space are lower than the other components (see values in red color in the third column of Table 7.2). For face images taken by LFC and reflex camera, the lower **EERs** are always from the V channel from the HSV color space and the Z channel from the CIEXYZ color space. On the other hand, lower system performance comes from using the green channel for LFC and reflex camera because the **EERs** are higher than the other components. For smartphone, the blue channel gives lower system performance. Similar conclusion can be drawn here: there is not a single color component that can significantly increase the face recognition performance than the others. However, the V channel from the HSV color space and the Z channel from the CIEXYZ color space give lower **EER** for two cameras.

7.1.4 Discussion

As introduced in the previous section, Yoo *et al.* [188] found out that YCbCr and YCg'Cr' color spaces can provide better performance than the other color spaces.

In [189], using the three components red, green, and blue separately from the RGB color space could give better recognition performance compared to the greyscale converted image. However, the above mentioned color spaces cannot significantly improve the face recognition performance in our study, which is similar to the findings presented by Hemery *et al.* [190]. We discovered that different color spaces can influence the system performance, depending on the different applications. In our case, it could be due to the acquisition devices used in our study and the special database developed for this work. Since we only consider image-based distortions, so the face recognition system might be not sensitive to those distortion types. On the other hand, if we add different distortions to face images that are represented by different color spaces, then these degraded face images can have different influence on different color spaces.

7.1.5 Summary

We investigate how different color space components affect the recognition system performance on degraded face samples images. Nine color components are selected: grayscale; red, green and blue channels from RGB color space; L channel from CIELab color space; Y channel from YCbCr color space; V channel from HSV color space; L channel from LSLM color space; and Z channel from CIEXYZ color space. We use three indicators to present system performance: histogram of comparison scores with their mean values and differences, DET curves, and EER. We can summarize from the experimental results that, all selected color components have similar influence to the performance of face recognition system, which is dependent on the acquisition devices and the experimental setups.

7.2 Influence of color space for the performance of degraded visible wavelength iris image recognition

With the introduction of visible wavelength iris recognition, color iris images are captured during the acquisition process. Compared to the traditional near infrared iris images, the representation of color information must be considered in visible wavelength iris recognition. Similar to the face modality, we investigate the influence of color space for the performance of degraded visible wavelength iris image recognition in this section.

7.2.1 Related works of color space for the visible wavelength iris recognition

There are not many studies on iris color space analysis in the literature. Boyce *et al.* [104] and Monaco [195] investigated the influence of different color space components on iris recognition performance. In order to convert between the ori-

Table 7.3: Experiment protocol for iris

	Enroll samples	Probe samples	Total samples
LFC	5 samples per eye per subject * 2eyes * 8 distortions * 5 levels * 50 subjects = 20000 samples	10 samples per eye per subject * 2eyes * 8 distortions * 5 levels * 50 subjects = 40000 samples	20000 + 40000 = 60000 samples
Smart-phone	5 samples per eye per subject * 2eyes * 8 distortions * 5 levels * 50 subjects = 20000 samples	10 samples per eye per subject * 2eyes * 8 distortions * 5 levels * 50 subjects = 40000 samples	20000 + 40000 = 60000 samples
Reflex	5 samples per eye per subject * 2eyes * 8 distortions * 5 levels * 50 subjects = 20000 samples	10 samples per eye per subject * 2eyes * 8 distortions * 5 levels * 50 subjects = 40000 samples	20000 + 40000 = 60000 samples

ginal RGB color space and one of the other color spaces, they first segmented and normalized the iris samples. Thus, an RGB iris template is used as the baseline image on which all color space transforms are employed. Since they only care about the transformation of the visible wavelength iris images, the near infrared component is omitted. The normalized template is then subjected to a color space transform. Once the transform is completed, comparison is performed on each channel of the color image independently. In addition to the RGB color space, CIE Lab, YCbCr, HSV, and CMYK color spaces are used in [104, 195]. The findings in their papers are: there is no single color space transformation was found to increase comparison performance across all components. However, individual components of certain color spaces showed potential as ideal candidates for iris recognition. In color spaces such as CIE Lab and YCbCr, the luminosity functions showed consistently high performance across all eye color classes. When the chromaticity is completely segmented from the luminosity, such as in the CIE Lab and YCbCr color spaces, the chromaticity shows to have high correlations between its two components indicating that their performance and viability as templates are similar. Overall, the traditional RGB color space showed strong performance.

7.2.2 Experimental setup

The degraded visible wavelength iris images are from GC² Multi-modality Biometric Database. The experiment protocol is illustrated in Table 7.3.

Color space

According to the analysis results from [104], three components from three color spaces other than grayscale have better performance than the other components: the Red channel from the RGB color space, the L channel from the CIE-Lab color space, and the Y channel from the YCbCr channel. Therefore, we evaluate the performance of the iris recognition system by representing an iris image in four color components: grayscale, Red, L, and Y. The color space transformations have been done in Matlab R2016a by using default scripts.

Iris recognition system

The iris recognition system is OSIRIS (Open Source for IRIS) version 4.1 [196]. The OSIRIS reference system is an open source iris recognition system developed in the framework of the BioSecure project [196]. OSIRIS is composed of four modules: segmentation, normalization, feature extraction and matching. Those modules are classical for iris recognition and follow the main steps proposed by Daugman's approach [31]:

- **Iris segmentation:** The first task consists in isolating the iris texture from other elements of the image such as eyelids, eyelashes, spotlights and/or shadows. These elements are considered as artifacts and have to be handled at this stage. Feature extraction and template matching are therefore limited to this iris region. In addition, the segmentation module generates a binary mask (used in the template matching module), which indicates which pixels of the image belong to iris texture.
- **Normalization:** The iris texture is mapped into a size-invariant band called the normalized iris image. This dimensionless coordinate system of the resulting image copes with the problem of pupil dilation. This transformation is carried out by exploiting a parameterization of the iris boundaries obtained by the segmentation module. The normalization process allows the alignment of any two iris images to be compared.
- **Feature extraction:** This stage aims at extracting the texture characteristics of a given iris. Discriminative features of iris texture are the basis for the comparison (matching) of any two images. The resulting template is a binary image, called irisCode, given as input to the comparison module.
- **Template comparison:** The final stage of iris recognition systems consists in deciding whether two templates belong to the same iris or not. To this end, a similarity or dissimilarity score is computed between the two templates to compare. The decision of acceptance or rejection is taken by comparing the

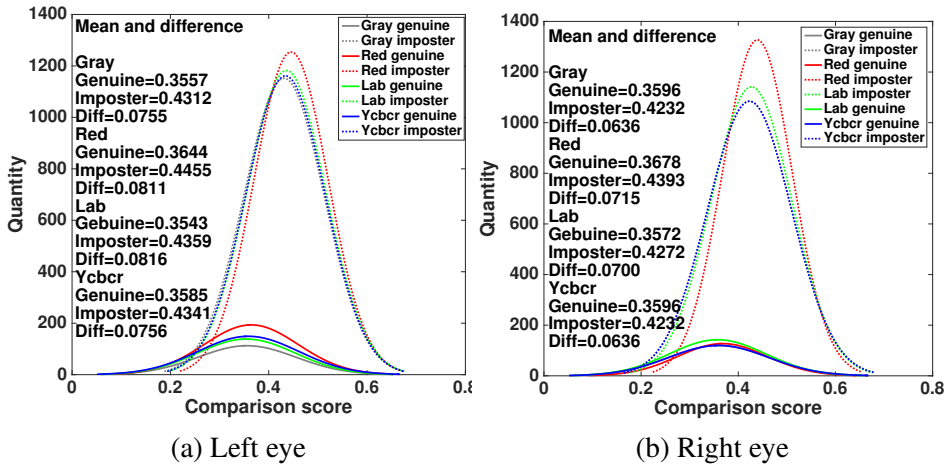


Figure 7.3: Comparison score and the difference of their mean values from left and right eye for LFC.

matching score to a threshold. The key at this stage is to fix this threshold appropriately, in order to take the correct decision.

7.2.3 Experimental results

7.2.4 Histogram of the comparison scores and the difference of their mean values

In order to evaluate the performance of iris recognition system on degraded iris images when taking into account color space, we first plot the fitted histogram of the comparison score and the difference of their mean values in Figures 7.3, 7.4, and 7.5. The x-axis represents the score and the y-axis represents the quantity of the comparison. The line plots (continued line for genuine comparison and dot line for imposter comparison) is the fitted line for the histogram of the comparison score. The mean values and their difference when using different color components to represent the iris images are also given in the Figures. The gray color represents the comparison score from grayscale iris images, the red color represents the red channel, the green color represents the L channel from CIE Lab color space, and blue color represents the Y channel from YCbCr color space.

From these three Figures we can see that, when the color space changed there is no big difference between the mean of the comparison scores. It means that using different components from selected color spaces cannot significantly affect the performance of the iris recognition system. However, the influence of color spaces is different for the three cameras. From Figure 7.3 we can see that, the difference

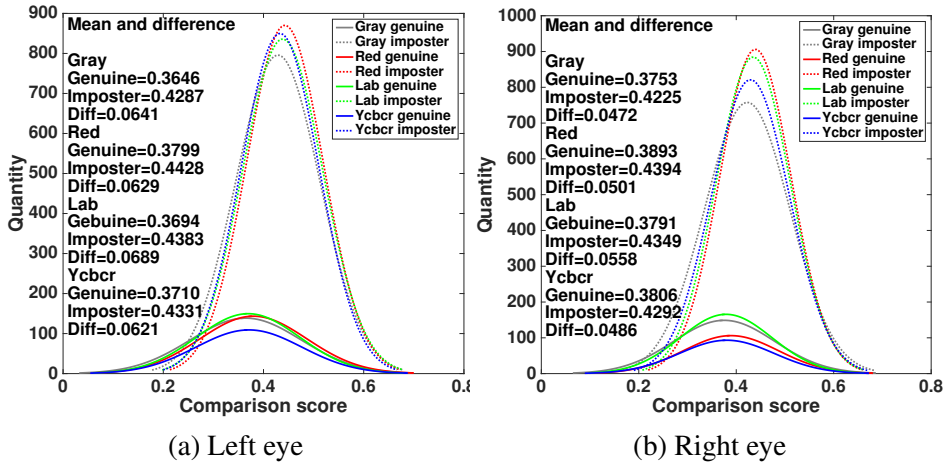


Figure 7.4: Comparison score and the difference of their mean values from left and right eye for smartphone.

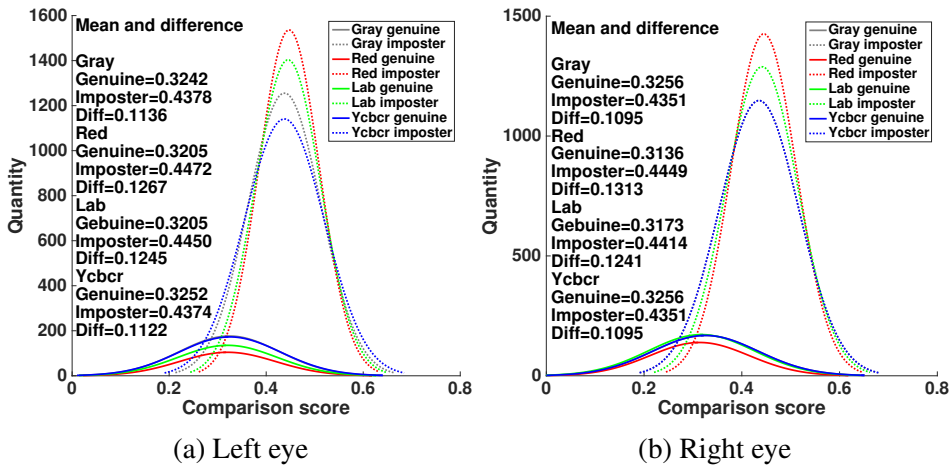


Figure 7.5: Comparison score and the difference of their mean values from left and right eye for reflex camera.

Table 7.4: EER obtained from iris recognition by using different color components

Color component	Gray	Red	L	Y
LFC				
Left	0.5409	0.5419	0.5413	0.5413
Right	0.5396	0.5417	0.5408	0.5405
Smartphone				
Left	0.5489	0.5664	0.5779	0.5409
Right	0.5258	0.5377	0.5645	0.5154
Reflex				
Left	0.6482	0.6890	0.6639	0.6466
Right	0.6462	0.7001	0.6793	0.6266

mean value between genuine score and imposter score by using L channel is larger than the other three color components for left eye (red channel for right eye). According to the rule proposed in [3], using L channel representing iris images has better recognition performance than using the other three color components for left eye from LFC (red channel is better for right eye). We also find that, the influence is different even for different eyes when using the same camera. From Figure 7.4 we observe that, for both left and right eyes, the L channel always has the better performance because the difference of mean comparison scores is greater than the other channels. In Figure 7.5, the better color component is the red channel.

From the analysis above we can conclude that, there is not one color component that can increase the performance of iris recognition system better than the others. However, for iris images from different eyes and different cameras, we can use alternative color component to represent iris images in order to obtain a better system performance.

EER

In Table 7.4 we can discover similar findings as for the comparison scores: by using different color components to represent iris image, the iris recognition performance is slightly affected. For iris images taken by LFC, EER obtained from gray components is lower than the other components (see values in red color in Table 7.4). For iris images taken by smartphone and reflex camera, the lower EER is always for the Y component from the YCbCr color space. Unlike the results from comparison score, the better color component is always the same for both eyes. Similar conclusion can be drawn here: not a single color component that can significantly increase the iris recognition performance compared to others. How-

ever, the Y channel from the YCbCr color space gives lower EER for two cameras.

7.2.5 Summary

We investigate how different color space components affect the recognition system performance on degraded visible wavelength iris samples images. Four color components are selected: grayscale, red channel from RGB color space, L channel from CIE Lab color space, and Y channel from YCbCr color space. We can summarize from experimental results that, there is not a single color component that can significantly increase the performance of iris recognition system.

7.3 Conclusion

According to the experimental results from both face and visible wavelength iris modalities, when using selected database and recognition systems, there is not a single color component that can significantly influence the performance of biometric recognition system. Therefore, the grayscale color space component, which is the default color component for selected face and iris recognition systems, will be used in the following experiments.

Chapter 8

Performance evaluation of no-reference image quality metrics for face and iris biometric images

The accuracy of face and iris recognition systems is significantly affected by the quality of sample images. The recent established standardization proposed several important aspects for the assessment of face sample quality. There are many existing no-reference IQMs that are able to assess natural image quality by taking into account similar image-based quality attributes as introduced in the standardization. However, whether such metrics can assess face sample quality is rarely considered. On the other hand, with the development of electronic color imaging, there are more and more researches about Visible Wavelength iris recognition. Compared to the near infrared iris images, using VW iris images acquired under unconstrained imaging conditions is a more challenging task for the iris recognition system. However, the number of quality assessment methods for VW iris images is limited. Therefore, it is interesting to investigate whether existing no-reference IQMs which are designed for natural images can assess the quality of VW iris images. In this chapter, we evaluate the performance of 15 selected no-reference IQMs on face and iris biometrics. The experimental results show that several of them can assess face and iris sample quality according to the systems performance. We also analyze the strengths and weaknesses of different IQMs as well as why some of them failed to assess face sample quality. Re-training an original metric by using a face or iris database can improve the performance of a such

metric. This chapter is based on Article F [10] and G [5], which are introduced in Section 1.3.

8.1 Introduction

Face has become one of the most commonly and successful modalities for biometric recognition in the past decade [26]. As face recognition is a mature technology, it has been used in both government (e.g. Australian and New Zealand customs services called SmartGate, law enforcement agencies in the United States) and civilian (e.g. sorting photographs, security payment) applications. The study in face recognition is motivated by the need for reliable, efficient, and security recognition methods in order to perform better identification and forensic investigations. However, face recognition is still a challenging issue when degraded face images are acquired [26]. In recent years, low-cost devices have enabled face recognition systems, and smartphone based face recognition systems received significant attention. Such facts make it difficult to ensure the quality of face images. It has been proven that face sample quality has a significant impact on the accuracy of biometric recognition [70]. Low face sample quality is a main reason for matching errors in biometric systems and may be the main weakness of some applications [70]. Biometric image quality assessment approaches are used for measuring image quality and they may help to improve the performance of face recognition systems. On the other hand, iris recognition is another commonly used technology in many government and civilian applications (e.g. border control in the United Kingdom and United Arab Emirates). However, most of the existing iris recognition systems rely on heavy imaging constraints captured in a stop-and-stare interface, at close distances and using near infrared (700-900 nm) wavelengths with sufficient quality. In recent years, thanks to the development of imaging technologies, there are more and more iris recognition systems that operate in the VW and in less constrained environments [197, 198, 199, 200, 148, 201, 104]. The VW iris imaging systems lead to acquire degraded iris samples due to less constrained environments that makes the sample quality assessment a major issue.

Recently, several standardizations on biometric sample quality have been finalized, especially for face and iris modalities: ISO/IEC JTC 1/SC 37 19794-5 Information technology - Biometrics - Biometric data interchange formats - Part 5: Face image data [202], ISO/IEC TR 29794-5 Information technology - Biometric sample quality - Part 5: Face image data [73], ISO/IEC JTC 1/SC 37 19794-6 Information technology - Biometrics - Biometric data interchange formats - Part 6: Iris image data [203], and ISO/IEC TR 29794-6 Information technology - Biometric sample quality - Part 6: Iris image data [74]. The standard in [202] presents requirements for the face image data record format as well as the instruction of photographing

high quality face images. Some important aspects should be considered in order to meet the basic face image quality requirements: pose angle, facial expression, visibility of pupils and irises, focus, illumination and so on. The standard in [73] proposes definition and specification of methodologies for computation of objective, quantitative quality scores for facial images. The standard in [203] presents requirements for the iris image data record format as well as the instruction of photographing high quality iris images. To meet the requirements of iris image quality, the following aspects need to be taken into account: usable iris area, iris-sclera contrast, iris-pupil contrast, pupil boundary shape, sharpness, frontal gaze-elevation, frontal gaze-azimuth, iris pupil concentricity and so on. The standard in [74] proposes definition and specification of methodologies for computation of objective, quantitative quality scores for iris images. Both image-based and modality-based face quality attributes are discussed in the standard.

Multi-modality biometric recognition technologies become more and more popular in recent years [6]. However, biometric sample quality assessment methods that can be used for the evaluation of multi-modality sample quality are rarely considered. It is necessary to investigate if it is possible to develop a quality metric that can assess the quality of biometric image samples from multiple modalities. Two kinds of quality attributes are usually considered when assessing biometric sample quality: image-based attributes and modality-based attributes. Image-based attributes are, for instance related to, contrast, sharpness etc. which are presented in all image-based biometric modalities (e.g. face, iris, palm print and so on). Modality-based attributes are dedicated for only one modality, such as pose symmetry in face biometric or eye reflection in iris biometric. As introduced in Chapter 4, using image-based quality attributes in the quality assessment approaches make it possible to assess image-based multi-modality biometric sample quality [6]. The goal of this chapter is to evaluate the performance of no-reference IQMs on face and iris images in order to assess the possibility of developing image-based multi-modality sample quality assessment metrics.

In this chapter, 15 no-reference IQMs are selected and evaluated. Three face recognition algorithms are used to evaluate the performance of face recognition system, and a near infrared iris recognition algorithm is adapted to the VW iris sample in order to evaluate iris recognition system performance. Face and VW iris images from the GC² multi-modality biometric database are used. The structure of this chapter is described as follows. We first present the experimental setup. Then the experimental results and their analysis for face and iris are illustrated, respectively. At last the summary of the evaluation and the conclusions are presented.

Table 8.1: Classification of the selected IQMs

IQMs	Distortion-specific	Generalized purposes
NSS	CONTRAST [119]	BIQI [129], BLIINDS2 [130], BRISQUE [131], ILNIQE2 [132]
Non NSS	JNBM [122], DCTSP [123], SH [124], CONTRAST2 [121], JPEG [127], PWN [126]	AQI [128], AQIP [128], dipIQ [204], SSEQ [133]

8.2 Experimental setup

8.2.1 Database and biometric systems

Face and **VW** iris images from the GC² multimodality biometric database are used in this chapter. The experiment protocols for face and **VW** iris images are the same as introduced in Chapter 7 (Table 7.1 for face modality, and Table 7.3 for iris modality). The open source face recognition system used here is 'The PhD (Pretty helpful Development functions for) face recognition toolbox' [191]. The detailed introduction of this system is in Section 7.1.1. The iris recognition system used here is OSIRIS (Open Source for IRIS) version 4.1 [196]. The detailed introduction of this system is in Section 7.2. The approaches used for the evaluation of biometric recognition system performance are: histogram of the comparison scores and their mean values, **DET** curves, and **EER**.

8.2.2 No-reference IQMs and their classification

Based on the survey and the availability of the source codes, we selected 15 no-reference **IQMs** for the performance evaluation. The reasons of selecting these **IQMs** are: 1) all of these **IQMs** have high correlation with the five most important image-based quality attributes [6]: for example, JNBM is made for blur distortion, which is one of the relevant distortions we introduced previously, 2) the implementation source code of these **IQMs** are publicly available. We classify these **IQMs** into two categories: 1) distortion specific, and 2) generalized purposes holistic **IQMs**. In each category, we separate **IQMs** into two groups: **NSS** based and non **NSS**-based **IQMs**. The classification of the selected **IQMs** is illustrated in Table 8.1. The introduction of each selected **IQMs** is already given in Section

4.5. As mentioned in the introduction part, we consider that face and VW iris images evolved in a subspace of the whole natural images space. Thus, the relevance of using NSS-based IQMs methods can be investigated. The implementations of these 15 no-reference IQMs are the original source codes provided by their authors. All parameters are the default settings in our experiments.

8.3 Experimental results for face modality

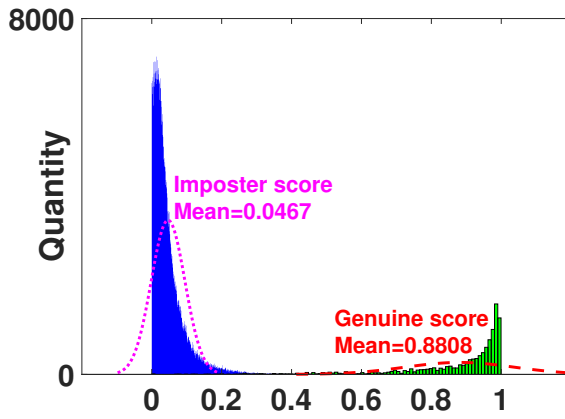
In this section, we present the experimental results for face modality. We only illustrate the results by using GF + KFA face recognition algorithm since the results from KFA and PC + KFA are very similar to GF + KFA.

8.3.1 Histogram of the comparison scores and their mean values

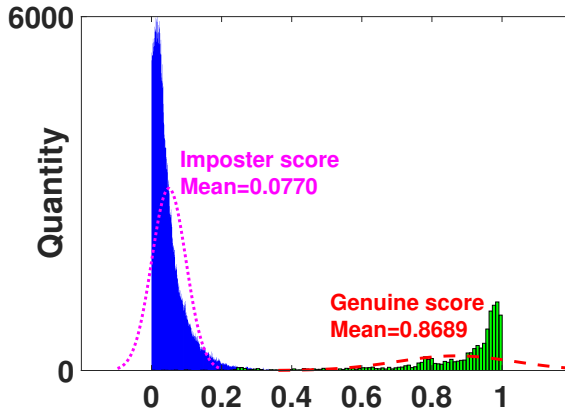
In order to evaluate the performance of the IQMs, we first plot the original comparison score by using GF + KFA recognition algorithm for three cameras in Figure 8.1. The x-axis represents the score and the y-axis represents the quantity of the comparison. The line plots (red '-' line for genuine comparison and magenta ':' line for imposter comparison) correspond to the fitted normal distributions. The mean value of the comparison score is given as well in Figure 8.1. As mentioned before, high quality biometric samples could generate relatively 'good' genuine comparison scores (in our case, the closer to 1 a score is, the more similar the two face samples are), which are well separated from imposter comparison scores [3]. We can observe from Figure 8.1 (a), (b), and (c) that genuine comparison scores are well separated from imposter comparison scores.

Here we only illustrate the interesting examples in Figure 8.2. The histogram of the genuine comparison score when omitting low quality samples by using 15 selected no-reference IQMs and GF + KFA recognition algorithm for three cameras are shown in Appendix A (Figures A.1, A.2, and A.3). For each sub-plot in Figure 8.2, the red continuous line represents the original comparison score (the same fitted red line from Figure 8.1); the magenta '-' line represents the comparison score when we omit 20% lowest quality face samples and keep the remaining 80% higher quality samples; the blue ':' line represents the comparison score when we omit 40% of the lowest quality face samples and keep the remaining 60% higher quality samples; and the green '-' line represents the comparison score when we omit 60% lowest quality face samples and keep only 40% highest quality samples in the database for the experiment. According to Grother's theory [3], we expect to observe the fitted line moves from left to right (mean comparison value becomes closer to 1) when we keep 80%, 60%, and 40% highest quality samples.

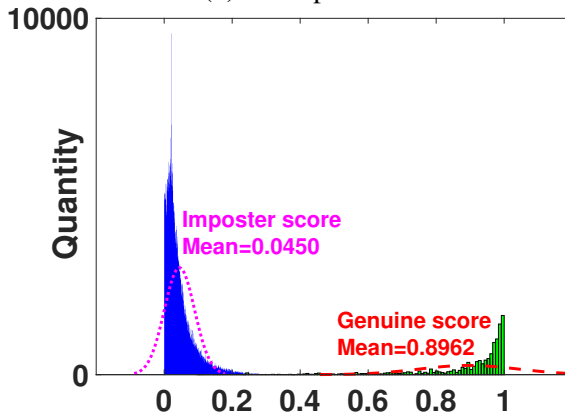
In Figure 8.2 (a), by using the assessment results from ILNIQE2 for LFC to omit low quality samples, we can observe the expected right shift for fitted lines (as well



(a) LFC

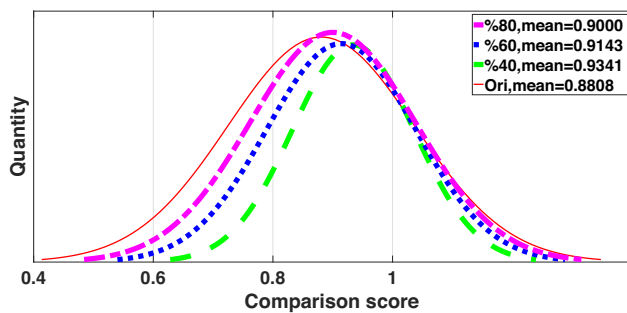


(b) Smartphone

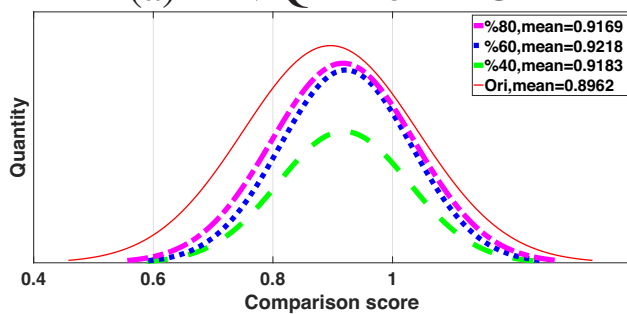


(c) Reflex

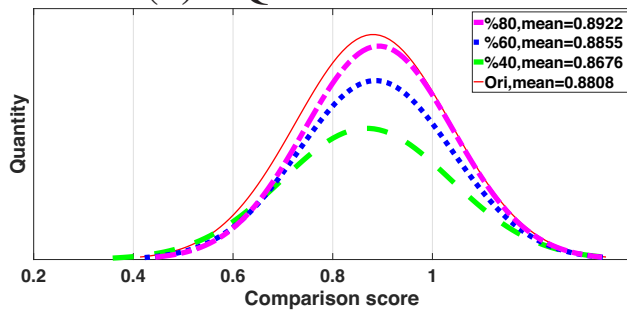
Figure 8.1: Comparison scores and their mean values for GF+KFA recognition algorithm for the three cameras.



(a) ILNIQE2 for LFC



(b) AQIP for Reflex



(c) JNBM for LFC

Figure 8.2: Examples of comparison scores and their mean values with omitting low quality samples by using GF+KFA recognition algorithm. The x-axis represents the comparison score, and the y-axis represents the quantity of the genuine comparison.

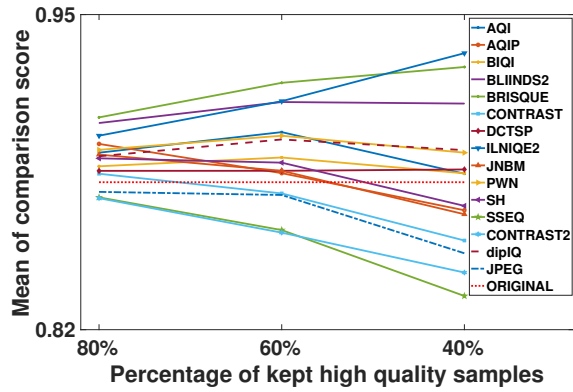
as the mean values). It means that these IQMs can assess face image quality and it is correlated with the performance of face recognition algorithm. In Figure 8.2 (b), the mean values increase from keeping 80% to 60% highest quality samples by using AQIP metric for reflex camera, however, the values decrease when there is only 40% highest quality samples left. Similar observations can be found for the other two cameras. In Figure 8.2 (c), the mean values become lower and lower than the original after omitting more and more low quality samples. This means that JNBM has a reversed correlation with the performance of GF + KFA recognition algorithm for LFC.

Additionally, we plot the mean values with omitting low quality samples in Figure 8.3 for three cameras in order to show the overall performance of IQMs. The x-axis represents the percentage of kept high quality samples and the y-axis represents the mean of comparison score. The red ':' line represents the original mean of comparison score. Same findings can be obtained from Figure 8.3. From the observation above we can summarize that, based on mean comparison scores, only BRISQUE can assess face quality based on the performance of GF + KFA face recognition algorithm for all three cameras; DCTSP can assess face quality for LFC and reflex camera; ILNIQE2 can assess face quality for LFC and smartphone. The rest of the IQMs either can assess face quality for only one camera or have low ability to assess face quality based on the system performance. However, AQIP, CONTRAST, JNBM, and SH (for LFC); AQI, AQIP, CONTRAST, DCTSP, JNBM, and SH (for smartphone); AQI, CONTRAST, JNBM, and SH (for reflex camera) have reversed correlation with the performance of GF + KFA recognition algorithm according to the histogram and the mean of comparison scores.

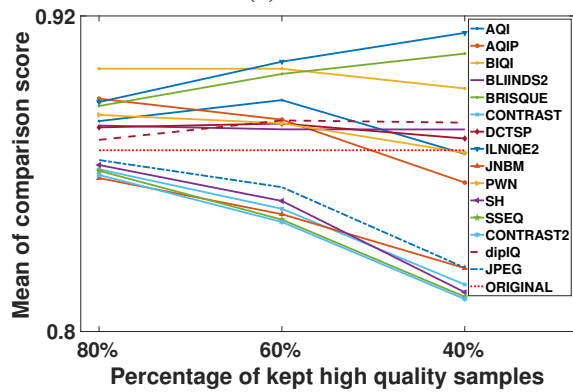
8.3.2 DET curve and EER

As mentioned before, we also obtain EER as an indicator to examine the performance of IQMs. The DET curves with EER for data with and without omitting low quality face samples for three cameras by using all selected IQMs are given in Appendix B (see Figures B.1, B.2, and B.3). Here we only illustrate interesting examples in Figure 8.4. For each sub-plot in Figure 8.4, the red continuous line represents the original DET curve; the magenta '- -' line represents the DET curve when we keep 80% highest quality face samples; the blue ':' line represents the comparison score when we keep 60% highest quality face samples; and the green '-.' line represents the comparison score when we keep only 40% highest quality face samples in the database for the experiment. If a DET curve is closer to the bottom-left point, it means that this set of data lead to a higher face recognition performance. Meanwhile, the lower EER value the better system performance.

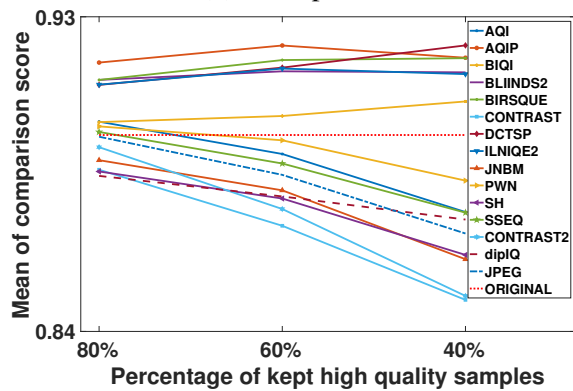
From Figure 8.4 (a) and (b) we can see that, DET curves shift closer to bottom-left



(a) LFC



(b) Smartphone



(c) Reflex

Figure 8.3: Tendency of mean comparison scores with omitting low quality samples for GF+KFA recognition algorithm.

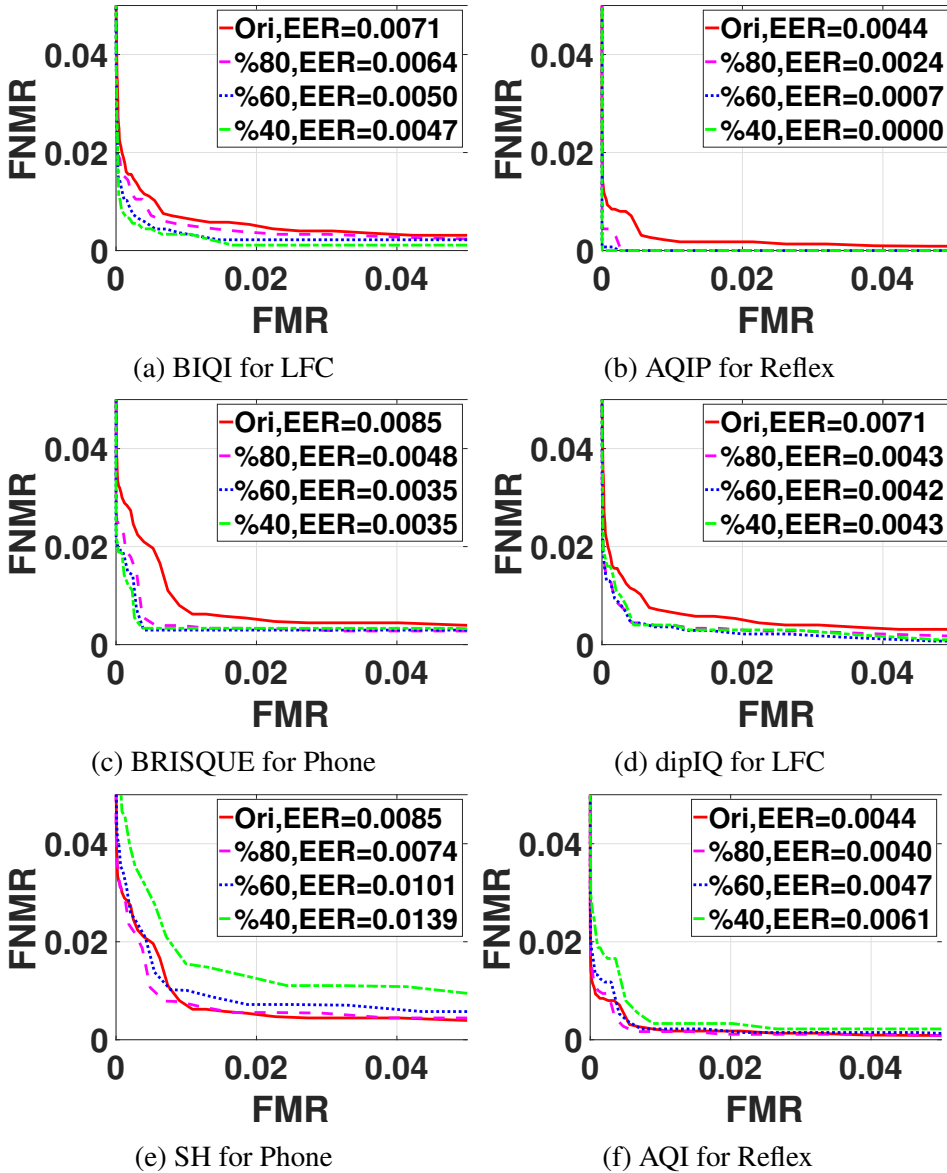
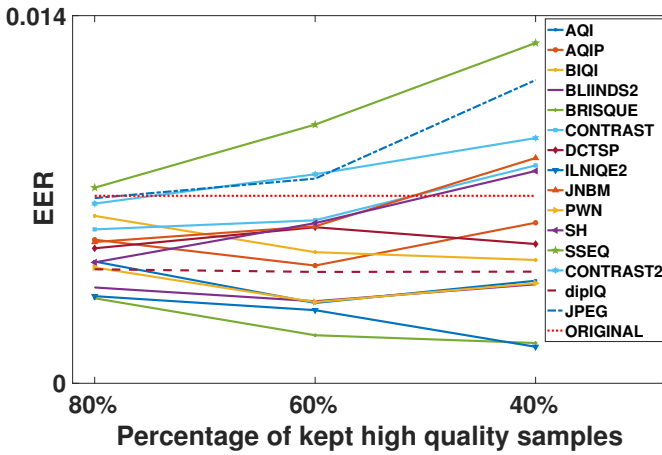


Figure 8.4: Examples of DET curves with EER for comparison score with and without omitting low quality samples by using GF+KFA recognition algorithm.

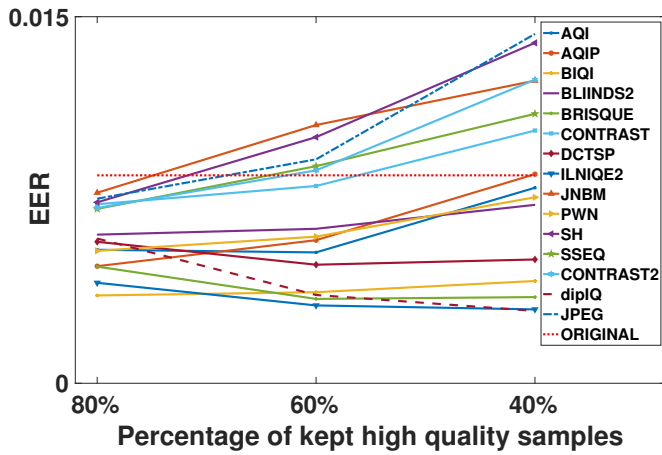
point when we keep 80%, 60%, and 40% highest quality samples by using the assessment results from BIQI and AQIP to omit low quality samples taken by LFC and reflex camera, respectively. It means that such IQMs can assess face image quality and it is correlated with the performance of face recognition algorithm. However, although the DET curves have no obvious shift when we keep 80%, 60%, and 40% highest quality samples, but the EER values have decreased by using the assessment results from BRISQUE when we omit low quality samples for smartphone (see Figure 8.4 (c)). In Figure 8.4 (d), three DET curves are on the bottom-left side of the original DET curve, but EER values are the same when keeping 80%, 60%, and 40% highest quality samples. We cannot conclude that such IQMs have 'bad' performance because all EER values are lower than the original when omitting low quality samples. We can observe from Figure 8.4 (e) and (f), SH for smartphone and AQI for reflex camera make the DET curves shift to top-right point when omitting low quality samples. This means that such IQMs have reversed correlation with the performance of GF + KFA recognition algorithm.

Additionally, we plot the tendency of EER values with omitting low quality samples in Figure 8.5 for three cameras in order to show the overall performance of IQMs. The x-axis represents the percentage of kept high quality samples and the y-axis represents the EER. The red ':' line represents the original EER without omitting low quality samples. Same findings can be obtained from Figure 8.5. From the observation above we can summarize that, based on DET curves and EER values when we keep 80%, 60%, and 40% highest quality samples, there are several IQMs can assess face sample quality: for LFC they are BIQI, ILNIQE2, and BRISQUE; for smartphone then are DCTSP, dipIQ, BRISQUE, and ILNIQE2; and for reflex camera they are BLIINDS2, ILNIQE2, and AQIP. On the other hand, some IQMs have reversed correlation with the performance of GF + KFA recognition algorithm and EER values become higher than the original: for LFC they are SSEQ, JPEG, CONTRAST2, JNBM, CONTRAST, and SH; for smartphone they are JPEG, SH, CONTRAST2, JNBM, SSEQ, and CONTRAST; for reflex camera they are CONTRAST, CONTRAST2, SH, AQI, JPEG, JNBM, SSEQ, PWN, and dipIQ. The rest of the IQMs either have little influence to the DET curves and EER values when omitting low quality face samples, or have fluctuation results. Therefore, ILNIQE2 is the only metric that can assess face sample quality for three cameras based on the DET curves and EER values.

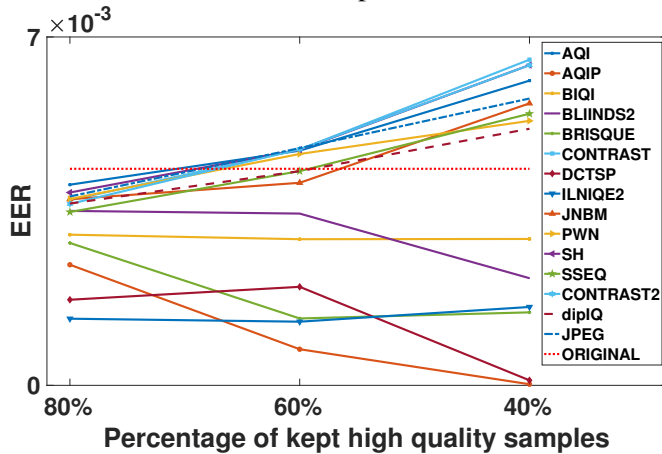
We also use EER values for all three cameras by omitting lowest quality face sample one by one until only one highest quality face sample is left from each subject as another indicator to assess the performance of selected IQMs. The full plots are shown in Appendix C (see Figures C.1, C.2, and C.3). Here we only give



(a) LFC



(b) Smartphone



(c) Reflex

Figure 8.5: Tendency of EER values with and without omitting low quality samples for GF+KFA recognition algorithm.

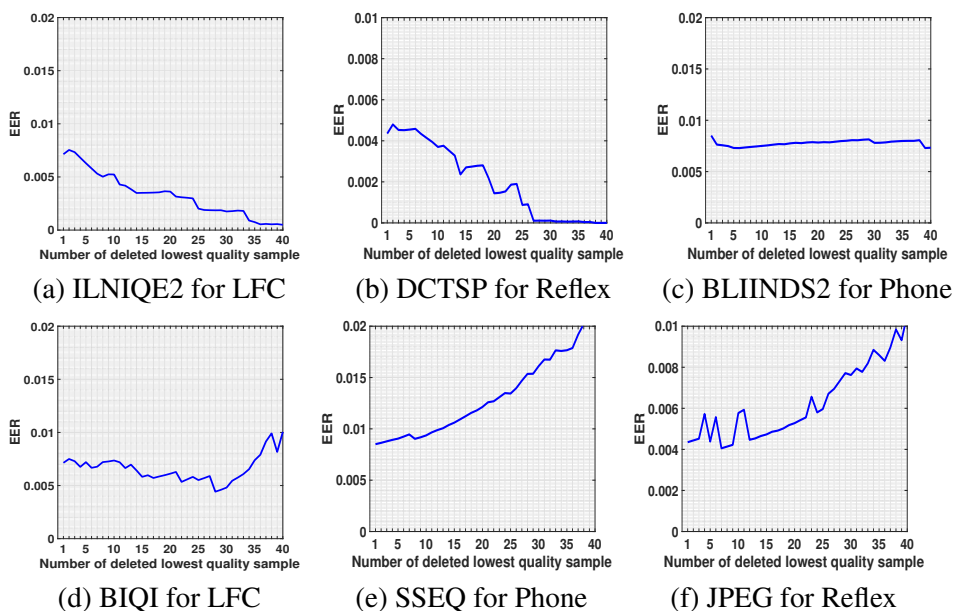


Figure 8.6: Examples of EER values with omitting low quality face samples one by one until the best quality sample left by using GF+KFA recognition algorithm.

the interesting examples that illustrate the change of EER values. The x-axis in Figure 8.6) represents the number of omitted lowest quality samples unit. There are 40 units per captured sample image per subject (eight distortions in five levels). Each unit has 750 images (15 captured sample image per subject). The y-axis represents the EER value. If the EER value has a smooth decreasing tendency when we omit lowest quality samples one by one, it means that the metric used for generating the quality scores can predict the face recognition algorithm well which represents the high performance of such IQMs. In Figure 8.6 (a) and (b) we can see that, by using the assessment results from ILNIQE2 and DCTSP to omit one lowest quality sample (taken by LFC and reflex camera, respectively) each time, the EER curves have a decreasing tendency. In Figure 8.6 (c), the EER curve from BLIINDS2 for smartphone is nearly flat. In Figure 8.6 (d), the EER curve from BIQI for LFC camera has fluctuation in the beginning, and the final trend of the curve is increasing and the EER value became higher in the end. On the other hand, as shown in Figure 8.6 (e) and (f), the EER values seem to increase when we use these metrics to assess face image quality.

In order to have an overview of the performance of selected IQMs represented by omitting lowest quality face sample one by one, we indicate whether a metric can improve the face recognition system performance, or have little influence to the

Table 8.2: Overview of the performance of selected IQMs for face modality

	LFC	Phone	Reflex	
AQI	Yellow	Red	Red	<div style="background-color: green; width: 100px; height: 15px; margin-bottom: 5px;"></div> <div style="background-color: yellow; width: 100px; height: 15px; margin-bottom: 5px;"></div> <div style="background-color: red; width: 100px; height: 15px;"></div>
AQIP	Yellow	Red	Green	
BIQI	Yellow	Yellow	Yellow	
BLIINDS2	Yellow	Yellow	Yellow	
BRISQUE	Yellow	Green	Yellow	
CONTRAST	Red	Red	Red	
DCTSP	Yellow	Yellow	Green	
ILNIQE2	Green	Green	Yellow	
JNBM	Red	Red	Red	
PWN	Yellow	Red	Red	
SH	Red	Red	Red	
SSEQ	Red	Red	Red	
CONTRAST2	Red	Red	Red	
dipIQ	Yellow	Yellow	Red	
JPEG	Red	Red	Red	

system (neutral), or decrease the system performance in Table 8.2. The green cells in the table represent that by using such metrics to omit lowest quality face sample one by one until only one highest quality face sample left from each subject, the system performance is improved. The yellow cells in the table represent the metrics are neutral, which have little influence on the system performance. The red cells in the table represent the metrics decrease the performance of face recognition system. From Table 8.2 we can observe that, based on EER values with omitting low quality face samples one by one until the best quality sample left for three cameras by using GF + KFA recognition algorithm, ILNIQE2 can assess face image quality for LFC and reflex camera. The rest of the IQMs can either assess face quality for only one camera or have low ability to assess face quality based on the system performance. However, CONTRAST, JNBM, SH, SSEQ, CONTRAST2, and JPEG decrease the performance of GF + KFA recognition algorithm for three cameras according to the results obtained from one by one omitted EER values.

8.3.3 Performance comparison between selected IQMs and ISO proposed IQMs

As mentioned in Section 3.2.1, several IQMs are proposed in the face standard [73]. Here we compare the performance of selected IQMs and ISO proposed IQMs: ISO1 [205], ISO2 [206], and ISO3 [207]. In Figure 8.7 we illustrate the DET curves with EER for LFC by using ISO proposed IQMs to omit low qual-

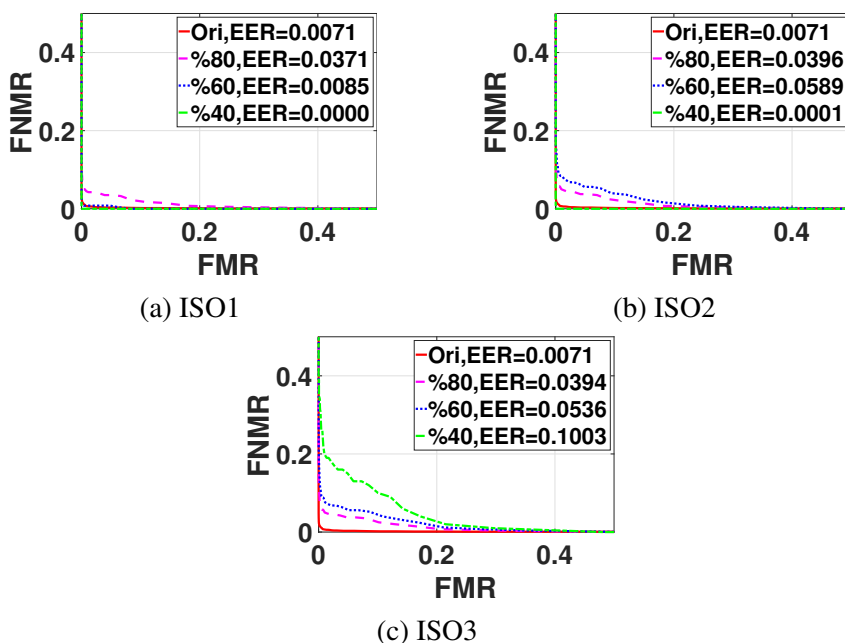


Figure 8.7: DET curves with EER for comparison score with and without omitting low quality samples for LFC by using ISO proposed IQMs (GF+KFA).

ity samples. From Figure 8.7 we can see that none of the metrics give expected DET shift and EER decrease when we omit low quality samples in the dataset. Similar observations can be found in Figure 8.8, which represent EER values with omitting low quality face samples one by one until the best quality sample left for reflex camera by using ISO proposed IQMs. Therefore, compared to the performance evaluation results for selected no-reference IQMs we see that several metrics have better performance than ISO proposed metrics.

8.3.4 Re-training ILNIQE2 on face database

From previous results, one specific metric, namely ILNIQE2 shows interesting results in terms of correlation between the provided quality scores and the performance results. Since this quality index has been trained on general purpose natural images, it would be interesting to investigate if results can be improved retraining it on face images. To perform the retraining, the color FERET database [40] has been selected, which has 269 subjects and there are two acquisition sessions for most of subjects. For each session, 11 different sample images were acquired which contain different face angles and expressions. We use 269 images (one sample image (the front face) per subject) from the FERET database to

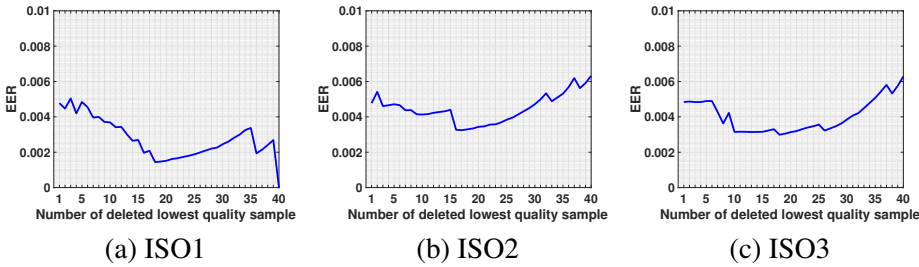
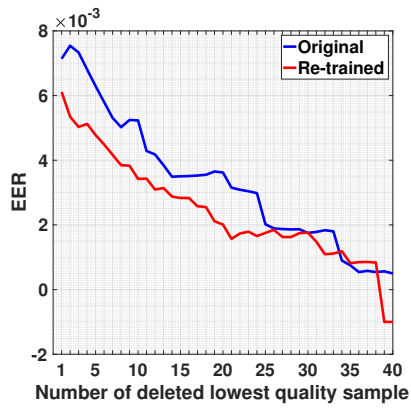


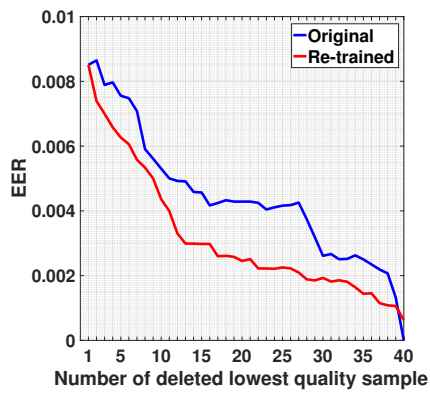
Figure 8.8: EER values with omitting low quality face samples one by one until the best quality sample left for reflex camera by using ISO proposed IQMs (GF+KFA).

re-train the ILNIQE2 metric. These 269 images are all high quality face images because the ILNIQE2 metric only requires pristine images for training. The re-trained metric is then used to re-conduct the experiment removing lowest quality samples one by one from each subject. The plots of EER values for three cameras are shown in Figure 8.9. The blue lines represent the original ILNIQE2 method, and the red lines represent the re-trained ILNIQE2 method. From Figure 8.9 we can see that, after the re-training process, the overall performance of the metric is improved because the red lines are under the blue thin lines. It means that the overall EER values from the re-trained method are lower than the original method. In addition, the improvement for reflex camera are greater than LFC and smartphone. By using the original ILNIQE2 to omit lowest quality samples from the database, the EER values are not smoothly decreasing, moreover, the EER increase after 18 unites of lowest samples are removed for reflex camera. However, by using the re-trained method, the line becomes smoother and has a decreasing tendency. Finally, the EER reach '0' when 24 unites of lowest quality samples are omitted. The difference of EER between the original and the re-trained method for reflex camera is obvious.

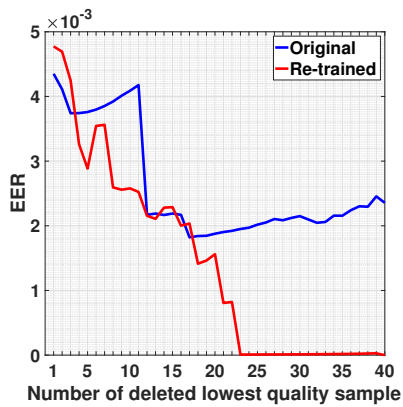
We would like to investigate if such improvement for reflex camera is due to the better prediction of re-trained ILNIQE2 for all distortions or for some distortions. Therefore, we illustrate EER curves for single distortions in Figure 8.10. Since there are eight distortions for each sample image, the total units become five instead of 40 as the case was in Figure 8.9. From Figure 8.10 we can see that the re-training process has little impact on high luminance and JPEG artifacts distortions. It reduces the performance of ILNIQE2 for low contrast and low luminance distortions because the average EER are higher after re-training, but the EER curves still have a decreasing tendency. Furthermore, the re-training has a positive effect for high contrast, Gaussian blur, motion blur, and Poisson noise distortions. The EER curves for the latter three distortions have an increasing tendency for the original



(a) LFC



(b) Smartphone



(c) Reflex

Figure 8.9: Comparison of EER by omitting lowest quality sample one by one using ILNIQE2 for each subject between the original method and the re-trained method.

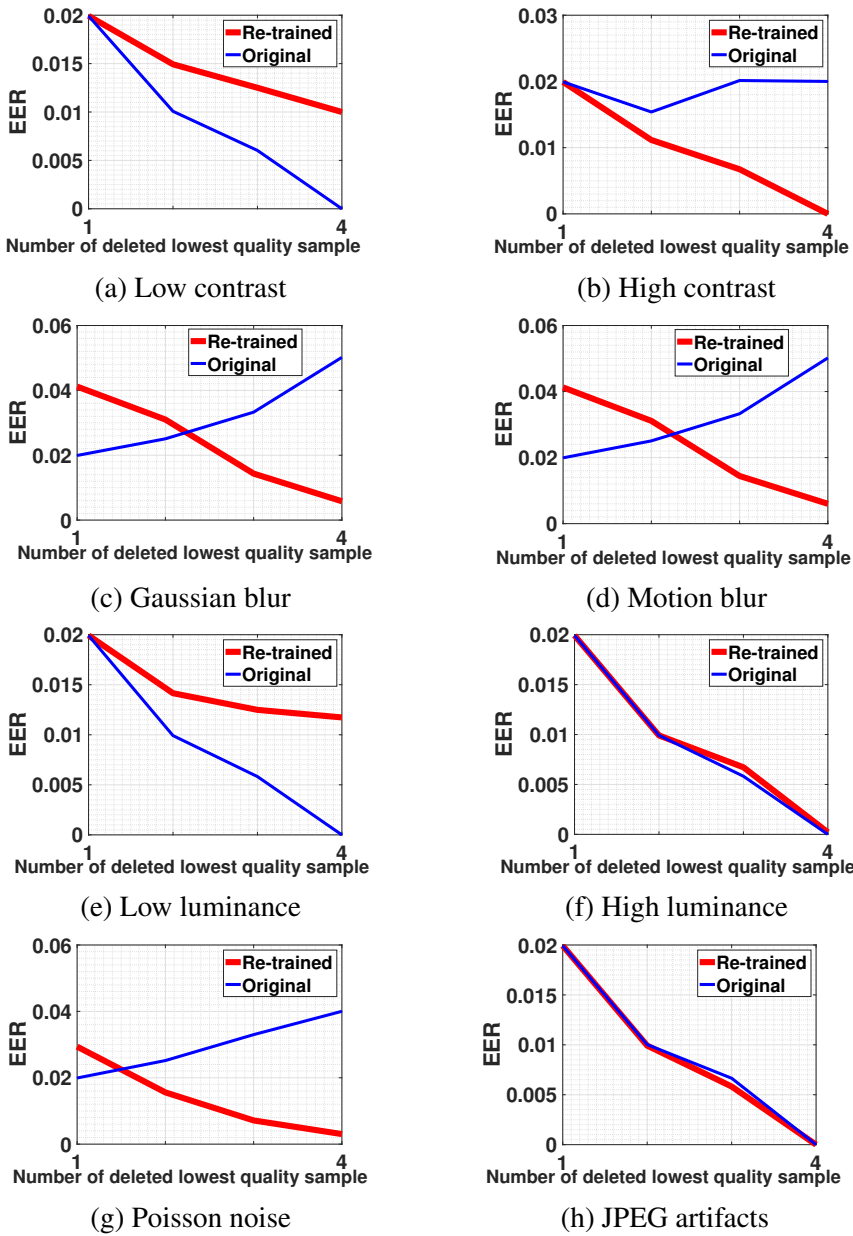
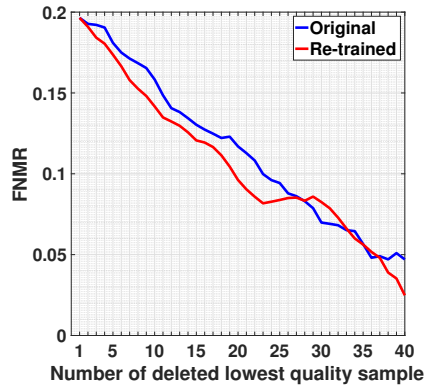
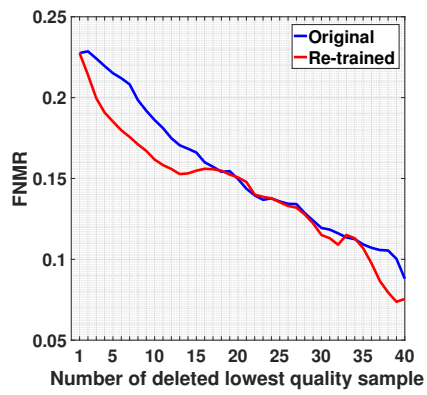


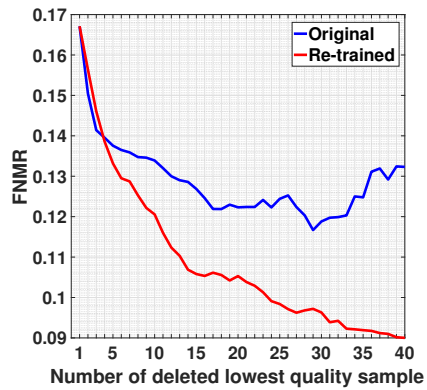
Figure 8.10: Comparison of EER between the original method and the re-trained method for each distortion for reflex camera.



(a) LFC



(b) Smartphone



(c) Reflex

Figure 8.11: Comparison of ERC by omitting lowest quality sample one by one using ILNIQE2 for each subject between the original method and the re-trained method.

method, however, they have a decreasing trend after the re-training process. It is worth noting that all curves after re-training have a decreasing tendency.

In order to further verify the performance of re-trained ILNIQE2, we use **ERC** to illustrate its performance before and after the re-training process. Figure 8.11 shows the **ERC** for all three cameras by omitting lowest quality face sample one by one until only one highest quality face sample is left from each subject. The x-axis in Figure 8.11 represents the number of omitted lowest quality samples unit, and the y-axis represents the **FNMR** value. The blue lines represent the original ILNIQE2 method, and the red lines represent the re-trained ILNIQE2 method. Similar to **EER**, if the **FNMR** value has a smooth decreasing tendency when we omit lowest quality samples one by one, it means that the metric used for generating the quality scores can predict the face recognition algorithm well which represents the high performance of such metric. By looking at plots (a) and (b) in Figure 8.11 we can see that, the performance of re-trained ILNIQE2 is improved before 28 units of lowest quality samples are omitted for LFC (17 units for smartphone). After that, the performance before and after the re-training process are similar. In Figure 8.11 (c), after 4 units of lowest quality samples are omitted for reflex camera, the performance of re-trained ILNIQE2 is improved almost 40% at the end. Same to the observation in Figure 8.9, the improvement for reflex camera is greater than LFC and smartphone in Figure 8.11. By using **ERC** as an indicator, we can still summarize that the re-training process can improve the performance of ILNIQE2.

8.3.5 Discussion

From the overall point of view, all the selected **IQMs** decrease the **EER** when keeping 80% and 60% high quality samples in the database according to their quality assessment scores (see Figure 8.5). The expected outcome is that when more low quality face samples are omitted the **EER** should decrease continuously. However, two kinds of unexpected outcomes are observed: 1) **EER** increases when more low quality samples are omitted but the **EER**, which is computed from the last 40% high quality face samples is still lower than the **EER** computed from the entire database (AQI, AQIP, BLIINDS2, PWN and DCTSP for LFC; AQI, AQIP, BIQI, BLIINDS2, and PWN for smartphone; BRISQUE for reflex camera); and 2) **EER** increases when omitting low quality face samples but the **EER**, which is computed from the last 40% high quality face samples becomes higher than the **EER** computed from the entire database (CONTRAST, CONTRAST2, JPEG, JNBM, SSEQ, and SH for LFC; CONTRAST, CONTRAST2, SH, SSEQ, JNBM, and JPEG for smartphone; AQI, CONTRAST, CONTRAST2, dipIQ, JPEG, JNBM, PWN, SH, and SSEQ for reflex camera). **IQMs** that do not belong to these two cases are then have better performance. In addition, **IQMs** in case 2) have lower ability to predict the performance of selected face recognition systems compared to

the IQMs in case 1). When we compare the EER by omitting lowest quality sample one by one until only the highest quality face sample left from each subject we can see that, it is difficult to have a very smooth gradual declining curve. However, by using some of the IQMs to omit the lowest quality samples, we can observe that the EER curves have an obvious tendency to drop. These IQMs are: ILNIQE2 for LFC; BRISQUE, DCTSP, ILNIQE2, and dipIQ for smartphone; AQIP, and DCTSP for reflex camera. These IQMs have better overall performance than the others and they can be used for the development of new image-based multimodality biometric sample quality assessment method. In addition, although some curves may have fluctuations at some point, the general trend is still decreasing: AQIP and BRISQUE for LFC; BIQI, BRISQUE, and ILNIQE2 for reflex camera. In order to improve the performance of these IQMs, an optimization process needs to be conducted. On the other hand, some IQMs lead to the gradually increasing EER curves when omitting lowest quality face samples. This outcome is the opposite of our expectation. Such IQMs are: AQI, CONTRAST, JNBM, SH, SSEQ, CONTRAST2, and JPEG for LFC; AQI, AQIP, CONTRAST, JNBM, PWN, SH, SSEQ, CONTRAST2, and JPEG for smartphone; AQI, CONTRAST, JNBM, PWN, SH, SSEQ, CONTRAST2, dipIQ, and JPEG for reflex camera. They have reversed correlation with the performance of selected face recognition algorithms.

Based on the experimental results discussed above we can summarize that, ILNIQE2 has an overall better performance than the other selected IQMs for all three cameras. It gives obvious decreased EER curves for LFC and smartphone when omitting lowest quality samples one by one. Its EER curve for reflex camera has a big drop in the middle, but we can still see a decreasing trend. Several IQMs have better performance than the others for at least one camera: AQIP, BRISQUE, and DCTSP. Including ILNIQE2, most of these better performing IQMs are from the generalized purposes holistic category according to our classification in Table 8.1, except DCTSP. We introduced eight different distortions to the face sample images, and for each distortion we have five different levels of degradation. Therefore, it is not difficult to understand why some generalized purposes holistic IQMs have better performance. This is mainly due to that their design is to assess the quality of an image that contains unknown and multiple distortions. However, AQIP, BRISQUE, DCTSP, and even for original ILNIQE2 can neither obtain a very smooth gradually declining EER curve nor perform good for all three cameras. One of the reasons could be that most of generalized purposes holistic IQMs are usually trained on natural image databases, for instance, BRISQUE, and ILNIQE2 are trained on the LIVE database [208]. However, not all type of distortions for image-based attributes in our dataset are introduced in the LIVE database, for example, motion blur and contrast changes are not included in the LIVE database.

Additionally, BRISQUE, and ILNIQE2 are also **NSS** based **IQMs**. Face images are a sub-category of natural images so we may expect that these generalized purposes holistic and **NSS** based **IQMs** can fail in some conditions.

As we can also see from the experimental results, by using the quality assessment scores from some **IQMs** to omit low quality samples, the **EER** increases instead of decreasing. It means that such **IQMs** have reversed correlation with the performance of selected face recognition system. These **IQMs** are: AQI, CONTRAST, CONTRAST2, JNBM, SH, and SSEQ (for all three cameras). Except AQI and SSEQ, all these **IQMs** are from distortion specific category, which are designed for the measurement of single type of distortion, such as JPEG or JPEG2000 compression distortions. Since these **IQMs** are tested under the condition of images containing only single type of distortion, they may not predict well the quality of the face samples that contain multiple distortions. If we look at the **EER** curves when omitting lowest quality face samples one by one using PWN for smartphone and reflex camera, we can find that the curves have a declining tendency at a certain interval (in the beginning for smartphone and smartphone). PWN is a metric used for the measurement of noise degradation and at some points the face sample images that have noise distortions are starting to be omitted. Before all noise degraded face samples are omitted the **EER** can decrease. After there is no noise degraded face samples left in the database, the **EER** stops decreasing because PWN cannot predict the face image quality from other types of distortions. This explains why we can observe such phenomenon. When we compare the performance between selected **IQMs** and ISO proposed **IQMs**, we can see that only ISO1 can reduce the **EER** when omitting low quality face samples. ISO2 and ISO3 give similar results to **IQMs** which have reversed correlation with the performance of selected face recognition algorithms. The reason is that they are designed for only single type of distortion and they cannot handle the multiple distortions under the condition in this section. Thus, the findings in this section show that this research work can be used in the future and is meaningful.

Finally, experimental results from the re-trained ILNIQE2 show that the database used for training the **IQMs** may influence the performance. The core of the ILNIQE2 metric is a pre-learned **NSS** fitted **MultiVariate Gaussian (MVG)** model. This model uses **NSS** features computed from pristine natural image (e.g. LIVE database) patches. This **MVG** model is therefore deployed as a pristine reference model against which to measure the quality of a given test image. On each patch of a test image, a best-fit **MVG** model is computed and then compared with the pre-learned pristine **MVG** model for the calculation of the quality score. However, as we mentioned, face images are a sub-category of natural images. It may not be appropriate to compare the best-fit **MVG** model from only face images with the

pre-learned **MVG** model from the entire portion of natural images. It could be explained by the variations between face images are less due to the similar structure of face images. The re-trained **MVG** model is then more appropriate for the calculation of quality scores for face images. Therefore, the performance of re-trained ILNIQE2 is better than the original.

8.3.6 Summary

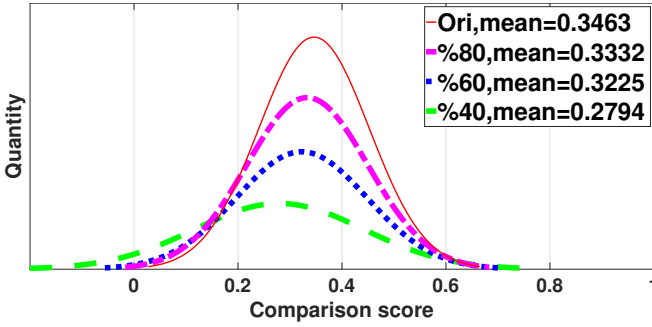
We evaluated the performance of selected no-reference **IQMs** for face biometric images on GC² Multi-Modality Biometric Database by using three face recognition algorithms. Three indicators are used to reflect the performance of **IQMs** according to the face recognition algorithms: histogram of mean comparison score, **DET** curve, and **EER** value. We illustrated the results by comparing between indicators with and without omitting certain percentage of low quality face samples. In addition, an experiment that re-trained a metric by using only face images is conducted. From the experimental results we can summarize that, before the re-training process, ILNIQE2 has a better performance than the other selected **IQMs** to assess the quality of face images based on the **DET** curves and **EER** values for two cameras: LFC and smartphone. The re-trained ILNIQE2 metric has better performance than its original for all three cameras and the performance for LFC and smartphone is further improved. Therefore, it is possible to use existing no-reference **IQMs** to assess the face sample quality, moreover, the optimization process can further improve the performance of **IQMs**. In general, selected distortion specific **IQMs** are not as good as the selected generalized purposes holistic **IQMs** due to the limitation of suitable degradation.

8.4 Experimental results for iris modality

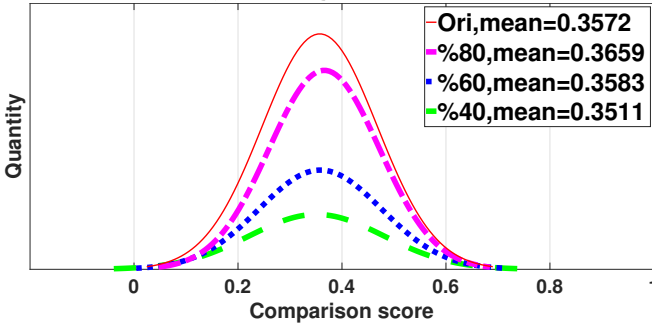
8.4.1 Histogram of the comparison scores and their mean values

Here we only illustrate the interesting examples in Figure 8.12 for iris modality. The histogram of the genuine comparison scores when omitting low quality samples by using 15 selected no-reference **IQMs** for three cameras are shown in Appendix A (Figures A.4, A.5, and A.6).

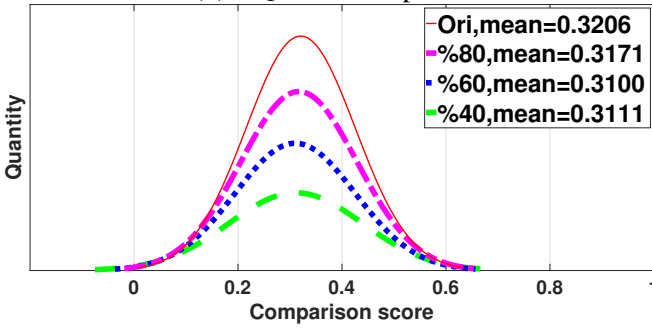
In Figure 8.12 (a), by using the assessment results from ILNIQE2 for LFC to omit low quality samples, we can observe the expected left shift for fitted lines (as well as the decreasing of mean values). It means that such **IQMs** can assess **VW** iris image quality and it is correlated with the performance of iris recognition algorithm. In Figure 8.12 (b), the mean values increase from keeping 80% to 60% highest quality samples by using AQI metric for smartphone, however, the values decrease when there is only 40% highest quality samples left. This means that AQI has



(a) ILNIQE2 for LFC



(b) AQI for Smartphone



(c) JPEG for Reflex

Figure 8.12: Examples of comparison scores and their mean values with omitting low quality samples.

reversed correlation with the performance of iris recognition algorithm for smartphone. In Figure 8.12 (c), all mean values are lower than the original, however, when only 40% highest quality samples left the mean value increases. This can be explained that when only a small part of the data left the system performance can be fluctuating and it might not be reliable.

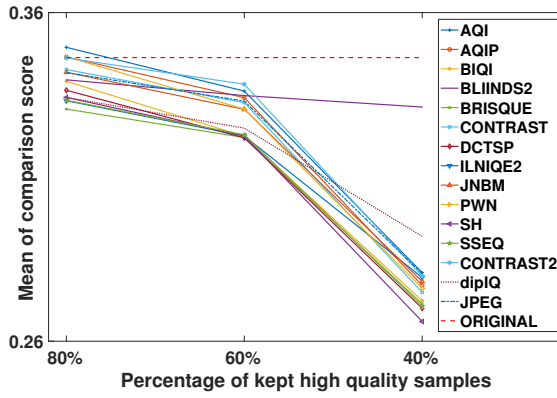
The plots of mean values when omitting low quality samples are illustrated in Figure 8.13 for three cameras. From Figure 8.13 (a) we can see that, when we use AQI, AQIP, CONTRAST2, and PWN to omit 20% of lowest quality iris samples, the mean comparison scores are higher than the original score. Similar findings can be observed for smartphone (AQI, AQIP, CONTRAST, and CONTRAST2) in Figure 8.13 (b). However, for the reflex camera, the mean comparison scores have an increasing tendency when more and more iris samples are omitted when we use CONTRAST, JNBM, and JPEG metrics (see Figure 8.13 (c)). Moreover, the mean comparison score becomes higher than the original mean comparison score when using CONTRAST2 to omit low quality score for reflex camera. The rest IQMs can assess VW iris sample quality according to the mean of comparison score.

8.4.2 DET curve and EER

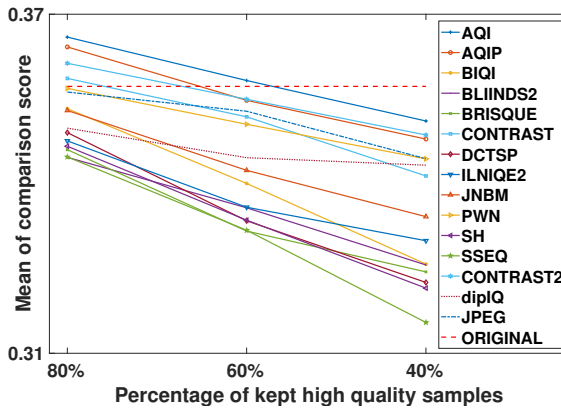
The interesting DET curves with EER for data with and without omitting low quality VW iris samples for three cameras by using IQMs are given in Figure 8.14. The DET curves with EER for data with and without omitting low quality iris samples for three cameras by using all 15 selected IQMs are given in Appendix B (see Figures B.4, B.5, and B.6).

From Figure 8.14 (a) and (b) we can see that, DET curves shift closer to bottom-left point when we keep 80%, 60%, and 40% highest quality samples by using the assessment results from PWN to omit low quality samples taken by smartphone and reflex camera, respectively. Especially we can see very obvious gap between each lines in Figure 8.14 (b). It means that such IQMs can assess VW iris image quality and it is correlated with the performance of iris recognition algorithm. However, the DET curves have no obvious shift and the EER values have no significant changes by using the assessment results from BLIINDS2 when we omit low quality samples for LFC (see Figure 8.14 (c)). In Figure 8.14 (d), DET curves shift closer to top-right point and EER values increase when we keep 80%, 60%, and 40% highest quality samples by using the assessment results from dipIQ to omit low quality samples taken by reflex camera. This means that such IQMs have a reversed correlation with the performance of iris recognition algorithm.

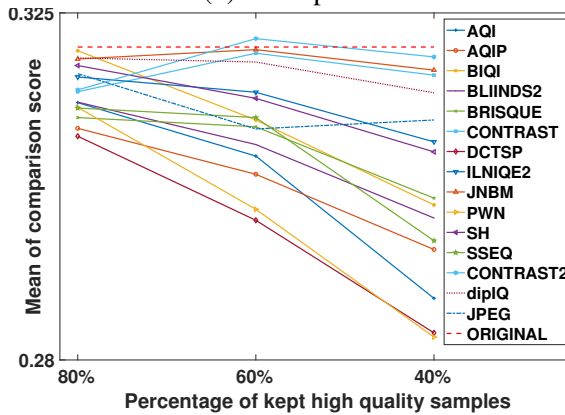
The tendency of EER values with omitting low quality samples for iris modality is given in Figure 8.15 for three cameras. From Figure 8.15 (a) we can see that, the



(a) LFC

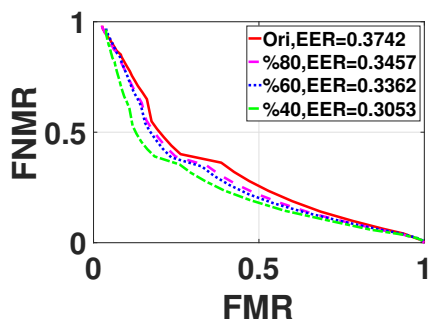


(b) Smartphone

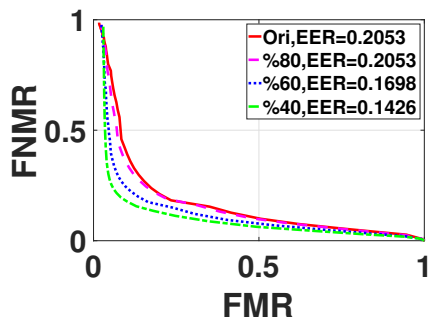


(c) Reflex

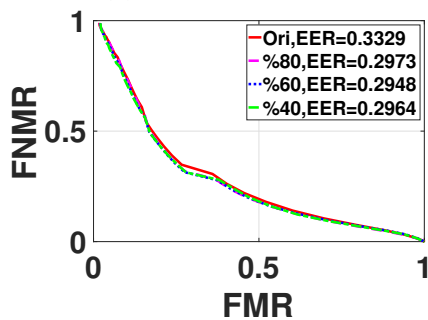
Figure 8.13: Tendency of mean comparison scores with omitting low quality samples.



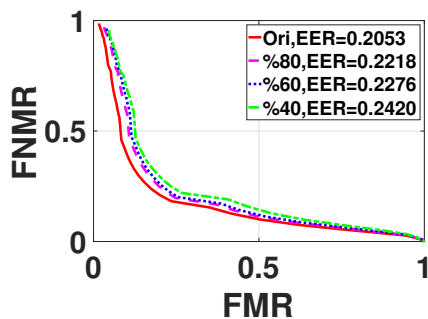
(a) PWN for Smartphone



(b) PWN for Relfex

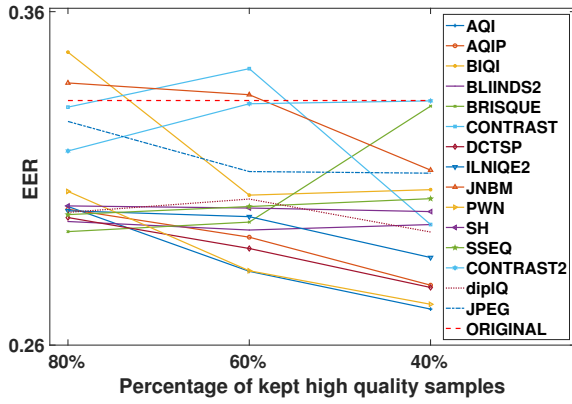


(c) BLIINDS2 for LFC

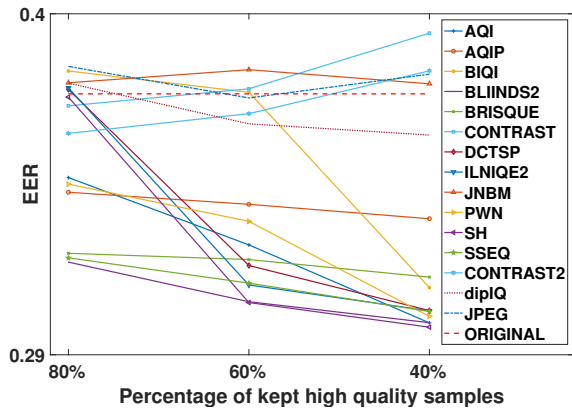


(d) dipIQ for Reflex

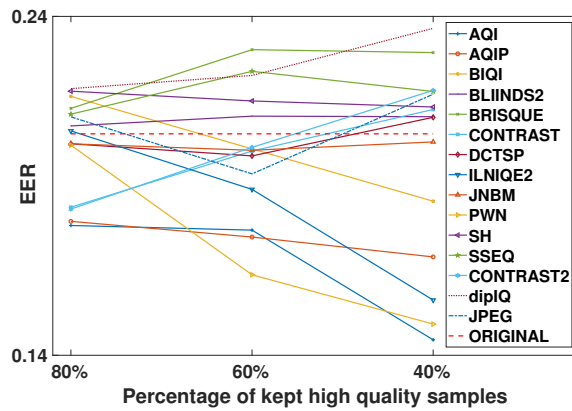
Figure 8.14: Examples of DET curves with EER for comparison score with and without omitting low quality samples.



(a) LFC



(b) Smartphone



(c) Reflex

Figure 8.15: Tendency of EER values with and without omitting low quality samples.

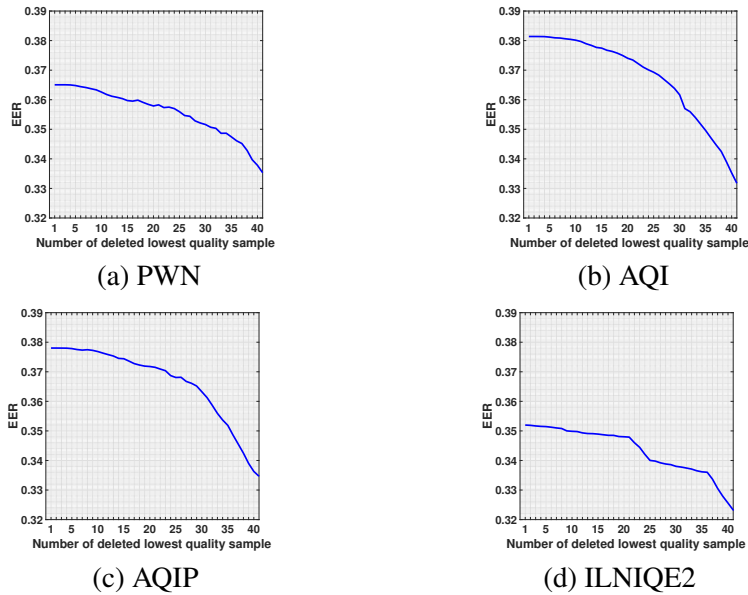


Figure 8.16: Examples of EER values with omitting low quality iris samples one by one until the best quality sample left for LFC.

tendency of EER values from JPEG, PWN, AQI, AQIP, and ILNIQE2 are obviously decreasing from 80% to 40% of kept high quality samples for LFC. Similar findings can be observed from Figure 8.15 (b) (DCTSP, PWN, SH, SSEQ, AQI, AQIP, BLIINDS2, and ILNIQE2) for smartphone and from Figure 8.15 (c) (PWN, AQI, AQIP, and ILNIQE2) for reflex camera. For the rest of IQMs, the EER values either higher than the original value or have increasing tendency. From the observation above we can summarize that, based on DET curves and EER values, four IQMs can assess VW iris quality for all three cameras: PWN, AQI, AQIP, and ILNIQE2.

The full plots of EER values for all three cameras by omitting lowest quality iris sample one by one until only one highest quality iris sample left from each subject are shown in Appendix C (see Figures C.4, C.5, and C.6). Here we only illustrate the four IQMs (PWN, AQI, AQIP, and ILNIQE2) that can assess iris quality for three cameras introduced above to discover the change of EER values. For iris modality, there are also 40 units per captured sample image per subject (eight distortions in five levels). But each unit has 1500 images (15 captured sample image per eye per subject). In Figures 8.16 and 8.17 we can see that, by using the assessment results from selected four IQMs to omit one lowest quality sample each time, the EER curves have decreasing tendency. However, in Figure 8.18,

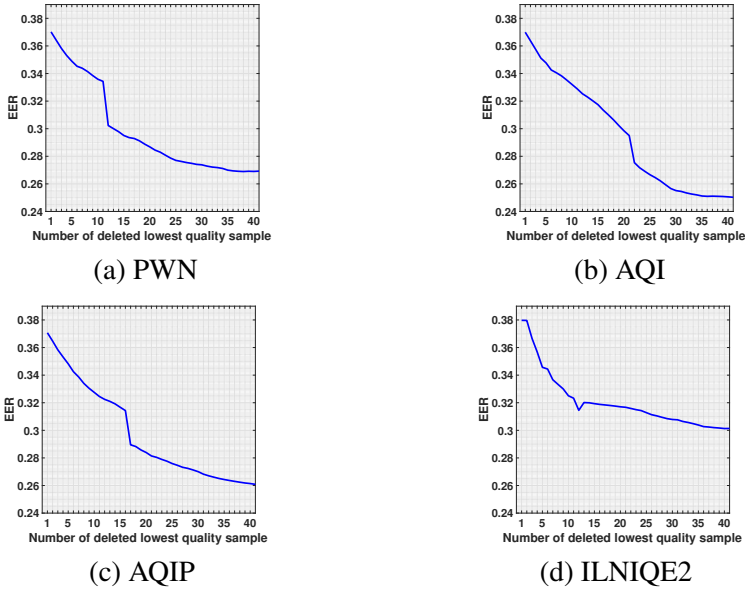


Figure 8.17: Examples of EER values with omitting low quality iris samples one by one until the best quality sample left for smartphone.

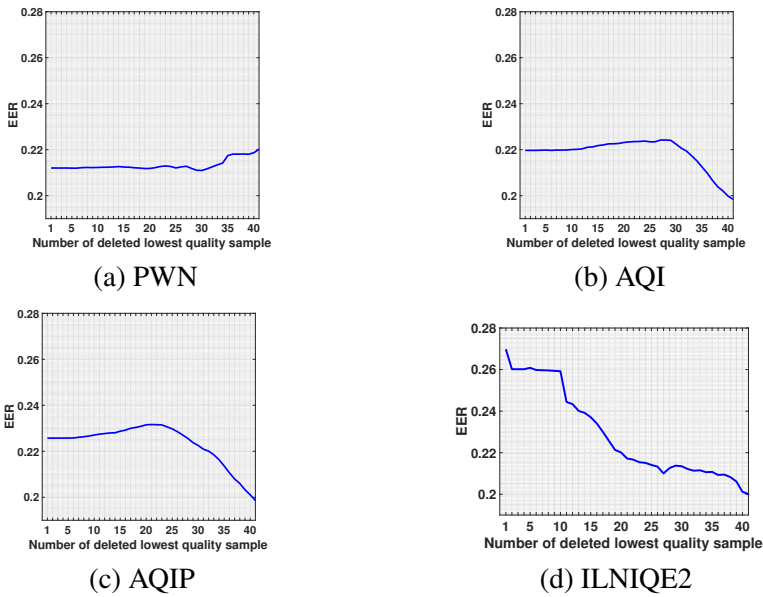


Figure 8.18: Examples of EER values with omitting low quality iris samples one by one until the best quality sample left for reflex camera.

Table 8.3: Overview of the performance of selected IQMs for iris modality

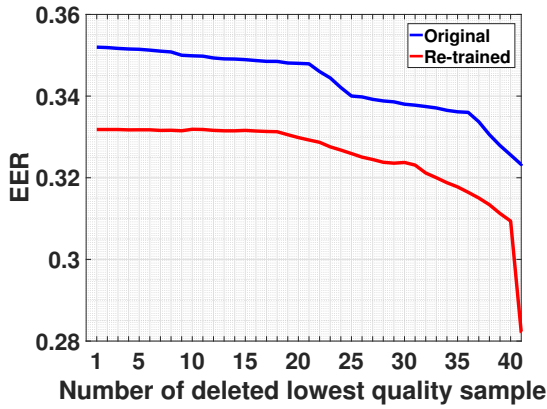
	LFC	Phone	Reflex
AQI	Improved performance	Improved performance	Neutral
AQIP	Improved performance	Improved performance	Neutral
BIQI	Decreased performance	Neutral	Neutral
BLIINDS2	Improved performance	Improved performance	Neutral
BRISQUE	Neutral	Improved performance	Neutral
CONTRAST	Neutral	Neutral	Improved performance
DCTSP	Neutral	Neutral	Neutral
ILNIQE2	Improved performance	Improved performance	Improved performance
JNBM	Neutral	Improved performance	Improved performance
PWN	Improved performance	Improved performance	Neutral
SH	Decreased performance	Improved performance	Neutral
SSEQ	Neutral	Improved performance	Neutral
CONTRAST2	Neutral	Neutral	Improved performance
dipIQ	Neutral	Neutral	Improved performance
JPEG	Neutral	Neutral	Improved performance

the [EER](#) values from AQI and AQIP for reflex camera increase in the beginning and decrease in the end. There is no obvious change of the [EER](#) values for PWN in the beginning, but the [EER](#) values increase in the end. Only [EER](#) values from ILNIQE2 in Figure 8.18) have no increasing tendency and decrease when 25 low quality units are omitted.

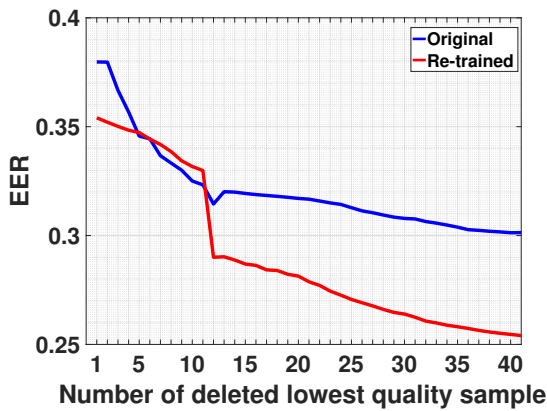
Here, we also illustrate the overview of the performance of [IQMs](#) in Table 8.3 for iris modality. We can observe that, based on [EER](#) values with omitting low quality iris samples one by one until the best quality sample left for three cameras, ILNIQE2 can assess iris image quality for three cameras. AQI and AQIP can assess iris quality for LFC and smartphone. JNBM can assess iris quality for smartphone and reflex camera. The rest of the [IQMs](#) can either assess iris quality for only one cameras, or have low ability to assess iris quality based on the system performance.

8.4.3 Re-training ILNIQE2 on VW iris database

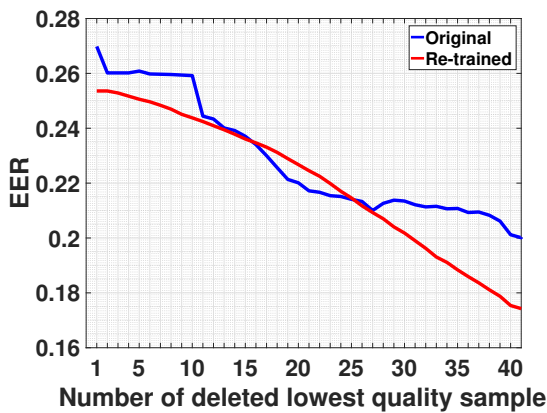
Similar to the face modality, ILNIQE2 shows better performance compared to other selected [IQMs](#). Therefore, we would like to know if results can be improved by retraining it on [VW](#) iris images. To perform the retraining, the UBIRIS .v2 database [44] has been selected, which the iris images were captured on non-constrained conditions (at-a-distance, on-the-move and on the visible wavelength). We use 241 images (one sample image per subject) in session one from the UBIRIS



(a) LFC

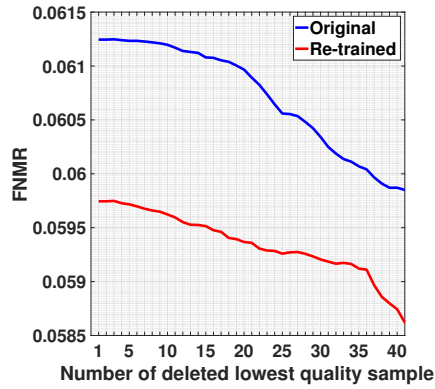


(b) Smartphone

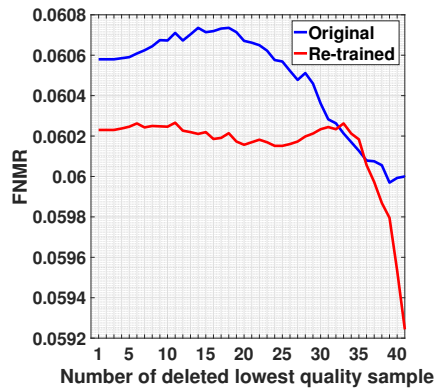


(c) Reflex

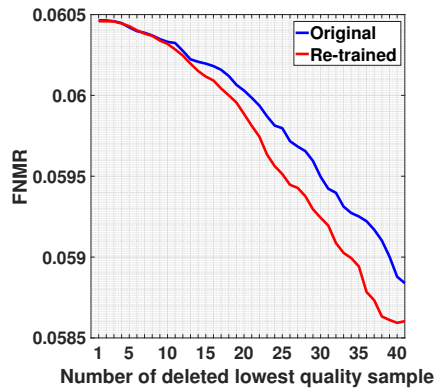
Figure 8.19: Comparison of EER by omitting lowest quality sample one by one using ILNIQE2 for each subject between the original method and the re-trained method.



(a) LFC



(b) Smartphone



(c) Reflex

Figure 8.20: Comparison of ERC by omitting lowest quality sample one by one using ILNIQE2 for each subject between the original method and the re-trained method.

.v2 database to re-train the ILNIQE2 metric. These 241 images are all high quality **VW** iris images. The re-trained metric is then used to re-conduct the experiment removing lowest quality samples one by one from each subject. The plots of **EER** values for three cameras are shown in Figure 8.19. The blue lines represent the original ILNIQE2 method, and the red lines represent the re-trained ILNIQE2 method. From Figure 8.19 we can see that, after the re-training process, the overall performance of the metric is improved because the red lines are under the blue lines. In addition, the improvement for LFC is greater than smartphone and reflex camera.

Again, we verify the performance of re-trained ILNIQE2 by using **ERC**. Figure 8.20 shows the **ERC** for all three cameras by omitting lowest quality iris sample one by one until only one highest quality iris sample is left from each subject. The blue lines represent the original ILNIQE2 method, and the red lines represent the re-trained ILNIQE2 method. By looking at plots (a) in Figure 8.20 for LFC, the overall **FNMR** values have an obvious drop. The re-trained ILNIQE2 has better performance than the original. In Figure 8.20 (b), the performance of re-trained ILNIQE2 is better than the original before 33 and after 36 units of lowest quality samples are omitted for smartphone. Moreover, the **FNMR** values drop fast and doubled the difference at the end. In Figure 8.20 (c), the improvement for reflex camera by using re-trained ILNIQE2 is greater and greater when keep omitting low quality iris samples. From the experimental results we can still summarize that the re-training process can improve the performance of ILNIQE2 for iris modality.

8.4.4 Summary

We evaluated the performance of 15 selected no-reference **IQMs** for **VW** iris biometric images on GC² Multi-Modality Biometric Database. Three indicators are used to reflect the performance of **IQMs** according to the iris recognition algorithms: histogram of mean comparison score, **DET** curve and **EER** value. We illustrated the results by comparing between indicators with and without omitting certain percentage of low quality iris samples. In addition, re-training a metric by using only **VW** iris database has been done. From the experimental results we can summarize that, before the re-training process, ILNIQE2 has a better performance than the other selected **IQMs** to assess the quality of iris images for three cameras based on the **EER** values. The re-trained ILNIQE2 metric has better performance than its original version, especially for LFC, based on the **EER** values and **ERC**.

8.5 Conclusion

From the experimental results for both face and **VW** iris modalities we can see that, there are several selected **IQMs** can assess biometric sample quality according to

the system performance, which addressed the third research question formulated in Section 1.2. Moreover, by re-training the ILNIQE2 metric using a modality specific database we can improve its performance, which addressed the last research question mentioned in Section 1.2. Therefore, it is possible to use existing no-reference IQMs to assess face and VW iris sample quality. The above mentioned findings can be used for the development of robust quality metrics for face and VW iris image quality, and furthermore, for multiple biometric modalities image quality assessment.

Chapter 9

Conclusion

The goal of this work was to investigate a common image-based multi-modality biometric sample quality assessment framework. Based on this framework, we evaluate the performance of existing no-reference IQMs on unconstrained multi-modality biometric samples. Assessing multi-modality biometric sample quality is a challenging task, since different biometric modalities have their own quality attributes. Nevertheless, our aim was to use no-reference IQMs correlated with biometric system performance for unconstrained multi-modality biometric samples, which is a complex and difficult task. Four research questions have been addressed in this work: 1) how to design a common framework to assess the quality of multi-modality biometric image samples, 2) what are the most important image-based quality attributes in the common framework, 3) how to use no-reference IQMs to assess the quality of multi-modality biometric image samples, and what is their performance, 4) how to optimize the no-reference IQMs in order to improve their performance on multi-modality biometric image samples.

First, we introduced the concept of biometrics, including fingerprint, face, iris recognition and performance of a biometric system in Chapter 2. Then we explain the differences between image quality and biometric sample quality in the same chapter. Thereafter, in Chapter 3 we investigated existing biometric sample quality assessment methods for contact-based and contactless fingerprint, face, and NIR-based and VW iris modalities. We also discover how to evaluate the performance of biometric sample quality assessment methods. Based on the knowledge gathered from existing biometric sample quality assessment, we proposed a common framework for the assessment of multi-modality biometric image quality in Chapter 4. In this common framework, we first surveyed common image-based image attributes of multi-modality sample quality assessment for unconstrained

biometric system, then classified and selected the most important attributes from them. We created a new multi-modality biometric image quality database for the evaluation of biometric image quality assessment methods. Totally 830250 images were captured by LFC, smartphone, and reflex camera for contactless fingerprint, VW iris, and face biometric modalities. In the final section of Chapter 4, we investigated existing IQMs and their applications for biometrics. This chapter addressed the research questions 1 and 2. In Chapter 5 we conducted experiments to know how image degradations influence the performance of fingerprint biometrics. Due to the lack of publicly available contactless fingerprint recognition system, we first reviewed ten existing contact-based fingerprint quality enhancement approaches in Chapter 6. Based on the review, we proposed a 3-step contactless fingerprint image enhancement method in order to adapt contactless fingerprint to the contact-based fingerprint recognition systems. However, by using the proposed method, the performance of the fingerprint recognition system is still lower than an accepted level. Therefore, we left contactless fingerprint modality for further works.

Chapter 7 focused on the influence of different color spaces for the performance of face and VW iris recognition. The experimental results indicated that there is little difference by using different color spaces for face and VW iris recognition. In Chapter 8 we evaluated the performance of 15 selected no-reference IQMs for face and VW iris biometric images. We used 1) histogram of the comparison scores, 2) DET curve, and 3) EER as indicators to represent the performance of selected IQMs on face and VW iris biometrics. Based on the performance, we optimized the best performed metric, namely ILNIQE2 by re-training it on face or VW iris databases. The performance of optimized ILNIQE2 metric has been further improved according to the system performance for both modalities. This chapter addressed the research questions 3 and 4. The above mentioned findings can be used for the development of robust quality metrics for face and VW iris image quality, and furthermore, for multiple biometric modalities image quality assessment.

Main contributions

- Proposed a common framework for the assessment of multi-modality biometric image quality. This framework can be used for the development of biometric sample quality assessment for any image-based modalities.
- Investigated, classified, and redefined five most important image-based attributes: contrast, sharpness, luminance, artifacts, and color, which can be used for the assessment of multi-modality biometric sample quality.
- Created a new multi-modality biometric image quality database that can be

used for the evaluation of biometric sample quality assessment methods. There are three modalities in this database: contactless fingerprint, face, and **VW** iris. The database contains 13500 raw fingerprint images, 2250 raw face images, and 4500 raw iris images. In addition, we applied eight distortions in five degradation levels to each raw image. Therefore, totally 830250 sample images were included in this database. We plan to make the database publicly available.

- Surveyed existing **IQMs** and their applications in fingerprint, face, and iris biometrics. This survey helped us to select appropriate **IQMs**.
- Investigated how image degradations influence the performance of a fingerprint recognition system and a fingerprint quality assessment method.
- Proposed a 3-step contactless fingerprint image quality enhancement method after the survey of ten existing contact-based fingerprint enhancement approaches.
- Discovered that the performance of biometric systems is not significantly affected by different color spaces in our experimental setups and conditions.
- Evaluation the performance of 15 selected no-reference **IQMs** for face and **VW** iris images. The evaluation results showed that several **IQMs** can assess biometric sample quality according to the system performance. The best performed metric 'ILNIQE2' has been optimized by conducting a re-training process, and the performance was better than the original.

In conclusion, our work has investigated the multi-modality quality assessment for unconstrained biometric samples. New framework, database, and an optimized metric for assessing the quality of face and **VW** iris biometric images have been proposed, and the work carried out in this thesis will be useful for future research and development in the multi-modality biometric image quality assessment area.

Perspectives

Instead of introducing distortions artificially to the database, we could simulate the real world distortions when acquiring biometric images. This can be done by changing the acquisition conditions. More image-based biometric modalities could be included in the database, such as palmprint, ear, vein, and so on.

The proposed 3-step contactless fingerprint image quality enhancement method could be further optimized in order to enhance contactless fingerprints to a certain

level so that they can be adapted to the contact-based fingerprint recognition system. On the other hand, develop a fingerprint recognition system for contactless fingerprint samples could be another option to enrich the final evaluation stage for selected no-reference IQMs.

We can select more no-reference IQMs for the performance evaluation on multi-modality biometric sample images. Moreover, re-training the ILNIQE2 by using a multi-modality database (mixed datasets with face and VW iris images) is an interesting experiment to be conducted. It could also be interesting to use a metric to help enhance the biometric sample image quality, so that the system performance can be improved.

Bibliography

- [1] Arun A Ross, Karthik Nandakumar, and Anil K Jain, “Handbook of biometrics,” *Inger-Verlag, New York*, 2007.
- [2] Fernando Alonso-Fernandez, Julian Fierrez, and Javier Ortega-Garcia, “Quality measures in biometric systems,” *IEEE Security & Privacy*, vol. 10, no. 6, pp. 52–62, 2012.
- [3] Patrick Grother and Elham Tabassi, “Performance of biometric quality measures,” *IEEE transactions on pattern analysis and machine intelligence*, vol. 29, no. 4, pp. 531–543, 2007.
- [4] Samarth Bharadwaj, Mayank Vatsa, and Richa Singh, “Biometric quality: a review of fingerprint, iris, and face,” *EURASIP Journal on Image and Video Processing*, vol. 2014, no. 1, pp. 34, 2014.
- [5] Xinwei Liu, Marius Pedersen, Christophe Charrier, and Patrick Bours, “Performance evaluation of no-reference image quality metrics for face biometric images,” *J. Electron. Imaging* 27(2), 023001 (2018), doi: 10.1117/1.JEI.27.2.023001, 2018.
- [6] Xinwei Liu, Marius Pedersen, and Christophe Charrier, “Image-based attributes of multi-modality image quality for contactless biometric samples,” in *Signal Processing and Integrated Networks (SPIN), 2016 3rd International Conference on*. IEEE, 2016, pp. 106–111.
- [7] Xinwei Liu, Marius Pedersen, Christophe Charrier, Patrick Bours, and Christoph Busch, “The influence of fingerprint image degradations on the performance of biometric system and quality assessment,” in *Biometrics*

Special Interest Group (BIOSIG), 2016 International Conference of the IEEE, 2016, pp. 1–6.

- [8] Xinwei Liu, Marius Pedersen, Christophe Charrier, Faouzi Alaya Cheikh, and Patrick Bours, “An improved 3-step contactless fingerprint image enhancement approach for minutiae detection,” in *Visual Information Processing (EUVIP), 2016 6th European Workshop on*. IEEE, 2016, pp. 1–6.
- [9] Xinwei Liu, Christophe Charrier, Marius Pedersen, and Patrick Bours, “Study on color space for the performance of degraded face image recognition,” in *Media Watermarking, Security, and Forensics Conference, IS&T Electronic Imaging 2018*, 2018.
- [10] Xinwei Liu, Marius Pedersen, Christophe Charrier, and Patrick Bours, “Can no-reference image quality metrics assess contactless visible wavelength iris sample quality?,” in *Image Processing (ICIP), 2017 IEEE International Conference on, Beijing, China, September 2017*. IEEE, 2017, pp. 1–5.
- [11] Xinwei Liu, Christophe Charrier, Marius Pedersen, and Patrick Bours, “Study on color space for the performance of degraded visible wavelength iris image recognition,” in *COmpression and Representation of Audiovisual Signals*, 2017.
- [12] Xinwei Liu, Christophe Charrier, Marius Pedersen, and Patrick Bours, “Performance evaluation of no-reference image quality metrics for visible wavelength iris biometric images,” in *26th European Signal Processing Conference (EUSIPCO 2018), Rome, Italy, September 2018*, 2018, Accepted.
- [13] Xinwei Liu, Marius Pedersen, Christophe Charrier, and Patrick Bours, “Can image quality enhancement methods improve the performance of biometric systems for degraded face images?,” in *The 9th Colour and Visual Computing Symposium 2018 (CVCS 2018), Gjøvik, Norway, September 2018*. IEEE, 2018, Accepted.
- [14] Colin Beavan, *Fingerprints: The Origins of Crime Detection and the Murder Case that Launched Forensic Science*, Hyperion Books, 2002.
- [15] Francis Galton, *Finger prints*, Macmillan and Company, 1892.
- [16] Anil Jain, Ruud Bolle, and Sharath Pankanti, *Biometrics: personal identification in networked society*, vol. 479, Springer Science & Business Media, 2006.

-
- [17] ISO/IEC FDIS, “2382-37 information technology – vocabulary – part 37 : Biometrics,” 2012-05-01.
- [18] Anil K Jain, Arun Ross, and Salil Prabhakar, “An introduction to biometric recognition,” *IEEE Transactions on circuits and systems for video technology*, vol. 14, no. 1, pp. 4–20, 2004.
- [19] Lawrence O’Gorman, “Comparing passwords, tokens, and biometrics for user authentication,” *Proceedings of the IEEE*, vol. 91, no. 12, pp. 2021–2040, 2003.
- [20] Salil Prabhakar, Sharath Pankanti, and Anil K Jain, “Biometric recognition: Security and privacy concerns,” *IEEE security & privacy*, vol. 99, no. 2, pp. 33–42, 2003.
- [21] A Jain, D Maltoni, D Maio, and J Wayman, “Biometric systems technology, design and performance evaluation,” *Springer-Verlag London limited, 2005*, 2005.
- [22] Lawrence O’Gorman, “Seven issues with human authentication technologies,” in *Proc. Workshop Automatic Identification Advanced Technologies (AutoID)*, 2002, pp. 185–186.
- [23] Davide Maltoni, Dario Maio, Anil K Jain, and Salil Prabhakar, *Handbook of fingerprint recognition*, Springer Science & Business Media, 2009.
- [24] Francis Lee Bailey and Henry B Rothblatt, *Investigation and preparation of criminal cases*, Lawyers Co-operative Publishing Company, 1985.
- [25] Dario Maio, Davide Maltoni, Raffaele Cappelli, James L Wayman, and Anil K Jain, “Fvc2002: Second fingerprint verification competition,” in *Pattern recognition, 2002. Proceedings. 16th international conference on*. IEEE, 2002, vol. 3, pp. 811–814.
- [26] Anil K Jain and Stan Z Li, *Handbook of face recognition*, Springer, 2011.
- [27] Michael David Kelly, “Visual identification of people by computer,” Tech. Rep., STANFORD UNIV CALIF DEPT OF COMPUTER SCIENCE, 1970.
- [28] Michael Kirby and Lawrence Sirovich, “Application of the karhunen-loeve procedure for the characterization of human faces,” *IEEE Transactions on Pattern analysis and Machine intelligence*, vol. 12, no. 1, pp. 103–108, 1990.

- [29] Wikipedia, “Iris (anatomy),” [https://en.wikipedia.org/wiki/Iris_\(anatomy\)](https://en.wikipedia.org/wiki/Iris_(anatomy)), Accessed: 2017-11-29.
- [30] Libor Masek et al., “Recognition of human iris patterns for biometric identification,” 2003.
- [31] John Daugman, “How iris recognition works,” *IEEE Transactions on circuits and systems for video technology*, vol. 14, no. 1, pp. 21–30, 2004.
- [32] Anil K Jain, Arun A Ross, and Karthik Nandakumar, “Introduction,” in *Introduction to Biometrics*, pp. 1–49. Springer, 2011.
- [33] Alvin Martin, George Doddington, Terri Kamm, Mark Ordowski, and Mark Przybocki, “The det curve in assessment of detection task performance,” Tech. Rep., National Inst of Standards and Technology Gaithersburg MD, 1997.
- [34] George Doddington, Walter Liggett, Alvin Martin, Mark Przybocki, and Douglas Reynolds, “Sheep, goats, lambs and wolves: A statistical analysis of speaker performance in the nist 1998 speaker recognition evaluation,” Tech. Rep., NATIONAL INST OF STANDARDS AND TECHNOLOGY GAITHERSBURG MD, 1998.
- [35] Patrick J Flynn, “Biometrics databases,” in *Handbook of Biometrics*, pp. 529–548. Springer, 2008.
- [36] “NIST special fingerprint database 4,” <https://www.nist.gov/srd/nist-special-database-4>, Accessed: 2017-12-01.
- [37] Javier Ortega-Garcia, J Fierrez-Aguilar, D Simon, J Gonzalez, M Faundez-Zanuy, V Espinosa, A Satue, I Hernaez, J-J Igarza, C Vivaracho, et al., “Mcyt baseline corpus: a bimodal biometric database,” *IEE Proceedings-Vision, Image and Signal Processing*, vol. 150, no. 6, pp. 395–401, 2003.
- [38] “Yale face database,” <http://vision.ucsd.edu/content/yale-face-database>, Accessed: 2017-12-02.
- [39] “AT&T face database,” <http://www.cl.cam.ac.uk/research/dtg/attarchive/facedatabase.html>, Accessed: 2017-12-02.
- [40] “FERET color face database,” <https://www.nist.gov/programs-projects/face-recognition-technology-feret>, Accessed: 2017-12-02.

-
- [41] AR Martinez and Robert Benavente, “The ar face database, 1998,” *Computer Vision Center, Technical Report*, vol. 3, pp. 5, 2007.
- [42] “CASIA iris database,” <http://biometrics.idealtest.org/dbDetailForUser.do?id=4>, Accessed: 2017-12-01.
- [43] Hugo Proença and Luís A Alexandre, “Ubiris: A noisy iris image database,” in *International Conference on Image Analysis and Processing*. Springer, 2005, pp. 970–977.
- [44] Hugo Proença, Silvio Filipe, Ricardo Santos, Joao Oliveira, and Luis A Alexandre, “The ubiris. v2: A database of visible wavelength iris images captured on-the-move and at-a-distance,” *IEEE Transactions on Pattern Analysis and Machine Intelligence*, vol. 32, no. 8, pp. 1529, 2010.
- [45] M.S. Hosseini, B.N. Araabi, and H. Soltanian-Zadeh, “Pigment melanin: Pattern for iris recognition,” *Instrumentation and Measurement, IEEE Transactions on*, vol. 59, no. 4, pp. 792–804, April 2010.
- [46] Bruno Dumas, Catherine Pugin, Jean Hennebert, Dijana Petrovska-Delacrétaz, Andreas Humm, Florian Evéquo, Rolf Ingold, and Didier Von Rotz, “Myidea-multimodal biometrics database, description of acquisition protocols,” *Proc. Third COST*, vol. 275, pp. 59–62, 2005.
- [47] Javier Ortega-Garcia, J Fierrez-Aguilar, D Simon, J Gonzalez, M Faundez-Zanuy, V Espinosa, A Satue, I Hernaez, J-J Igarza, C Vivaracho, et al., “Mcyt baseline corpus: a bimodal biometric database,” *IEE Proceedings-Vision, Image and Signal Processing*, vol. 150, no. 6, pp. 395–401, 2003.
- [48] Sonia Garcia-Salicetti, Charles Beumier, Gérard Chollet, Bernadette Dorizzi, Jean Jardins, Jan Lunter, Yang Ni, and Dijana Petrovska-Delacrétaz, “Biomet: A multimodal person authentication database including face, voice, fingerprint, hand and signature modalities,” in *Audio-and Video-Based Biometric Person Authentication*. Springer, 2003, pp. 1056–1056.
- [49] “WVU multi-modality biometric database,” <https://biic.wvu.edu/data-sets/multimodal-dataset>, Accessed: 2017-12-02.
- [50] Peter G Engeldrum, *Psychometric scaling: a toolkit for imaging systems development*, Imcotek, 2000.
- [51] Ruud Janssen, *Computational image quality*, vol. 101, SPIE press, 2001.

- [52] D Benini et al., “ISO/IEC 29794-1 biometric quality framework standard,” *jtcl/sc37/working group*, 2006.
- [53] Eyung Lim, Xudong Jiang, and Weiyun Yau, “Fingerprint quality and validity analysis,” in *Image Processing. 2002. Proceedings. 2002 International Conference on*. IEEE, 2002, vol. 1, pp. I–I.
- [54] LinLin Shen, Alex Kot, and Wai Mun Koo, “Quality measures of fingerprint images,” in *AVBPA*. Springer, 2001, pp. 266–271.
- [55] Mayank Vatsa, Richa Singh, Afzel Noore, and Max M Houck, “Quality-augmented fusion of level-2 and level-3 fingerprint information using dsm theory,” *International Journal of Approximate Reasoning*, vol. 50, no. 1, pp. 51–61, 2009.
- [56] Martin Aastrup Olsen, Haiyun Xu, and Christoph Busch, “Gabor filters as candidate quality measure for nfiq 2.0,” in *Biometrics (ICB), 2012 5th IAPR International Conference on*. IEEE, 2012, pp. 158–163.
- [57] Yi Chen, Sarat C Dass, and Anil K Jain, “Fingerprint quality indices for predicting authentication performance,” in *AVBPA*. Springer, 2005, vol. 3546, pp. 160–170.
- [58] Elham Tabassi and Patrick Grother, “Fingerprint image quality,” in *Encyclopedia of Biometrics*, pp. 482–490. Springer, 2009.
- [59] Oliver Bausinger and Elham Tabassi, “Fingerprint sample quality metric nfiq 2.0.,” in *BIOSIG*, 2011, pp. 167–171.
- [60] Xingguang Li, Zhenan Sun, and Tieniu Tan, “Comprehensive assessment of iris image quality,” in *Image Processing (ICIP), 2011 18th IEEE International Conference on*. IEEE, 2011, pp. 3117–3120.
- [61] Craig Belcher and Yingzi Du, “A selective feature information approach for iris image-quality measure,” *IEEE Transactions on Information Forensics and Security*, vol. 3, no. 3, pp. 572–577, 2008.
- [62] Nathan D Kalka, Jinyu Zuo, Natalia A Schmid, and Bojan Cukic, “Image quality assessment for iris biometric,” *Biometric technology for human identification III*, vol. 6202, no. 1, pp. 62020D, 2006.
- [63] Zhuoshi Wei, Tieniu Tan, Zhenan Sun, and Jiali Cui, “Robust and fast assessment of iris image quality,” *Lecture notes in computer science*, vol. 3832, pp. 464, 2006.

-
- [64] Yuqing He, Ting Liu, Yushi Hou, and Yuanbo Wang, “A fast iris image quality evaluation method based on weighted entropy,” in *International Symposium on Photoelectronic Detection and Imaging 2007: Image Processing*. International Society for Optics and Photonics, 2008, vol. 6623, p. 66231R.
- [65] Yi Chen, Sarat C Dass, and Anil K Jain, “Localized iris image quality using 2-d wavelets,” in *International conference on biometrics*. Springer, 2006, pp. 373–381.
- [66] Jitao Sang, Zhen Lei, and Stan Z Li, “Face image quality evaluation for iso/iec standards 19794-5 and 29794-5,” in *International Conference on Biometrics*. Springer, 2009, pp. 229–238.
- [67] Rein-Lien Vincent Hsu, Jidnya Shah, and Brian Martin, “Quality assessment of facial images,” in *Biometric Consortium Conference, 2006 Biometrics Symposium: Special Session on Research at the*. IEEE, 2006, pp. 1–6.
- [68] M Subasic, S Loncaric, T Petkovic, H Bogunovic, and V Krivec, “Face image validation system,” in *Image and Signal Processing and Analysis, 2005. ISPA 2005. Proceedings of the 4th International Symposium on*. IEEE, 2005, pp. 30–33.
- [69] Brendan F Klare and Anil K Jain, “Face recognition: Impostor-based measures of uniqueness and quality,” in *Biometrics: Theory, Applications and Systems (BTAS), 2012 IEEE Fifth International Conference on*. IEEE, 2012, pp. 237–244.
- [70] Xiufeng Gao, Stan Z Li, Rong Liu, and Peiren Zhang, “Standardization of face image sample quality,” in *International Conference on Biometrics*. Springer, 2007, pp. 242–251.
- [71] Timo Ojala, Matti Pietikainen, and Topi Maenpaa, “Multiresolution gray-scale and rotation invariant texture classification with local binary patterns,” *IEEE Transactions on pattern analysis and machine intelligence*, vol. 24, no. 7, pp. 971–987, 2002.
- [72] ISO/IEC, “ISO/IEC 29794-4 information technology – biometric sample quality – part 4: Finger image data,” 2010.
- [73] ISO/IEC, “ISO/IEC 29794-5 information technology – biometric sample quality – part 5: Face image data,” 2010.

- [74] ISO/IEC, “ISO/IEC 29794-6 information technology – biometric sample quality – part 6: Iris image data,” 2014.
- [75] Fernando Alonso-Fernandez, Julian Fierrez, Javier Ortega-Garcia, Joaquin Gonzalez-Rodriguez, Hartwig Fronthaler, Klaus Kollreider, and Josef Bigun, “A comparative study of fingerprint image-quality estimation methods,” *IEEE Transactions on Information Forensics and Security*, vol. 2, no. 4, pp. 734–743, 2007.
- [76] Mohammad Omar Derawi, Bian Yang, and Christoph Busch, “Fingerprint recognition with embedded cameras on mobile phones,” in *International Conference on Security and Privacy in Mobile Information and Communication Systems*. Springer, 2011, pp. 136–147.
- [77] Yeegahng Song, Chulhan Lee, and Jaihie Kim, “A new scheme for touchless fingerprint recognition system,” in *Intelligent Signal Processing and Communication Systems, 2004. ISPACS 2004. Proceedings of 2004 International Symposium on*. IEEE, 2004, pp. 524–527.
- [78] Ruggero Donida Labati, Angelo Genovese, Vincenzo Piuri, and Fabio Scotti, “Contactless fingerprint recognition: a neural approach for perspective and rotation effects reduction,” in *Computational Intelligence in Biometrics and Identity Management (CIBIM), 2013 IEEE Workshop on*. IEEE, 2013, pp. 22–30.
- [79] Fengling Han, Jiankun Hu, Mohammed Alkhathami, and Kai Xi, “Compatibility of photographed images with touch-based fingerprint verification software,” in *Industrial Electronics and Applications (ICIEA), 2011 6th IEEE Conference on*. IEEE, 2011, pp. 1034–1039.
- [80] Vincenzo Piuri and Fabio Scotti, “Fingerprint biometrics via low-cost sensors and webcams,” in *Biometrics: Theory, Applications and Systems, 2008. BTAS 2008. 2nd IEEE International Conference on*. IEEE, 2008, pp. 1–6.
- [81] Ruggero Donida Labati, Vincenzo Piuri, and Fabio Scotti, “Neural-based quality measurement of fingerprint images in contactless biometric systems,” in *Neural Networks (IJCNN), The 2010 International Joint Conference on*. IEEE, 2010, pp. 1–8.
- [82] Chulhan Lee, Sanghoon Lee, and Jaihie Kim, “A study of touchless fingerprint recognition system,” in *Joint IAPR International Workshops on Statistical Techniques in Pattern Recognition (SPR) and Structural and Syntactic Pattern Recognition (SSPR)*. Springer, 2006, pp. 358–365.

-
- [83] Bian Yang, Guoqiang Li, and Christoph Busch, “Qualifying fingerprint samples captured by smartphone cameras,” in *Image Processing (ICIP), 2013 20th IEEE International Conference on*. IEEE, 2013, pp. 4161–4165.
- [84] Chulhan Lee, Sanghoon Lee, Jaihie Kim, and Sung-Jae Kim, “Preprocessing of a fingerprint image captured with a mobile camera,” in *International Conference on Biometrics*. Springer, 2006, pp. 348–355.
- [85] BY Hiew, Andrew BJ Teoh, and David CL Ngo, “Preprocessing of fingerprint images captured with a digital camera,” in *Control, Automation, Robotics and Vision, 2006. ICARCV’06. 9th International Conference on*. IEEE, 2006, pp. 1–6.
- [86] Hugo Proença, “Quality assessment of degraded iris images acquired in the visible wavelength,” *IEEE Transactions on Information Forensics and Security*, vol. 6, no. 1, pp. 82–95, 2011.
- [87] Lothar Breitenbach and Pravir Chawdhry, “Image quality assessment and performance evaluation for multimodal biometric recognition using face and iris,” in *Image and Signal Processing and Analysis, 2009. ISPA 2009. Proceedings of 6th International Symposium on*. IEEE, 2009, pp. 550–555.
- [88] Nathan D Kalka, Jinyu Zuo, Natalia A Schmid, and Bojan Cukic, “Estimating and fusing quality factors for iris biometric images,” *IEEE Transactions on Systems, Man, and Cybernetics-Part A: Systems and Humans*, vol. 40, no. 3, pp. 509–524, 2010.
- [89] Hartwig Fronthaler, Klaus Kollreider, and Joseph Bigun, “Automatic image quality assessment with application in biometrics,” in *Computer Vision and Pattern Recognition Workshop, 2006. CVPRW’06. Conference on*. IEEE, 2006, pp. 30–30.
- [90] Changlong Jin, Hakil Kim, Xuenan Cui, Eunsoo Park, Junchul Kim, Jinsoo Hwang, and Stephen Elliott, “Comparative assessment of fingerprint sample quality measures based on minutiae-based matching performance,” in *Electronic Commerce and Security, 2009. ISECS’09. Second International Symposium on*. IEEE, 2009, vol. 1, pp. 309–313.
- [91] Arun Ross, Karthik Nandakumar, and Anil K Jain, “Introduction to multi-biometrics,” in *Handbook of Biometrics*, pp. 271–292. Springer, 2008.
- [92] Anders Eriksson and Pär Wretling, “How flexible is the human voice?-a case study of mimicry,” in *Fifth European Conference on Speech Communication and Technology*, 1997.

- [93] Wilson R Harrison, "Suspect documents. their scientific examination," 1958.
- [94] Nalini K Ratha, Jonathan H Connell, and Ruud M Bolle, "An analysis of minutiae matching strength," in *International Conference on Audio-and Video-Based Biometric Person Authentication*. Springer, 2001, pp. 223–228.
- [95] Anil K Jain and Arun Ross, "Multibiometric systems," *Communications of the ACM*, vol. 47, no. 1, pp. 34–40, 2004.
- [96] Arun A Ross, Karthik Nandakumar, and Anil K Jain, *Handbook of multi-biometrics*, vol. 6, Springer Science & Business Media, 2006.
- [97] Ahmad Nazri Zamani, Mat Kamil Awang, Nazaruddin Omar, and Shahrin Azuan Nazeer, "Image quality assessments and restoration for face detection and recognition system images," in *Modeling & Simulation, 2008. AICMS 08. Second Asia International Conference on*. IEEE, 2008, pp. 505–510.
- [98] Gerald O Williams, "Iris recognition technology," in *Security Technology, 1996. 30th Annual 1996 International Carnahan Conference*. IEEE, 1996, pp. 46–59.
- [99] Andrea F Abate, Michele Nappi, Daniel Riccio, and Gabriele Sabatino, "2d and 3d face recognition: A survey," *Pattern recognition letters*, vol. 28, no. 14, pp. 1885–1906, 2007.
- [100] Kamal Nasrollahi and Thomas B Moeslund, "Face quality assessment system in video sequences," in *European Workshop on Biometrics and Identity Management*. Springer, 2008, pp. 10–18.
- [101] Marius Pedersen, Nicolas Bonnier, Jon Yngve Hardeberg, and Fritz Albrechtsen, "Attributes of image quality for color prints," *Journal of Electronic Imaging*, vol. 19, no. 1, pp. 011016–011016, 2010.
- [102] Robert K Rowe, Kristin A Nixon, and Stephen P Corcoran, "Multispectral fingerprint biometrics," in *Information Assurance Workshop, 2005. IAW'05. Proceedings from the Sixth Annual IEEE SMC*. IEEE, 2005, pp. 14–20.
- [103] Pradeep Buddharaju and Ioannis Pavlidis, "Multispectral face recognition: fusion of visual imagery with physiological information," *Face biometrics for personal identification*, pp. 91–108, 2007.

-
- [104] Christopher Boyce, Arun Ross, Matthew Monaco, Lawrence Hornak, and Xin Li, “Multispectral iris analysis: A preliminary study,” in *Computer Vision and Pattern Recognition Workshop, 2006. CVPRW’06. Conference on*. IEEE, 2006, pp. 51–51.
- [105] Thrasyvoulos N Pappas and David L Neuhoff, “Least-squares model-based halftoning,” in *SPIE/IS&T 1992 Symposium on Electronic Imaging: Science and Technology*. International Society for Optics and Photonics, 1992, pp. 165–176.
- [106] Fredrik Nilsson, “Objective quality measures for halftoned images,” *JOSA A*, vol. 16, no. 9, pp. 2151–2162, 1999.
- [107] RF Hess, A Bradley, and L Piotrowski, “Contrast-coding in amblyopia i. differences in the neural basis of human amblyopia,” *Proceedings of the Royal Society of London B: Biological Sciences*, vol. 217, no. 1208, pp. 309–330, 1983.
- [108] Albert Abraham Michelson, *Studies in optics*, Courier Corporation, 1995.
- [109] Paul Whittle, “The psychophysics of contrast brightness.,” 1994.
- [110] Eli Peli, “Contrast in complex images,” *JOSA A*, vol. 7, no. 10, pp. 2032–2040, 1990.
- [111] Kresimir Matkovic, László Neumann, Attila Neumann, Thomas Psik, and Werner Purgathofer, “Global contrast factor-a new approach to image contrast.,” *Computational Aesthetics*, vol. 2005, pp. 159–168, 2005.
- [112] Jorge Caviedes and Franco Oberti, “A new sharpness metric based on local kurtosis, edge and energy information,” *Signal Processing: Image Communication*, vol. 19, no. 2, pp. 147–161, 2004.
- [113] Samira Bouzit and Lindsay MacDonald, “Colour difference metrics and image sharpness,” in *Color and Imaging Conference*. Society for Imaging Science and Technology, 2000, vol. 2000, pp. 262–267.
- [114] Elena A Fedorovskaya, “Image quality as a problem of computational vision,” in *IS AND TS PICS CONFERENCE*. Society for Imaging Science & Technology, 2003, pp. 22–28.
- [115] “Lytro,” <https://www.lytro.com/>, Accessed: 2017-12-07.

- [116] Xinwei Liu, Marius Pedersen, and Jon Yngve Hardeberg, “Cid: Iq—a new image quality database,” in *International Conference on Image and Signal Processing*. Springer, 2014, pp. 193–202.
- [117] Marius Pedersen and Jon Yngve Hardeberg, “Survey of full-reference image quality metrics,” *Foundations and Trends in Computer Graphics and Vision*, vol. 7, no. 1, pp. 1–80, 2012.
- [118] Zhou Wang, Alan C Bovik, Hamid R Sheikh, and Eero P Simoncelli, “Image quality assessment: from error visibility to structural similarity,” *IEEE transactions on image processing*, vol. 13, no. 4, pp. 600–612, 2004.
- [119] Yuming Fang, Kede Ma, Zhou Wang, Weisi Lin, Zhijun Fang, and Guangtao Zhai, “No-reference quality assessment of contrast-distorted images based on natural scene statistics,” *IEEE Signal Processing Letters*, vol. 22, no. 7, pp. 838–842, 2015.
- [120] Karen Panetta, Chen Gao, and Sos Agaian, “No reference color image contrast and quality measures,” *IEEE transactions on Consumer Electronics*, vol. 59, no. 3, pp. 643–651, 2013.
- [121] Ke Gu, Weisi Lin, Guangtao Zhai, Xiaokang Yang, Wenjun Zhang, and Chang Wen Chen, “No-reference quality metric of contrast-distorted images based on information maximization,” *IEEE transactions on cybernetics*, 2016.
- [122] Rony Ferzli and Lina J Karam, “A no-reference objective image sharpness metric based on the notion of just noticeable blur (jnb),” *IEEE transactions on image processing*, vol. 18, no. 4, pp. 717–728, 2009.
- [123] Yu Han, Xiaoming Xu, and Yunze Cai, “Novel no-reference image blur metric based on block-based discrete cosine transform statistics,” *Optical Engineering*, vol. 49, no. 5, pp. 050501–050501, 2010.
- [124] Arthur Leclaire and Lionel Moisan, “No-reference image quality assessment and blind deblurring with sharpness metrics exploiting fourier phase information,” *Journal of Mathematical Imaging and Vision*, vol. 52, no. 1, pp. 145–172, 2015.
- [125] Gwendoline Blanchet and Lionel Moisan, “An explicit sharpness index related to global phase coherence,” in *Acoustics, Speech and Signal Processing (ICASSP), 2012 IEEE International Conference on*. IEEE, 2012, pp. 1065–1068.

-
- [126] Tong Zhu and Lina Karam, “A no-reference objective image quality metric based on perceptually weighted local noise,” *EURASIP Journal on Image and Video Processing*, vol. 2014, no. 1, pp. 5, 2014.
- [127] Zhou Wang, Hamid R Sheikh, and Alan C Bovik, “No-reference perceptual quality assessment of jpeg compressed images,” in *Image Processing. 2002. Proceedings. 2002 International Conference on*. IEEE, 2002, vol. 1, pp. I–I.
- [128] Salvador Gabarda and Gabriel Cristóbal, “Blind image quality assessment through anisotropy,” *JOSA A*, vol. 24, no. 12, pp. B42–B51, 2007.
- [129] Anush Krishna Moorthy and Alan Conrad Bovik, “A two-step framework for constructing blind image quality indices,” *IEEE Signal processing letters*, vol. 17, no. 5, pp. 513–516, 2010.
- [130] Michele A Saad, Alan C Bovik, and Christophe Charrier, “Dct statistics model-based blind image quality assessment,” in *Image Processing (ICIP), 2011 18th IEEE International Conference on*. IEEE, 2011, pp. 3093–3096.
- [131] Anish Mittal, Anush Krishna Moorthy, and Alan Conrad Bovik, “No-reference image quality assessment in the spatial domain,” *IEEE Transactions on Image Processing*, vol. 21, no. 12, pp. 4695–4708, 2012.
- [132] Lin Zhang, Lei Zhang, and Alan C Bovik, “A feature-enriched completely blind image quality evaluator,” *IEEE Transactions on Image Processing*, vol. 24, no. 8, pp. 2579–2591, 2015.
- [133] Lixiong Liu, Bao Liu, Hua Huang, and Alan Conrad Bovik, “No-reference image quality assessment based on spatial and spectral entropies,” *Signal Processing: Image Communication*, vol. 29, no. 8, pp. 856–863, 2014.
- [134] Lixiong Liu, Yi Hua, Qingjie Zhao, Hua Huang, and Alan Conrad Bovik, “Blind image quality assessment by relative gradient statistics and adaboosting neural network,” *Signal Processing: Image Communication*, vol. 40, pp. 1–15, 2016.
- [135] Mohamad El Abed, Alexandre Ninassi, Christophe Charrier, and Christophe Rosenberger, “Fingerprint quality assessment using a no-reference image quality metric,” in *Signal Processing Conference (EUSIPCO), 2013 Proceedings of the 21st European*. IEEE, 2013, pp. 1–5.
- [136] Zhigang Yao, Jean-Marie Le Bars, Christophe Charrier, and Christophe Rosenberger, “Fingerprint quality assessment combining blind image quality, texture and minutiae features,” in *ICISSP 2015*, 2015.

- [137] Ayman Abaza, Mary Ann Harrison, Thirimachos Bourlai, and Arun Ross, “Design and evaluation of photometric image quality measures for effective face recognition,” *IET Biometrics*, vol. 3, no. 4, pp. 314–324, 2014.
- [138] Abhishek Dutta, Raymond Veldhuis, and Luuk Spreeuwers, “Predicting face recognition performance using image quality,” *arXiv preprint arXiv:1510.07119*, 2015.
- [139] Fang Hua, Peter Johnson, Nadezhda Sazonova, Paulo Lopez-Meyer, and Stephanie Schuckers, “Impact of out-of-focus blur on face recognition performance based on modular transfer function,” in *Biometrics (ICB), 2012 5th IAPR International Conference on*. IEEE, 2012, pp. 85–90.
- [140] Cécile Fiche, Patricia Ladret, and Ngoc-Son Vu, “Blurred face recognition algorithm guided by a no-reference blur metric,” in *Image Processing: Machine Vision Applications III*, 2010, vol. 7538, pp. 75380U–75380U.
- [141] Tai Pang Chen, Xudong Jiang, and Wei-Yun Yau, “Fingerprint image quality analysis,” in *Image Processing, 2004. ICIP’04. 2004 International Conference on*. IEEE, 2004, vol. 2, pp. 1253–1256.
- [142] Eun-Kyung Yun and Sung-Bae Cho, “Adaptive fingerprint image enhancement with fingerprint image quality analysis,” *Image and Vision Computing*, vol. 24, no. 1, pp. 101–110, 2006.
- [143] Elham Tabassi and Charles L Wilson, “A novel approach to fingerprint image quality,” in *Image Processing, 2005. ICIP 2005. IEEE International Conference on*. IEEE, 2005, vol. 2, pp. II–37.
- [144] Anil K Jain, Jianjiang Feng, and Karthik Nandakumar, “Fingerprint matching,” *Computer*, vol. 43, no. 2, 2010.
- [145] Choonwoo Ryu, Seong G Kong, and Hakil Kim, “Enhancement of feature extraction for low-quality fingerprint images using stochastic resonance,” *Pattern Recognition Letters*, vol. 32, no. 2, pp. 107–113, 2011.
- [146] Kenneth Ko, “User’s guide to nist biometric image software (nbis),” *NIST Interagency/Internal Report (NISTIR)-7392*, 2007.
- [147] Philip Sedgwick, “Spearman’s rank correlation coefficient,” *BMJ*, vol. 349, pp. g7327, 2014.
- [148] Kiran B Raja, Ramachandra Raghavendra, Vinay Krishna Vemuri, and Christoph Busch, “Smartphone based visible iris recognition using deep sparse filtering,” *Pattern Recognition Letters*, vol. 57, pp. 33–42, 2015.

-
- [149] Kiran B Raja, Ramachandra Raghavendra, Martin Stokkenes, and Christoph Busch, "Multi-modal authentication system for smartphones using face, iris and periocular," in *Biometrics (ICB), 2015 International Conference on*. IEEE, 2015, pp. 143–150.
- [150] Ramachandra Raghavendra, Kiran B Raja, Bian Yang, and Christoph Busch, "Combining iris and periocular recognition using light field camera," in *Pattern Recognition (ACPR), 2013 2nd IAPR Asian Conference on*. IEEE, 2013, pp. 155–159.
- [151] Jack Hollingum, "Automated fingerprint analysis offers fast verification," *Sensor Review*, vol. 12, no. 3, pp. 12–15, 1992.
- [152] Shlomo Greenberg, Mayer Aladjem, Daniel Kogan, and Itshak Dimitrov, "Fingerprint image enhancement using filtering techniques," in *Pattern Recognition, 2000. Proceedings. 15th International Conference on*. IEEE, 2000, vol. 3, pp. 322–325.
- [153] Ramachandra Raghavendra, Christoph Busch, and Bian Yang, "Scaling-robust fingerprint verification with smartphone camera in real-life scenarios," in *Biometrics: Theory, Applications and Systems (BTAS), 2013 IEEE Sixth International Conference on*. IEEE, 2013, pp. 1–8.
- [154] Barry G Sherlock, DM Monro, and K Millard, "Fingerprint enhancement by directional fourier filtering," *IEE Proceedings-Vision, Image and Signal Processing*, vol. 141, no. 2, pp. 87–94, 1994.
- [155] Lin Hong, Yifei Wan, and Anil Jain, "Fingerprint image enhancement: Algorithm and performance evaluation," *IEEE transactions on pattern analysis and machine intelligence*, vol. 20, no. 8, pp. 777–789, 1998.
- [156] Dario Maio and Davide Maltoni, "Direct gray-scale minutiae detection in fingerprints," *IEEE transactions on pattern analysis and machine intelligence*, vol. 19, no. 1, pp. 27–40, 1997.
- [157] S Greenberg, "Adaptive anisotropic filter applied for fingerprint enhancement," *submitted for publication*, 1999.
- [158] Guang-Zhong Yang, Peter Burger, David N Firmin, and SR Underwood, "Structure adaptive anisotropic image filtering," *Image and Vision Computing*, vol. 14, no. 2, pp. 135–145, 1996.
- [159] Xiping Luo and Jie Tian, "Knowledge based fingerprint image enhancement," in *Pattern Recognition, 2000. Proceedings. 15th International Conference on*. IEEE, 2000, vol. 4, pp. 783–786.

- [160] Jiangang Cheng and Jie Tian, "Fingerprint enhancement with dyadic scale-space," *Pattern Recognition Letters*, vol. 25, no. 11, pp. 1273–1284, 2004.
- [161] Anil Jain, Lin Hong, and Ruud Bolle, "On-line fingerprint verification," *IEEE transactions on pattern analysis and machine intelligence*, vol. 19, no. 4, pp. 302–314, 1997.
- [162] Nabil Jean Naccache and Rajjan Shinghal, "Spta: A proposed algorithm for thinning binary patterns," *IEEE transactions on Systems, Man, and Cybernetics*, , no. 3, pp. 409–418, 1984.
- [163] Safar Hatami, Reshad Hosseini, Mahmoud Kamarei, and Hossein Ahmadi, "Wavelet based fingerprint image enhancement," in *Circuits and Systems, 2005. ISCAS 2005. IEEE International Symposium on*. IEEE, 2005, pp. 4610–4613.
- [164] Vutipong Areekul, Ukrit Watchareeruetai, Kittiwat Suppasriwasuseth, and Sawasd Tantaratana, "Separable gabor filter realization for fast fingerprint enhancement," in *Image Processing, 2005. ICIP 2005. IEEE International Conference on*. IEEE, 2005, vol. 3, pp. III–253.
- [165] Sharat Chikkerur, Alexander N Cartwright, and Venu Govindaraju, "Fingerprint enhancement using stft analysis," *Pattern recognition*, vol. 40, no. 1, pp. 198–211, 2007.
- [166] Nobuyuki Otsu, "A threshold selection method from gray-level histograms," *IEEE transactions on systems, man, and cybernetics*, vol. 9, no. 1, pp. 62–66, 1979.
- [167] Soweon Yoon, Jianjiang Feng, and Anil K Jain, "Latent fingerprint enhancement via robust orientation field estimation," in *Biometrics (IJCB), 2011 International Joint Conference on*. IEEE, 2011, pp. 1–8.
- [168] Jianjiang Feng, Jie Zhou, and Anil K Jain, "Orientation field estimation for latent fingerprint enhancement," *IEEE transactions on pattern analysis and machine intelligence*, vol. 35, no. 4, pp. 925–940, 2013.
- [169] RECOMMENDATION ITU-R BT, "Studio encoding parameters of digital television for standard 4: 3 and wide-screen 16: 9 aspect ratios," 1995.
- [170] Jae S Lim, "Two-dimensional signal and image processing," *Englewood Cliffs, NJ, Prentice Hall, 1990, 710 p.*, 1990.

-
- [171] David S Bright and Eric B Steel, “Two-dimensional top hat filter for extracting spots and spheres from digital images,” *Journal of Microscopy*, vol. 146, no. 2, pp. 191–200, 1987.
- [172] Karel Zuiderveld, “Contrast limited adaptive histogram equalization,” in *Graphics gems IV*. Academic Press Professional, Inc., 1994, pp. 474–485.
- [173] Masahiro Kawagoe and Akio Tojo, “Fingerprint pattern classification,” *Pattern recognition*, vol. 17, no. 3, pp. 295–303, 1984.
- [174] A Ravishankar Rao, *A taxonomy for texture description and identification*, Springer Science & Business Media, 2012.
- [175] Michael Kass and Andrew Witkin, “Analyzing oriented patterns,” *Computer vision, graphics, and image processing*, vol. 37, no. 3, pp. 362–385, 1987.
- [176] T Chang, “Texture analysis of digitized fingerprints for singularity detection,” in *Proc. 5th Int. Conf. Pattern Recognition*, 1980, pp. 478–480.
- [177] John G Daugman, “Uncertainty relation for resolution in space, spatial frequency, and orientation optimized by two-dimensional visual cortical filters,” *JOSA A*, vol. 2, no. 7, pp. 1160–1169, 1985.
- [178] Anil K Jain and Farshid Farrokhnia, “Unsupervised texture segmentation using gabor filters,” *Pattern recognition*, vol. 24, no. 12, pp. 1167–1186, 1991.
- [179] Neurotechnology Inc., “VeriFinger,” <http://www.neurotechnology.com>, Accessed: 2017-12-08.
- [180] Anil K Jain and Jianjiang Feng, “Latent palmprint matching,” *IEEE Transactions on Pattern Analysis and Machine Intelligence*, vol. 31, no. 6, pp. 1032–1047, 2009.
- [181] Luis Torres, Jean-Yves Reutter, and Luis Lorente, “The importance of the color information in face recognition,” in *Image Processing, 1999. ICIP 99. Proceedings. 1999 International Conference on*. IEEE, 1999, vol. 3, pp. 627–631.
- [182] Jae Young Choi, Yong Man Ro, and Konstantinos N Plataniotis, “Color local texture features for color face recognition,” *IEEE transactions on image processing*, vol. 21, no. 3, pp. 1366–1380, 2012.

- [183] Creed Jones and A Lynn Abbott, "Color face recognition by hypercomplex gabor analysis," in *Automatic Face and Gesture Recognition, 2006. FGR 2006. 7th International Conference on*. IEEE, 2006, pp. 6–pp.
- [184] Chengzhang Wang, Baocai Yin, Xiaoming Bai, and Yanfeng Sun, "Color face recognition based on 2dpca," in *Pattern Recognition, 2008. ICPR 2008. 19th International Conference on*. IEEE, 2008, pp. 1–4.
- [185] Jian Yang and Chengjun Liu, "A general discriminant model for color face recognition," in *Computer Vision, 2007. ICCV 2007. IEEE 11th International Conference on*. IEEE, 2007, pp. 1–6.
- [186] Jae Young Choi, Yong Man Ro, and Konstantinos N Plataniotis, "Color face recognition for degraded face images," *IEEE Transactions on Systems, Man, and Cybernetics, Part B (Cybernetics)*, vol. 39, no. 5, pp. 1217–1230, 2009.
- [187] Andrew W Yip and Pawan Sinha, "Contribution of color to face recognition," *Perception*, vol. 31, no. 8, pp. 995–1003, 2002.
- [188] Seunghwan Yoo, Rae-Hong Park, Dong-Gyu Sim, and Nowon-gu Wolgye-dong, "Investigation of color spaces for face recognition.," in *MVA, 2007*, pp. 106–109.
- [189] Patrick Bours and Kirsi Helkala, "Face recognition using separate layers of the rgb image," in *Intelligent Information Hiding and Multimedia Signal Processing, 2008. IHHMSP'08 International Conference on*. IEEE, 2008, pp. 1035–1042.
- [190] Baptiste Hemery, Jean-Jacques Schwartzmann, and Christophe Rosenberger, "Study on color spaces for single image enrolment face authentication," in *Pattern Recognition (ICPR), 2010 20th International Conference on*. IEEE, 2010, pp. 1249–1252.
- [191] Štruc Vitomir, "The phd toolbox: Pretty helpful development functions for face recognition," 2012.
- [192] Vitomir Štruc and Nikola Pavešić, "The complete gabor-fisher classifier for robust face recognition," *EURASIP Journal on Advances in Signal Processing*, vol. 2010, no. 1, pp. 847680, 2010.
- [193] Chengjun Liu, "Capitalize on dimensionality increasing techniques for improving face recognition grand challenge performance," *IEEE transactions on pattern analysis and machine intelligence*, vol. 28, no. 5, pp. 725–737, 2006.

-
- [194] Peter Kovesei, “Image features from phase congruency,” *Videre: Journal of computer vision research*, vol. 1, no. 3, pp. 1–26, 1999.
- [195] Matthew K Monaco, *Color space analysis for iris recognition*, West Virginia University, 2007.
- [196] Nadia Othman, Bernadette Dorizzi, and Sonia Garcia-Salicetti, “Osiris: An open source iris recognition software,” *Pattern Recognition Letters*, vol. 82, pp. 124–131, 2016.
- [197] James R Matey, David Ackerman, James Bergen, and Michael Tinker, “Iris recognition in less constrained environments,” in *Advances in Biometrics*, pp. 107–131. Springer, 2008.
- [198] Craig Fancourt, Luca Bogoni, Keith Hanna, Yanlin Guo, Richard Wildes, Naomi Takahashi, and Uday Jain, “Iris recognition at a distance,” in *International Conference on Audio-and Video-Based Biometric Person Authentication*. Springer, 2005, pp. 1–13.
- [199] Kelly N Smith, V Paul Pauca, Arun Ross, Todd Torgersen, and Michael C King, “Extended evaluation of simulated wavefront coding technology in iris recognition,” in *Biometrics: Theory, Applications, and Systems, 2007. BTAS 2007. First IEEE International Conference on*. IEEE, 2007, pp. 1–7.
- [200] Kang Ryoung Park and Jaihie Kim, “A real-time focusing algorithm for iris recognition camera,” *IEEE Transactions on Systems, Man, and Cybernetics, Part C (Applications and Reviews)*, vol. 35, no. 3, pp. 441–444, 2005.
- [201] Kiran B Raja, R Raghavendra, and Christoph Busch, “Visible iris imaging: A novel imaging solution for improved iris recognition,” in *Imaging Systems and Techniques (IST), 2015 IEEE International Conference on*. IEEE, 2015, pp. 1–6.
- [202] ISO/IEC, “19794-5 biometric data interchange formats - part 5: Face image data,” 2011-03-04.
- [203] ISO/IEC, “19794-6 biometric data interchange formats - part 6: Iris image data,” 2011-03-04.
- [204] Kede Ma, Wentao Liu, Tongliang Liu, Zhou Wang, and Dacheng Tao, “di-piq: Blind image quality assessment by learning-to-rank discriminable image pairs,” *IEEE Transactions on Image Processing*, vol. 26, no. 8, pp. 3951–3964, 2017.

- [205] Ce Liu, William T Freeman, Richard Szeliski, and Sing Bing Kang, “Noise estimation from a single image,” in *Computer Vision and Pattern Recognition, 2006 IEEE Computer Society Conference on*. IEEE, 2006, vol. 1, pp. 901–908.
- [206] Pina Marziliano, Frederic Dufaux, Stefan Winkler, and Touradj Ebrahimi, “A no-reference perceptual blur metric,” in *Image processing. 2002. Proceedings. 2002 international conference on*. IEEE, 2002, vol. 3, pp. III–III.
- [207] Jeonghun Yang, Hyuk Choi, and Taejeong Kim, “Noise estimation for blocking artifacts reduction in dct coded images,” *IEEE Transactions on circuits and systems for video technology*, vol. 10, no. 7, pp. 1116–1120, 2000.
- [208] Hamid R Sheikh, Zhou Wang, Lawrence Cormack, and Alan C Bovik, “Live image quality assessment database release 2,” 2005.

Appendix A

Figures of histogram of the comparison scores and their mean values

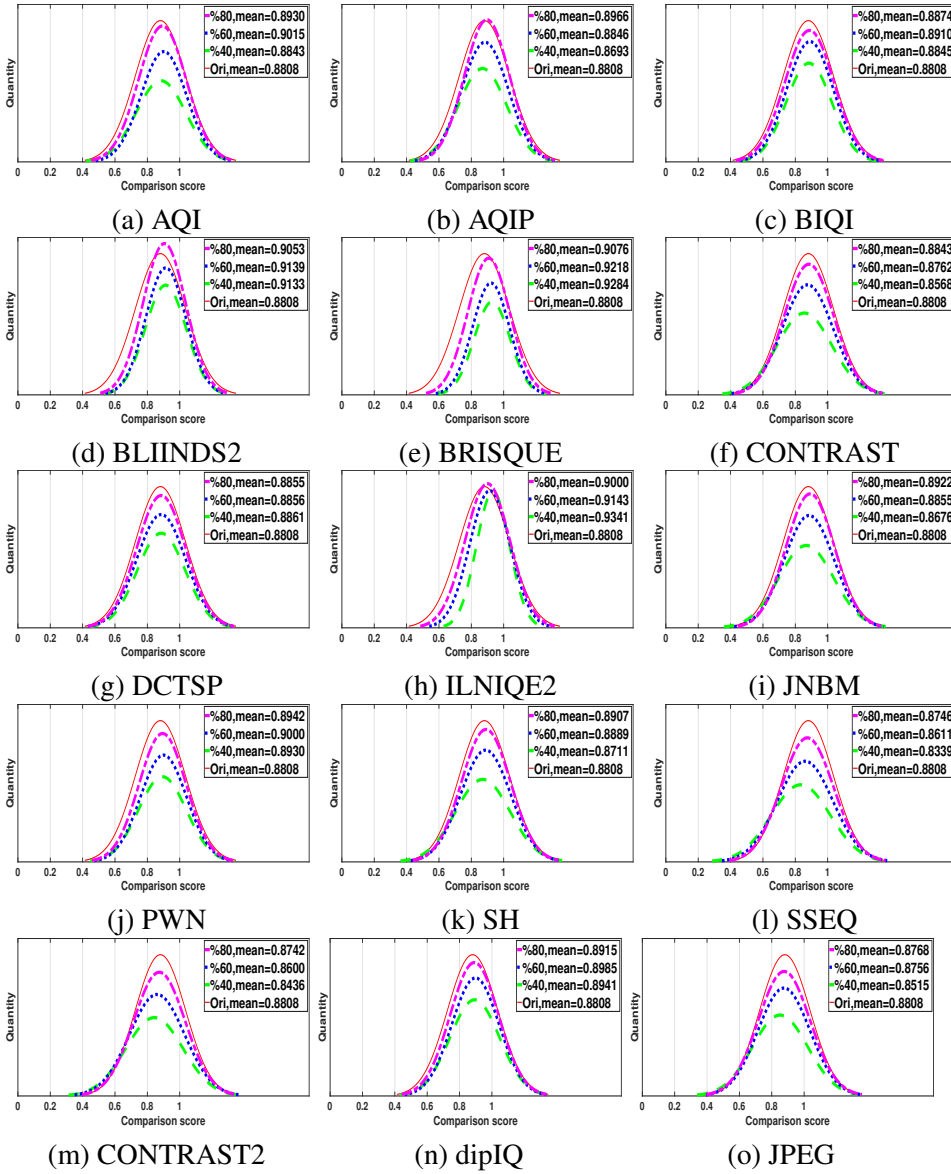


Figure A.1: Comparison scores and their mean values with omitting low quality face samples for LFC by using GF+KFA face recognition algorithm.

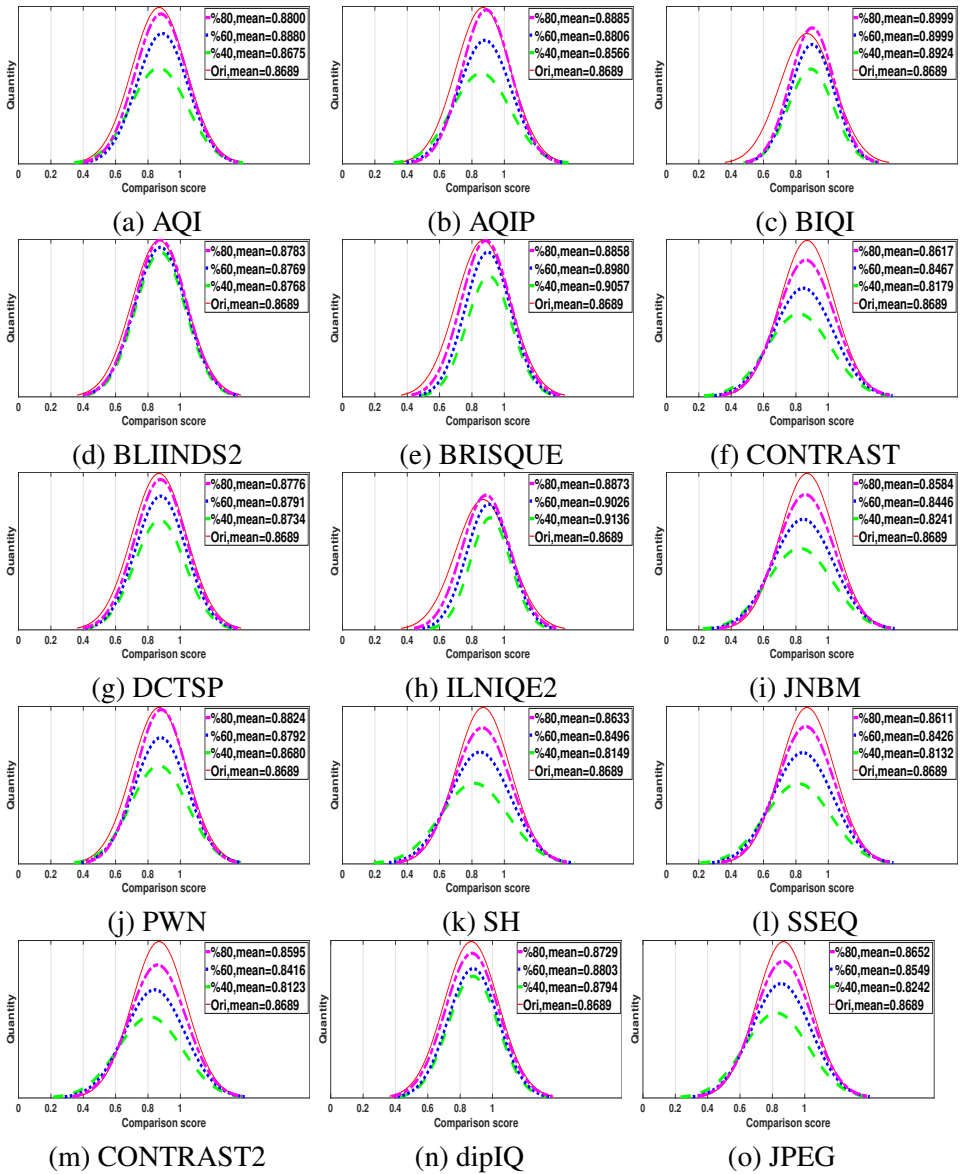


Figure A.2: Comparison scores and their mean values with omitting low quality face samples for smartphone by using GF+KFA face recognition algorithm.

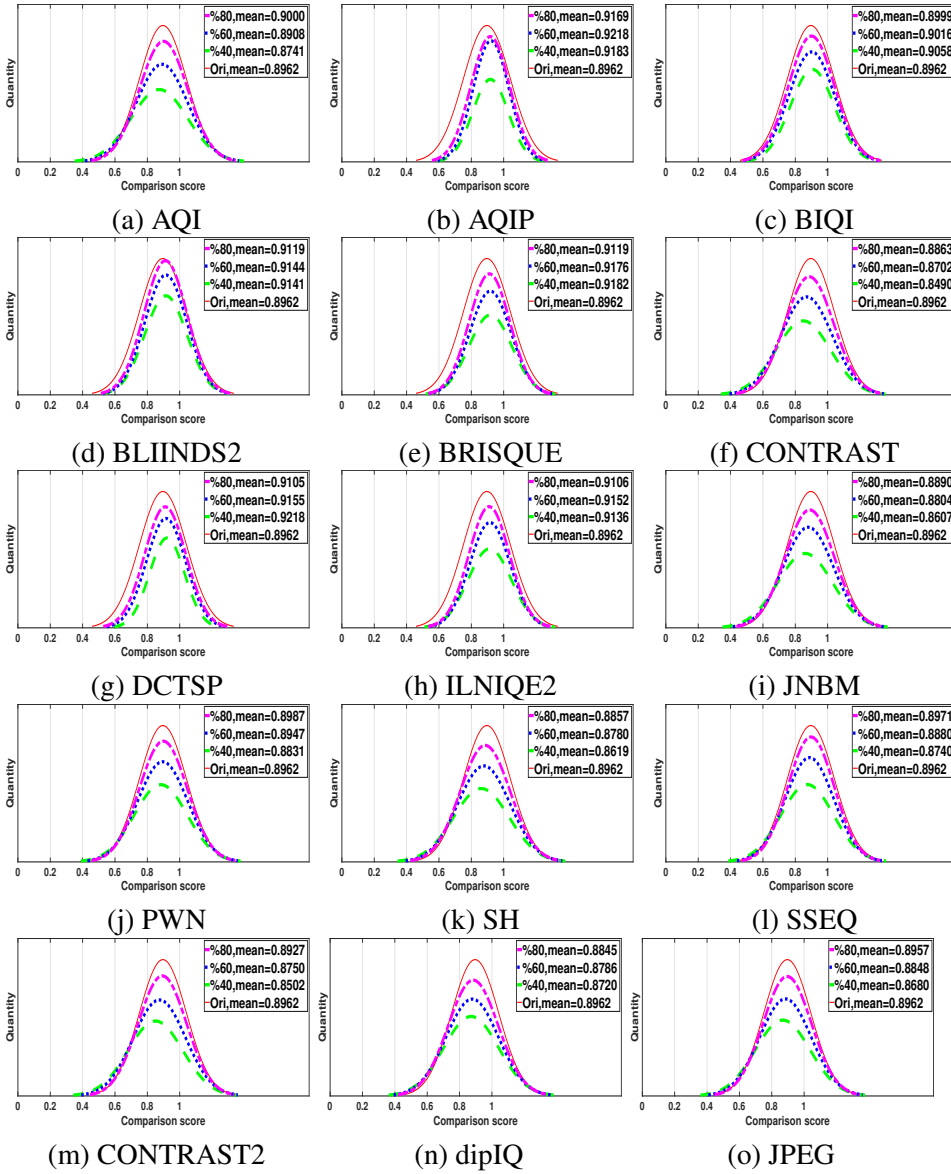


Figure A.3: Comparison scores and their mean values with omitting low quality face samples for reflex camera by using GF+KFA face recognition algorithm.

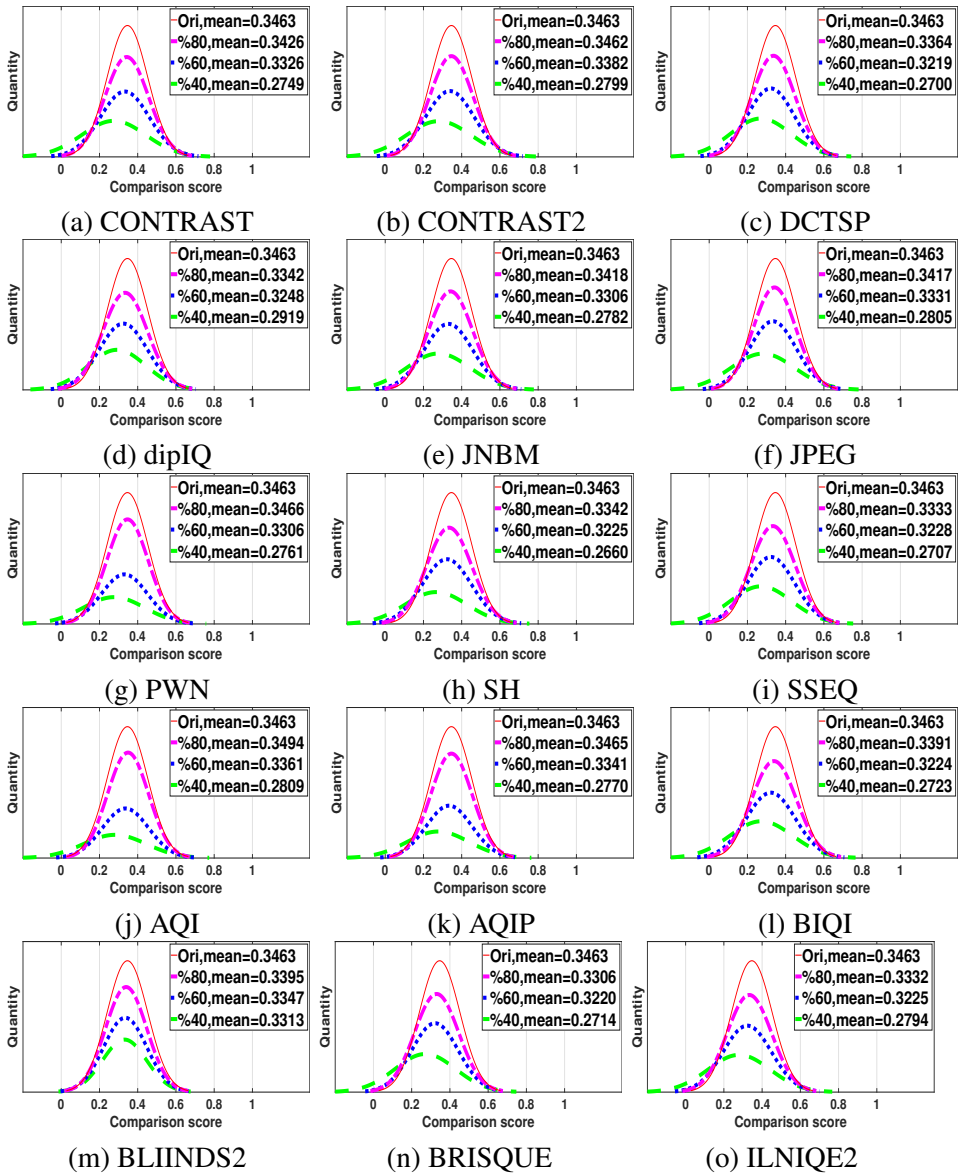


Figure A.4: Comparison scores and their mean values with omitting low quality iris samples for LFC.

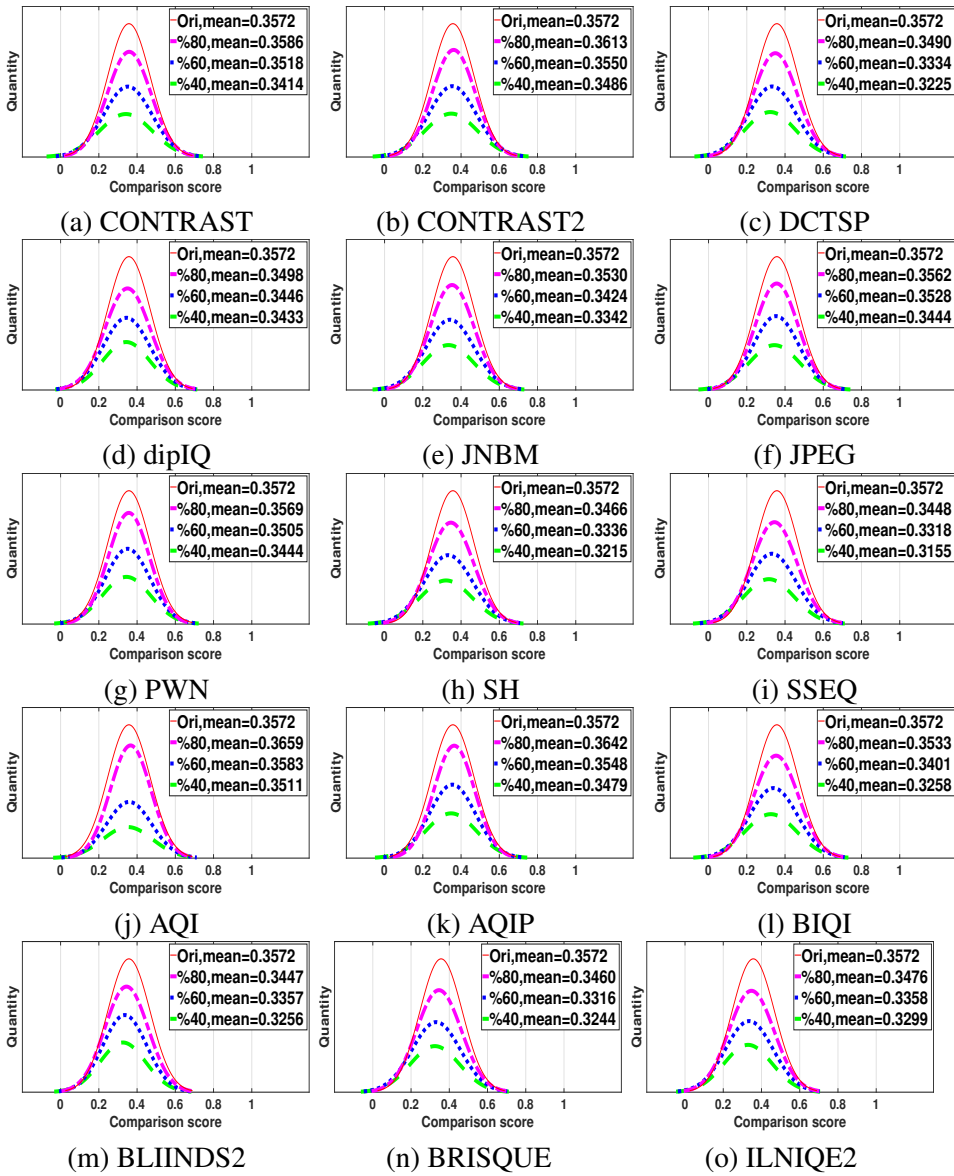


Figure A.5: Comparison scores and their mean values with omitting low quality iris samples for smartphone.

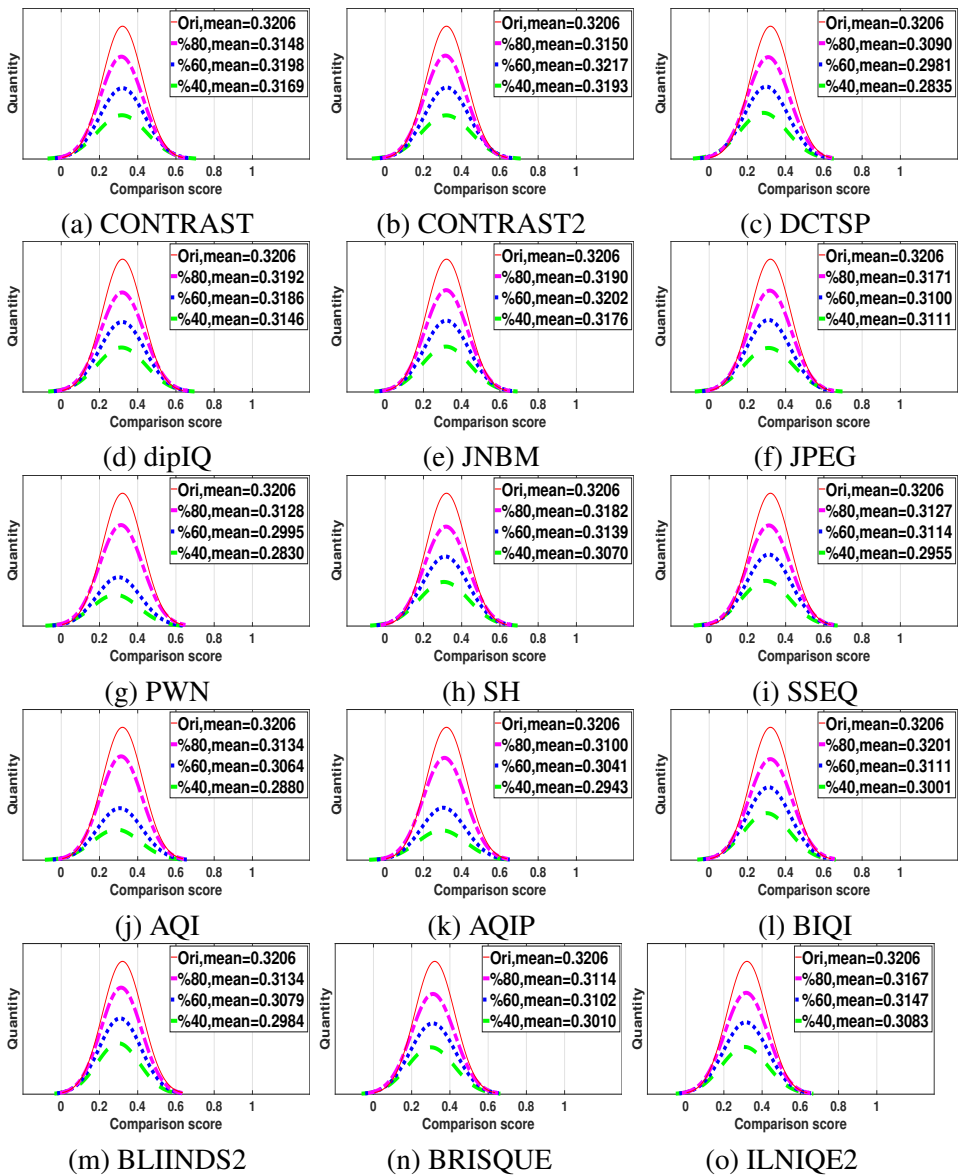


Figure A.6: Comparison scores and their mean values with omitting low quality iris samples for reflex camera.

Appendix B

Figures of DET curves with EER for comparison score with and without omitting low quality samples

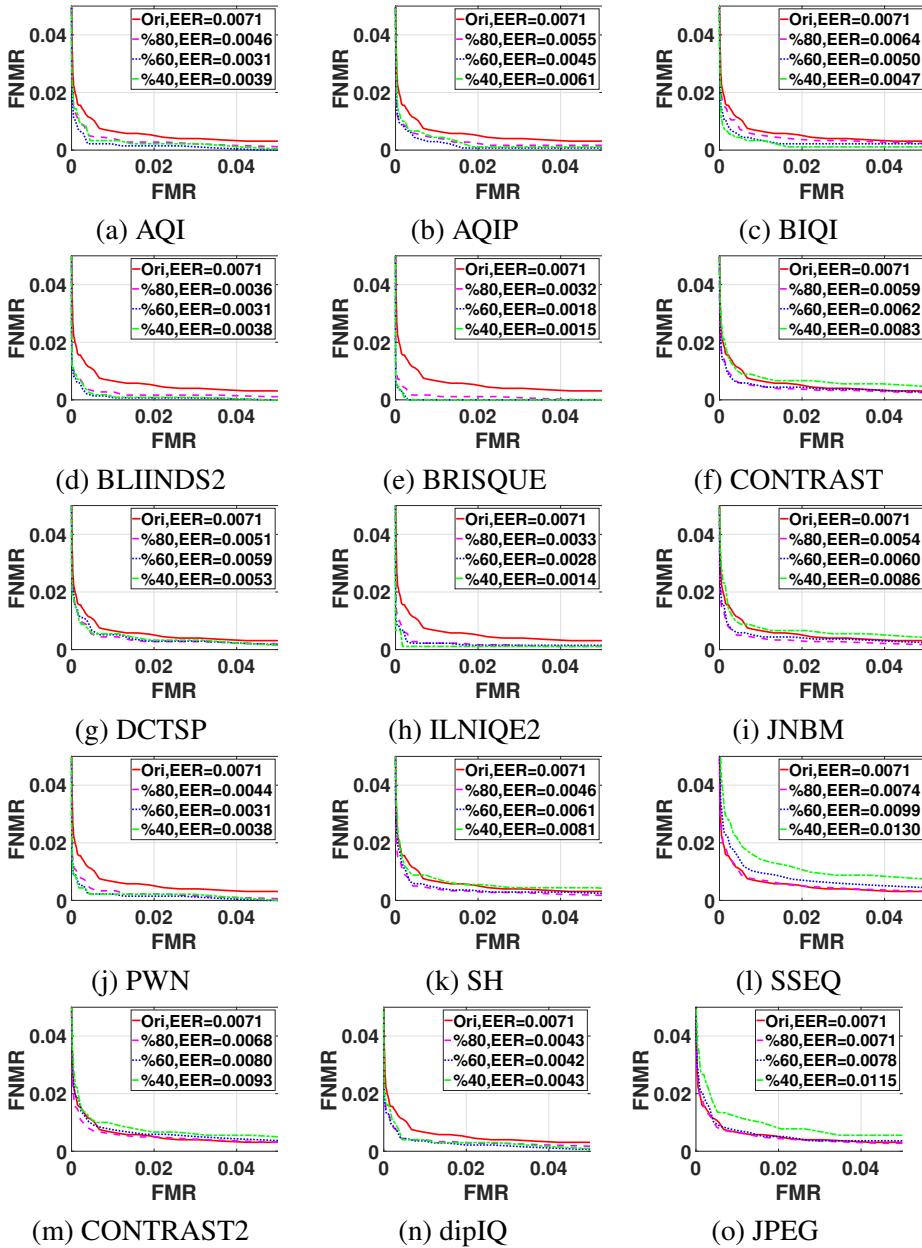


Figure B.1: DET curves with EER for comparison score with and without omitting low quality face samples for LFC by using GF+KFA face recognition algorithm.

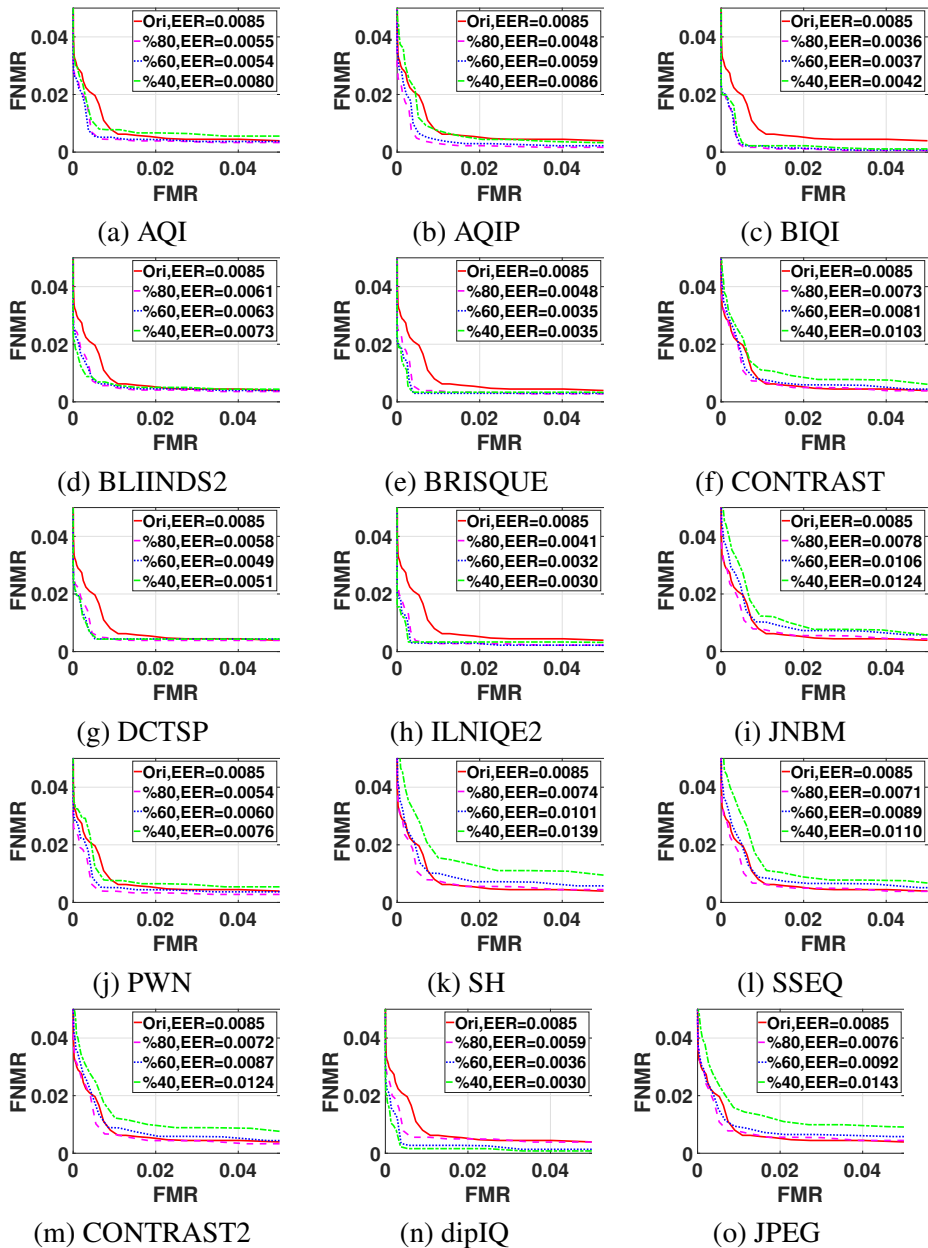


Figure B.2: DET curves with EER for comparison score with and without omitting low quality face samples for smartphone by using GF+KFA face recognition algorithm.

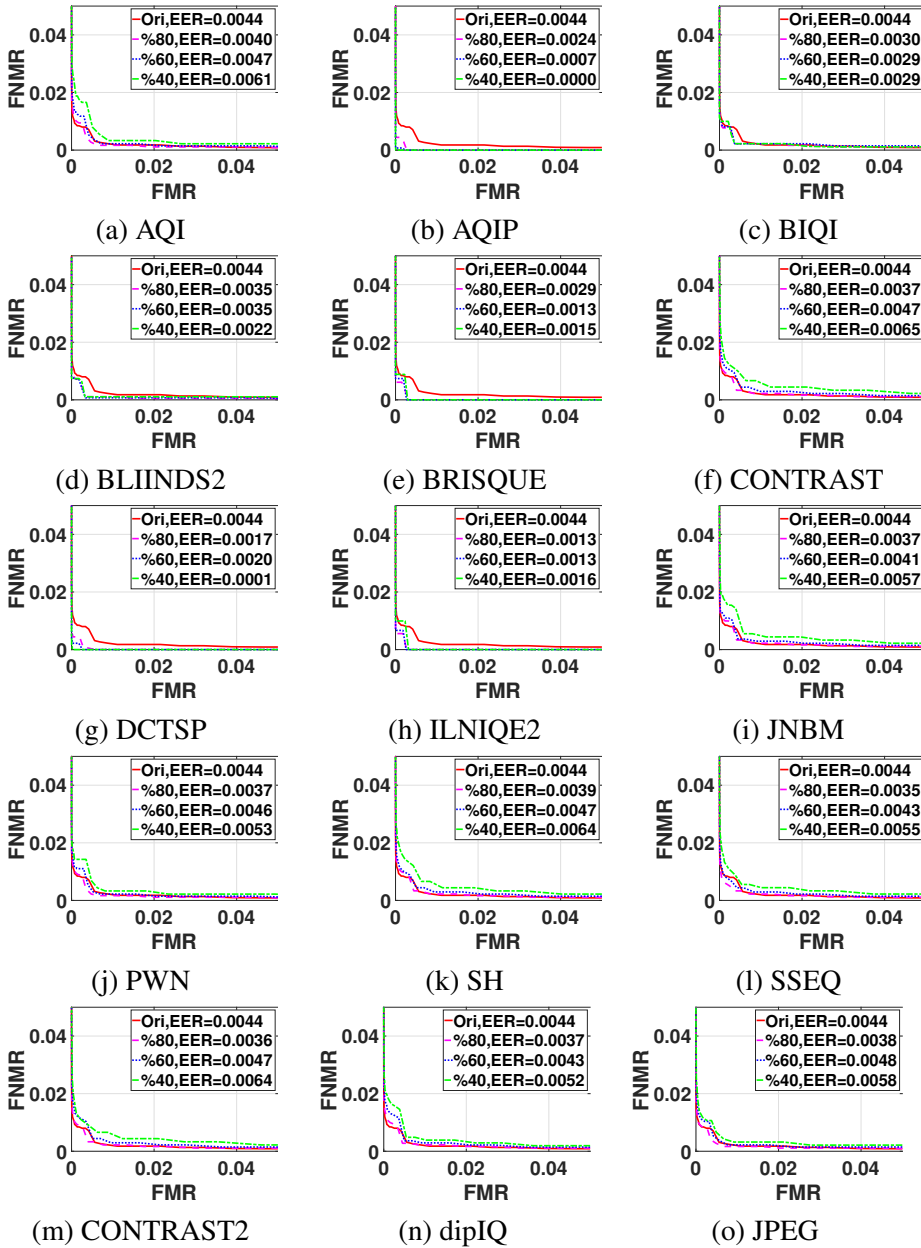


Figure B.3: DET curves with EER for comparison score with and without omitting low quality face samples for reflex camera by using GF+KFA face recognition algorithm.

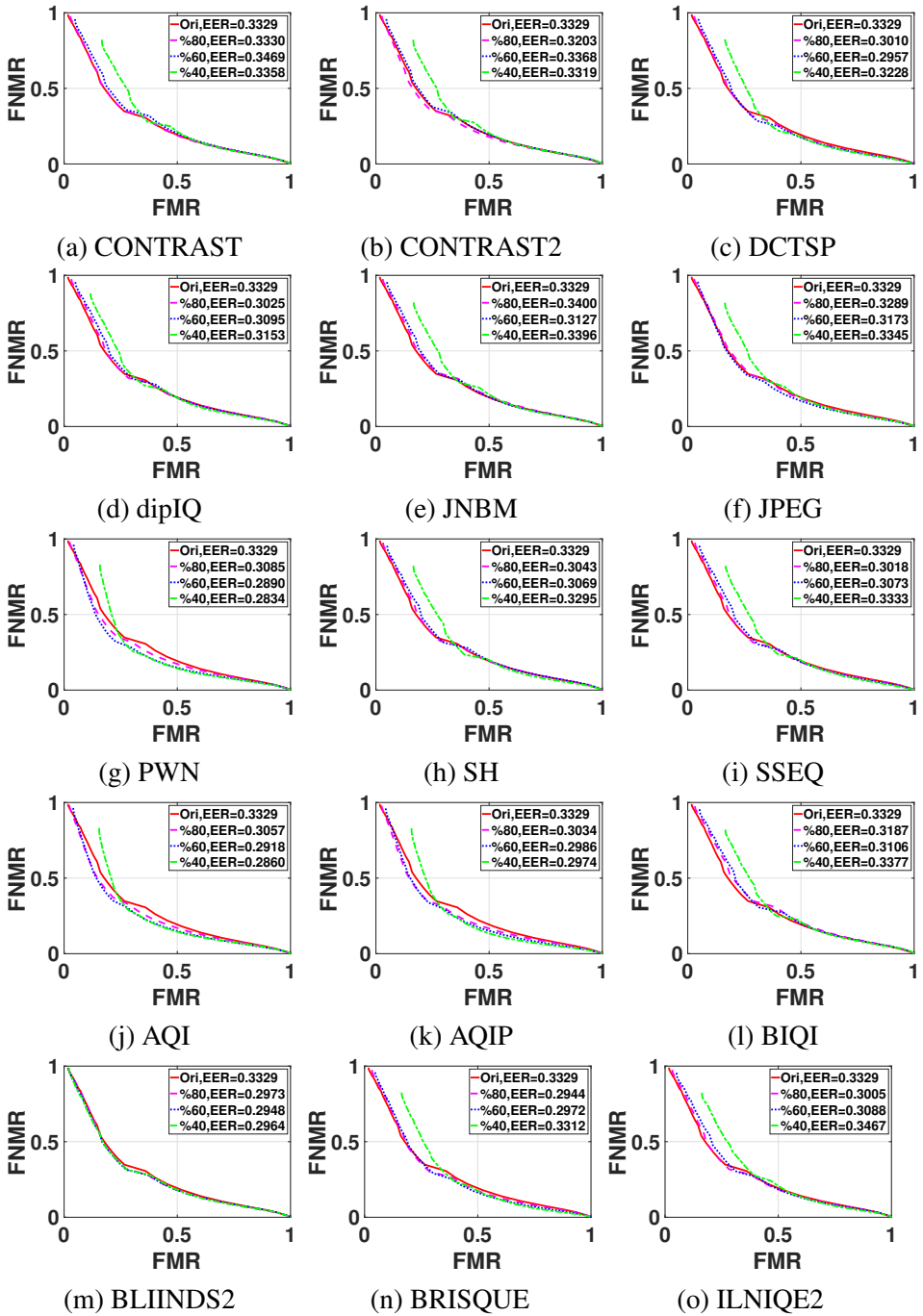


Figure B.4: DET curves with EER for comparison score with and without omitting low quality iris samples for LFC.

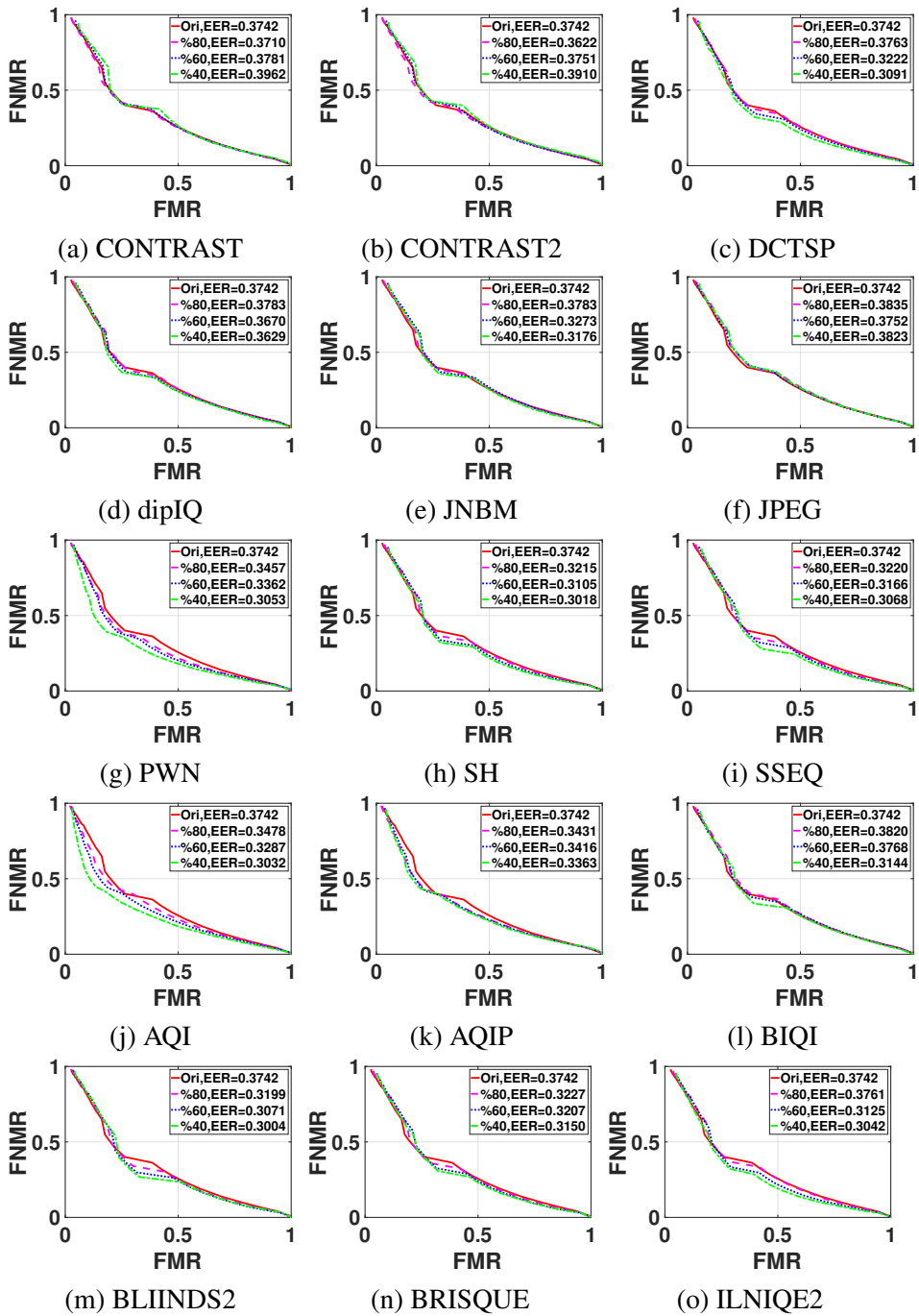


Figure B.5: DET curves with EER for comparison score with and without omitting low quality iris samples for smartphone.

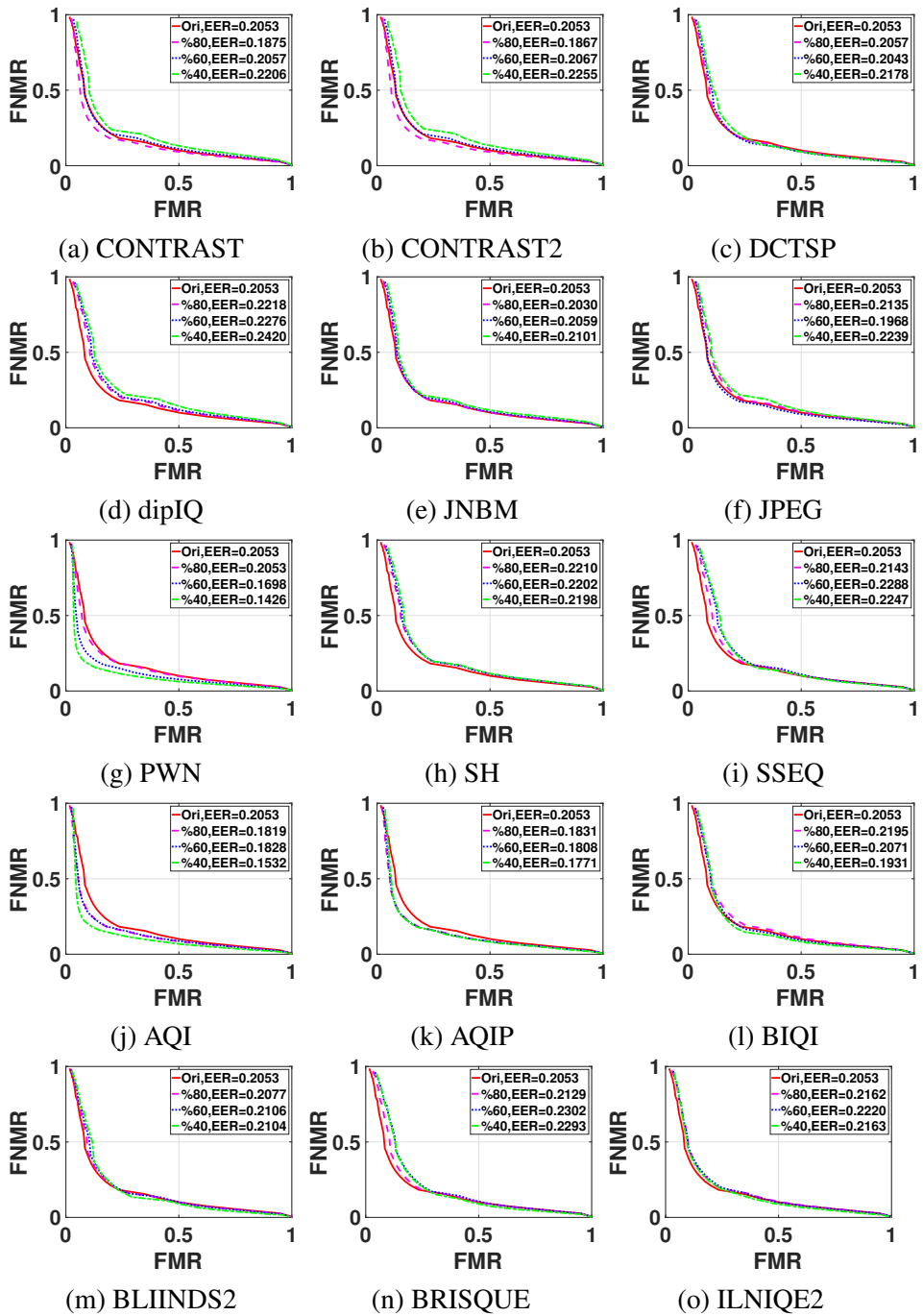


Figure B.6: DET curves with EER for comparison score with and without omitting low quality iris samples for reflex camera.

Appendix C

**Figures of EER values with
omitting low quality face samples
one by one until the best quality
sample left**

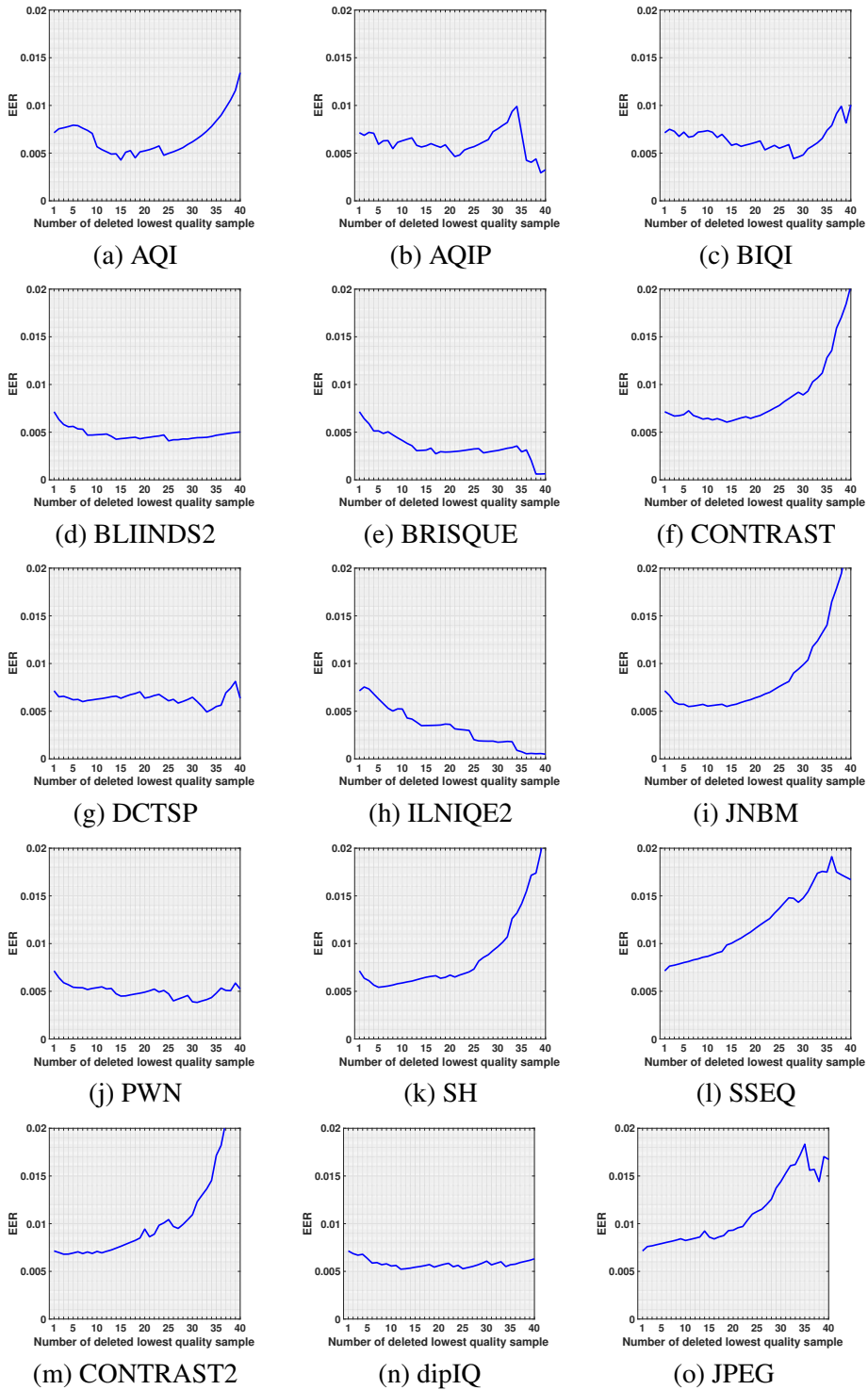


Figure C.1: EER values with omitting low quality face samples one by one until the best quality face sample left for LFC by using GF+KFA face recognition algorithm.

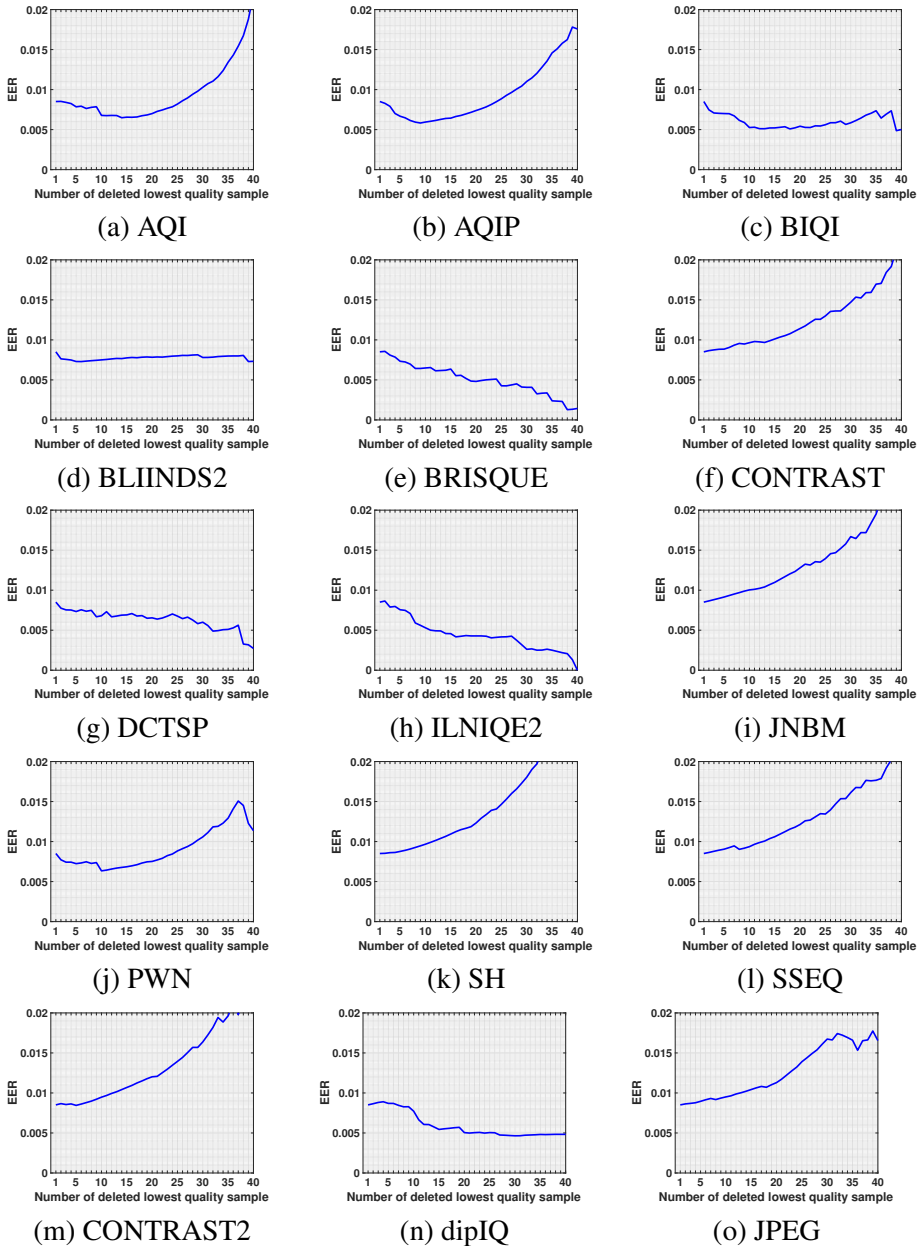


Figure C.2: EER values with omitting low quality face samples one by one until the best quality face sample left for smartphone by using GF+KFA face recognition algorithm.

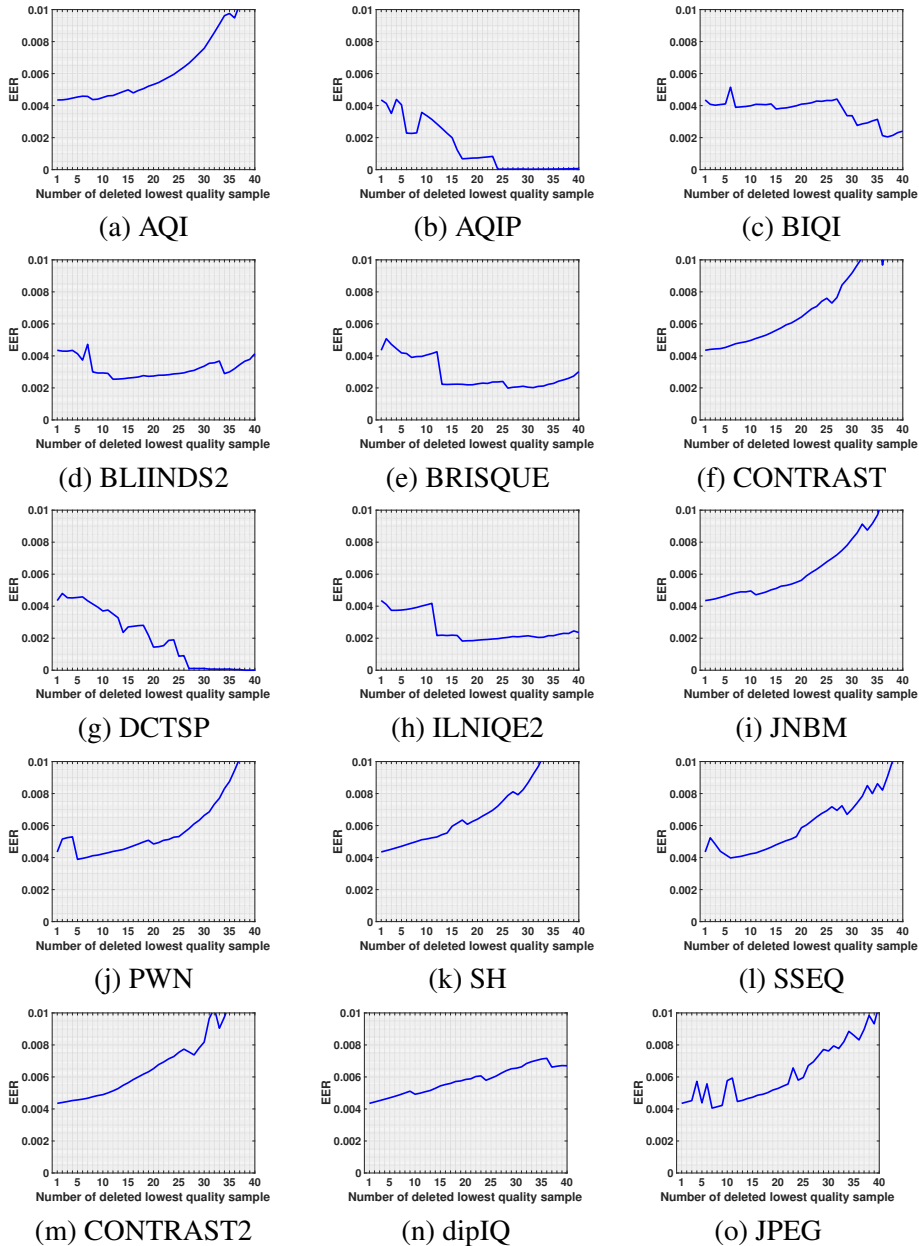


Figure C.3: EER values with omitting low quality face samples one by one until the best quality face sample left for reflex camera by using GF+KFA face recognition algorithm.

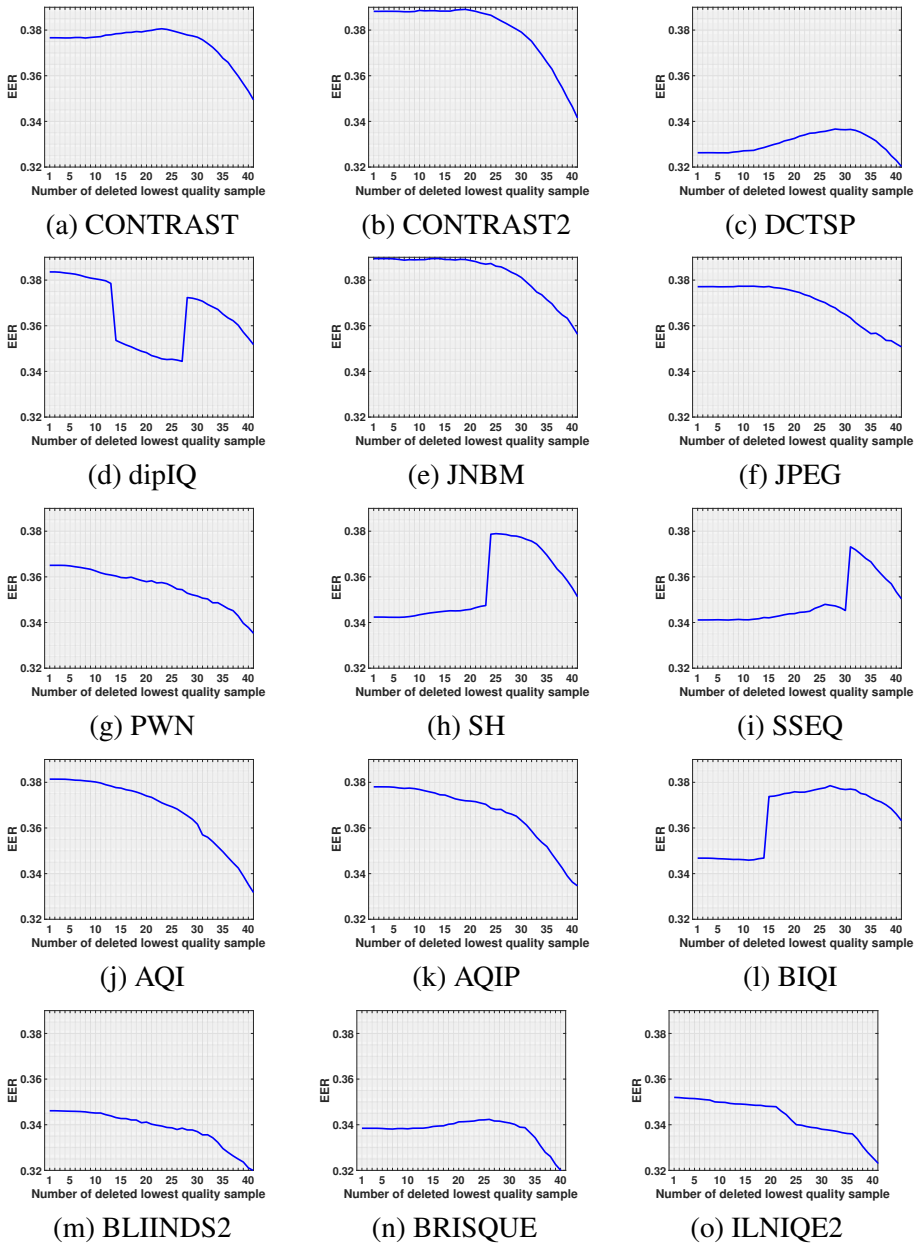


Figure C.4: EER values with omitting low quality face samples one by one until the best quality iris sample left for LFC.

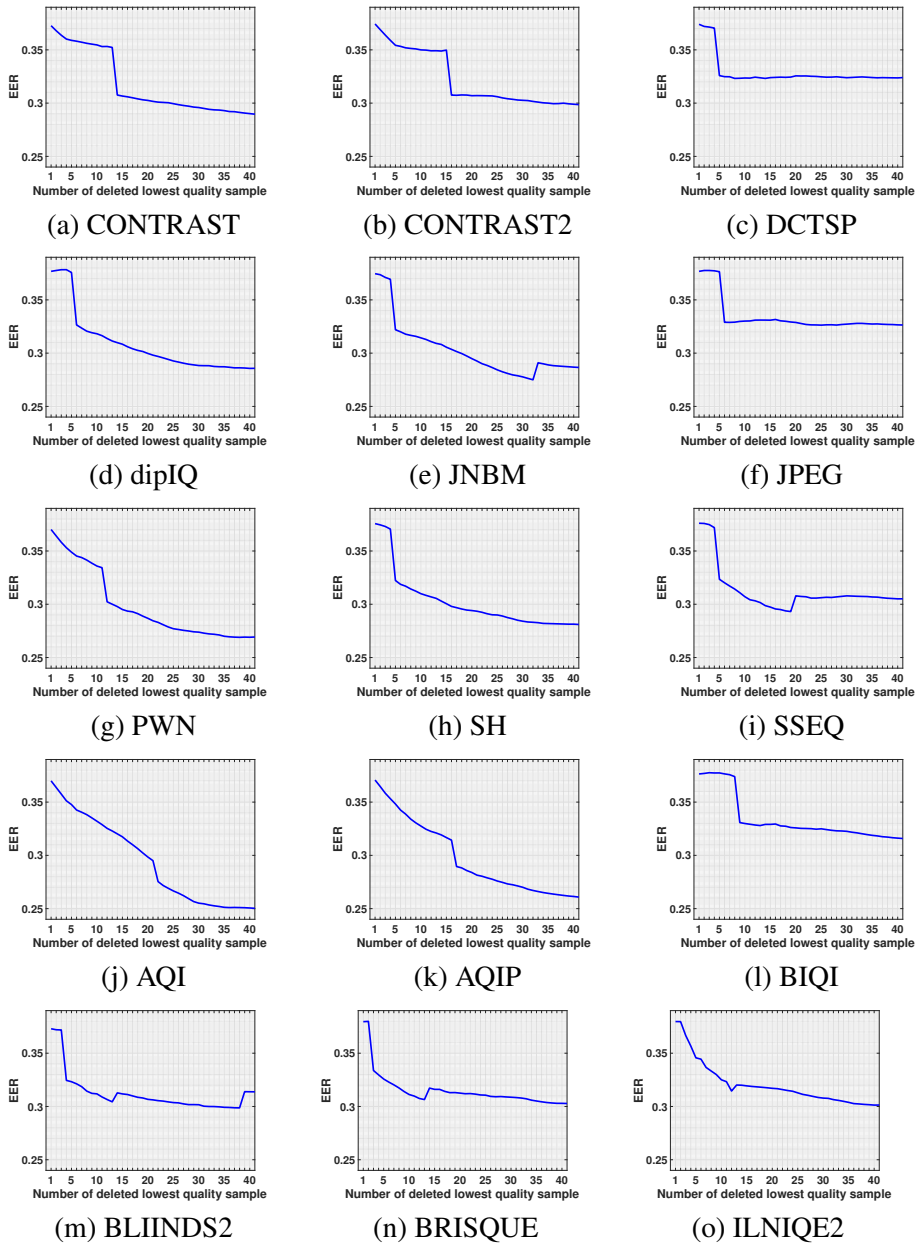


Figure C.5: EER values with omitting low quality face samples one by one until the best quality iris sample left for smartphone.

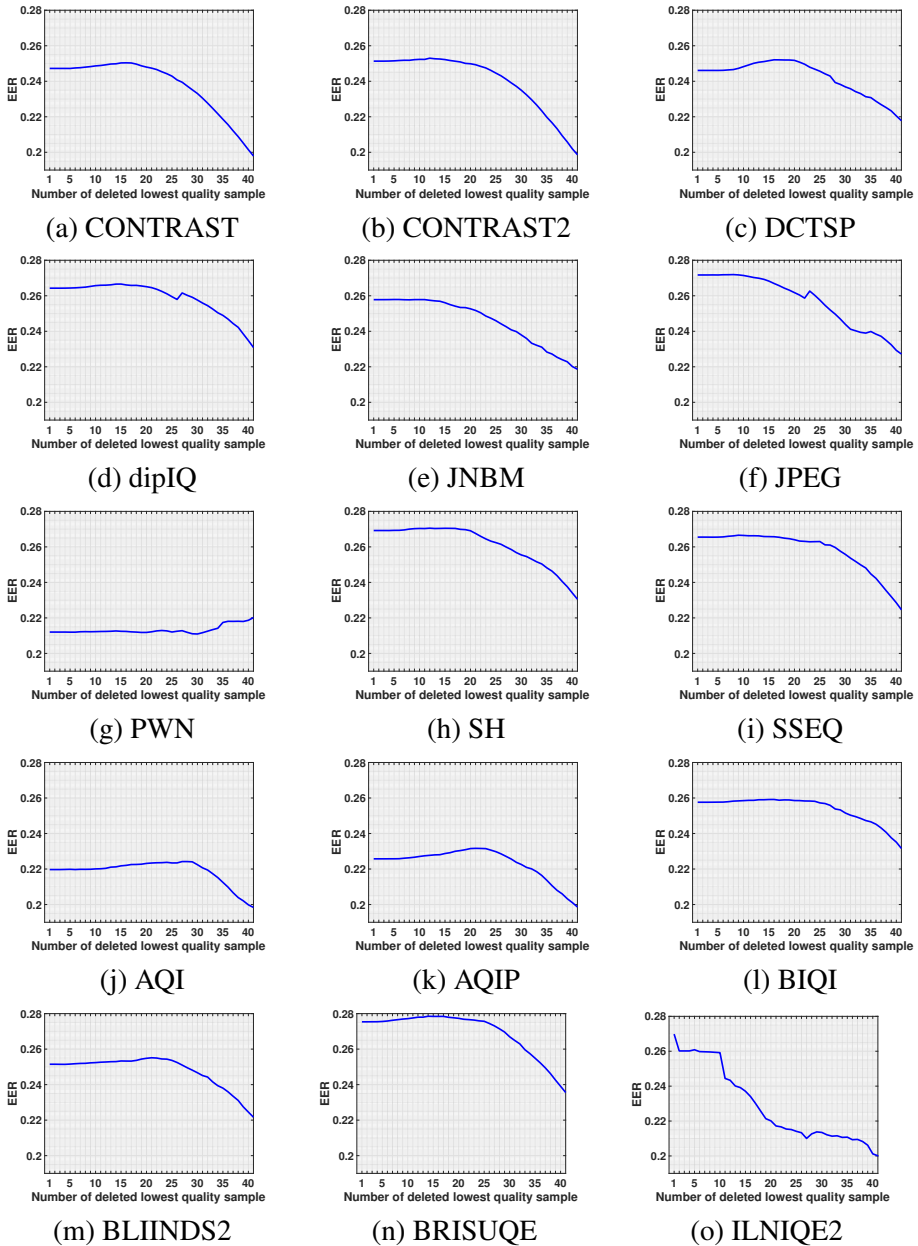


Figure C.6: EER values with omitting low quality face samples one by one until the best quality iris sample left for reflex camera.